



HAL
open science

La cryosphère marine et continentale du domaine nord-ouest groenlandais: dynamique récente (Holocène) et lien avec le contexte climatique et océanographique régionale

Eleanor Georgiadis

► **To cite this version:**

Eleanor Georgiadis. La cryosphère marine et continentale du domaine nord-ouest groenlandais: dynamique récente (Holocène) et lien avec le contexte climatique et océanographique régionale. Environmental Sciences. Université de Bordeaux; Université laval, 2020. English. NNT : . tel-03475990

HAL Id: tel-03475990

<https://theses.hal.science/tel-03475990>

Submitted on 11 Dec 2021

HAL is a multi-disciplinary open access archive for the deposit and dissemination of scientific research documents, whether they are published or not. The documents may come from teaching and research institutions in France or abroad, or from public or private research centers.

L'archive ouverte pluridisciplinaire **HAL**, est destinée au dépôt et à la diffusion de documents scientifiques de niveau recherche, publiés ou non, émanant des établissements d'enseignement et de recherche français ou étrangers, des laboratoires publics ou privés.

THÈSE EN COTUTELLE PRÉSENTÉE

POUR OBTENIR LE GRADE DE

DOCTEUR DE

**L'UNIVERSITÉ DE BORDEAUX (France)
ET DE L'UNIVERSITÉ LAVAL (Canada)**

ÉCOLE DOCTORALE SCIENCES ET ENVIRONNEMENTS U. BX

SPÉCIALITÉ SÉDIMENTOLOGIE ET PALÉOCLIMAT

DÉPARTEMENT DE BIOLOGIE U. LAVAL

SPÉCIALITÉ OCÉANOGRAPHIE

Par Eleanor GEORGIADIS

**The marine and continental cryosphere in NW Greenland: Holo-
cene dynamics under a changing climate and interplay with the
oceanographic context**

Sous la direction de Jacques GIRAUDEAU
et de Guillaume MASSE

Soutenue le 30 avril 2020

Membres du jury :

Mme.	SEIDENKRANTZ, Marit-Solveig	Professeur, University of Aarhus, Danemark	Rapporteur
M.	KNIES, Jochen	Directeur de Recherche, Geological Survey of Norway, Norvège	Rapporteur
Mme.	ESCUTIA, Carlota	Directrice de Recherche, Spanish National Research Council, Espagne	Examineur
M.	LAJEUNESSE, Patrick	Professeur, Université Laval, Canada	Examineur
M.	MARTINEZ, Philippe	Professeur, Université de Bordeaux, France	Examineur
Mme.	SICRE, Marie-Alexandrine	Directrice de Recherche CNRS, Sorbonne Université, France	Examineur
M.	GIRAUDEAU, Jacques	Directeur de Recherche CNRS, Université de Bordeaux, France	Co-directeur
M.	MASSE, Guillaume	Chargé de Recherche CNRS, Université Laval, Canada	Co-directeur
Mme.	RIBEIRO, Sofia	Chargée de Recherche, Geological Survey of Denmark, Danemark	Invité

Titre : La cryosphère marine et continentale du domaine Nord-Ouest groënlandais (détroit de Nares) : dynamique récente (holocène) et en lien avec le contexte climatique et océanographique régional.

Résumé :

Le détroit de Nares constitue l'un des trois domaines de l'Archipel Arctique Canadien (AAC) reliant l'océan Arctique à la baie de Baffin. Le transport d'eau d'origine pacifique via l'AAC alimente l'essentiel de la circulation océanique de la partie nord et occidentale de la baie de Baffin. Le potentiel d'eau douce atteint, plus au sud, la mer du Labrador, et module ainsi les caractéristiques physico-chimiques des eaux de surface et de sub-surface de cette région, siège de la formation d'une des composantes majeures de la circulation profonde de l'Atlantique Nord (Labrador Sea Water).

Le détroit de Nares, à la frontière est de l'AAC, est à 80% couvert de glace de mer pendant 11 mois de l'année sous l'influence (1) de l'apport de banquise multi-annuelle provenant de l'océan Arctique au Nord, et (2) de la formation *in situ* de glace de mer. L'histoire hydrologique de cette région est donc intimement liée à celle de ces deux composantes. Par ailleurs, ce couvert de glace régule le transport d'eaux dessalées et de glace vers la baie de Baffin, et entretient l'existence d'une zone ouverte : la polynie des eaux du nord.

La polynie des eaux du nord est aujourd'hui essentiellement une polynie à chaleur latente. L'arc de glace du bassin de Kane empêche la dérive de glace de mer et d'icebergs vers la baie de Baffin, pendant que les vents puissants chassent la glace formée à la surface de la polynie. Deux processus physiques importants ont alors lieu : (1) la formation de glace de mer en continue entretient la formation de saumures ou « brines », des eaux salées et froides, et (2) sous l'effet du vent, les masses d'eaux de surface sont déviées vers l'île d'Ellesmere. Un mouvement vertical est initié par la plongée des brines et le pompage d'Ekman résultant du déplacement des masses d'eaux par le vent induit la remontée d'eaux atlantiques chaudes, riches en nutriment. La remontée d'eaux atlantiques peut promouvoir la fonte de la glace en surface, ce qui confère à la polynie des eaux du nord son caractère sensible. La productivité primaire

est alimentée en continu par des eaux pacifiques riches en silicates à travers le détroit de Nares et la remontée d'eaux atlantiques riches en nitrates dans la polynie, jusqu'à la rupture estivale du pont de glace qui entraîne l'entrée de glace dans la polynie et l'arrêt de la remontée de nitrates. Depuis les années 1980, la durée moyenne du pont de glace est en diminution, engendrant une chute de la productivité.

Le détroit de Nares a été affecté durant la période post-glaciaire par (1) un retrait rapide des calottes groenlandaise et innuitienne, initialement ancrées sur le fond et convergeant au niveau du détroit de Nares, (2) une baisse importante du niveau marin (rebond isostatique) et (3) des conditions variables de glace de mer pérenne ou saisonnière. Ces trois phénomènes, dont la chronologie et le synchronisme à l'échelle régionale sont très mal contraints, font du détroit de Nares un domaine unique d'examen de la réponse de la cryosphère marine et continentale à un changement climatique rapide tel celui amplifié aujourd'hui dans les régions arctiques sous le forçage du réchauffement global.

Les archives sédimentaires prélevées lors des campagnes (2014 et 2016) du NGCC Amundsen dans le cadre de l'ANR GREENEDGE et du programme canadien ARCTICNET offrent une opportunité unique de reconstituer l'histoire post-glaciaire à tardi-holocène de la région.

Notre travail repose sur une analyse multi-proxies de ces archives incluant pour chaque carotte une étude sédimentologique approfondie (granulométrie et lithofaciès), une analyse micropaléontologique (assemblages de foraminifères benthiques et planctoniques), des mesures géochimiques continues de la distribution d'éléments majeurs et mineurs (banc XRF core-scanner), des analyses minéralogiques (q-XRD) et des mesures biogéochimiques (biomarqueurs de la glace de mer IP₂₅ et HBI III).

Nos résultats nous ont amené à proposer un âge d'ouverture pour le détroit de Nares situé entre 9 et 8.3 mille ans avant l'actuel (cal. ka BP), avec un âge probable autour de 8.4-8.3 cal. ka BP. Les conditions environnementales suivant la connexion de l'Océan Arctique avec la baie de Baffin ont été très variables durant le maximum thermique holocène (induisant de très fortes températures atmosphériques) ainsi qu'à cause de l'apport important d'eau de fonte lié au recul des calottes. Dans un environnement plus glacio-distal, un minimum de couvert de glace de mer est observé entre 8.1 et 7.5 cal. ka BP. Avec la chute de températures atmosphériques, le couvert de glace de mer

saisonnaire est établi de façon régulière à partir de 7.5 cal. ka BP, mais ce n'est qu'à partir de 5.5 cal. ka BP que le pont de glace du bassin de Kane s'inscrit durablement au printemps et en été. La polynie est initiée à partir de 5.5 cal. ka BP, mais elle repose sur une chaleur essentiellement latente. Ce n'est qu'à partir de 4.5 cal. ka BP, lorsque les températures atmosphériques sont assez froides, que la formation de brines est assez importante pour engendrer le transport vertical d'eaux atlantiques. A partir de 3.7/3.0 cal. ka BP, le pont de glace nord est présent de façon quasi-pérenne, ce qui empêche l'entrée de glace de mer arctique épaisse dans le détroit de Nares et abouti à la fragilisation du pont de glace dans le bassin de Kane. Le détroit de Nares devient libre de glace de façon saisonnière et, du fait de l'absence de convection, les eaux de la région nord de la baie de Baffin deviennent stratifiées. Le rétablissement du pont de glace du bassin de Kane est limité à une courte période centrée autour de 500 ans avant l'actuel.

Mots clés : Calotte ; glace de mer ; climat ; Holocène ; Arctique ; paléoenvironnements

Title: The marine and continental cryosphere in NW Greenland: Holocene dynamics under a changing climate and interplay with the oceanographic context

Abstract:

Nares Strait is one of the three channels of the Canadian Arctic Archipelago (CAA), which connect the Arctic Ocean to Baffin Bay. The CAA throughflow is a major component of ocean circulation in western Baffin Bay. Nares Strait borders the CAA to the east, separating Ellesmere Island from Greenland, and is 80% covered in sea ice 11 months of the year. The heavy sea ice cover is constituted of (1) arctic (multi-year) sea ice having entered the strait by the north, and (2) locally formed first year sea ice, which consolidates the ice cover. The hydrological history of the area is intimately linked to the formation of land-fast sea ice in the strait, constituting ice arches. The sea-ice cover in Nares Strait regulates freshwater (liquid and solid) export towards

Baffin Bay, and is integral to the formation of an area of open water in northernmost Baffin Bay: the North Water polynya.

Nares Strait has been at the heart of major geomorphological changes over the past 10,000 years. Its deglacial and post-glacial history is marked by (1) rapid retreat of the Greenland and Innuitian ice-sheets which coalesced along Nares Strait during the Last Glacial Maximum, (2) post-glacial shoaling associated to isostatic rebound, and (3) variable multi-year and seasonal sea ice conditions. Little is known about the evolution of these three environmental components of the Nares Strait history, and they are poorly constrained in terms of chronology and synchronism with other regional changes. Nares Strait and its eventful Holocene history provide a unique case study of the response of the marine and continental cryosphere to rapid climate change, such as that affecting Arctic regions in modern times.

The marine sediment archives that were retrieved during the ANR GreenEdge and ArcticNet (2014 and 2016) cruises of the CCGS Amundsen offer a unique opportunity to investigate the Deglacial to Late Holocene history of Nares Strait. Our reconstructions are based on a multi-proxy study of these cores, including sedimentologic (grain size and lithofacies), geochemical (XRF), mineralogical (q-XRD) micropaleontological (planktic and benthic foraminiferal assemblages), and biogeochemical (sea ice biomarkers IP₂₅ and HBI III).

Our results include an age for the deglacial opening of Nares Strait between 9.0 and 8.3 cal. ka BP, with the event likely occurring closer to the later bracket of the timeframe (i.e. ca 8.4-8.3 cal. ka BP). This event established the throughflow from the Arctic Ocean towards northernmost Baffin Bay. Environmental conditions were highly unstable in the Early Holocene, and marine primary productivity was limited. A period of minimum sea ice cover occurred from ca 8.1 to 7.5 cal. ka BP, during the Holocene Thermal Maximum, when atmospheric temperatures were higher than today in Nares Strait. Sea ice cover became more stably established as a seasonal feature around 7.5 cal. ka BP and primary productivity related to ice edge blooms increased. Eventually, the duration of the ice arches increased and they were present in spring and into the summer from 5.5 to 3.7 cal. ka BP, which allowed the inception of the North Water polynya. The North Water reached its maximal potential between 4.5 and 3.7 cal. ka BP, when warmer Atlantic-sourced water upwelled in the polynya, providing nutrients for

primary productivity. The establishment of a near-perennial ice arch in northern Nares Strait prevented export of multi-year sea ice into Nares Strait and hindered the formation of the southern ice arch, ultimately resulting in a less productive polynya over the past ca 3.0 cal. ka BP.

Keywords : ice-sheet ; sea ice ; climate ; Holocene ; Arctic ; paleoenvironments

Unités de recherche

UMR CNRS-Université de Bordeaux 5805 EPOC (Environnements et Paléoenvironnements Océaniques et Continentaux)

OASU – Université de Bordeaux

Allée Geoffroy Saint-Hilaire – CS 50025

33615 Pessac CEDEX, France

UMI CNRS-Université Laval 3376 TAKUVIK

Département de Biologie et Québec Océan

Université Laval

Pavillon Alexandre-Vachon

1045, avenue de la Médecine

G1V 0A6, Québec, Canada

Table des matières

Résumé	ii
Abstract	iv
Table des matières	vi
Liste des figures, tableaux, illustrations	x
Listes des abréviations, sigles, acronymes	xiii
Remerciements	xiv
Avant-propos	xx
Introduction	1
1. Atmospheric and oceanic circulation in the Arctic	1
1.1 General (simplified) circulation	1
1.2 The Arctic Oscillation	5
2. Hydrology in Nares Strait	9
2.1 Oceanographic circulation	9
2.2 Sea ice conditions	13
3. The North Water polynya (Pikialasorsuaq)	17
3.1 Physical processes	17
3.2 Biological significance of the NOW polynya	20
4. Holocene history of Nares Strait	22
4.1 Importance of Holocene archives	22
4.2 Previous work on the Holocene history of Nares Strait	23
5. Objectives of current work and dissertation layout	25
5.1 Objectives	25
5.2 Dissertation layout	27
Chapter 1 Deglacial to Postglacial history of Nares Strait, Northwest Greenland: a marine perspective from Kane Basin	29
1.1 Résumé	29
1.2 Abstract	29
1.3 Introduction	30
1.4 Regional settings	31
1.5 Material and methods	34
1.5.1 Sedimentological analyses	34
1.5.2 XRF core-scanning	34
1.5.3 Chronology and radiocarbon dating in Nares Strait	35
1.6 Results and interpretations	36
1.6.1 Age model and sedimentation rates in core AMD14-Kane2b	36

1.6.3 Relationship between XRD data, grain size, and sediment sources	40
1.6.4 Lithological units and sedimentological processes	40
1.7 Discussion.....	48
1.7.1 <i>Ca.</i> 9.0 cal. ka BP: ice sheet retreat in Kane Basin	49
1.7.2 <i>Ca.</i> 9.0-8.3 cal. ka BP: ice-proximal to ice-distal environment in Kane Basin	49
1.7.3 <i>Ca.</i> 8.3 cal. ka BP: the opening of Kennedy Channel.....	51
1.7.4 <i>Ca.</i> 8.3-8.1 cal. ka BP: increased iceberg delivery to Kane Basin	53
1.7.5 <i>Ca.</i> 8.1-7.5 cal. ka BP: rapid retreat of the GIS in Kane Basin	53
1.7.6 <i>Ca.</i> 7.5-0 cal. ka BP: deglaciation of Washington Land	54
1.8 Conclusion	54
1.9 Supplements.....	57
Chapter 2 Holocene deglaciation of the southern sector of Nares Strait: insight from Talbot Fjord.....	62
2.1 Résumé	62
2.2 Abstract.....	62
2.3 Introduction	63
2.4 Study site.....	64
2.4.1 Holocene History and modern-day glacial activity.....	64
2.4.2 Regional geology and sediment sources	65
2.4 Material and Methods	67
2.4.1 Material: marine sediment core AMD16-233	67
2.4.2 Chronology	68
2.5 Mineralogical and geochemical analyses	71
2.5.1 Quantitative bulk mineralogy.....	71
2.5.2 AVAATECH XRF-core scanning.....	71
2.5.3 Statistical analysis of the geochemical dataset.....	73
2.6 Sedimentological analyses	73
2.6.1 Thin sections.....	73
2.6.2 Grain size	73
2.7 Results.....	74
2.7.1 Relationship between semi-quantitative elemental (XRF) and quantitative mineralogical (q-XRD) composition of sediment.....	74
2.7.2 Lithofacies: sedimentological characteristics and source material	75
2.8 Discussion.....	80
2.8.1 Paleoenvironmental interpretation of XRF core scanning data.....	80
2.8.2 Reconstruction of sedimentary environments, and link with regional context	80
2.8.3 Ice proximal environment at the entrance of Talbot Fjord (>9.8 cal ka BP)	81
2.8.4 Deglaciation of southern Nares Strait (>9.8-8.5 cal ka BP)	83

2.8.5 Ice-distal environment (8.5-0 cal ka BP).....	88
2.9 Conclusion	89
2.10 Supplements	91
Chapter 3 Local and regional controls on Holocene sea ice dynamics and oceanography in Nares Strait, Northwest Greenland	98
3.1 Résumé	98
3.2 Abstract	98
3.3 Introduction	99
3.4 Material and methods	102
3.4.1 Sediment core AMD14-Kane2b.....	102
3.4.2 Sea ice biomarkers	103
3.4.3 Foraminifera	104
3.5 Results and interpretations	105
3.5.1 Sea ice biomarkers	105
3.5.2 Foraminifera	107
3.6 Results and interpretations	110
3.6.1 Deglaciation of Kane Basin (<i>ca.</i> 9.0–8.3 cal. ka BP).....	110
3.6.2 Maximum influence of Atlantic Water in Kane Basin (<i>ca.</i> 8.3-7.4 cal. ka BP).....	113
3.6.3 Increased drift-ice and shallowing of Kane Basin (<i>ca.</i> 7.4-5.5 cal. ka BP)	114
3.6.4 Establishment of modern oceanography in Nares Strait and the inception of ice arches (<i>ca.</i> 5.5-3.0 cal. ka BP).....	116
3.6.5 Decline of sea ice cover in Kane Basin (<i>ca.</i> 3.0-0 cal. ka BP)	119
3.7 Conclusion	119
Chapter 4 Holocene dynamics of the North Water, northernmost Bafin Bay: a perspective from the western sector of the polynya	123
4.1 Résumé	123
4.2 Abstract	123
4.3 Introduction	124
4.4 Material and Methods	129
4.4.1 Sediment core AMD16-233.....	129
4.4.2 Biomarker measurements.....	129
4.4.3 Micropaleontological (foraminifera) assemblages	130
4.4.3 XRD mineralogy	131
4.5 Results and interpretations	132
4.5.1 General trends in the proxy records of core AMD16-233.....	132
4.5.2 Environmental significance of the proxy records.....	134
4.6 Discussion	141
4.6.1 Heavy sea-ice cover during Early Holocene ice sheet retreat, and maximum Atlantic influence (>9.8-8.4 cal. ka BP)	141

4.6.2 Transition from multi-year to seasonal sea-ice cover, and from oligotrophic to more productive conditions at the core site, with reduced Atlantic influence (8.4-6.5 cal. ka BP)	142
4.6.3 Enhanced productivity, and inception of the North Water polynya (6.5-3.7 cal. ka BP)	145
4.6.4 Reduced productivity and enhanced stratification (3.7-1.9 cal. ka BP)	148
4.6.5 Collapse of the Trinity-Wykeham ice shelf limited recovery of North Water productivity (1.9 cal. ka BP-0)	149
4.7 Summary and conclusion	150
Chapter 5 Nares Strait: a driver of local and regional ocean, ice and climate dynamics	155
5.1 Introduction	155
5.2 Nares Strait environmental dynamics drive local change in the area.....	155
5.2.1 Ice shelf development in the northern Nares Strait area	155
5.2.2 Mitigation of local climate, and influence on human dynamics	157
5.3 Further-reached implication of the Holocene history of Nares Strait.....	161
5.3.1 Silicate pump	161
5.3.2 Potential implications on North Atlantic Holocene circulation.....	162
5.4 Conclusion and implications of Nares Strait dynamics on modern and future ocean circulation and climate	169
Conclusion and perspectives.....	172
References	178

Liste des figures, tableaux, illustrations

Liste des Figures

Figure 1.1: Circulation in the Arctic Ocean.....	2
Figure 1.2: Estimated fluxes of inflow to and outflow from the Arctic.	3
Figure 1.3: Age of sea ice in the Arctic Ocean.	4
Figure 1.4: Schematic global atmospheric circulation, with compartmentalised wind cells, adapted from the general model of Held et Hou (1980) and represented only for the northern hemisphere.	5
Figure 1.4: Schematic representation of the Arctic Oscillation and its effect on northern hemisphere climate.	5
Figure 1.6: Simplified examples of cyclonic (CCR) and anticyclonic circulation regime (ACCR) of atmospheric circulation in the Arctic Ocean.....	7
Figure 1.7: Schematic representation of oceanic and atmospheric pressure patterns in a positive and a negative phase.....	8
Figure 1.8: Oceanographic circulation in Nares Strait.	10
Figure 1.9: Sea-ice conditions in Nares Strait.	13
Figure 1.10: Winter (November to March) AO index and number of ice arch days.....	16
Figure 1.11: Approximate location of the North Water polynya (Pikialasorsuaq) in northern Baffin Bay.	17
Figure 1.12: Schematic representation of the physical processes linked to the North Water Polynya in southern Nares Strait.	18
Figure 1.13: Schematic representation of the biological significance of the North Water Polynya.....	21
Figure 1.14: Holocene archives in the Nares Strait area.	23
Figure 1.15: Location of cores AMD14-Kane2b and AMD16-233.....	26
Figure 2.1: Schematic circulation in the Canadian and northern Greenland sectors of the Arctic Ocean and within Nares Strait.	32
Figure 2.2: Geology of Northwest Greenland and Ellesmere Island along Nares Strait.	34
Figure 2.3: ²¹⁰ Pb and ¹³⁷ Cs profiles in AMD14-Kane2b CASQ core and box core.	35
Figure 2.4: Core AMD14-Kane2b age model and sedimentation rates.	37
Figure 2.5: 3.5 kHz chirp profile across the coring location.	41
Figure 2.6: Sedimentological results and elemental signature of the detrital fraction of core AMD14-Kane2b.....	42
Figure 2.7: Comparison of sieved grain size data from AMD14-Kane2b and paleoceanographic proxies from HLY03-05CG in Hall Basin (Jennings et al., 2011).	50
Figure 2.8: GIS and IIS retreat in Nares Strait.	52
Figure 3.1: Study area in NW Greenland and location of core AMD16-233 shown on a MODIS satellite image.	65
Figure 3.2: Synthetic geological map of the study area.	66
Figure 3.3: Age model and sedimentation rates of core AMD16-233.....	69
Figure 3.4: Correlation matrix of sediment provenance and normalised elemental counts.....	74
Figure 3.5: Sedimentologic and geochemical data from core AMD16-233.....	79
Figure 3.6: Schematic representation of ice sheet extent in Nares Strait.....	83
Figure 3.7: Retreat of Innuitian and Greenland Ice Sheets in southern Nares Strait before 9.8 cal. ka BP.	84
Figure 3.8: Ice sheet retreat in southern Nares Strait and along a west-central axis in Kane Basin.	85
Figure 3.9: Further ice sheet retreat in southern Nares Strait and along the west central axis in Kane Basin, reaching location AMD1-Kane2b around 9.0 cal. ka BP.	86
Figure 3.10: Further ice sheet retreat in northern Kane Basin, until the opening of Nares Strait was completed around 8.5 cal. ka BP.	87
Figure 4.1: Schematic circulation in the Canadian and northern Greenland sectors of the Arctic Ocean and Baffin Bay and within Nares Strait, and inter-annual variations in sea ice cover in Nares Strait.....	101
Figure 4.2: Sedimentation rates (from Georgiadis et al., 2018), HBI (IP ₂₅ and HBI III) concentrations and fluxes in core AMD14-Kane2b.	106

Figure 4.3: Benthic and planktic foraminifera concentrations and fluxes, percentages of agglutinated foraminifera, abundance of calcareous species in core AMD14-Kane2b, and the hierarchical clustering dendrogram of the distance matrix computed in R.	108
Figure 4.4: Benthic and planktic foraminiferal fluxes, percentages of agglutinated foraminifera, and abundance of benthic foraminifera species used to reconstruct paleoenvironments in Kane Basin, plotted next to IP ₂₅ and HBI III fluxes in core AMD14-Kane2b on an age scale.....	112
Figure 4.5: Comparison of benthic and planktic foraminiferal fluxes, abundance of selected benthic foraminiferal species, and IP ₂₅ and HBI III fluxes in AMD14-Kane2b with regional records.	115
Figure 4.6: Schematic representation of positive and negative phases of the Arctic Oscillation, and of sea ice conditions in Nares Strait, adapted from Steele et al. (2004).	118
Figure 5.1: Study area and location of core AMD16-233 and other nearby records.	126
Figure 5.2: Variable surface conditions in the North Water related to the presence and absence of the Kane Basin ice arch, and variable sea ice conditions at the core site.	128
Figure 5.3: Depth scale of benthic and planktic foraminiferal concentration and fluxes, IP ₂₅ and HBI III concentrations and fluxes, BSi content, and sedimentation rates.	133
Figure 5.4: Close-up of selected benthic foraminiferal species, biomarker concentrations, and sediment provenance in the IRD-rich interval of core AMD16-233.....	134
Figure 5.5: Depth scale of benthic and planktic foraminiferal fluxes, major contributing species in the benthic foraminiferal assemblage, percentage of linings, and relative contributions of calcareous and agglutinated taxa in the bulk assemblage of core AMD16-233.	135
Figure 5.6: Time scale of benthic and planktic foraminiferal fluxes, IP ₂₅ and HBI III fluxes, BSi content in the mineralogical suite, and relative abundance of selected benthic foraminiferal species in core AMD16-233.	137
Figure 5.7: Same as Figure 5.6, but with IP ₂₅ and HBI III fluxes, and other regional records.	144
Figure 5.8: Schematic representation of surface conditions in Nares Strait and northernmost Baffin Bay and polynya dynamics, including wind-driven Ekman transport, brine convection, and upwelling.	146
Figure 6.1: Study area with location of cores AMD14-Kane2b and AMD16-233.	156
Figure 6.2: Comparison of data from cores AMD14-Kane2b and AMD16-233 with local records.....	158
Figure 6.3: Comparison between diatom productivity-related proxies in Baffin Bay and our record of silicate drawdown in southern Nares Strait.	162
Figure 6.4: Map of the North Atlantic showing modern surface circulations (adapted from Rashid et al., 2017) and location of marine sediment cores discussed in the text.	166
Figure 6.5: Comparison of sea ice dynamics in Nares Strait with oceanographic proxies in the Labrador Sea and Baffin Bay.	168
Figure 6.6: Comparison of the winter atmospheric Arctic Oscillation (AO) index, with the seasonal duration of ice arches in Nares Strait (adapted from Vincent et al., 2019)	171

Liste des Tableaux

Table 2.1: AMS radiocarbon ages on selected carbonate material.....	38
Table 2.2: Details of CT scans and thin sections for each lithologic unit of core AMD14-Kane2b and summarised descriptions and interpretations.....	43
Table 3.1: Radiocarbon dated material in core AMD16-233, and calibrated ages using $\Delta R = 0$, $\Delta R = 335$, and $\Delta R = 264 \pm 74$ years.....	70
Table 3.2: Close-up of X-rays, photographs and thin sections of the different lithofacies of core AMD16-233.	77
Table 4.1: List of foraminifera taxa used to reconstruct paleoenvironmental conditions from core AMD14-Kane2b and their original references.	104
Table 5.1: List of foraminifera taxa used to reconstruct paleoenvironmental conditions from core AMD16-233 and their original references.	130
Table 6.1: Marine sediment cores and studies used to compare with our records.	165

Liste des Figures et Tableaux Supplémentaires

Figure 2.2: XRF data plotted against grain size data.	57
Figure 2.10: Location of the radiocarbon ages in Nares Strait reported in England (1999) and Bennike (2002) and their calibrated ages with $\Delta R = 240 \pm 51$ years.	60
Figure 3.11: Correlation matrix of XRD-derived sediment source proportions, and XRF core-scanning semi-quantitative elemental composition of the sediment in core AMD16-233.	93
Figure 3.12: Correlation matrix of the XRD source data and Al-normalised XRF data, and correlation matrix of the XED source data and XRF core-scanner data normalised to the sum of all counts used in the main text of this paper.	94
Figure 3.13: Correlation matrix of XRD-derived mineralogical data and normalised (sum) XRF-derived semi-quantitative elemental composition of the sediment of core AMD16-233.	95
Figure 3.14: Zr:Al plotted against % (silt + sand).	96
Figure 3.15: Downcore profile of the minerals composing the sediment of core AMD16-233.	96
Table 2.3: Radiocarbon ages as reported in England (1999) and Bennike (2002) and calibrated with $\Delta R = 240 \pm 51$ years.	58
Table 2.4: Radiocarbon dated material from core HLY03-05CG (Jennings et al., 2011), calibrated with $\Delta R = 240 \pm 51$ years.	60
Table 3.3: Mineralogical assemblages of the sources present in the Nares Strait area (Andrews and Eberl, 2011).	91
Table 3.4: ΔR of living, pre-bomb molluscs collected in or near to Nares Strait and their distance to the core site.	21
Table 3.3: Mineralogical assemblages of the sources present in the Nares Strait area (Andrews and Eberl, 2011).	91

Listes des abréviations, sigles, acronymes

AMOC: Atlantic Meridional Oceanic Circulation

AO: Arctic Oscillation

BIC: Baffin Island Current

CAA: Canadian Arctic Archipelago

MODIS: Moderate Resolution Imaging Spectroradiometer

NOW: North Water

TDS: Transpolar Drift Stream

WCG: West Greenland Current

Remerciements

[Eng] Before getting into the acknowledgments, I apologise for the length of this section. This PhD ended in a very peculiar way, and I have gone straight from dissertation-writing-isolation to near worldwide lockdown, which has given me too much time to write the acknowledgments. I am convinced that never has a PhD student benefited from as much help as I have during the past 3.5 to 4 years. I have a long list of people to thank, and wish I could have thanked them in person but the irony is that I was unable to organise a “pot de these” (the traditional party organised by PhD students at the University of Bordeaux following their defence, where everyone in the building stops what they are doing to join in the festivities). In my defence, it’s not entirely my fault that I have so many people to thank: as well as being great scientists, my supervisors are also amazing “people persons” and (nearly) everyone wants to work with them. This opened the door to many collaborations for me and I have travelled from couch to couch thanks to the generosity of many friends in order to visit leaders in Arctic research all over the world.

[Fr] Je suis persuadée que jamais une thèse n’a reçue autant de support que celui dont j’ai bénéficié ces 3.5 à 4 dernières années. L’ironie du sort a voulu que je ne puisse pas accueillir toutes les personnes à qui j’avais promis le « pot de thèse du siècle » pour les remercier de leur aide, soutien émotionnel ou logistique. (Il m’arrive encore de penser que cette pandémie est le fruit d’un complot organisé par un de mes directeurs pour éviter à tout prix de prendre part à un pot « véguane »). Quoi qu’il en soit, ce n’est que partie remise, le pot du siècle n’est pas annulé mais seulement reporté !

[Eng] I would like to start with acknowledging the amazing French University system which not only enabled me to pursue a higher education for free, but also provided me with a monthly stipend for the near entirety of my studies. Without this I would never have been able (nor even envisaged) to continuing to study beyond high school. This PhD was enabled thanks to funding from IdEx (U. Bordeaux) and CRSNG (U. Laval) to wish I am forever indebted for trusting this incredible project.

[Eng] I wish to acknowledge the members of the jury who took the time to read this dissertation and take part in the long online defence, providing engaging questions and fruitful comments. I warmly thank **Philippe Martinez** for presiding over the defence and making all the special arrangements entailed by an online defence. Special thanks go out to **Jochen Knies** and **Marit-Solveig Seidenkrantz**, the examiners of this PhD, for going through the dissertation in detail and raising engaging points during the defence. Thank you, **Patrick Lajeunesse** for helping me with the geophysical data throughout my PhD and sharing your knowledge of polar geology during my defence. I sincerely thank **Carlota Escutia** and **Marie-Alexandrine Sicre** who took time in their busy schedules to provide constructive comments regarding deglacial processes and sea ice dynamics – I wish we could have met in person and engaged in further discussions on these subjects. I thank **Sofia Ribeiro** for being an ever present and encouraging figure throughout my PhD and

providing critical thoughts during my defence. Finally, thank you to **Connie Lovejoy** and **Frederick Garabetian** and my supervisors, **Guillaume Massé** and **Jacques Giraudeau**, for their help in organising the online defence.

[Fr] Cette thèse fait suite à un stage de master, dirigé par **Jacques Giraudeau** et **Philippe Martinez** à l'université de Bordeaux, avec l'implication de **Guillaume Massé** qui m'a accueillie à l'université Laval pour un court échange. Je souhaite remercier Jacques, Guillaume et Philippe qui m'ont ouvert la porte à la recherche, et m'ont fait confiance alors que ce n'était pas tout de suite évident que j'allais m'en sortir. Merci à Philippe qui a continué à suivre mon projet, même quand son nom n'apparaissait plus en tant que directeur dans ma recherche. Je serai éternellement reconnaissante à Jacques et à Guillaume, mes directeurs de thèse, d'avoir consacré tant d'efforts à la constitution de mon dossier de doctorat en cotutelle malgré leurs emplois du temps déjà chargés. Ils m'ont, une fois de plus, fait confiance en m'accordant un projet de recherche ambitieux et magnifique – et ce, en dépit du fait qu'ils avaient conscience à ce moment-là de mon habitude à faire tout à la dernière minute et de ma tendance sévère d'être tête-en-l'air. C'est facile de prendre un thésard avec des valeurs sûres – ce qui était, en revanche, pas mon cas. Je suis venue de très, très loin. Je dois tous mes progrès à mes directeurs qui ont été présents lorsqu'il le fallait pendant la thèse mais qui m'ont aussi laissé une grande part d'autonomie, un équilibre qui m'a permis de développer une indépendance en tant que jeune chercheuse. Mon travail de thésarde a été grandement facilité par leur gentillesse, leur disponibilité et leur patience (qui dépasse ce que je savais humainement possible) – et leur sens d'humour *rires gênants*. C'est aussi grâce à mes directeurs, en particulier à Guillaume, que j'ai pu vivre l'expérience unique d'avoir participé à une mission océanographique où j'ai franchis les 80° nord à bord de l'*Amundsen*. Je remercie Jacques et Guillaume d'être des chercheurs sympathiques avec qui (presque) tout le monde a envie de travailler, ce qui m'a ouvert la voie à de nombreuses collaborations et m'a fait voyager pour échanger avec et me former auprès de grands chercheurs dans le domaine arctique. Vous m'avez appris que la science n'est pas juste des résultats sur un ordi (ou imprimés sur du papier, pour les plus anciens), que la science est aussi un prétexte pour échanger avec d'autres êtres-humains et parfois même de faire la fête. J'espère que je serai, un jour, quand je serai vieille, une directrice de thèse aussi sage que vous. « Allez, j'en fais pas trop, sinon vous allez prendre la grosse tête » comme dirait Jacques.

[Fr] Parmi les profs remarquables que j'ai pu rencontrer grâce à cette thèse en cotutelle, je souhaite remercier en particulier **Jean-Eric Tremblay** et **Patrick Lajeunesse** qui ont été présents pour moi à l'université Laval, et qui ont éclairé mes résultats à la lumière de la spécialité qui leur est propre. Jean-Eric et Patrick ont généreusement accepté d'évaluer mon examen doctoral et ma présentation de projet, apportant ainsi qualité et diversité des disciplines au sein de mon jury. Je remercie encore Patrick pour son aide dans la réflexion et l'écriture de mon premier papier, ainsi que pour sa participation au jury d'évaluation de cette thèse.

[Fr] S'il y a quelqu'un qui a toujours été présente pour moi au cours de cette thèse, c'est bien **Caroline Guilmette**. Depuis le début de la thèse (et même pendant mon séjour rapide à U. Laval pendant mon master), Caro était à mes côtés – ou plutôt, plus justement, j'étais aux côtés de Caro qui gérait tout – dans le labo, à continuellement préparer, passer et repasser des échantillons au GC-MS. C'est Caro qui m'a formée, avec beaucoup de rigueur et de patience, à la préparation et aux mesures d'HBI, et qui m'a laissée avec confiance travailler dans son laboratoire. J'ai également eu la grande chance d'avoir accompagné Caro sur l'*Amundsen* pour récupérer les carottes du leg2b de la campagne ArcticNet 2016, et même d'avoir aidé à ranger le camp de glace à Qiqiktarjuaq avec elle (expérience unique !). Jamais je n'ai rencontré une personne aussi dévouée à son travail et rigoureuse dans tout ce qu'elle fait. C'est également Caro qui me rassurait lorsque j'avais des baisses de moral, comme tous les thésards, à U. Laval. Merci, Caro, d'être une personne formidable, tant professionnellement que personnellement. J'ai une chance inouïe d'avoir travaillé avec toi pour ce projet de recherche.

[Fr] Je remercie chaleureusement **Gab (Joyal, OG)** qui m'a accueillie les bras ouverts lorsque je débarquais à Québec pour ma deuxième année de thèse, en m'offrant un chez moi au sein de sa magnifique maison. Je dois avouer que c'était également super pratique d'habiter avec un grand génie de la sismique et de la bathy pour discuter de ces sujets que je maîtrise très moyennement. Enfin, merci aussi de m'avoir mis en contact avec Gab Deslongchamps, me permettant de me loger à Québec pour ma dernière année de thèse. Un grand, grand merci à **Anne** également qui m'a généreusement fourni des vêtements pour que je survive à l'hiver québécois, et qui m'a fait découvrir le Mont Saint Anne dans Charlevoix, les tic-tacs de la nature et les champignons homard !

[Fr] Pour ma troisième année de doc qui s'est faite à Québec, c'est **Gab (Deslongchamps)** qui m'a ouvert sa porte et donné un toit. Je pense qu'une grande partie de cette thèse a vu le jour grâce à toi : tu as sauvé mon équilibre mental en dernière année de thèse et je ne te remercierai jamais assez. Tu as su m'appâter pour m'éloigner du microscope et m'emmener aux cours de yoga gratuits, aux pub quizz, aux soirées et à Pohégamook. Merci à ton cercle d'amis (et en particulier à Julien, Jérémie, Valérie, Pat, Arnaud, ... et bien sûr Félix et Mowgli) de m'avoir accueillie comme si je vous connaissais depuis toujours. Merci pour toutes tes petites intentions aux quotidiens qui m'ont donné l'énergie qu'il me fallait pour persévérer dans la fin du doctorat. En somme je dirais que les Gabriel(e) à Québec sont de vrais anges gardiens.

[Eng] I am eternally grateful to **Anne Jennings, Sofia Ribeiro** and **Audrey Limoges** for inspiring me as a young (female) researcher and for being mentors that have always been patient with me as I made my first steps in research. Were it not for Anne, Sofia and Audrey, I would have seen very little women during my PhD and I was fortunate to have found exceptional role models in them. I wish to thank you for teaching me to be rigorous in scientific reasoning and writing. It was wonderfully engaging to discuss the history of Nares Strait and the North Water with you. I am grateful to have had my thoughts challenged by you: you were

kind to me as I sometimes (often) made mistakes and embarrassed myself, though you always made me feel comfortable and respected me, even as a (very) junior researcher.

[Eng] Thank you to everyone at INSTAAR for making my stays such a great experience, not once but twice! **Natalia**, thank you for being such an amazing host for my first time in Boulder. I must admit that my first night in your house was one of the scariest experiences of my life, but you did such an amazing job of making me feel at home once you knew I was actually in your house. You took me out to explore Colorado during both my stays, taking me to Denver, Evergreen, Breckenridge and Buena Vista. You truly are an incredible friend, with the best parents! **Lineke** and **Jan**, you made me feel very welcome at your home and it was wonderful to meet **Nora**, thank you so much for having me during my second stay in Boulder! Thank you to both **Anne** and **Tom Marchitto** for hosting my stay at INSTAAR. I would like to acknowledge Tom's incredible patience as he trained me at preparing samples in the clean room. Tom, I have not forgotten about our trace element data! I will draft a paper eventually! I further thank Anne for teaching me how to properly identify tricky foraminifera, by being patient and looking at the tiniest details. I also extend my thanks to **John Morton** for helping me out in the clean room and running my samples, and to **John Andrews** who patiently talked me over some of my q-XRD results.

[Fr] Je remercie sincèrement les collègues à UQAR pour leur participation dans ce projet. Merci à **Guillaume St-Onge** pour les bons conseils et commentaires pertinents du premier papier. Un grand merci à **Jean-Carlos Montero-Serrano** de m'avoir accueillie à ISMER/UQUAR et pour m'avoir formée à la préparation des échantillons q-XRD, ainsi que pour les commentaires concernant le papier sédimento/minéralogie de la AMD16-233. Je remercie très chaleureusement **Myriam Caron** qui a été présente tout au long de cette thèse et qui a fait un travail formidable et laborieux sur le paléomag, les conditions de surface et la sédimentation lithique dans la baie de Baffin et le détroit de Nares. J'ai eu énormément de chance d'avoir pu échangé avec toi ces quatre dernières années et je suis très sincèrement RAVIE d'avoir pu m'appuyer sur ton travail de thèse tout au long de ma thèse.

[Fr] Enfin, je remercie tous les **collègues d'EPOC**. Le support logistique de **Pascal, Isabelle, Olivier, Muriel, Marie-Claire** et **Bernard** a été particulièrement précieux dans la réalisation de ce projet. Merci à **Naima** et **Frédérique** qui ont fait un travail formidable pendant le master de Naima dont j'ai profité lors de travaux annexes sur les foraminifères planctoniques de la carotte AMD14-Kane2b. J'aimerais remercier en particulier **Sébastien Zaragosi** qui a consacré des heures et des heures depuis la fin de mon master à m'apprendre à faire l'acquisition numérique des lames minces, à analyser de façon pertinente la sédimentologie des carottes de cette thèse, et à maîtriser CorelDraw. Le regret que je garderai en lien avec cette thèse c'est de ne pas avoir eu le temps ou de pas avoir été assez présente pour partager la convivialité du laboratoire et vous connaître davantage.

[Fr] Je remercie **Brieuc**, puis **Antoine** et **Paul** d'avoir été des camarades de bureau parfaits, sympathiques et tout plein d'humour ! Ça a été un réel plaisir de venir travailler en votre compagnie à Bordeaux ! Je remercie **tous les thésards d'EPOC**, les anciens et les nouveaux (je ne citerai pas de noms parce que je sais que je vais en oublier, mais j'espère que vous savez qui vous êtes !) pour avoir entretenu une si bonne ambiance au sein de la petite famille de thésards d'EPOC. J'aurais tellement aimé passer plus de temps avec vous au cours de cette thèse. Je vous souhaite à tous tout le meilleur pour la suite !

[Fr] J'ai un certain nombre d'anges gardiens à remercier à Bordeaux, ceux qui m'ont hébergée, nourrie, soutenue, qui ont fait la navette tout au long de cette thèse. Je suis sincèrement redevante à **Kelly**, qui m'a mise en contact avec Lara et Mario (merci à eux !) qui m'ont ouvert chaleureusement leur porte pour mes séjours bordelais. Merci énormément à **Cassandra** qui m'a accueillie à bras ouverts chez elle et m'a soutenue tout au long du doc. Un grand, grand merci à **Antoine** qui m'a hébergée maintes fois, qui m'a fourni serviette, nourriture, bière, et qui est même venu jusqu'à Montréal pour me rendre visite et rester au fond d'un trou sale ! Je remercie enfin **Mélanie et son chat**, qui ne m'ont peut-être pas accueillie systématiquement, mais qui ont pris le risque de m'héberger après un ou deux soirée(s) particulièrement arrosée(s). A bientôt en Irlande du Nord, Mélanie !

[Fr] Je remercie mes copines de prépa Blandine, Pauline, Alison et Amélie d'avoir été des amies formidables depuis... longtemps maintenant ! Les soirées en votre compagnie sont les meilleures ! Un merci tout particulier à Amélie, sa famille et Alexis qui m'ont accueillie chaleureusement à Bordeaux au cours du doc.

[Eng] I would like to thank my family for being so supportive as I studied ever longer. A special thanks goes out to my mum who was the catalyst of my love of nature, through her curiosity and admiration of all plants and animals. A most loving thank you goes out to Conor who supported my (hopefully stress-induced) mood swings and was ever so patient as I pursued this very international PhD. Thank you to Wilma and Barry for being such amazing and supportive people, and for boosting my moral by sending me Xmas and birthday presents all the way over to Canada.

[Eng] Finally, a big shout out to all contributors to published work from the Nares Strait area, who inspired and enabled many of the reconstructions and theories proposed in this dissertation thanks to their rigorous and honest work.

Avant-propos

Cette thèse est composée de quatre articles qui ont été ou ont vocation d'être publiés dans des revues scientifiques internationales. Ces articles traitent de la déglaciation et des conditions post-glaciaires à tardiholocènes du détroit de Nares, au nord-ouest du Groenland, en relation avec le contexte climatique et océanographique régional. Les articles sont suivis d'un chapitre synthétique où nos résultats sont confrontés à d'autres travaux, en considérant la dynamique Holocène de la cryosphère marine et continentale non seulement comme un produit du changement climatique, mais également comme un moteur dans la dynamique locale et potentiellement régionale. Une introduction générale, préalable aux articles, présente le site d'étude et les phénomènes étudiés, et la thèse termine par une conclusion résumant les résultats principaux et les plaçant dans le contexte des travaux présentés dans la littérature, tout en mettant en perspectives nos résultats.

Le premier papier (chapitre 1) traite de la déglaciation de la partie centrale du détroit de Nares (bassin de Kane), sur la base d'une étude sédimentologique et géochimique de la carotte sédimentaire AMD14-Kane2b. Il a été soumis à *Climate of the Past* le 26 juin 2018, et publié le 18 décembre 2018.

Le deuxième papier (chapitre 2) s'intéresse à la déglaciation de la partie sud du détroit de Nares, à travers une étude multi-proxy (sédimentologique, minéralogique et géochimique) de la carotte sédimentaire AMD16-233. Il sera soumis à un journal scientifique (e.g., *Paleoceanography and Paleoclimatology*; *Journal of Quaternary Science*) à l'automne 2020.

Le troisième papier (chapitre 3) s'appuie sur des mesures de biomarqueurs de la glace de mer (IP_{25} et HBI III) et des assemblages de foraminifères benthiques de la carotte AMD14-Kane2b pour reconstruire la dynamique de la glace de mer dans le bassin de Kane. Il a été soumis le 4 octobre 2019 à *Marine Geology*, et accepté le 25 décembre 2019. Il sera publié dans l'édition d'avril 2020 de ce journal.

Le quatrième papier (chapitre 4) s'appuie sur les résultats des trois papiers précédents et sur les mesures de biomarqueurs et les assemblages de foraminifères benthiques de la carotte AMD16-233 pour reconstruire l'histoire de la polynie des eaux du nord. Ce papier sera publié au mois de mai 2020 dans une revue scientifique internationale (e.g., *The Holocene*; *Earth and Planetary Science Letters*).

Introduction

The present work focusses on the Holocene evolution of the marine and continental cryosphere in Nares Strait. This general introduction lays out the regional context, the understanding of which is fundamental to apprehend an in-depth study of the Holocene history of Nares Strait encompassing geomorphological and oceanographic aspects of its evolution. The introduction starts with a brief presentation of atmospheric and oceanic circulation in the Arctic Ocean, and includes a section describing one of the main drivers of atmospheric circulation changes in the Arctic, the pattern known as the Arctic Oscillation. A second section describes modern oceanographic circulation and sea ice regimes in Nares Strait based on field studies and modelling. The third part of this introduction is dedicated to the North Water Polynya, which opens to the south of Nares Strait due to unique physical processes, and includes a short section on the biological significance of the North Water. In a fourth section, attention is focused on the importance of Holocene archives of past climate, and we present what was known prior to this work regarding the Holocene history of Nares Strait. Questions which will have emerged throughout this introduction will be addressed in the final section of the introduction in which we define the objectives of the current work and present the layout of the dissertation.

1. Atmospheric and oceanic circulation in the Arctic

1.1 *General (simplified) circulation*

The Arctic Ocean, together with its bordering seas, is a Mediterranean-type body of water: it is circled by continent, while narrow straits and channels connect it to the Pacific and Atlantic Oceans, and it is affected by thermohaline circulation (Aagaard et al., 1985). Water from the Atlantic Ocean reaches the Arctic Ocean through the Barents Sea and Fram Strait, while Pacific water enters via Bering Strait (Figure 1.1). Atlantic water is high in salt owing to greater evaporation relative to precipitation, whereas the Pacific receives much of this evaporation as rain, as well as inputs from continental rivers, and is therefore fresher. The Arctic Ocean plays a key role in the salinity budget of the Atlantic and Pacific oceans. Pacific-sourced water exits the Arctic through Fram Strait and the Canadian Arctic Archipelago (CAA), returning a significant amount of freshwater to the Atlantic Ocean (Melling, 2000). Fluxes across major straits of the Arctic Ocean are illustrated in Figure 1.2.

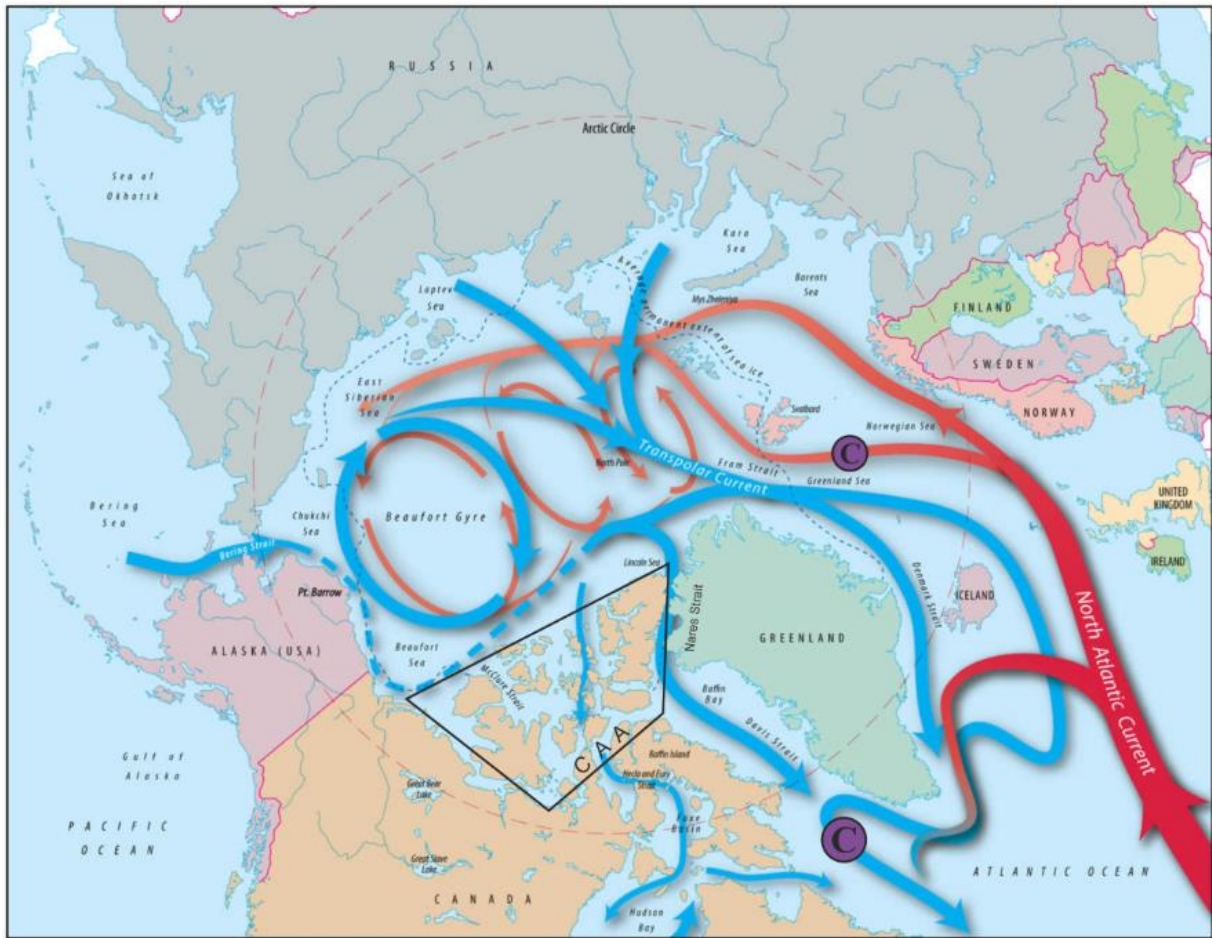


Figure 1.1: Circulation in the Arctic Ocean. Blue arrows represent cold, relatively fresh water, and red arrows warm, salty water. The location of the main convection centres are marked by purple disks in the Greenland and Labrador Seas (adapted from <https://www.whoi.edu/>). CAA: Canadian Arctic Archipelago

The water undergoes temperature and salinity modifications as it enters and circulates in the Arctic Ocean, as part of the thermohaline circulation. While one third of freshwater is supplied to the Arctic via the Pacific inflow, the other two thirds are provided by rivers pouring into the Eurasian, Russian, Beaufort and Chukchi Seas (Figure 1.2) (Aagaard and Carmack, 1989; Serreze et al., 2006). The fresh layer of surface water forms the Polar Mixed Layer (PML) which is separated from the underlying water masses by a strong halocline. The PML usually only reaches depths of ~5-10 m, but as the Arctic has become increasingly ice-free in recent years, wind-driven mixing has significantly deepened the PML in some areas of the Arctic Ocean (Rainville et al., 2011). In the Barents and Greenland Seas, more saline (denser) Atlantic water dives under the fresher surface water, and becomes the warmest layer of the Arctic Ocean. It is sometimes referred to as “the Atlantic layer of the Arctic Ocean”, but it is modified by injections of cold brines as sea ice is formed at the surface, and is therefore more commonly named “Arctic Intermediate Water” (AIW) (Aagaard et al., 1985). The depth of the AIW usually extends from 200 to 500 m, and temperatures decrease as AIW circulates from the Eurasian Basin ($\theta < 2^{\circ}\text{C}$) towards the Canadian Basin ($\theta \sim 0.5^{\circ}\text{C}$), with salinities comprised between 34.5 and 34.8 psu as it is enriched with brines from the continental shelf seas that border the Arctic Ocean (Aagaard et al., 1985; Jones, 2001). Deeper water originates from convection in

the gyre of the Greenland Sea, which, together with convection in the Labrador Sea (Figure 1.1), drives the Atlantic meridional overturning circulation (e.g., Brakstad et al., 2019). Wind-driven brine production on the continental shelves creates dense water which mixes with AIW and participates in the maintenance of the halocline (Aagaard, 1981). The densest shelf waters cascade down the continental slopes and mix with water below the halocline, producing the highest salinity Arctic bottom water and ventilating the depths of the Arctic Ocean (e.g., Aagaard et al., 1985; Swift et al., 1983). Given the presence of a 290 m deep sill in the Lincoln Sea off North Greenland, only the PML and upper layers of the AIW are able to enter Nares Strait from the north (Münchow et al., 2011), while shallower sills in the other channels of the CAA further restrict the depth of AIW transported toward Baffin Bay. Deeper water masses of the Arctic Ocean join the Atlantic Ocean only through the 2600 m deep Fram Strait.

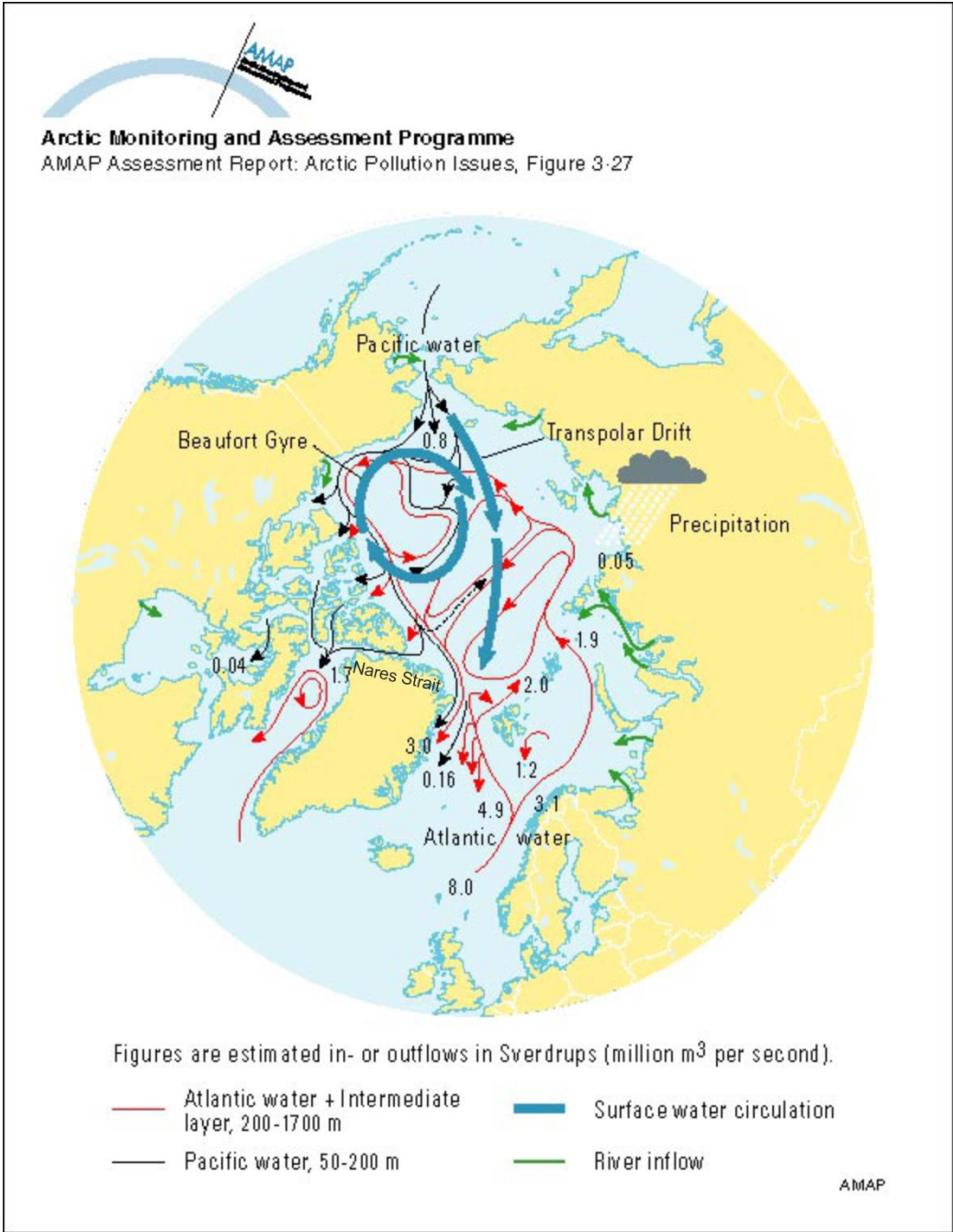


Figure 1.2: Estimated fluxes of inflow to and outflow from the Arctic (source: AMAP)

Both observational and model-derived datasets are highly variable regarding sea ice and freshwater fluxes through Fram Strait and the CAA (McGeehan and Maslowski, 2012). A common feature of large scale studies on Arctic ice export is, however, that the focus is often on ice loss through Fram Strait, while freshwater fluxes through the Canadian Arctic Archipelago (CAA) are less well understood. Yet, some estimates rank the freshwater export through Nares Strait as equivalent to that through Fram Strait (Beszczynska-Möller et al., 2011). Furthermore, the freshwater flux through the CAA is predicted to increase by ~48% on centennial time scales, compared to only 3% in Fram Strait (according to a study by Haak and the MPI group, which was cited by Vellinga et al. (2008) and McGeehan and Maslowski (2012)). Baffin Bay is a major source of freshwater towards the Labrador Sea, where the convection of deep water is an important driver of the AMOC. Belkin et al. (1998) called for the necessity of further investigation of freshwater flux through the CAA, as they proposed that the Great Salinity Anomaly of the 1980s was possibly due to enhanced freshwater export through the CAA that reached the Labrador Sea via Baffin Bay. Kwok (2005) also noted the potential of freshwater export through the CAA to affect convection in the Labrador Sea. The channels of the CAA are all the more interesting to study in the context of Arctic sea-ice export vs. build-up in the Lincoln Sea, because of their unique sea-ice regime which has historically led to a complete blockage of ice movement in the winter, particularly in Nares Strait (e.g., Kwok, 2005), while a trend of early collapse of the ice barriers has led to increased freshwater flux through the channels in recent years (Münchow, 2016). Nares Strait appears to be the most important of the three CAA channels in terms of export of Arctic sea-ice towards Baffin Bay (Kwok, 2006), as it receives some of the oldest sea ice in the Arctic (Haas et al., 2006; Ryan and Münchow, 2017; Figure 1.3).

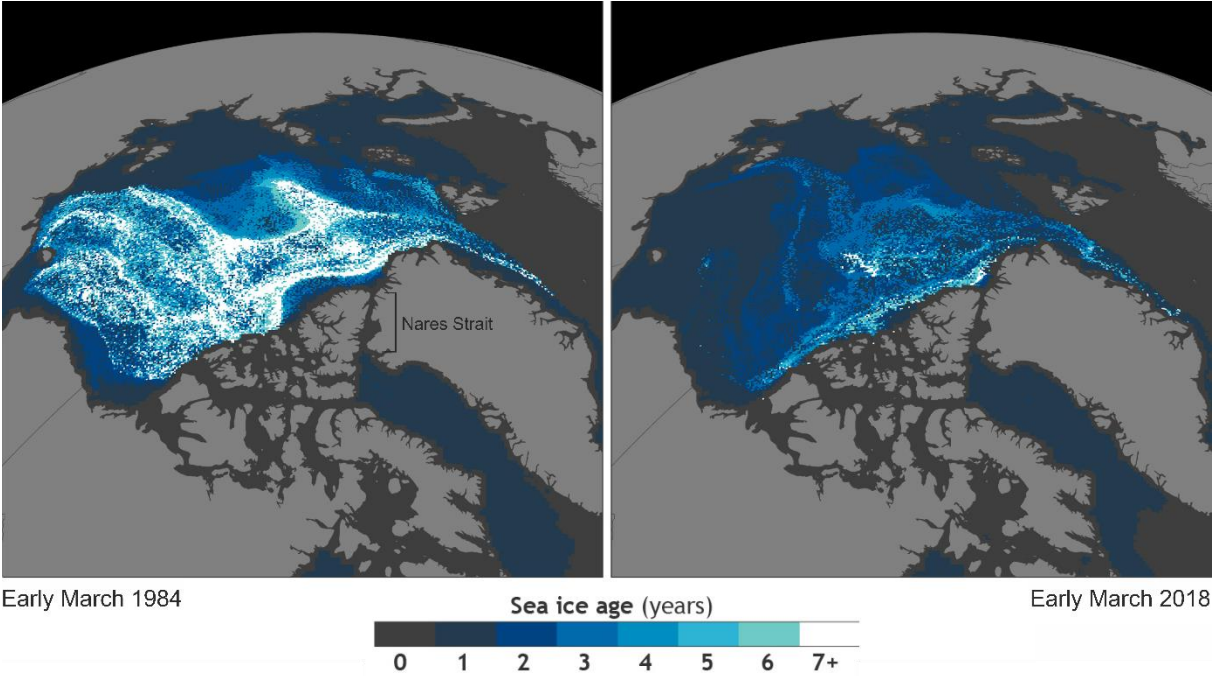


Figure 1.3: Age of sea ice in the Arctic Ocean. Note that, as the occurrence of old sea ice has decreased in recent years, the oldest sea ice tends to be found to the north of Nares Strait. Source: NOAA Climate.gov; data: Mark Tschudi

Overall, the Arctic Ocean is highly stratified and there is little interaction between layers (e.g., McLaughlin et

al., 1996). The strong halocline plays a vital role in the maintenance of the Arctic sea-ice cover, as it prevents warmer, underlying water from reaching the surface (Rainville et al., 2011). The circulation of surface layers (including sea ice) is driven by atmospheric circulation regimes and sea level pressure (SLP) differences in the Arctic and mid-latitudes (e.g., Rigor et al., 2002; Serreze et al., 2016).

According to the simplified model of global atmospheric circulation (Held and Hou, 1980), the Arctic is generally under the influence of an atmospheric high (Polar High), owing to the global solar-driven formation of wind cells (Figure 1.4). The core of the anticyclone is located in the Western Arctic, creating the Beaufort Gyre. Several atmospheric circulation modes are associated with major differences in SLP affecting High and Sub-Arctic latitudes, one of the most studied modes being the Arctic Oscillation (AO). The AO has a significant role in the build-up and the export of Arctic sea ice.

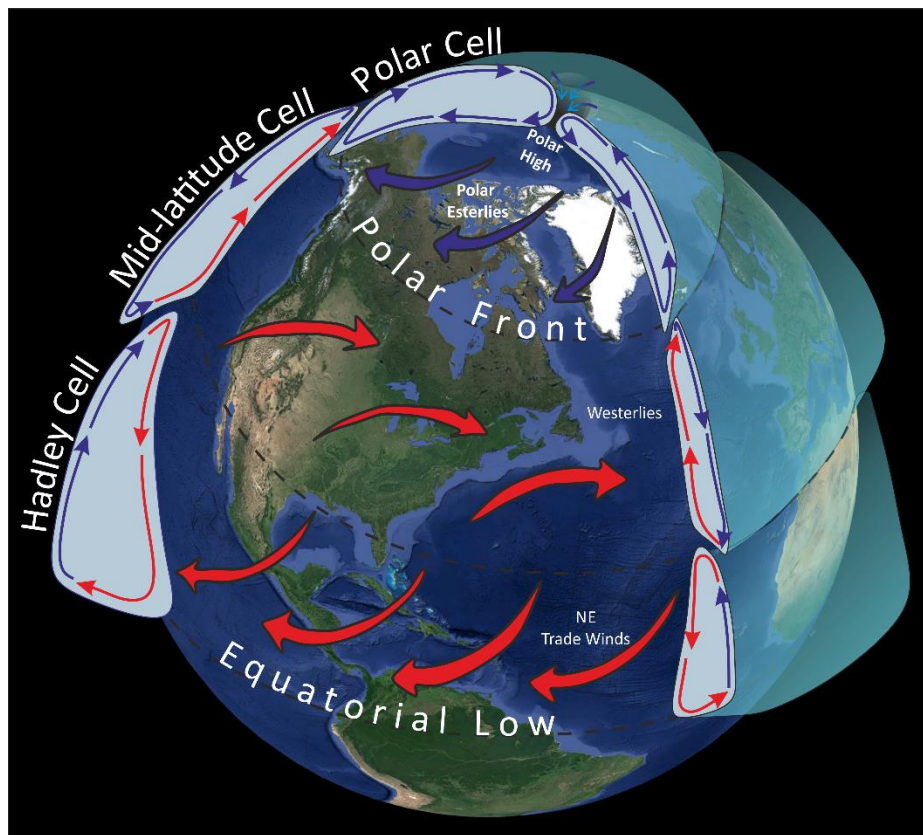


Figure 1.4: Schematic global atmospheric circulation, with compartmentalised wind cells, adapted from the general model of Held et Hou (1980) and represented only for the northern hemisphere.

1.2 The Arctic Oscillation

The Arctic Oscillation (AO) refers to an atmospheric circulation pattern that affects the northern hemisphere climate, by shifting the location of the jet stream poleward (during the positive phase) or equatorward (during the negative phase) (Figure 1.5). During the positive phase of the AO, the polar high is weaker than average, and the coldest storms are confined to high latitudes by a strong ring of circum-polar winds. During the negative AO phase, the polar high is concentrated above the Beaufort Gyre (Figure 1.5) the circum-polar wind belt is weakened and distorted, and cold air masses and storminess are able to reach the mid-latitudes.

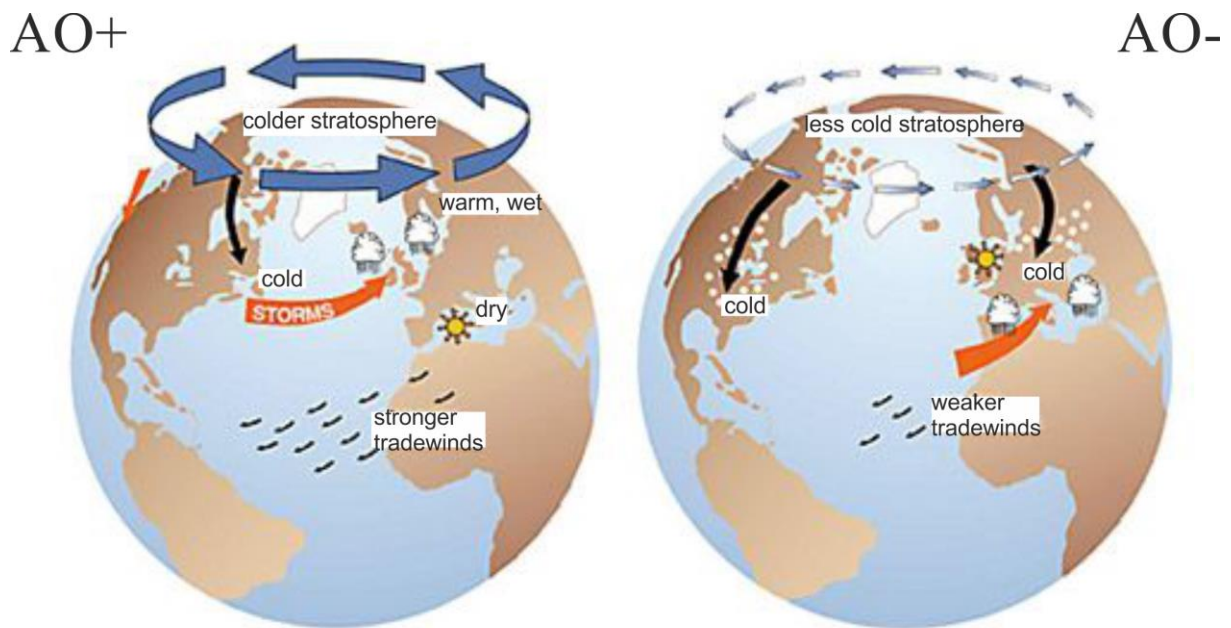


Figure 1.5: Schematic representation of the Arctic Oscillation and its effect on northern hemisphere climate (image: J. Wallace, University of Washington)

The AO displays seasonal variability, with the strongest effect of the AO occurring in the winter and able to persist into the summer (e.g., Dumas et al., 2003; Rigor et al., 2002). The calculation of the AO index is complex, and involves several stages of reanalysis and weighting to extract a monthly, seasonal or yearly AO index. The theoretical basis of the calculation of the AO index will be explained hereafter, based on Figure 1.6, in order to better understand how the AO affects circulation in the Arctic Ocean. First, the outermost sea surface height isoline in the Arctic Ocean is located (H in Figure 1.6-a; L in Figure 1.6-b). The sea surface height at this location is then subtracted from the sea surface height at the centre of the isolines (L in Figure 1.6-a; H in Figure 1.6-b), and divided by the distance between the two points. The result is positive in a positive phase of the AO, and negative in a negative phase of the AO (Figure 1.6).

In a positive phase of the AO, the weaker pressure at the centre of the isolines draws atmospheric circulation poleward (red arrow in Figure 1.6-a), resulting in cyclonic winds due to the Coriolis effect. Theoretically, the cyclonic winds promote the export of sea ice as it is driven by wind and deviated to the right by the Coriolis effect (Figure 1.6-a). In practice, enhanced export of sea ice through Fram Strait during strong positive phases of the AO in the 1990s has indeed been evidenced in observational datasets (e.g., Rigor et al., 2002).

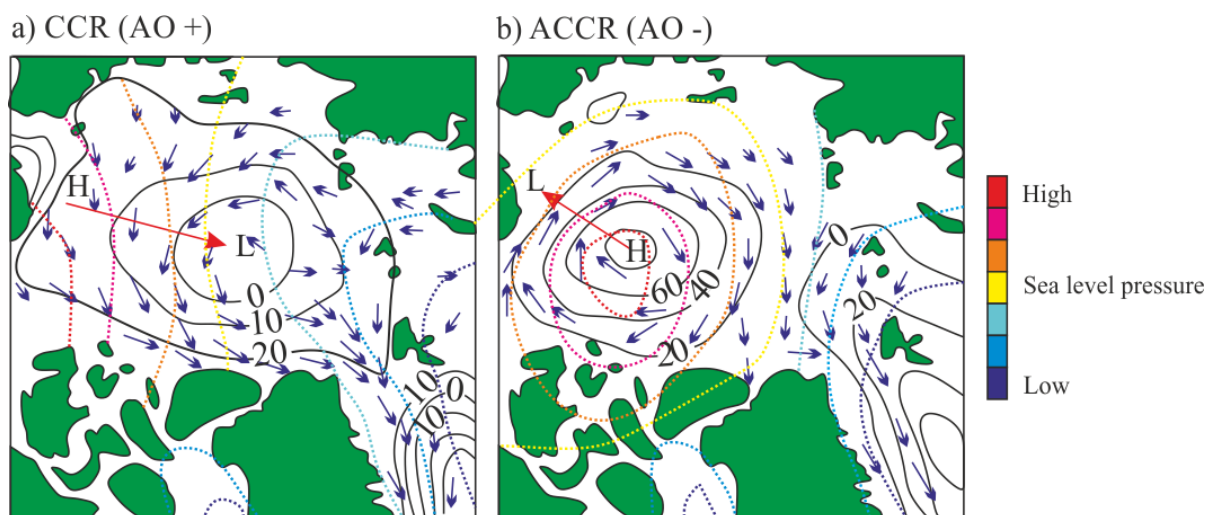


Figure 1.6: Simplified examples of cyclonic (CCR) and anticyclonic circulation regime (ACCR) of atmospheric circulation in the Arctic Ocean (modified from <https://whoi.edu>). Solid black lines represent sea level height isolines (cm), dashed coloured lines represent sea level pressure (hPa). H corresponds to the sea level height maximum, located along the outer (inner) sea level height isoline in CCR (ACCR), and L corresponds to the minima in sea level height, located along the inner (outer) sea level height isoline in ACCR (CCR). Red arrows represent the atmospheric pressure gradient, and blue arrows the direction of sea ice motion.

Conversely, in a negative phase of the AO, high atmospheric pressure at the centre of the isolines pushes atmospheric circulation outward (red arrow in Figure 1.6-b), creating anticyclonic winds due to the Coriolis effect. Sea ice is, in turn, converged towards the centre the Beaufort Gyre under the influence of the wind and the Coriolis effect. While the accumulation of multi-year sea-ice in the Lincoln Sea has indeed been tied to negative phases of the AO (e.g., Serreze et al., 2016), extremely low indices of the AO have also been linked to enhanced export of sea ice through Fram Strait (i.e. in the winter of 2009-10, Stroeve et al., 2011). This unexpected observation was explained by a potential shift in the character of the AO, with the most recent events having carried the thicker, multi-year sea ice towards the Eastern Arctic, rather than the Lincoln Sea. It was suggested that previous years of record-low sea-ice cover (e.g., 2007) may have also preconditioned the ice in the area, by reducing its thickness, thus increasing its mobility (Dumas et al., 2003; Stroeve et al., 2011). When the AO index is close to zero, an overall reduction of sea ice motion is observed (Steele et al., 2004).

The AO also affects sea ice (e.g., Kwok, 2000) and ocean (e.g., Steele et al., 2004) circulation in the Arctic Ocean via the Transpolar Drift Stream (TDS; Figure 1.7). Looking at changes in the TDS is particularly relevant to investigating environmental conditions in Nares Strait, since the trajectory of the TDS appears to dictate the origin of surface water and sea ice arriving towards Nares Strait (Figure 1.7). The lower-than-usual Beaufort High is contracted during a positive phase of the AO, allowing a westward shift of the TDS (Figure 1.7-a). In this configuration, the weaker TDS originates closer to the Bering Strait, sometimes branching out into the Beaufort Gyre, and ultimately terminating to the west of Fram Strait, towards the Canadian Arctic (Kwok et al., 2010; Steele

and Boyd, 1998). Steele et al. (2004) speculate that shifts of the Atlantic/Pacific front may be associated to the AO index. Positive phases of the AO may lead to a stronger influence of Pacific-sourced water off Northern Greenland (Figure 1.7-a; Steele et al., 2004). In a negative phase of the AO, the Beaufort High is large and strong, and the TDS is shifted eastward (Figure 1.7-b). The TDS efficiently transports sea ice from the Eastern Arctic towards Fram Strait, sustaining open water off Siberia thus enhancing new ice formation (Rigor et al., 2002). The sea ice exported through Fram Strait via the TDS in a negative phase of the AO is hence more likely to be thinner first year ice, while multi-year sea ice builds-up in the Beaufort Gyre (Rigor et al., 2002). The circulation pattern associated to negative phases of the AO may ultimately reduce the influence of Pacific-sourced water in Northern Greenland (Figure 1.7-b, Steele et al., 2004).

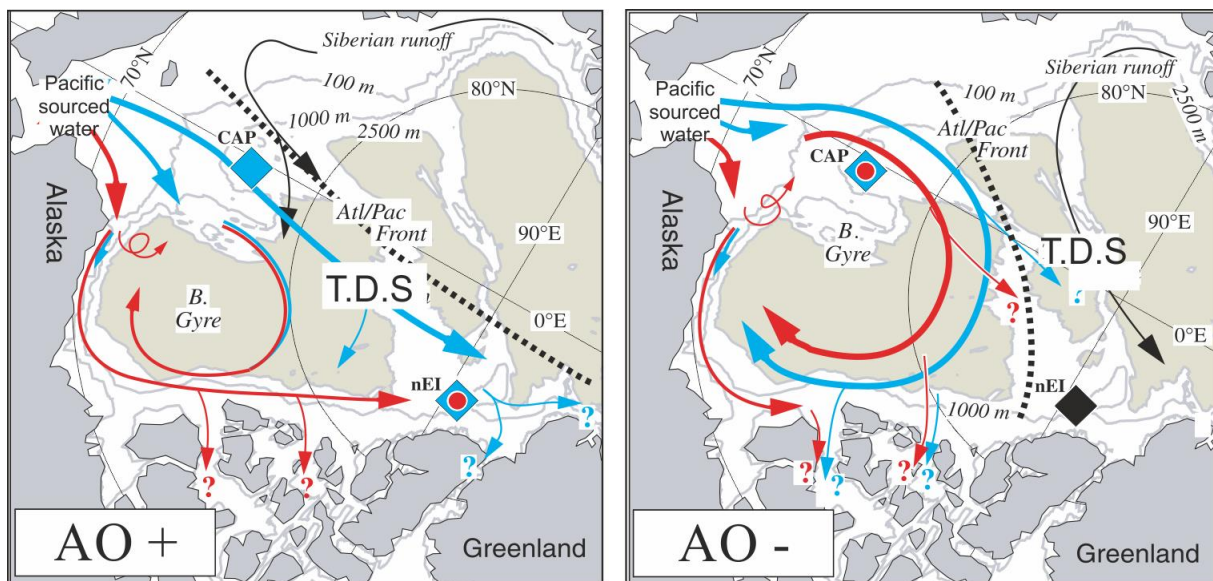


Figure 1.7: Schematic representation of oceanic and atmospheric pressure patterns in a positive and a negative phase of the Arctic Oscillation.

Other modes of variability also play a major role in the export of sea ice through Fram Strait, e.g. thermodynamic factors (Kwok and Untersteiner, 2011). Another SLP mode impacting Arctic sea-ice cover is the Dipole Anomaly, which in its positive phase, increases wind-driven export of sea-ice through Fram Strait (Wang et al., 2009). It has however been acknowledged that the preconditioning of thinning Arctic sea-ice linked to previous years of positive phases of the AO, plays a major role in facilitating sea ice export linked to the Dipole Anomaly, thus hinting at a stronger influence of the AO on longer time scales (Dumas et al., 2003; Wang et al., 2009).

Although it is agreed that sea level difference between the Lincoln Sea and northernmost Baffin Bay is the main driver of the flow in Nares Strait (e.g., Kliem and Greenberg, 2003; Münchow et al., 2006), studies that have considered SLP patterns (i.e. AO and Dipole Anomaly) have found that they only explain a small portion of the variability on instrumental time scales (McGeehan and Maslowski, 2012; Samelson and Barbour, 2008). The particular sea ice regime in Nares Strait is paramount in regulating freshwater export through Nares Strait (Münchow, 2016; Shroyer et al., 2015).

2. Hydrology in Nares Strait

2.1 Oceanographic circulation

Nares Strait is a long (*ca* 500 km) and narrow channel that connects the Arctic Ocean to Baffin Bay, and separates Ellesmere Island from Greenland (Figure 1.8-a and b). The sea level difference between the Lincoln Sea and Baffin Bay is the main driver of the southward flow, the speed of which accelerates in the narrower sections of the strait, i.e. Robeson Channel (400 m deep, 21 km wide), Kennedy Channel (340 m deep, 30 km wide) and Smith Sound (600 m deep, 50 km wide) and slows down in the wider basins, i.e. Hall Basin (800 m deep, 70 km wide), Kane Basin (220 m deep, 170 km) and, ultimately, the north of Baffin Bay upon its exit from Nares Strait (Figure 1.8-b).

The oceanographic circulation in Nares Strait is poorly constrained owing to a number of challenges facing the acquisition of field data. The heavy sea ice cover poses a collision threat to both instruments and ships, and the scarcity of plankton during the polar night decreases the backscatter needed for ADCP measurements. Other difficulties encountered so close to the north pole include violent storms, and a weak horizontal magnetic field which necessitate appropriate adaptations to field material (e.g., Münchow and Melling, 2008). Fluxes through Nares Strait are highly variable, on both seasonal and inter-annual bases (Münchow, 2016; Münchow et al., 2011; Rabe et al., 2010), while short-term flux variability is strongly influenced by tidal cycles (Münchow and Melling, 2008). Although temperature vs. salinity profiles provide a general idea of the origin of the water masses in the strait, they are affected by wind-powered mixing and deeper incorporation of meltwater in spring and summer, and brine rejection in autumn. Nutrients are however used successfully to identify Atlantic- vs. Pacific-sourced water in Nares Strait using the differences of dissolved phosphate to nitrogen ratios between the two pools (Jones, 2003; Jones and Eert, 2004; Münchow et al., 2007).

Overall, the shipborne temperature and salinity measurements in Nares Strait, which have only been acquired during summer (usually August) in open water conditions, have been mostly consistent in terms of water column structure since the 1960s (Franceschetti, 1964; Moynihan, 1971; Palfrey and Day, 1968). They tend to show a highly stratified water column and a predominantly southward flow. Measurements performed under the ice in the spring have evidence slight differences in the water column (Muench, 1971). Moored instruments have recorded year-long to multi-annual data, and have confirmed seasonal and inter-annual variations in water column characteristics and along-channel fluxes (e.g., Münchow and Melling, 2008; Rabe et al., 2010). These datasets also provide evidence of a warming trend in recent years (Münchow et al., 2011).

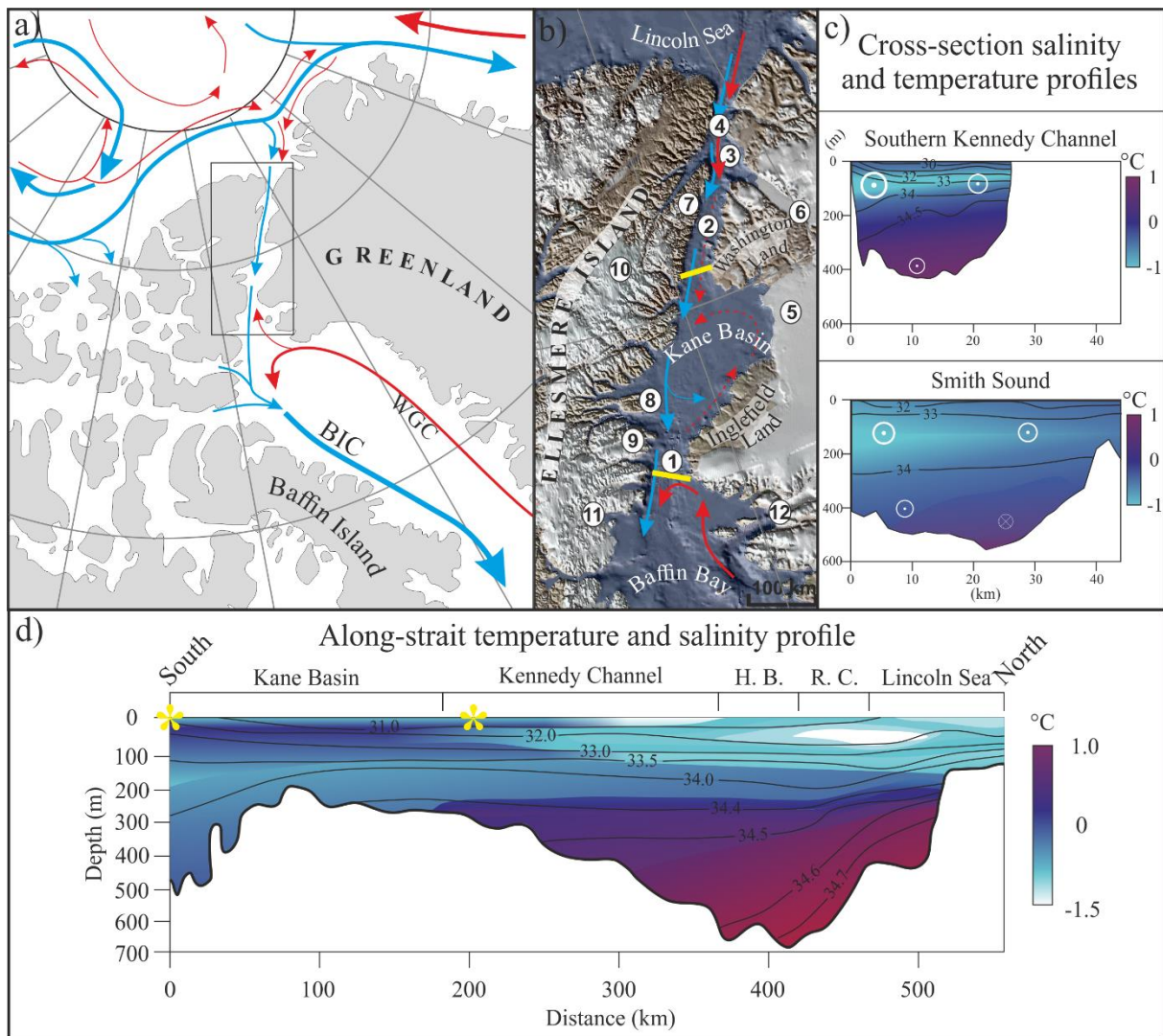


Figure 1.8: Oceanographic circulation in Nares Strait. a) schematic ocean circulation in the Arctic Ocean, Baffin Bay and Nares Strait, blue arrows represent fresher surface water, and red arrows Atlantic-sourced deeper water; b) schematic circulation in Nares Strait, dashed red lines correspond to the potential circulation of Atlantic water in Nares Strait; c) cross-sections of temperature and salinity profiles in Nares Strait in August 2003 (Münchow et al., 2007) and general direction of flow; d) along-strait temperature and salinity profile in August 1971 (Sadler, 1976) (H. B.: Hall Basin; R. C.: Robeson Channel). The locations of cross-section profiles in c) are shown as yellow lines in b) and yellow asterisks in d). Numbers in b) refer to: 1- Smith Sound; 2- Kennedy Channel; 3- Hall Basin; 4- Robeson Channel; 5- Humboldt Glacier; 6- Petermann Glacier; 7- Judge Daly Promontory; 8- Bache Peninsula; 9- Johan Peninsula; 10- Agassiz Ice Cap; 11- Talbot Fjord; 12- Qaanaaq Fjord.

The water in Nares Strait is generally more stratified in its deeper, northern sector than in the south (Figure 1.8-d). The warmest ($\theta < 1^{\circ}\text{C}$) and most saline ($S < 34.8$ psu) water is found at depths in Hall Basin (Sadler, 1976). Waters with salinities above 34.54 psu (e.g., measured by Sadler (1976) in Hall Basin, Figure 1.8-d) either originate from the north, or are locally enriched by brine injection if they entered from Baffin Bay where the water is fresher

(Münchow et al., 2011). Münchow et al. (2011) hypothesise that water with the highest salinities ($S = 34.82$ psu and $\theta = 0.20^\circ\text{C}$), found below 330 m, originate from Atlantic-sourced water (constituting the Arctic Intermediate Water, AIW) laying below 350 m depth on the Canadian Shelf of the Arctic Ocean (to the west of Nares Strait), which would have to surpass a 300 m sill in the Lincoln Sea. However, Jackson et al. (2014) estimated that Atlantic water from the Eurasian Basin coming from the Northwest Greenland shelf (to the east of Nares Strait) is a more likely source of the water below 100 m in Nares Strait. It is possible that a front exists between Atlantic water coming from the Canadian Basin and Atlantic water coming from the Eurasian Basin, depending on the larger Arctic Ocean circulation, and, notably, the Arctic Oscillation (Figure 1.7; Steele et al., 2004). What is agreed however, is that surface water appear to be predominantly Pacific-derived water from the western Arctic (Jackson et al., 2014; Münchow et al., 2007). At depth, the southward flow of the denser Atlantic-sourced water is gradually obstructed by upward sloping bathymetry during its travel south in Kennedy Channel (Münchow et al., 2007). Oceanographic data from Kane Basin is extremely sparse, and only snap-shots are available, i.e. no mooring instruments have been deployed there. Shipborne measurements in northern Kane Basin in August 1971 recorded a potentially well mixed water column and the incorporation of meltwater at depth, with cold ($\theta < -1.6^\circ\text{C}$) and fresh ($30.0 < S < 33.0$ psu) water in the top 100 m, and more saline ($S \sim 34$ psu) and warmer ($\theta \sim -0.4^\circ\text{C}$) bottom water. Under-ice measurements from north-western Kane Basin in May 1969 recorded colder ($\theta < -1.8^\circ\text{C}$) and more saline ($32.6 < S < 33.0$ psu) water in the top 100 m compared to summer datasets, and a greater presence of relatively high salinity ($S \sim 34.5$ psu) and warmer ($\theta \sim -0.20^\circ\text{C}$) bottom water (Muench, 1971). The under-ice water column is thus likely characterised by less meltwater and solar heating at the surface relative to ice-free summer conditions, while sea ice also provides isolation from wind-stress and reduces downward mixing. The water exiting Nares Strait is concentrated on the western side of Smith Sound, and is essentially fresher and cooler than the water having entered through Robeson Channel due to the ca 220 m sill in northern Kane Basin (Münchow et al., 2007). Overall, the water in the upper 200 m forms a continuum of water from the Arctic Ocean to Smith Sound through Nares Strait, while the southward transport of deeper (more saline and warmer) water is gradually excluded by sills. As this shallow water body, encompassing the core of the flow, travels southward above the more sluggish bottom waters, the sharp horizontal gradient in salinity introduces strong shear (Rabe et al., 2012).

Using phosphate vs. nitrate ratios, Münchow et al. (2007) identify Pacific-sourced water as composing more than 75% of the 0-100 m surface water in Robeson Channel. In Kennedy Channel, the top 100 m of the water column remains predominantly Pacific-sourced, whereas this contribution falls to 50% in Smith Sound (Jones, 2003; Münchow et al., 2007), hinting at enhanced mixing of the water column southward. A mix of Pacific- and Atlantic-sourced water is identified between ca 100 and 300 m (Jones, 2003; Münchow et al., 2007). Deeper water masses display an increasing fraction of denser Atlantic-sourced water, which makes up nearly 70% of the total water flux exiting Smith Sound (Münchow et al., 2007).

The oceanographic circulation is driven by the sea level drop between the Lincoln Sea and Baffin Bay, while predominantly northerly winds trap the core of the flow against the Ellesmere Island coast (Münchow and Melling, 2008; Rabe et al., 2010). On average, the velocity of the current in Nares Strait sits around $30 \text{ cm}\cdot\text{s}^{-1}$, while maximum velocities of up to $60 \text{ cm}\cdot\text{s}^{-1}$ have been measured near the surface in Robeson Channel and decrease

with depth to maximums of $ca\ 10\ \text{cm}\cdot\text{s}^{-1}$ in the lowermost 100 m along Nares Strait (Münchow et al., 2007, 2006). Surface conditions greatly impact current velocities and fluxes, as sea-ice cover isolates the underlying water while surface velocities increase significantly under the influence of wind-stress following sea ice break-up (Münchow, 2016; Rabe et al., 2010). The bathymetry in Nares Strait drops rapidly from the Ellesmere coast, while the seabed slopes more gently from Greenland. The core of the southward flow, entering Nares Strait from the Lincoln Sea, is generally concentrated in the deeper, western side of the strait (Münchow et al., 2007). As with water column characteristics, little is known about ocean circulation in Kane Basin. Aerial radar photography along with aircraft and ship-based sightings of drifting icebergs enabled Nutt (1966) to identify a cyclonic circulation pattern in Kane Basin. It is thought the core of the Nares Strait flow is channelled along the bathymetric low in western Kane Basin, while the eastern sector of the basin is relatively sheltered from northerly wind, and is affected by a more sluggish circulation (Dunbar, 1979; Nutt, 1966). A northward counter current likely follows the eastern trough in Kane Basin, producing a cyclonic circulation pattern (Figure 1.8-b). Ultimately, the southward flow is funnelled through Smith Sound upon its exit from Kane Basin. A branch of the West Greenland Current travels up the eastern side of Smith Sound, potentially following the eastern trough in Kane Basin (Figure 1.8-a, b, c), and constitutes a counter current entering Nares Strait from the south (Bailey, 1956; Moynihan, 1971; Sadler, 1976). As this northward flow faces upward sloping bathymetry at the entrance of Kane Basin, it is deviated to the west and recirculates southwards (Münchow et al., 2007). As of yet, the extent of the West Greenland Current into Kane Basin remains uncertain, although it is thought to be limited to occasional events of strong southerly winds over Smith Sound (Dumont et al., 2010; Ingram et al., 2002; Sadler, 1976), and probably generally depends on the strength of the West Greenland Current.

The main driver of the southward flow in Nares Strait is the $ca\ 10\ \text{cm}$ sea level difference between the Lincoln Sea and Baffin Bay (Münchow and Melling, 2008). The sea surface elevations in the area are largely due to steric height, i.e. the salinity of the fresher Pacific water gradually increases on its journey towards the Atlantic Ocean, increasing in density, and thus decreasing sea surface elevation between the Arctic and Atlantic Oceans (Steele and Ermold, 2007). McGeehan and Maslowski (2012) propose that oceanographic dynamics in northernmost Baffin Bay can additionally influence the sea surface height gradient. Based on simulations, they determine that when the ingress of the West Greenland Current (WGC) into northernmost Baffin Bay decreases, the volume and sea surface elevation in northern Baffin Bay are reduced. This strengthens the elevation gradient, thereby increasing fluxes through Nares Strait. They thus suggest that the seasonally weaker northward flow of the WGC (derived from their simulations, and evidenced by Rykova et al. (2009) and Tang et al. (2004) from field studies) may increase the elevation gradient in winter and spring, partly explaining larger fluxes through Nares Strait during these seasons. McGeehan and Maslowski (2012) also mention that local hydrology in northern Baffin Bay may influence sea surface height, via local cooling and brine formation which would both decrease sea surface elevation, potentially increasing fluxes through Nares Strait.

In addition to sea level forcing, surface layers are also strongly influenced by northerly wind-stress, which may explain up to 80% of flux variance (Rabe et al., 2012). Wind-strength above Nares Strait has been shown to be correlated to the AO index (Samelson and Barbour, 2008), which may be a consequence of the expansion of the

Beaufort High above the Lincoln Sea in a positive phase of the AO (reinforcing the pressure gradient between north and south Nares Strait), and, conversely, an extended Icelandic Low towards the Lincoln Sea in a negative phase of the AO (Steele et al., 2004; Stroeve et al., 2011). However, the wind only exercises significant pressure when the surface is mobile, i.e. when the sea-ice cover has broken-up (Münchow, 2016; Rabe et al., 2010). Sea ice dynamics are thus integral in understanding fluxes through Nares Strait.

2.2 Sea ice conditions

Nares Strait displays particular surface conditions which fall within either of the three following states at any given time (Figure 1.9): (1) immobile land-fast ice cover, (2) open water scattered with mobile drift-ice, (3) open water with very little or no drift-ice.

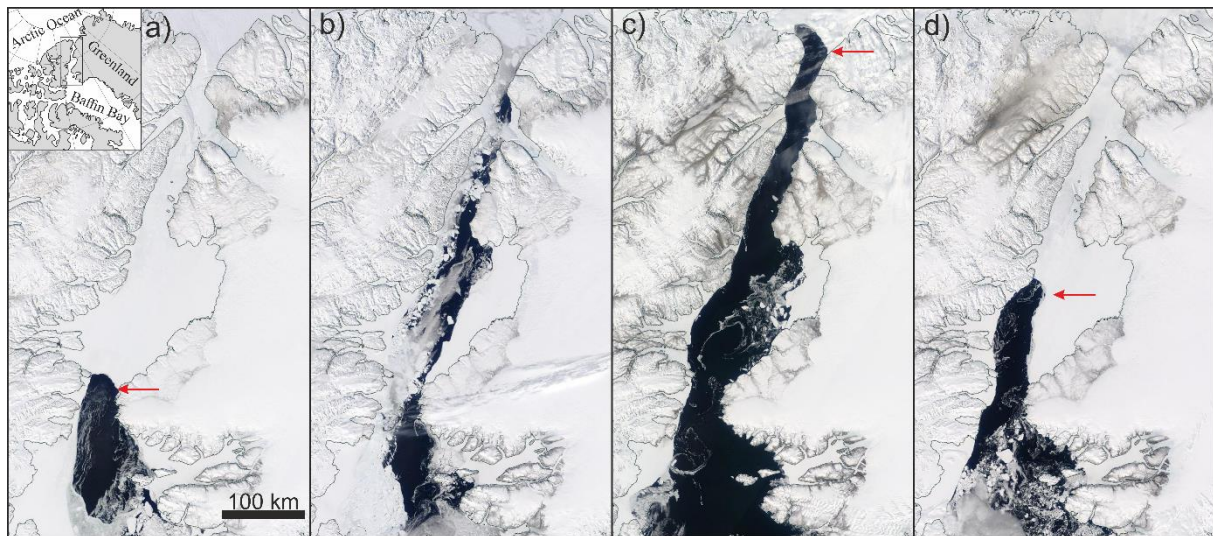
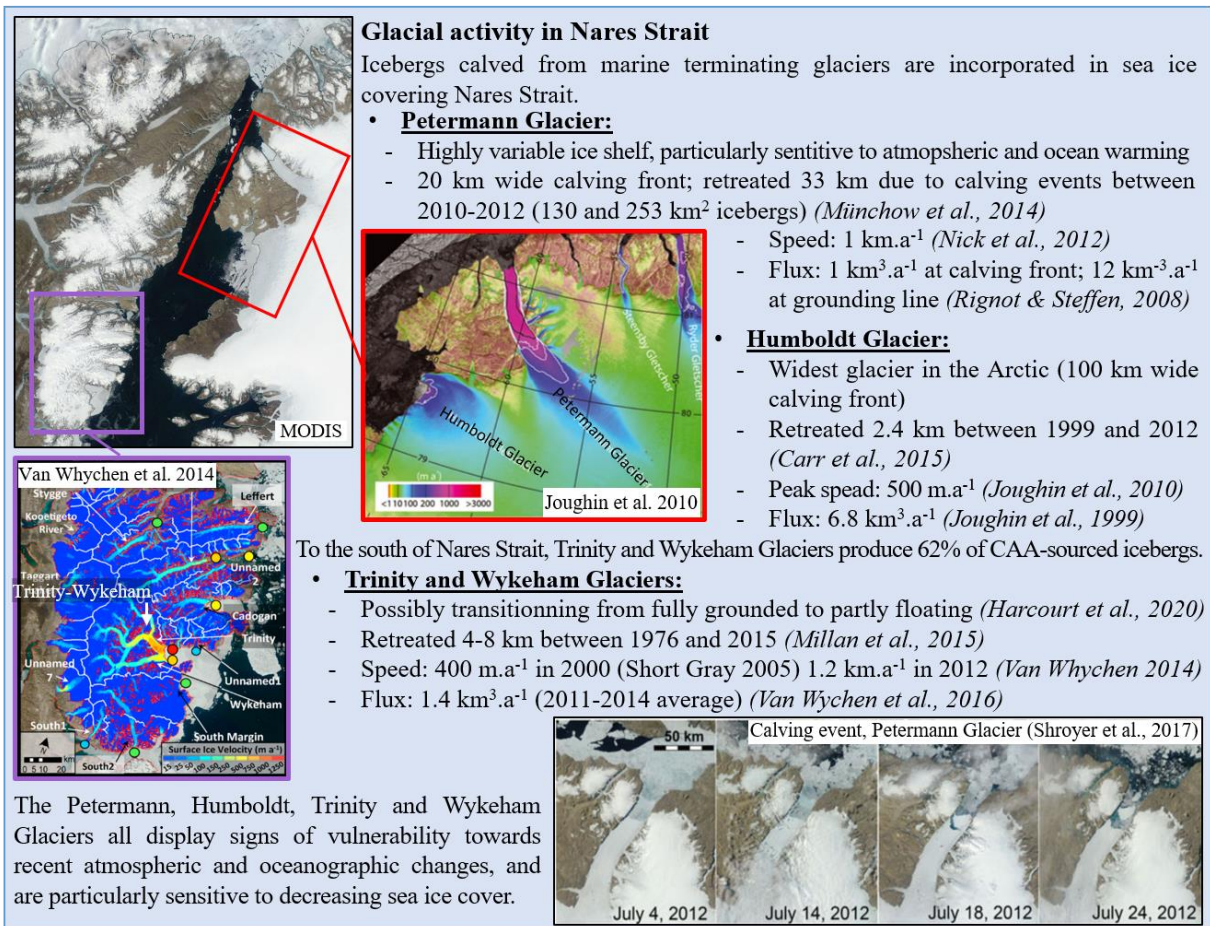


Figure 1.9: Sea-ice conditions in Nares Strait. a) immobile land-fast sea ice in Nares Strait: the Kane Basin ice arch (red arrow) prevents sea ice from exiting Nares Strait (May 2018); b) mobile sea ice in Nares Strait: in the absence of ice arches, Arctic sea ice is transported to Baffin Bay via Nares Strait (May 2019); c) open water conditions in Nares Strait: the northern ice arch (red arrow) prevents Arctic sea-ice from entering Nares Strait (June 2009); d) the Kane Basin ice arch occasionally forms further north in Kane Basin (May 2014). Satellite images from MODIS (<https://worldview.earth.nasa.gov/>).

Following the break-up of Arctic sea ice in the summer and autumn, mobile pack-ice drifts into Nares Strait. It is carried along the channel by surface currents and swept by northerly winds towards the south of the strait. Situated at the southern edge of the Lincoln Sea, Nares Strait receives some of the oldest and thickest sea ice of the Arctic (Haas et al., 2006; Ryan and Münchow, 2017; Figure 1.3). The Petermann and Humboldt Glaciers also calve significantly large icebergs in Hall and Kane Basins, respectively (e.g., Carr et al., 2015; Münchow et al., 2014; Nick et al., 2012; Shroyer et al., 2017; Thomas et al., 2009; cf. Insert 1 for more information on glacial activity in Nares Strait). The particular morphology of Nares Strait promotes the build-up of ice in Kane Basin, as the sluggish, cyclonic circulation in this wider basin, particularly in its sheltered eastern side, slows down the drifting pack ice (Dunbar, 1979; Nutt, 1966). Eventually, the large pieces of thick Arctic and glacial ice becomes trapped in



Insert 1: Glacial activity in Nares Strait

the bottleneck between Inglefield Land and Johan Peninsula in southern Kane Basin (Figure 1.8; Figure 1.9). *In situ*-formed sea ice consolidates the ice cover as it becomes land-fast (Dunbar, 1979, 1975) when atmospheric temperatures drop in late autumn and winter (Barber et al., 2001). The ice edge in southern Nares Strait takes an arch-like shape between the constricted shores of the strait, usually in southern Kane Basin, but ice arches have been observed at various locations within Nares Strait (Figure 1.9-a-d; e.g., Figure 1.8; Vincent, 2019). The ice covering Nares Strait and terminating in southern Kane Basin is referred to as the ‘southern ice arch’, or the ‘Kane Basin ice arch’, also known as an ice ‘bridge’ (Figure 1.9-a). The southern ice arch is a recurrent feature in Nares Strait, thought to occur seasonally. When it is present, the ice arch prevents ice from drifting into northernmost Baffin Bay, while northerly winds and southward ocean currents sweep away newly formed ice, creating a polynya named the North Water (Melling et al., 2001). Occasionally, an ice arch forms to the north of Nares Strait, in the Lincoln Sea, by the convergence of thick multi-year Arctic sea ice which becomes land-fast along the northern shores of Northwest Greenland and northern Ellesmere Island (Figure 1.9-c; Moore and McNeil, 2018). When this northern ice arch is present, before or after the formation of the Kane Basin ice arch, it prevents the incursion of Arctic sea ice through Robeson Channel, and can promote a polynya in the north of Nares Strait (Kozo, 1991). Although this northern polynya has been less studied than its southern counterpart, the northern ice arch has become an important feature in recent years when the southern ice arch has failed to form, promoting “anomalous” open conditions in the entire Nares Strait (in 2009 for example, Figure 1.9-c; Vincent, 2013). We have found no

evidence that either of the ice arches in Nares Strait have survived past summer (although Vincent (2019) notes a collapse of the southern ice arch as late as September 17th in 1980), and their ultimate, seasonal collapse leads to the export of Arctic sea ice for several months per year. In recent years, studies have shed light on the physical processes involved with ice arch breakup, showing that the effect of wind (Dumont et al., 2009) and tides (Vincent, 2020) initiate the break-up of the ice as it thins in the summer months. The trend in earlier collapses in the satellite era may thus be explained by increasingly thinner ice in Nares Strait which reduces the ice arch's resistance to wind and tidal action (e.g., Vincent 2020).

Despite the importance of ice arch formation in regional (and potentially global) oceanography, little is known about the long-term (i.e. longer than decadal scale) dynamics of sea ice in Nares Strait. Sparse observation from the field date back to the early 1950s, and even sparser historical records of the presence of the Kane Basin ice arch are found in early Arctic expeditions and whaling logbooks (Dunbar, 1979, 1973, 1969, 1951; Dunbar and Dunbar, 1972), while satellite imagery for the area is available starting in 1979 (Vincent, 2019). Local inhabitants in the coastal villages in Greenland and the Canadian Islands state that ice arches have been used to cross the channels of CAA since 1860 (ICC, 2017), attesting that they have been present historically. However, to our knowledge, there is no further information available concerning the precise seasonal duration of the ice arch prior to the satellite era. Succeeding generations of researchers have placed the average date of break-up of the ice arch gradually earlier in the summer. Dunbar (1969) states that the “ice bridge usually breaks up in late July or August”, with examples of ice arch collapse in early August in 1966, and in mid-August in 1967. Based on satellite images between 1996 and 2002, Kwok (2005) documents typical ice arch formation between November and March, and break-up around July. An overview of satellite images between 1979 and 1996 shows that the duration of the ice arch significantly decreased in the 1990s compared to the 1980s (Barber et al., 2001). Although more recent observations show a recovery in the late 1990s and early 2000s, the trend between 1979 and 2019 has been a decrease in sea ice duration (Figure 1.10; Vincent, 2019), having culminated in 2007 with total absence of ice arch consolidation (Münchow, 2016). It may appear as though we are currently witnessing a drastic change in sea ice dynamics in Nares Strait (Moore and McNeil, 2018). However, although sea ice cover in northernmost Baffin Bay and Nares Strait seems to be affected by multi-decadal variability (Preußner et al., 2015), longer-term trends are difficult to assess owing to the relatively short period of observation afforded by seasonally-resolved datasets.

The formation of ice arches plays an integral role in the export of Arctic sea ice and liquid freshwater through Nares Strait. Models (McGeehan and Maslowski, 2012; Rasmussen et al., 2011; Shroyer et al., 2015), satellite-derived estimations (Kwok, 2005; Kwok et al., 2010) and field measurements (Münchow, 2016; Ryan and Münchow, 2017) agree that freshwater flux through Nares Strait is drastically restricted when ice motion is halted by ice arches, and significantly increased when sea ice is mobile in the absence of ice arches. Based on salinity and current measurements from moored instruments in Kennedy Channel, Münchow (2016) calculated that “volume flux increased by 45%, ocean freshwater flux increased by 69%, and ice freshwater flux increased by 46%” between the first three-year period of measurements in 2003-06, when sea ice was motionless for an average 5.4 months/year, and the second in 2007-09, when ice was motionless for an average 2.4 month/year. In addition to sea surface elevation forcing, atmospheric control via wind strength is a major driver of surface fluxes through

Nares Strait when ice arches are absent, particularly during the winter and early spring months when winds are the strongest (Samelson et al., 2006; Samelson and Barbour, 2008; Shroyer et al., 2015). Therefore, the later formation, earlier collapse, or complete absence of ice arches affect freshwater (liquid and solid) export all the more in a changing climate, since the ice arches have historically restricted surface fluxes during the winter and spring. Meanwhile, model simulations by Dumont et al. (2009) demonstrate that the strength of the Kane Basin ice arch depends on the thickness of the ice forming the arch, which determines its resistance to the strong northerly winds in Nares Strait. The combined finding by Samelson et al. (2006) and Dumont et al., (2009) implies that the effect of wind-stress is likely to be twofold: (1) under the highest wind-stress the duration of the Kane Basin arch may be decreased, while (2) fluxes in the resulting mobile surface layers are enhanced by the strong winds. Similar regulating mechanisms depending on ice thickness and wind stress may also play a major role on the establishment of the northern ice arch in the Lincoln Sea (Moore and McNeil, 2018). Samelson and Barbour (2008) find that wind strength in Nares Strait is proportionate to the atmospheric pressure difference between north and south Nares Strait, and go on to show a correlation (albeit with a 3-year lag) between this pressure gradient and the Arctic Oscillation (AO). While we are not aware of any studies that have tied modern ice arch formation to SLP patterns (and particularly the AO), looking at the duration of the Kane Basin ice arch (as documented by Vincent, 2019) and the winter AO index over the past 40 years (from <https://www.pmel.noaa.gov/arctic-zone/detect>), there appears to be a general decrease in ice arch duration during periods of recurrent positive winter AO (Figure 1.10). Longer time series for ice arch presence may however be necessary to draw any conclusion on the potential controlling role of the AO.

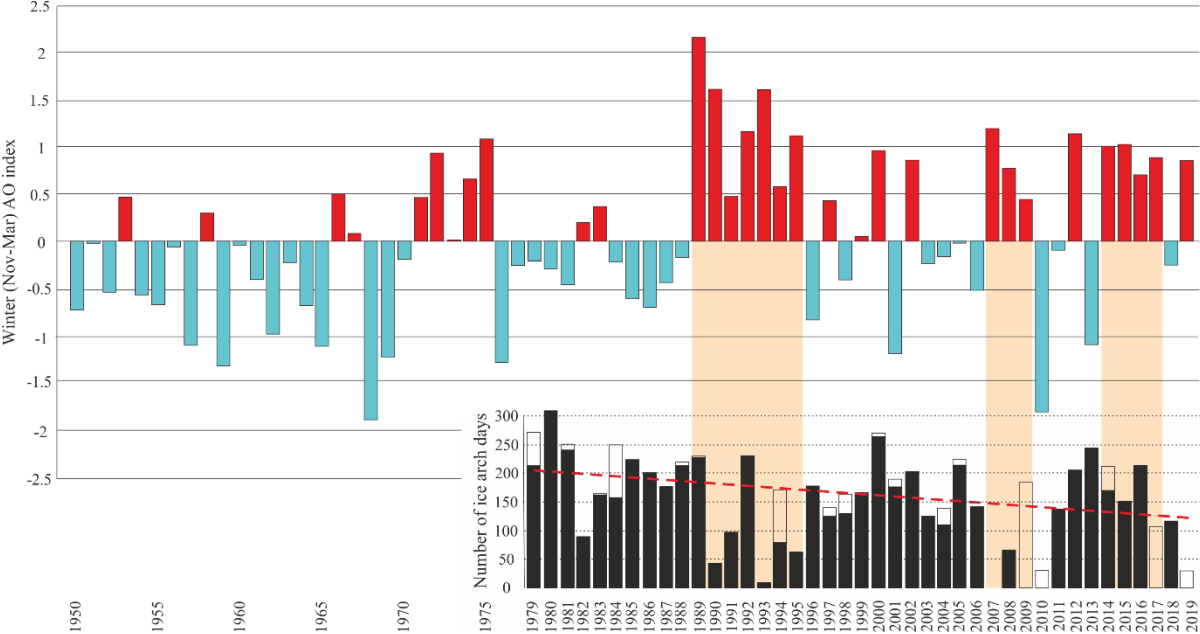


Figure 1.10: Winter (November to March) AO index and number of ice arch days. Periods marked by consecutive positive AO winters are highlighted in light orange (source of AO index: <https://www.pmel.noaa.gov/arctic-zone/detect>). Filled black rectangles represent number of days/year of presence of the southern ice arch, blank rectangles include the northern ice arch, and red dashed line

corresponds to the trend in ice arch duration (adapted from Vincent, 2019).

The consequences of a shifting ice regime in Nares Strait range from increases in freshwater flux toward Baffin Bay (Münchow, 2016), to the drainage of old Arctic ice from the Lincoln Sea (Ryan and Münchow, 2017), and include ecological upheaval in marine biological communities (Kalenitchenko et al., 2019) and land-based ecosystems via the influence of the North Water polynya (e.g., Mosbech et al., 2018). Concerns have also been voiced by local inhabitants which depend heavily on resources from the North Water (ICC, 2017). Despite the major significance of the North Water polynya, we know relatively little about the implications of a changing sea ice regime on productivity in the area.

3. The North Water polynya (Pikialasorsuaq)

3.1 Physical processes

The North Water polynya is an area of open water at the south of the Kane Basin ice arch (Figure 1.11). The first historically documented presence of open sea in northern Baffin Bay dates back to July 1st 1616 (Dunbar and Dunbar, 1972), but Inuit and Paleo-Inuit people have travelled to the location for millennia, establishing year-round and seasonal settlements (Schledermann, 1980). It became known to explorers and whalers as “the North Water”, while Inuit people call it “Pikialasorsuaq” (the great upwelling), and has also been referred to as the NOW polynya more recently in the scientific literature.

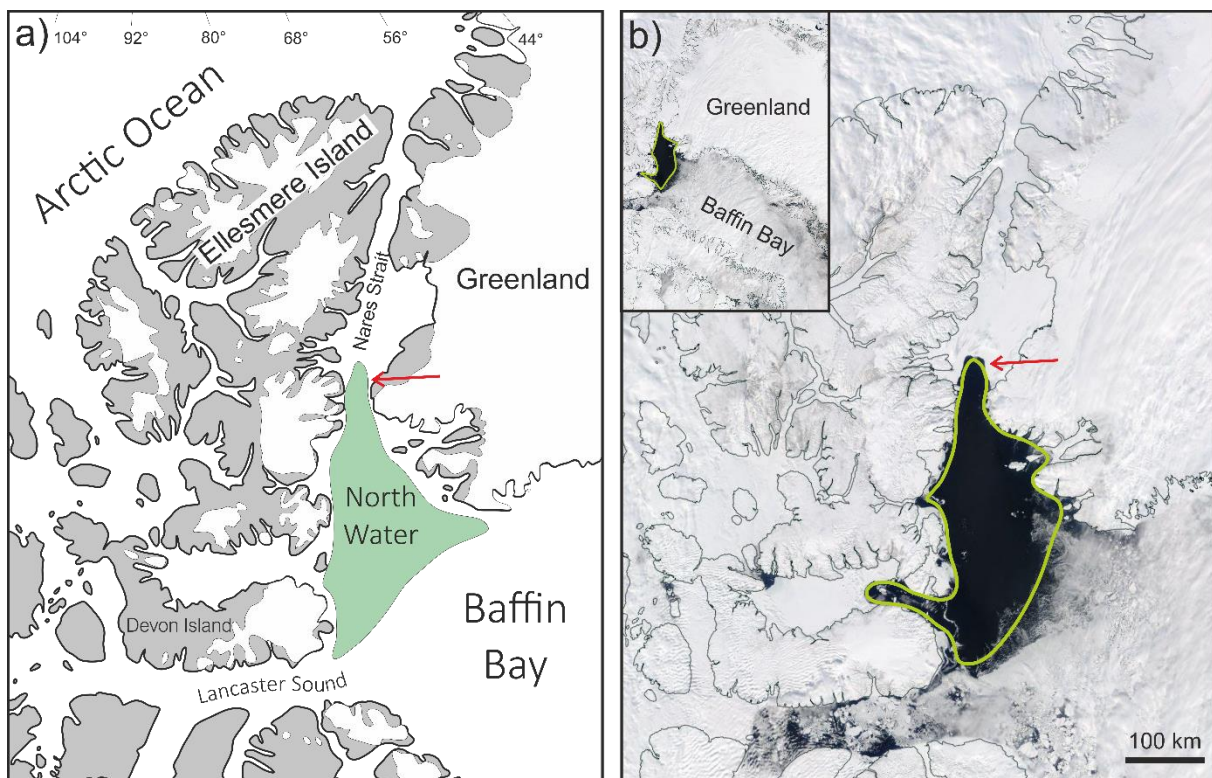


Figure 1.11: Approximate location of the North Water polynya (Pikialasorsuaq) in northern Baffin Bay; schematic representation in a) and satellite images in b). Red arrow represents typical location of the Kane Basin ice arch. MODIS satellite image from <https://worldview.earth.nasa.gov/> (May 2016).

The North Water Polynya extends from Greenland to Arctic Canada in northern Baffin Bay. Its surface area can reach approximately 80,000 km², with its northern border usually defined by the Kane Basin ice arch, while its southern limit is more variable in space and time as well as being less distinguishable (Figure 1.11).

A number of observational (e.g., Bâcle et al., 2002; Barber et al., 2001; Heinemann, 2018; Ingram et al., 2002; Marsden et al., 2004; Melling et al., 2001; Mundy and Barber, 2001) and modelling (e.g., Biggs and Willmott, 2001; Dumont et al., 2010; Yao and Tang, 2003) studies have contributed to our understanding of the physical processes involved in the opening and maintenance of the North Water, along with ocean-ice-atmosphere interactions and feedback mechanisms. The main physical processes linked to the North Water are summarised in Figure 1.12.

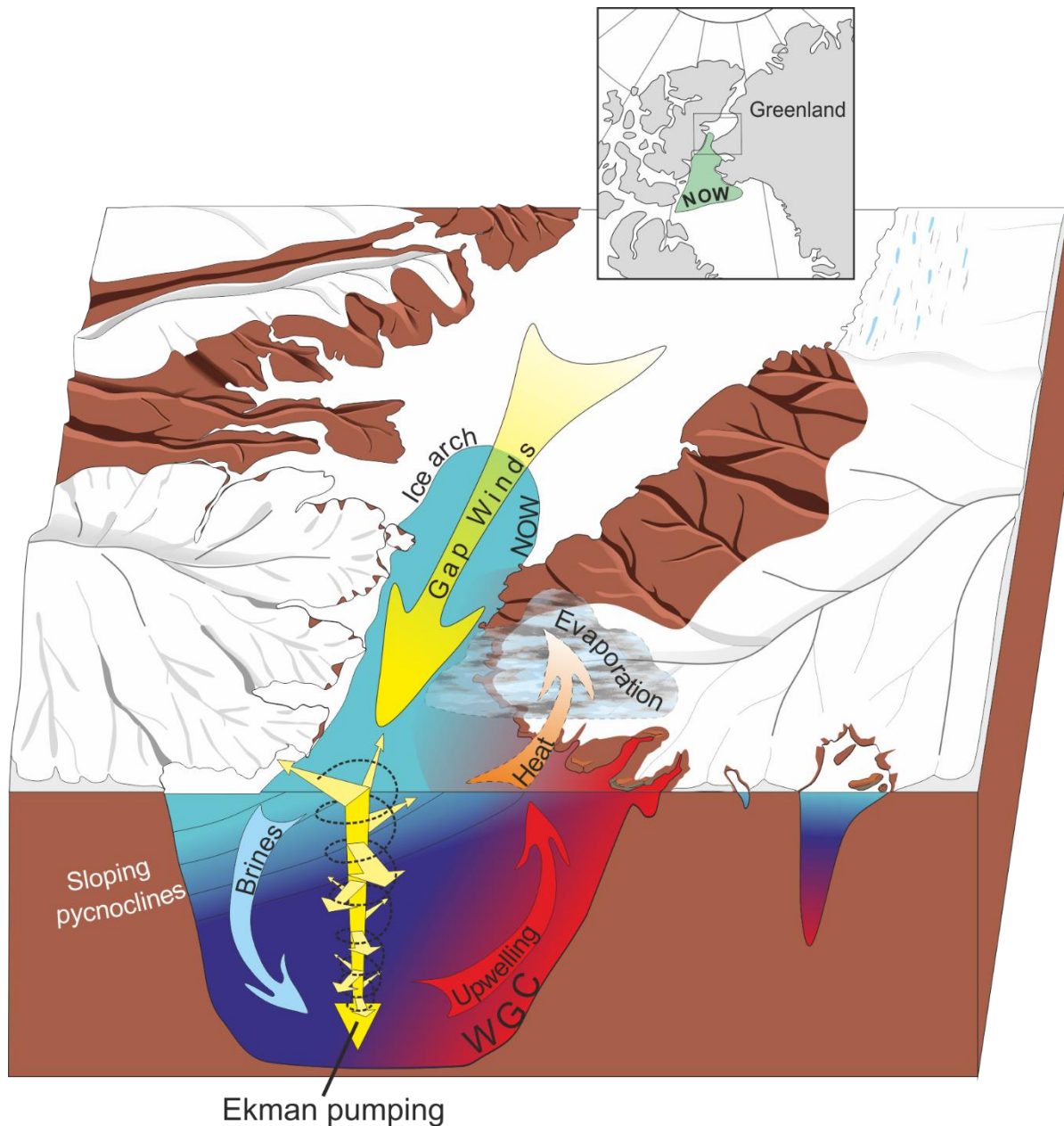


Figure 1.12: Schematic representation of the physical processes linked to the North Water Polynya in southern Nares Strait. WGC: West Greenland Current; NOW: North Water

The North Water has been identified essentially as a latent polynya, although it also shares characteristics of sensible polynyas. Latent polynyas necessitate a stable margin, usually represented by land, from which wind can drive sea ice away and produce open water (e.g., Darby et al., 1995). In the case of the North Water, the stable margin is represented by the Kane Basin ice arch, over which blow strong, orographically channelled winds Ito, H., 1982. Wind Through a Channel—Surface Wind Measurements in Smith Sound and Jones Sound in Northern Baffin Bay. *J. Appl. Meteorol.* 21, 1053–1062. [https://doi.org/10.1175/1520-0450\(1982\)021<1053:WTACWM>2.0.CO;2](https://doi.org/10.1175/1520-0450(1982)021<1053:WTACWM>2.0.CO;2)

Samelson, R.M., Barbour, P.L., 2008. Low-Level Jets, Orographic Effects, and Extreme Events in Nares Strait: A Model-Based Mesoscale Climatology. *Mon. Weather Rev.* 136, 4746–4759. <https://doi.org/10.1175/2007MWR2326.1>

. Winds above Smith Sound are extremely strong (*ca* 20 m.s⁻¹) due to gap winds produced by the funnelling of the along strait winds between Johan Peninsula (in Ellesmere Island) and Inglefield Land (in Greenland) (Heinemann, 2018; Figure 1.12). The opening of the North Water is thus initiated by the mechanical removal of newly formed sea ice away from the stable ice margin in southern Kane Basin. The water exposed is significantly warmer than the air above it (i.e. *ca* 20°C warmer), driving the release of heat towards the atmosphere (Steffen and Ohmura, 1985), while the surface layer is susceptible of being further warmed by solar radiation due to its low albedo (Ingram et al., 2002). A net moisture transfer from the open sea towards the atmosphere is driven by the higher saturation specific humidity in the warmer air above the polynya, and results in the formation of clouds and fog above the North Water (Boisvert et al., 2012; Figure 1.12). These clouds may act as an important feedback mechanism in promoting the melting of sea-ice cover downwind (effectively enlarging the surface of the polynya) as they tend to retain heat (Boisvert et al., 2012). The heat and moisture transfer in the North Water plays an important role on climate in the area, increasing air temperatures and precipitation (Marshall et al., 2007; Maxwell, 1981), enhancing snowfall and promoting surface accumulation on nearby ice caps (Mair et al., 2009). The heat transfer towards the atmosphere is also thought to create a local atmospheric low, thereby inducing a positive feedback on the north-south pressure gradient in Nares Strait responsible for the strong winds in Nares Strait (Marsden et al., 2004).

The loss of heat from the ocean is partially compensated by latent heat emitted by sea ice formation, but colder water is ultimately produced. The strong winds remove newly-formed ice as it is produced (estimated at a rate equivalent to 1.2 m.month⁻¹ according to Yao and Tang, 2003). The continuous formation of sea ice results in salt rejection, which contribute to increasing the density of chilled water, ultimately producing brines which are thought to be the source of deep and bottom water of Baffin Bay (Bourke et al., 1989; Sadler, 1976). The Ekman transport resulting from the removal of the surface layer, and divergence from the Greenland coast, causes an upwelling of underlying water from the east (Melling et al., 2001; Figure 1.12). It was hypothesised by Bâcle et al. (2002) that penetrative brine convection may enhance the upwelling of less dense water from the WGC, a claim that is supported by model simulations (Yao and Tang, 2003). According to modelling work by Dumont et al. (2010), the upwelling is however strongest when the Kane Basin ice arch presents an edge which is perpendicular to the northerly winds (such as the configuration in 2014; Figure 1.9-d) so that Ekman transport is most efficient. Dumont et al. (2010) also show that sloping of the pycnocline due to baroclinic adjustment associated to the Nares Strait outflow can further promote upwelling of warmer WGC water in the east. Although the initiating opening mechanism

of the North Water is the removal of thin ice by wind, the upwelling of warmer Atlantic-derived water from the WGC may contribute to melting sea ice in the eastern sector of the polynya (consisting in the sensible component of the polynya), and has been estimated to account for up to 1/3 of the heat lost at the surface (Melling et al., 2001; Figure 1.12).

The North Water is thus marked by dichotomy between its eastern (Greenland) and western (Ellesmere Island) sectors. The western side of the polynya is dominated by the Nares Strait outflow and characterised by fresher Pacific-sourced surface water, while warmer Atlantic-sourced water is found in the eastern side (Tremblay et al., 2002), both at depth and at the surface through Ekman pumping. Furthermore, brine sinking, Ekman-induced downwelling and strong northerly winds in the western part of the North Water increase the depth of the mixed layer, whereas the upper mixed layer is shallow, warmer and more saline in the east (Mei et al., 2002). The physical processes that occur in the North Water are not only important for oceanographic circulation, but they also influence productivity in the polynya (Mei et al., 2002).

3.2 Biological significance of the NOW polynya

As an area of open water surrounded by thick sea ice cover, the North Water is often described as an Arctic oasis (e.g., Deming et al., 2002; Jeppesen et al., 2018). The occurrence of open water in the early spring following the polar night, allows for a precocious phytoplankton bloom starting 2-3 months prior to general ice retreat in the region (Lovejoy et al., 2002). Productivity in the polynya supports a large ecosystem, attracting a number of migratory species and year-round residents (e.g., Born et al., 2004; Hobson et al., 2002; Stirling, 1997; Teilmann et al., 1999; Figure 1.13).

Phytoplankton blooms are initiated earlier (April) in the eastern sector of the North Water and later propagate towards the west (in May). As well as this east vs. west temporal disparity, the North Water is characterised by distinct community assemblages between its eastern and western, and northern and southern sectors, which also vary over time in their respective regions (Lovejoy et al., 2002; Figure 1.13). The spatial disparity in phytoplankton productivity in the North Water is likely due to differential physical forcing (Mei et al., 2002; Vidussi et al., 2004). Field observations have shown that the western North Water displays more diversity in the community structures but is overall less productive, mainly due to a greater depth of the mixed layer, while diatoms dominate the phytoplankton bloom in the eastern sector of the polynya, where sensible heat favours a shallowed mixed layer (Lovejoy et al., 2002; Mei et al., 2002; Vidussi et al., 2004; Figure 1.13). Pacific-sourced water outflowing from Nares Strait supplies the North Water with silicate, but is depleted in nitrate; the opposite is true for Atlantic-sourced water upwelling in the eastern polynya (Tremblay et al., 2002). Tremblay et al. (2002) suggest that silicate content is sufficient to meet diatom productivity in the entire polynya, and that nitrate, which is supplied largely by the upwelling, is the limiting nutrient. They add, however, that were the Nares Strait outflow dominated by Atlantic-, as opposed to Pacific-sourced water, silicate would become the limiting nutrient. Tremblay et al. (2002) also demonstrate that silicate drawdown and subsequent dissolution in the bottom water of the North Water constitutes a trap that reduces the amount of silicate available for productivity in Baffin Bay. The overall biomass of phytoplankton production in the North Water is determined by the nutrient inventory of the surface water, with

productivity continuing until exhaustion of the limiting nutrient (Lewis et al., 1996; Mei et al., 2002; J.-E. Tremblay et al., 2002). Field observations thus demonstrate that while the North Water is a latent heat polynya, its sensible component is largely responsible for the high productivity rates observed there today.

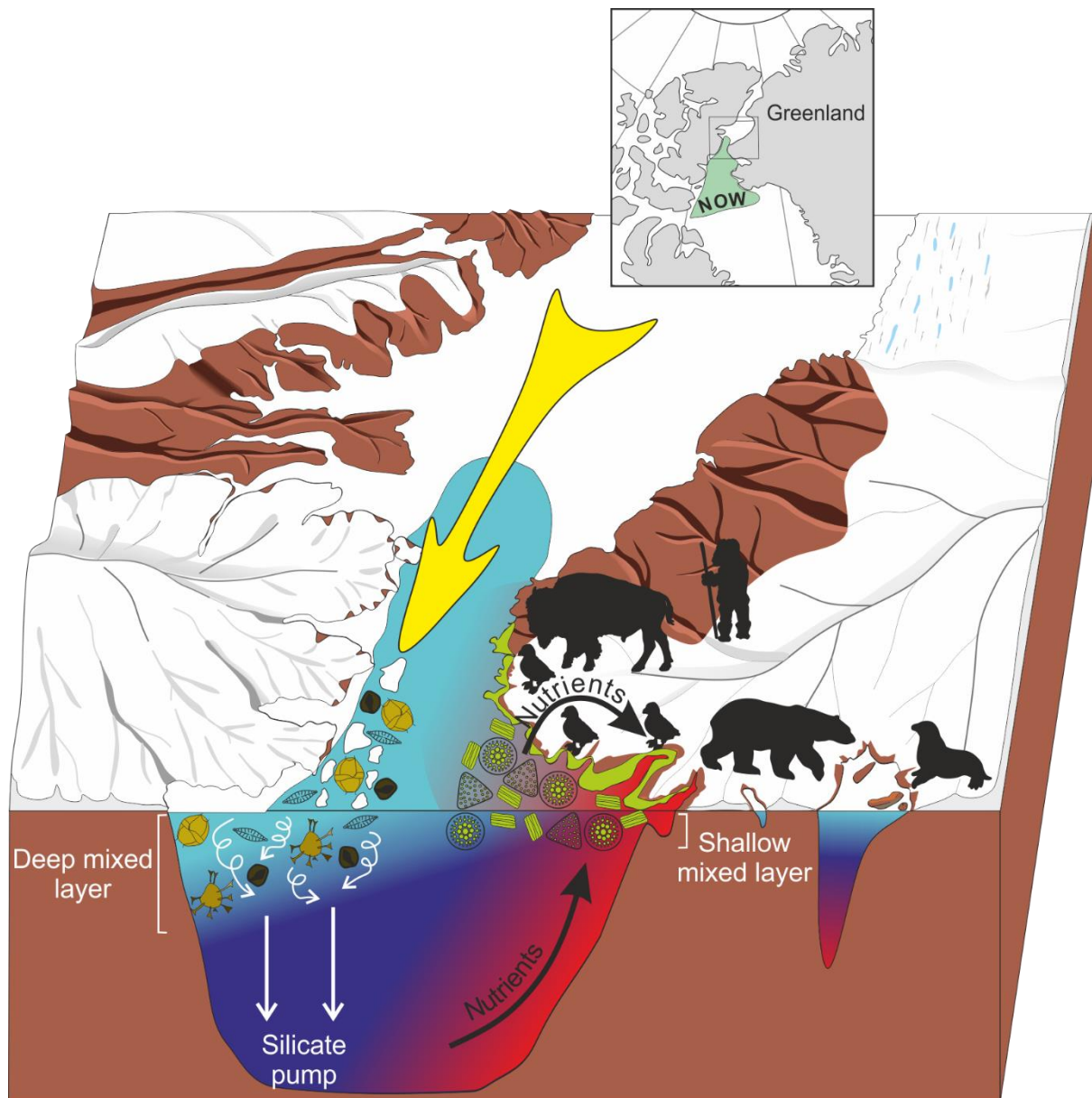


Figure 1.13: Schematic representation of the biological significance of the North Water Polynya

This primary productivity supports a polynya ecosystem ranging from zooplankton to birds, and includes large marine mammals such as whales, seals and polar bears (e.g., Born et al., 2004; Hobson et al., 2002; Stirling, 1997; Teilmann et al., 1999). Birds feeding from the polynya are particularly important for the region, as they are responsible for the transfer of nutrients from ocean to land (González-Bergonzoni et al., 2017; Outridge et al., 2016; Figure 1.13). In addition to being prey for certain land species (e.g., the Arctic Fox), the little auk are an engineer species in that their fertilising guano increases vegetation near their nesting grounds which can sustain herbivores such as muskoxen and Arctic hare (González-Bergonzoni et al., 2017; Hastrup et al., 2018; Mosbech et al., 2018). The congregation of marine and land mammals along the Greenland coast of the North Water illustrates the fact

that the eastern sector of the polynya is more productive than the west owing to the upwelling (Born et al., 2004; Heide-Jørgensen et al., 2016; Figure 1.13). Inuit and Paleo-Inuit settlements have been established in the area for millennia, drawn by the marine and land resources offered by the polynya (e.g., Dietz et al., 2018; Gotfredsen et al., 2018; Hastrup et al., 2018; Schledermann, 1980). The ice arch in Nares Strait also played an important role in human migrations, as the ice bridges were used to cross over channels of the CAA, and was an important cross road for cultural exchange (e.g., Grønnow and Sørensen, 2004); until restrictions were put in place to stop freedom of movement over the international Nares Strait at the beginning of the cold war (Dick, 2001). It has been hypothesised that fluctuations in occupation of the area evidenced by archaeological investigations may be linked to ice arch and polynya dynamics (Hastrup et al., 2018). However, no sufficiently well resolved marine records of surface conditions in Nares Strait and the North Water exist to support this claim. More recently, the decreasing seasonal duration of ice arches in Nares Strait over the past 40 years (Vincent, 2019) has been accompanied by decreasing productivity in the North Water evidenced by satellite imagery (Marchese et al., 2017) which is thought to be due to poor nutrient supply by increased stratification and reduced upwelling (Bergeron and Tremblay, 2014). According to Inuit communities, higher ranking species of the food chain have also been affected by these changes (ICC, 2017). Evidently, with such a rich ecosystem at stake in the wake of a changing climate, further investigation on the response of the ice arch-polynya tandem system to climate forcing is highly needed.

4. Holocene history of Nares Strait

4.1 Importance of Holocene archives

Delving into the past history of a particular area can reveal how it has previously responded to climate change, better equipping us in order to understand how it is currently changing or may change in the future under similar forcing. The Holocene is the period covering the last 11.7 calibrated thousand years before present (cal. ka BP), and follows the Last Glacial Maximum (LGM; 26.5-ca. 19 cal. ka BP) and the Deglaciation (post ca. 19 cal ka BP). Locally (western Canadian Arctic Archipelago), the Holocene was characterised by orbitally-induced high temperatures between 11.7 and 7.8 cal. ka BP (Holocene Thermal Maximum, HTM), followed by a gradual cooling which accelerated after ca 2 cal. ka BP (Lecavalier et al., 2017). The cooling trend terminated around 0.3 cal ka BP, with the last three centuries being marked by rapid warming (Lecavalier et al., 2017). Atmospheric temperatures are expected to increase by 1-2.5°C within the next decade and by 3.5-7.5°C by the end of the century (IPCC, 2007a, 2007b). The $\delta^{18}\text{O}$ -derived atmospheric temperature from the Agassiz Ice Core documents that HTM temperatures were close to those predicted for the next decade (Lecavalier et al., 2017). Holocene archives are thus particularly interesting, not just to establish a pre-industrial base-line of environmental conditions, but also to shine a light on paleoenvironmental conditions under a warmer climate (MacDonald, 2010). Although the HTM may be a close parallel to predicted atmospheric temperatures, major differences arise from the fact that the world was transitioning out of the LGM, with deglacial conditions persisting in the High Arctic well into the Holocene, particularly in the western CAA (Briner et al., 2016). During the LGM, the CAA was covered by the Innuitian Ice Sheet (IIS), cutting off the connection between the Arctic Ocean and Baffin Bay (e.g., England et al., 2006). This

makes it important to characterise the geomorphological evolution of the area before drawing direct conclusion between environmental reconstructions and climatic forcing.

4.2 Previous work on the Holocene history of Nares Strait

The deglaciation of the CAA is poorly constrained. The chronology of glacial retreat in Nares Strait relies essentially on radiocarbon dating of molluscs found on raised beaches (e.g., England, 1999, and references therein), and on cosmogenic dating (Ceperley et al., 2020; Reusche et al., 2018; Zreda et al., 1999), providing discrete ages for ice retreat at a specific location. Prior to the current work, only one marine sediment core had been retrieved in northern Nares Strait (HLY03-01-05GC; Figure 1.14-a), and it constituted the only continuous (and spatially integrated) record of the transition between a pro-glacial marine environment towards an open gateway (Jennings et al., 2011). The chronology of events is complicated by a lack of knowledge concerning reservoir ages in Nares Strait. The modern reservoir age is difficult to assess owing to the scarcity of pre-bomb collections of molluscs. The reservoir age derived from these collections are not necessarily representative of the reservoir age of bottom water in Nares Strait due to the discrepancy between collection depths (0-85 m) and the living depth of carbonated organisms found in marine sediment cores (depths >220 m). The reservoir age is also susceptible to have evolved over time with major changes in oceanography linked to ice sheet retreat and post-glacial rebound. Radiocarbon dating in the CAA is further complicated by non-systematic discrepancies between ages yielded from deposit- vs. suspension-feeding molluscs, the so-called “*Portlandia* effect” (England et al., 2013).

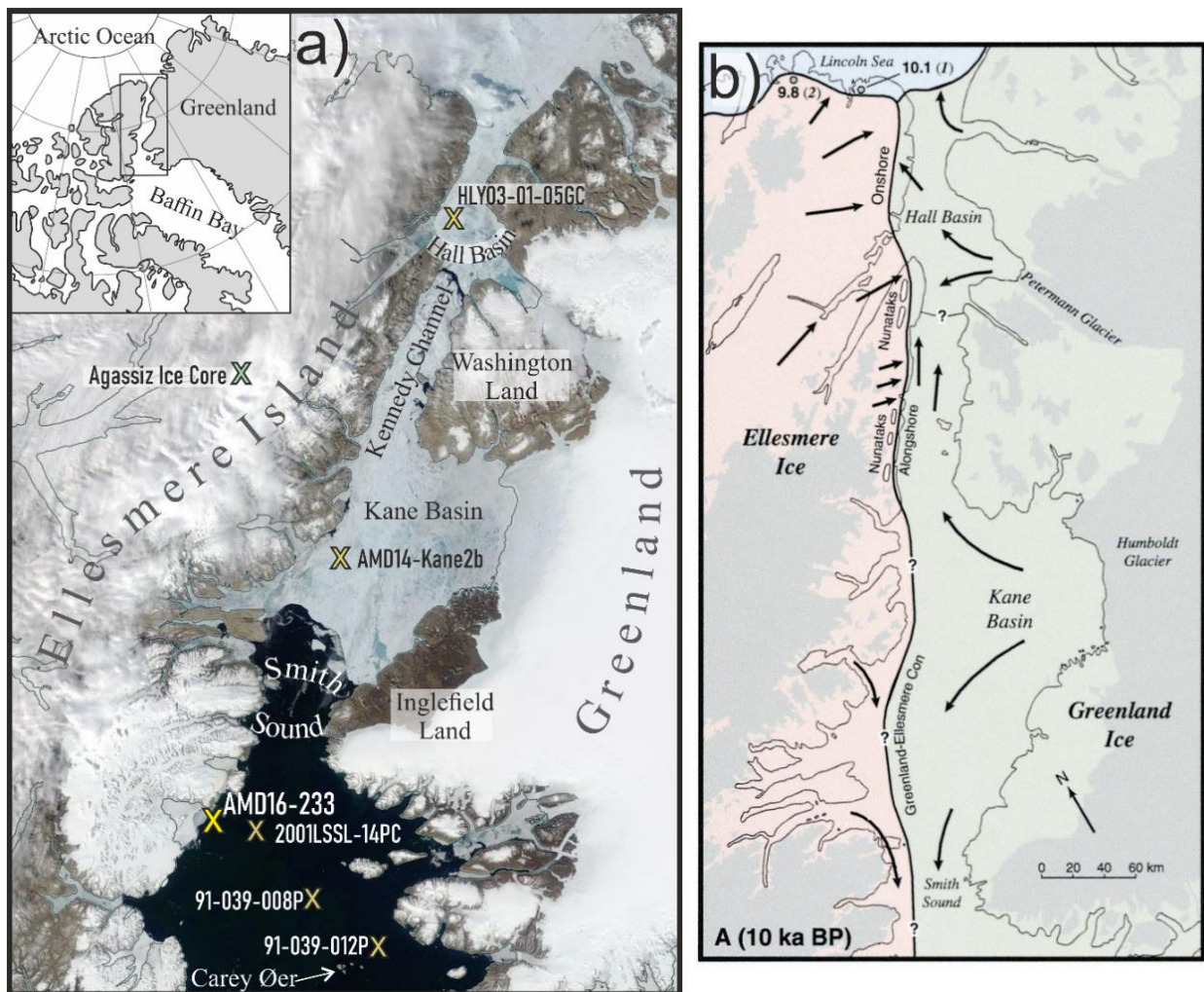
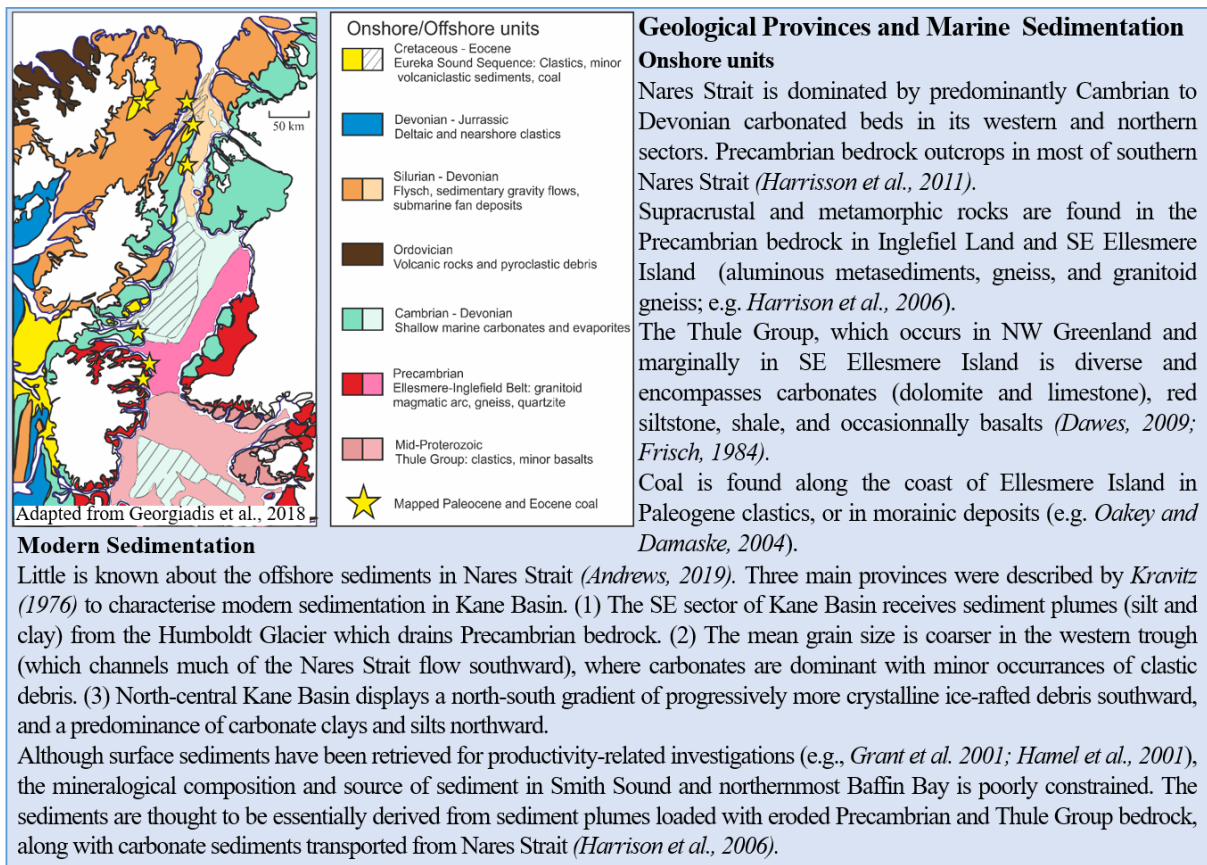


Figure 1.14: Holocene archives in the Nares Strait area. a) Location of marine sediment cores in Nares Strait and northernmost Baffin Bay, with from north to south: HLY03-01-05GC (Jennings et al., 2011), AMD14-Kane2b (this study), AMD16-233 (this study), 2001LSSL-14PC (Jennings et al., 2019), and 91-039-008P and 91-039-012P (Blake et al., 1996; Knudsen et al., 2008; Levac et al., 2001).; b) reconstruction of the LGM extent of the Greenland and Innuitian Ice Sheets in Nares Strait based on land-bound fieldwork (England, 1999).

A brief synthesis of the Holocene history of Nares Strait is summarised as follows.

The IIS coalesced with the Laurentide Ice Sheet along Parry Channel in the western CAA, and with the Greenland Ice Sheet (GIS) in the east (England et al., 2006). According to the occurrence of erratic boulders from Greenland on Ellesmere Island, the GIS extended over most of the length of Nares Strait and coalesced with the IIS along the eastern coast of Ellesmere Island (Blake, 1977; Christie, 1983, 1967; cf. Insert 2 for a general presentation of the geological context in Nares Strait). An extensive review of geological and radiocarbon datasets by England (1999) established that the occupation of Nares Strait by glacial ice took place between ca 22 and ca 9 cal. ka BP (Figure 1.14-b). The occurrence of older molluscs in the north and south of Nares Strait entails that deglaciation began at the extremities of the strait (around 10 cal ka BP, $\Delta R = 240 \pm 51$ years), with the central

Kennedy Channel and northern Kane Basin opening later. The altitude of raised beaches along the channels of the CAA made it possible to fairly accurately measure isostatic rebound (England et al., 2006) helping to constrain models of ice sheet dynamics in the area (Lecavalier et al., 2014). The major uncertainty emanating from England's (1999) review was the exact timing of the later ice retreat in Kennedy Channel. No shells older than 8.1 cal. ka BP ($\Delta R = 240 \pm 51$ years) were found on the coasts of Kennedy Channel (England, 1999), while glacial deposits on islands in Kennedy Channel yielded average cosmogenic ages of ca 10,000 years (Zreda et al., 1999). A transition from pro-glacial laminated sediment towards hemipelagic mud was recorded in Hall Basin, possibly signalling retreat of glacial ice in Kennedy Channel and the complete opening of Nares Strait at ca 8.6 cal ka BP ($\Delta R = 240 \pm 51$ years; Jennings et al., 2011). The lack of other marine sediment archives within Nares Strait is an impediment to the establishment of a fully integrated scheme of glacial retreat in the strait. Furthermore, the oceanographic evolution of Nares Strait is nearly entirely based on the marine sediment core from northern Nares Strait. Micropaleontological (benthic foraminifera) assemblages attest to shoaling of the water column (due to isostasy), with however a continuous influence of Atlantic-sourced water at the bottom of Hall Basin throughout the Holocene (Jennings et al., 2011). A shift in micropaleontological assemblages and isotopic geochemistry infers a rapid transition towards more sea ice-related productivity, which coincides with the lithologic transition between laminated to bioturbated mud at ca 8.6 cal. ka BP. Poor resolution of the datasets owing to reduced sedimentation rates prevents the identification of any other significant paleoenvironmental change in Hall Basin in the Mid- to Late Holocene (Jennings et al., 2011). Resolving details in paleoenvironmental reconstruction has also been a challenge to the south of Nares Strait. Two marine sediment records were retrieved in northernmost Baffin Bay, but gaps of several hundred to several thousands of years between the composites of the piston and trigger weight cores make it difficult (or impossible) to assess downstream consequence of the opening of Nares Strait, or to produce a continuous reconstruction of paleoenvironmental conditions (Knudsen et al., 2008; Levac et al., 2001). As for Kane Basin, the offshore glacial retreat during the Early Holocene and the evolution of oceanographic and sea ice dynamics are entirely unknown.



Insert 2: Geological context

Achieving more confidence in the timing of the opening of Nares Strait would help constrain the modelling of ice sheet dynamics and the isostatic response. It is also a case study for the opening of an oceanic gateway and atmospheric channel in response to climate forcing. Furthermore, the establishment of the connection between the Arctic Ocean and Baffin Bay is likely to have majorly impacted regional and global oceanic circulation. Locally, reconstructing geomorphologic reorganisation in Nares Strait is paramount to understanding the establishment of oceanographic circulation within the strait and the evolution of sea ice dynamics which depend so heavily on geomorphology and atmospheric forcing. This project was instigated to address these issues.

5. Objectives of current work and dissertation layout

5.1 Objectives

The current work is based on the multi-proxy investigation of two marine sediment cores retrieved in Kane Basin (AMD14-Kane2b) and northernmost Baffin Bay (AMD16-233) (Figure 1.15), during ArcticNet campaigns of the CCGS *Amundsen* in 2014 and 2016, respectively.



Figure 1.15: Location of cores AMD14-Kane2b and AMD16-233 on MODIS satellite image (<https://worldview.earth.nasa.gov/>.)

The first objective of this work is to characterise glacial retreat and ice sheet dynamics as viewed from Kane Basin and from the western sector of Smith Sound. This fundamental task will include defining the spatial evolution of Kane Basin as the glacial ice margin retreated, and providing a new perspective on the complete opening of Nares Strait in an attempt to better date this event. In Smith Sound, we will attempt to document the local deglaciation of the south-eastern sector of Ellesmere Island, and the deglaciation of Nares Strait will be viewed through the lens of downstream Nares Strait.

The second objective of this project is to reconstruct post-glacial hydrological conditions in Kane Basin and the western sector of the North Water. Our records will provide new insight regarding the establishment of the modern oceanographic circulation in Nares Strait in relation to its geomorphological reorganisation and to paleoclimatic changes. We also aim at reconstructing surface conditions in hope of characterising the response of

surface conditions towards oceanographic and atmospheric forcing.

Establishing a robust chronological frame for both cores will be the backbone of this work, as it will help to provide the most precise dating of events possible.

Finally, Nares Strait will be considered in a wider context, and its role as a driver of change rather than the subject of external (and internal) forcing will be explored in a synthetic chapter. In particular, we will explore the possible influence of hydrology in Nares Strait on the more general oceanography in Baffin Bay.

5.2 Dissertation layout

This dissertation consists of four chapters which present our main results, followed by a synthetic chapter, before we conclude and reflect on the limits of the work presented here. The objectives of each chapter is synthesised in Insert 3.

Chapters 1 and 2 of this manuscript concern the geomorphological reorganisation of Nares Strait. These chapters are presented as two scientific papers, one based on core AMD14-Kane2b, the other on core AMD16-233. The two studies apply a similar analytical strategy to each core. Sedimentary environments are reconstructed based on a thorough sedimentological study, while the mineralogical and/or geochemical composition of the sediment is used to identify sediment provenance. The methodology and age models of the cores are detailed in each paper. These two approaches are complimentary in that they enable us to draw a continuous spatio-temporal scheme of the deglaciation for each of the study sites.

Chapters 3 and 4 are related to oceanography and sea ice dynamics, and their Holocene evolution. These chapters are presented as one article per core, and rely on chapters 1 and 2 I to lay out the geomorphological setting at each location. The proxies used in chapters 3 and 4 are micropaleontological (benthic and planktic foraminiferal assemblages), and biogeochemical (sea ice biomarkers IP₂₅ and HBI III).

Each article includes a section of the material (marine sediment core) and methods used for each study.

Our findings will be explored in a broader, regional context in a final synthetic chapter (chapter 5).

Objectives	Dissertation layout
<p><u>Provide a robust chronological and mechanistic view of the postglacial ice sheet retreat and geomorphological setting:</u></p> <ul style="list-style-type: none"> - Deglaciation of Kane Basin & complete opening of Nares Strait - Deglaciation of SE Ellesmere Island, downstream point of view of ice sheet retreat in southern Nares Strait, and of the opening of Nares Strait 	<ul style="list-style-type: none"> - <u>Chapter 1:</u> Radiocarbon dating, and sedimentological and geochemical study of core AMD14-Kane2b - <u>Chapter 2:</u> Radiocarbon dating, and sedimentological, geochemical and mineralogical study of core AMD16-233
<p><u>Reconstruct the Holocene evolution of ocean circulation and sea-ice dynamics</u></p> <ul style="list-style-type: none"> - In Kane Basin (ice arch) - In the western sector of the North Water 	<ul style="list-style-type: none"> - <u>Chapter 3:</u> Micropaleontologic and biogeochemical study of core AMD14-Kane2b - <u>Chapter 4:</u> Micropaleontologic and biogeochemical study of core AMD16-233
<p><u>Consider broader regional implications of the Holocene history of Nares Strait</u></p>	<p><u>Chapter 5:</u> Synthesis</p>

Insert 3: Objectives and dissertation layout

Chapter 1 Deglacial to Postglacial history of Nares Strait, Northwest Greenland: a marine perspective from Kane Basin

1.1 Résumé

Une carotte de sédiments marins récupérée dans le bassin de Kane, la partie centrale du détroit de Nares, a été analysée pour contraindre la chronologie de la déglaciation du détroit. L'étude s'appuie sur un modèle d'âge basée sur 19 âges ^{14}C afin de dater l'ouverture postglaciaire de cette porte de l'Arctique et son évolution holocène. Les paléo-environnements glacio-marins sont reconstruits à partir d'une étude sédimentologique et géochimique. Au site de carottage, la sédimentation marine pro-glaciaire a commencé *ca* 9,0 cal. ka BP après le retrait de la calotte. Les contributions variables de sable et de clastes suggèrent des conditions de glace de mer et une activité glaciaire oscillantes, ayant persisté jusqu'à *ca* 7,5 cal. ka BP sous l'influence combinée des températures atmosphériques chaudes et du refroidissement proglaciaire induit par la proximité des calottes glaciaires innuitiennes et groenlandaises. Un intervalle riche en débris glaciaires (IRD) est interprété comme l'effondrement de la calotte dans le détroit de Kennedy *ca* 8,3 cal. ka BP, marquant l'ouverture complète du détroit de Nares et la connexion initiale entre la mer de Lincoln et la baie de Baffin. Le transport et le dépôt de sédiments par les icebergs sont particulièrement élevés entre *ca* 8,3 et *ca* 7,5 cal. ka BP suite à l'effondrement de la calotte dans le détroit de Kennedy, qui a probablement déclenché l'accélération des flux des calottes groenlandaise et innuitienne vers le détroit de Nares. Cette accélération a conduit au retrait rapide de la calotte groenlandaise dans l'est du bassin de Kane vers 8,1 cal. ka BP, comme en témoigne un changement notable dans la géochimie des sédiments dans la carotte. La diminution progressive des apports de carbonate dans le bassin de Kane entre $\sim 8,1$ et $\sim 4,1$ cal. ka BP reflète la déglaciation tardive de la terre de Washington. La remontée isostatique postglaciaire du bassin de Kane peut être observé dans notre archive par l'augmentation du vannage d'argiles induit par le rapprochement du fond marin vers les courants océaniques de sub-surface. La réduction d'IRD entre 7,5 et 1,9 cal. ka BP est à mettre en relation avec le recul des calottes sur terre et la réductions du nombre de terminaisons marines des calottes.

1.2 Abstract

A radiocarbon-dated marine sediment core retrieved in Kane Basin, central Nares Strait, was analysed to constrain the timing of the postglacial opening of this Arctic gateway and its Holocene evolution. This study is based on a set of sedimentological and geochemical proxies of changing sedimentary processes and sources that provide new insight into the evolution of ice sheet configuration in Nares Strait. Proglacial marine sedimentation at the core site initiated *ca.* 9.0 cal. ka BP following the retreat of grounded ice. Varying contributions of sand and clasts suggest unstable sea ice conditions and glacial activity, which subsisted until *ca.* 7.5 cal. ka BP under the combined influence of warm atmospheric temperatures and proglacial cooling induced by the nearby Inuitian (IIS) and Greenland (GIS) ice sheets. An interval rich in ice-rafted debris (IRD) is interpreted as the collapse of the ice saddle in Kennedy Channel *ca.* 8.3 cal. ka BP that marks the complete opening of Nares Strait and the initial connection between the Lincoln Sea and northernmost Baffin Bay. Delivery of sediment by icebergs was strengthened between *ca.* 8.3 and

ca. 7.5 cal. ka BP following the collapse of the buttress of glacial ice in Kennedy Channel that triggered the acceleration of GIS and IIS fluxes toward Nares Strait. The destabilisation in glacial ice eventually led to the rapid retreat of the GIS in eastern Kane Basin at about 8.1 cal. ka BP as evidenced by a noticeable change in sediment geochemistry in our core. The gradual decrease in carbonate inputs to Kane Basin between ~ 8.1 and ~ 4.1 cal. ka BP reflects the late deglaciation of Washington Land. The shoaling of Kane Basin can be observed in our record by the increased winnowing of lighter particles as the glacio-isostatic rebound brought the seabed closer to subsurface currents. Reduced iceberg delivery from 7.5 to 1.9 cal. ka BP inferred by our dataset may be linked to the retreat of the bordering ice sheets on land that decreased their number of marine termini.

Eleanor Georgiadis^{1,2}, Jacques Giraudeau¹, Philippe Martinez¹, Patrick Lajeunesse², Guillaume St-Onge³, Sabine Schmidt¹, and Guillaume Massé²

¹Université de Bordeaux, CNRS, UMR 5805 EPOC, 33615 Pessac, France

²Université Laval, UMI 3376 TAKUVIK, Québec, G1V 0A6, Canada

³Université du Québec à Rimouski and GEOTOP Research Center, Institut des sciences de la mer de Rimouski (ISMER), Rimouski, G5L 3A1, Canada

Climate of the Past, 14, 1991–2010, 2018 (<https://doi.org/10.5194/cp-14-1991-2018>)

1.3 Introduction

The Holocene history of Nares Strait, Northwest Greenland, has remained somewhat cryptic despite investigations during the past four decades (e.g., Blake, 1979; Jennings et al., 2011; Kelly and Bennike, 1992; Mudie et al., 2006). Nares Strait is a key gateway for Arctic seawater and ice toward the Atlantic Ocean, contributing to up to half of the volume of water transported through the Canadian Arctic Archipelago (CAA), which provides fresh water to the Labrador Sea and influences deep water formation (Belkin et al., 1998; McGeehan and Maslowski, 2012; Münchow et al., 2006). Nares Strait supplies one of the most productive regions of the Arctic, the North Water polynya, with nutrient-rich Pacific water (Jones, 2003; Jones and Eert, 2004) and maintains its very existence by trapping sea and calved glacial ice in ice arches in the north and south of the strait (Melling et al., 2001; Mundy and Barber, 2001).

Despite the importance of Nares Strait, intrinsic investigations into its late Pleistocene history, which is intimately linked with the dynamics of the bordering Innuitian (IIS) and Greenland (GIS) ice sheets, are relatively sparse and much of our knowledge relies on land-based studies. Debate initially surrounded early studies of glacial configuration in the CAA with some authors concluding that the CAA channels were not blocked during the Last Glacial Maximum (LGM) (Franklin Ice Complex theory; e.g., England, 1976), while others argued that the IIS coalesced with the bordering Greenland and Laurentide ice sheets (e.g., Blake, 1970). The presence of erratic boulders originating from Greenland on Ellesmere Island (England, 1999), cosmogenic nuclide surface-exposure dating (Zreda et al., 1999), and radiocarbon dating on mollusc shells (e.g., Bennike et al., 1987; Blake, 1992; Kelly

and Bennike, 1992) finally settled the argument in favour of the latter narrative by supporting the coalescence of the IIS and GIS along Nares Strait between 19 and ca. 8 ¹⁴C ka BP (~ 22–8.2 cal. ka BP, $\Delta R = 240$). England (1999) reviewed all land-based evidence available at that time and proposed a complex deglacial history of Nares Strait, featuring the late break-up of glacial ice in central Nares Strait (i.e. Kennedy Channel). These land-based studies have been complemented by Jennings et al. (2011) and Mudie et al. (2006) investigations of marine sediment cores collected in Hall Basin, northernmost Nares Strait, which record a change in a number of environmental proxies ca. 8.3 ¹⁴C ka BP (ca. 8.5 cal. ka BP, $\Delta R = 240$). More recently, the geophysical mapping of submarine glacial landforms by Jakobsson et al., (2018) provided additional insight regarding the retreat of Petermann Glacier in Hall Basin, and new surface-exposure dating on moraines in Washington Land demonstrates that the Humboldt Glacier, eastern Kane Basin, abandoned a previous position of stability ca. 8.3 ± 1.7 ka BP (Reusche et al., 2018). To date, little is known about the downstream consequences of the opening of the strait, despite the recovery of multiple marine archives in northernmost Baffin Bay (Blake et al., 1996; Knudsen et al., 2008; Levac et al., 2001; St-Onge and St-Onge, 2014). Several aspects of the evolution of northernmost Baffin Bay have been explored with regards to ice sheet retreat in the area (Blake et al., 1996), ice sheet dynamics (St-Onge and St-Onge, 2014), and changes in sea ice conditions and marine productivity during deglacial and postglacial times (Knudsen et al., 2008; Levac et al., 2001; St-Onge and St-Onge, 2014). Unfortunately, however, these archives do not cover a continuous record of the Holocene and the sediments deposited around and before the opening of the strait were not recovered or are unable to provide any further information on the timing and consequences of the event.

Here we present sedimentological, geochemical, and geochronological data obtained from a 4.25 m long marine sediment core (AMD14-Kane2b) retrieved in Kane Basin, central Nares Strait. This core provides a continuous sedimentary record spanning the last ca. 9.0 kyr, i.e. from the inception of the Early Holocene retreat of the GIS and IIS in Nares Strait to modern times. Our set of sedimentological and geochemical records derived from this study presents the first offshore evidence of an ice-free environment in Kane Basin in the Early Holocene and offers a unique opportunity to explore the local dynamics of ice sheet retreat leading to the opening of the strait and the establishment of the modern oceanographic circulation pattern.

1.4 Regional settings

Nares Strait is a long (530km) and narrow channel separating Northwest Greenland from Ellesmere Island, Arctic Canada, connecting the Arctic Ocean to the Atlantic Ocean in Baffin Bay (Figure 2.1). Kane Basin is the central, wide (120km large at its broadest point, totalling an area of approximately 27000 km²), and shallow (220 m deep) basin within Nares Strait. It separates Smith Sound (600 m deep, 50 km wide) in the south of the strait from Kennedy Channel (340 m deep, 30 km wide) in the north. A smaller but deeper basin, Hall Basin (800 m deep), where the Petermann Glacier terminates, connects Kennedy Channel to the Robeson Channel (400 m deep, 21 km wide) in the northernmost sector of the strait.

The oceanographic circulation in Nares Strait consists of a generally southward-flowing current driven by the

barotropic gradient between the Lincoln Sea and Baffin Bay (Kliem and Greenberg, 2003; Münchow et al., 2006), while the baroclinic temperature balance generates strong, northerly winds that affect surface layers (Münchow et al., 2007; Rabe et al., 2012; Samelson and Barbour, 2008). The relative influence of the barotropic vs. baroclinic factors that control the currents in Nares Strait is highly dependent on the presence of sea ice that inhibits wind stress when land-fast (Münchow, 2016; Rabe et al., 2012). Long-term ADCP measurements of flow velocity record average speeds of $20\text{--}30\text{cm s}^{-1}$ in Kennedy Channel (Münchow et al., 2006; Rabe et al., 2012) and $10\text{--}15\text{cm s}^{-1}$ in Smith Sound (Melling et al., 2001) with the highest velocities measured in the top 100 m of the water column. Strong currents peaking at 60 cm s^{-1} have been measured instantaneously in Robeson Channel (Münchow et al., 2007). The speed of the flow decreases in the wider sections of Nares Strait. A northward current has been shown to enter Kane Basin from northern Baffin Bay (Bailey, 1956; Melling et al., 2001; Muench, 1971; Münchow et al., 2007). Temperature and salinity isolines imply that an anticlockwise circulation takes place in the surface layers of Kane Basin, while the deeper southward flow of Arctic water is channelled by bottom topography and concentrated in the basin's western trough (Moynihan, 1971; Muench, 1971; Münchow et al., 2007).

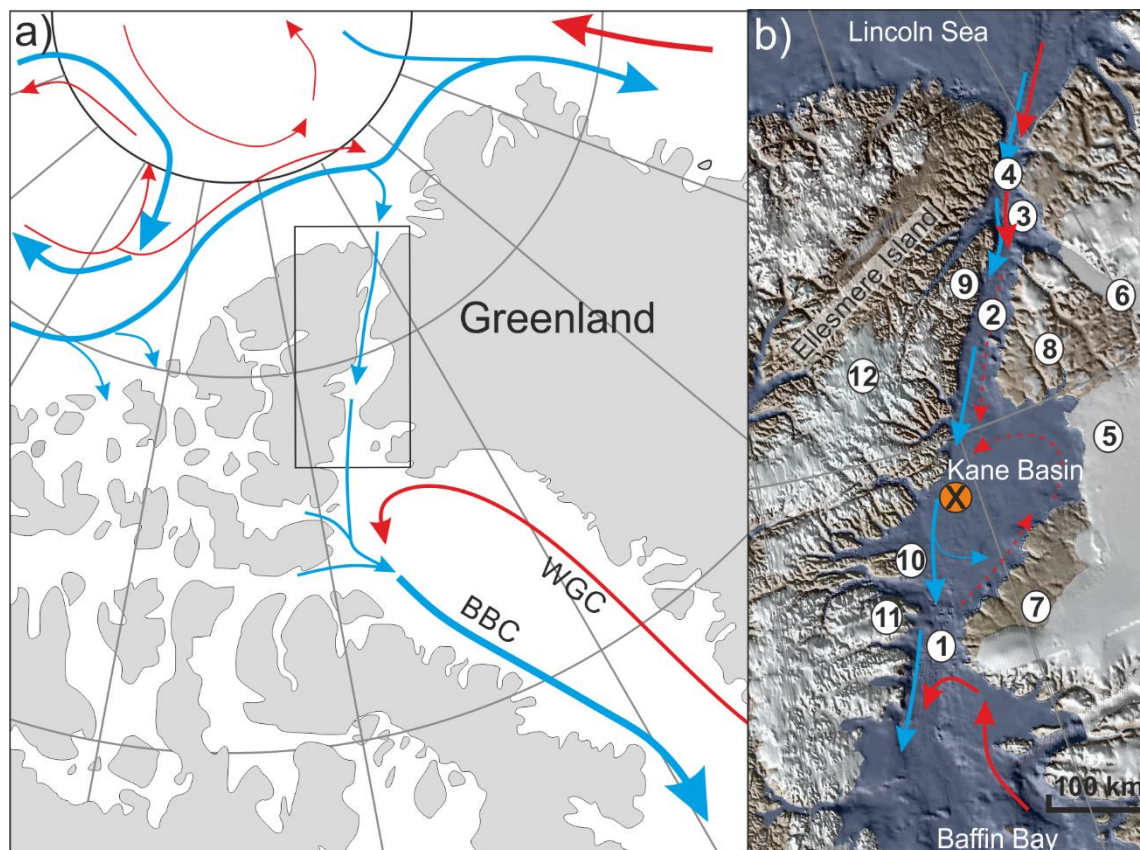


Figure 2.1: Schematic circulation in the Canadian and northern Greenland sectors of the Arctic Ocean (a) and within Nares Strait (b). The location of core AMD14-Kane2b is marked by a cross. Blue arrows represent Arctic water and red arrows predominantly Atlantic water. WGC: West Greenland Current, BBC: Baffin Bay Current. 1 – Smith Sound; 2 – Kennedy Channel; 3 – Hall Basin; 4 – Robeson Channel; 5 – Humboldt Glacier; 6 – Petermann Glacier; 7 – Inglefield Land; 8 – Washington Land; 9 – Judge Daly Promontory; 10 – Bache Peninsula; 11 – Johan Peninsula;

12 – Agassiz Ice Cap.

Sea ice concentration in Nares Strait is usually over 80% from September to June (Barber et al., 2001). The state of the ice varies between mobile (July to November) and fast ice (November to June). The unique morphology of the strait leads to the formation of ice arches in Nares Strait when sea ice becomes land-fast in the winter. The ice arches are a salient feature in the local and regional oceanography of Nares Strait: they not only block sea ice from drifting southward in the strait, sustaining the existence of the NOW Polynya (Barber et al., 2001), but they also control the export of low-salinity Arctic water into Baffin Bay (Münchow, 2016). The main iceberg sources for the strait are Petermann Glacier in Hall Basin and Humboldt Glacier in Kane Basin, both outlets of the GIS.

The Greenland coast bordering Kane Basin is relatively flat. In Inglefield Land the Precambrian basement is exposed, displaying supracrustal crystalline rocks and metamorphic rocks, essentially reported as aluminous metasediments and gneisses or granitoid gneisses, with some references to quartzite (Figure 2.2, Koch, 1933; Dawes, 1976; Dawes and Garde, 2004; Harrison et al., 2006, and references therein). Dawes and Garde (2004) postulated that this Precambrian basement also underlies the 100km wide Humboldt Glacier, a claim that is supported by the dominance of crystalline material delivered in modern glacimarine sediments in front of the Humboldt Glacier (Figure 2.2, Kravitz, 1976). To the north, the Precambrian basement in Washington Land is overlaid by Cambrian, Ordovician, and Silurian dolomites, limestones, and evaporites (Koch, 1929a, b; Harrison et al., 2006, and references therein). The Ellesmere shore of Kane Basin rises abruptly from sea level and is punctured by narrow fjords, penetrating inland for nearly 100km (Kravitz, 1982). In southern Kane Basin, the same Precambrian crystalline rocks outcrop to form the Ellesmere– Inglefield Precambrian Belt. The central and northern sectors of Ellesmere Island's coast mainly comprise Cambrian to Devonian carbonates and evaporates. Fluviodeltaic quartz sandstone, volcanistic sandstone, minor arkose, and sometimes coal are found in the Paleogene Eureka Sound sequence that occurs along the western coast of Kane Basin, on the Ellesmere Island flank of Kennedy Channel, and on Judge Daly Promontory (Christie, 1964, 1973; Kerr, 1967, 1968; Miall, 1982; Oakey and Damaske, 2004). Coal-bearing Paleogene clastics also occur along the coast of Bache Peninsula and in morainic deposits on Johan Peninsula in southwestern Kane Basin (Figure 2.2, Kalkreuth et al., 1993).

Kravitz (1976) described modern sedimentation in Kane Basin according to three main provinces defined on the basis of mineralogical and grain size characteristics. The first province covers the eastern, central, and southern part of the basin in which the predominant crystalline clay and silt sediments are water-transported off Humboldt Glacier and Inglefield Land. The second province, in the west of the basin, includes a higher fraction of ice-transported materials, mostly carbonates with clastic debris occurring in the deeper trough. Northern Kane Basin makes up the third province in which water-transported, mostly carbonate sediments from Washington Land are deposited in its northernmost part, while ice-transported crystalline particles are more common in the southern part of this province.

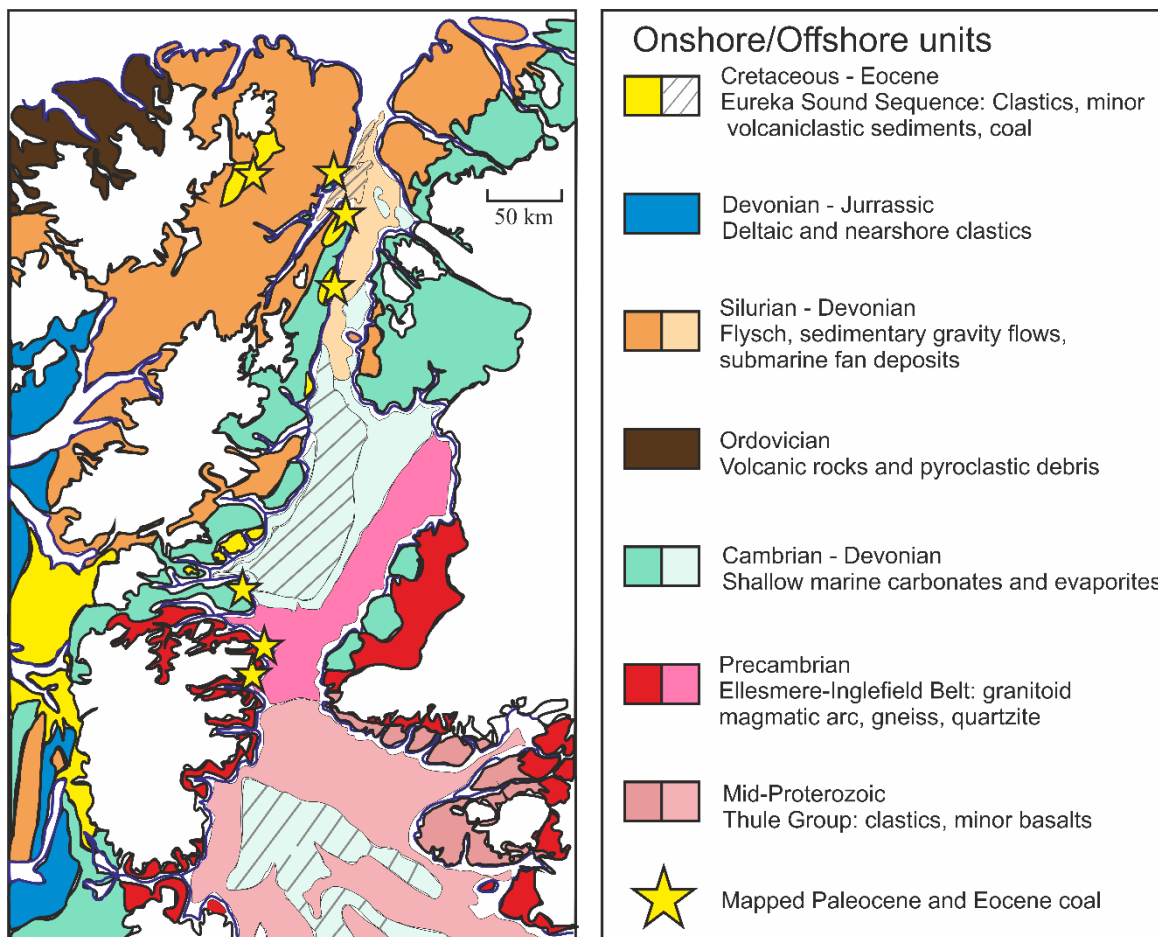


Figure 2.2: : Geology of Northwest Greenland and Ellesmere Island along Nares Strait. Adapted from Harrison et al. (2011).

1.5 Material and methods

Sediment core AMD14-Kane2b was retrieved at 217 m of water depth in Kane Basin, Nares Strait (79.31.140° N; 70.53.287° W) during the 2014 ArcticNet expedition of the CCGS *Amundsen*. This core was collected with a wide-square section (25 cm × 25 cm) gravity corer (Calypso Square or “CASQ”) and immediately subsampled onboard using large U channels.

1.5.1 Sedimentological analyses

The description of the various lithofacies was based on the visual description of the core and high-resolution images using a computed tomography (CT) scanner (Siemens SOMATOM Definition AS+ 128 at the Institut National de la Recherche Scientifique, Quebec, Canada). Changes in sediment density were estimated from variations in the CT numbers, which were processed according to Fortin et al. (2013). To complement CT analyses, a series of thin sections covering two intervals were sampled across major fraction of sands and identifiable ice-rafted debris (IRD), expressed as % weight of the bulk dry sediment.

1.5.2 XRF core-scanning

High-resolution (5 mm) X-ray fluorescence (XRF) core-scanning was conducted along the archive using an

AVAATECH XRF core-scanner. The semi-quantitative elemental composition of the sediment was measured throughout the whole archive with the exception of two units, which contain large clasts. Measurements were acquired with generator settings of 10, 30, and 50 kV in order to detect elements in the range of Al to Ba. Elemental ratios or normalisation to the sum of all elements except Rh and Ag, whose counts are biased during data acquisition, were used to minimise the effects of grain size and water content on elemental counts (Tjallingii et al., 2007; Weltje and Tjallingii, 2008). XRF core-scanner-derived elemental ratios have been used as a time-efficient method to assess down-core variations in grain size (e.g., Bahr et al., 2014; Guyard et al., 2013; Mulder et al., 2013) and/or sediment sources for detrital material in similar high-latitude locations (e.g., Bervid et al., 2016; Møller et al., 2006). The applicability of this approach in Kane Basin is tested in the present study by using Ti/K and Fe/Ca as proxies for grain size and sediment source, respectively. We also demonstrate a correlation between normalised K counts and clay content in core AMD14-Kane2b.

1.5.3 Chronology and radiocarbon dating in Nares Strait

The chronology is based on a set of 18 radiocarbon ages obtained from mixed benthic foraminifera samples and unidentified mollusc shells. The core top is dated at -5 yearsBP (1955 CE) based on ^{210}Pb measurements and a comparison with the ^{210}Pb profile (Figure 2.3) obtained from a box core collected at the same coring site.

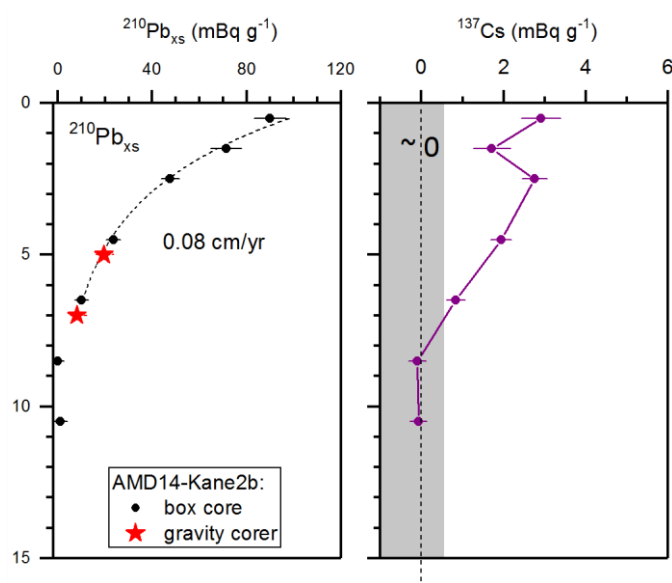


Figure 2.3: ^{210}Pb and ^{137}Cs profiles in AMD14-Kane2b CASQ core (red stars) and box core (black circles). $^{210}\text{Pb}_{\text{xs}}$ data points in the top part of AMD14-Kane2b CASQ core have been shifted to obtain the best correspondence of the plots, yielding a material loss of 4 cm at the top of the CASQ core.

Reservoir ages in Nares Strait are difficult to assess owing to the scarcity of pre-bomb specimens in collections of marine shells from the area. Only three molluscs were dated in Nares Strait with ΔR ranging between ca. 180 and ca. 320 years, comparing relatively well with molluscs from the western sector of northernmost Baffin Bay (ΔR of ca. 140 and ca. 270), while molluscs collected near Thule, Northwest Greenland, yielded negative ΔR (McNeely

et al., 2006). Coulthard et al. (2010) proposed a regional ΔR for the CAA of 335 years based on the McNeely et al. (2006) dataset of pre-bomb radiocarbon-dated molluscs and taking into account the general oceanographic circulation in the CAA. However, unlike in other passages of the CAA, which present shallow sills at their southern extremities, younger Atlantic water from Baffin Bay enters Nares Strait – or at least Kane Basin – from the south (Bailey, 1957; Muench, 1971; Münchow et al., 2007). We thus choose to correct ^{14}C ages in this study with the average ΔR of the three pre-bomb collected mollusc shells in Nares Strait, i.e. 240 ± 51 years, bearing in mind that reservoir ages are likely between 0 and 335 years and may have changed through time as a consequence of the major oceanic reorganisation in Nares Strait. Radiocarbon dating in Nares Strait is further complicated by the proximity of old carbonate rocks that are prone to introducing additional uncertainties in the ^{14}C ages yielded by deposit feeding molluscs (England et al., 2013). The non-systematic discrepancies between ages yielded from deposit feeders and those from suspension-feeding molluscs – the so-called *Portlandia* effect (England et al., 2013) – cannot be corrected. However, this represents a greater challenge for land-bound studies that pinpoint the timing of the deglaciation of a given location based on the oldest mollusc found in that location. In contrast, when establishing the age model of sediment cores, the age vs. depth relationship reveals any outliers that can be identified as either (1) remobilised by ice rafting, slumping, or bioturbation or (2) potentially affected by the *Portlandia* effect. Hence, we deem the *Portlandia* effect to be of minor concern in the establishment of the age model in this study despite the possible inclusion of deposit feeders in our radiocarbon dataset. The ^{14}C ages were calibrated with the Marine13 curve (Reimer et al., 2013) using Calib7.1 (Stuiver et al., 2020) with a marine reservoir age correction of 640 years ($\Delta R = 240 \pm 51$ years). We computed an age–depth model for core AMD14-Kane2b based on radiocarbon-dated material using CLAM 2.2 (Blaauw, 2010) as a smooth spline with a smoothing level of 0.4 and assuming that a 20 cm long clast-rich deposit (300–320 cm) was deposited near instantaneously at the scale of our chronology.

1.6 Results and interpretations

1.6.1 Age model and sedimentation rates in core AMD14-Kane2b

According to our chronology, core AMD14-Kane2b covers approximately the last 9.0kyr (Figure 3.4). The comparison of the ^{210}Pb profiles of core AMD14-Kane2b and the box core collected at the same location reveals the relatively good recovery of the topmost sediments in the CASQ core permitted by the large diameter of this corer (sediment loss of ca. 4cm; Figure 3.3). Fourteen of the ^{14}C ages yielded consistent values along a smooth spline, while four outlying radiocarbon ages were excluded from the age model. Only one mollusc fragment was dated (at 301.5 cm) and yielded an age of > 43 ka; it is thus clearly remobilised (Table 2.1). A whole mollusc shell at 238.5cm yielded a radiocarbon age about 1kyr older than expected and is the only specimen we suspect of being affected by the *Portlandia* effect. Two mixed benthic foraminifera samples yielded ages older than expected and most likely include older specimens.

Major changes in depositional environments, most particularly during the time interval corresponding to the lower half of our sediment core, explain the wide range of sedimentation rates. High sedimentation rates are

observed between the base and ca 250 cm, where they decrease from ca. 220 to 30 cm.ka⁻¹, and after which sedimentation rates increase to reach 50 cm.ka⁻¹ at 120 cm before decreasing again to ca. 20 cm.ka⁻¹ at the top of the core.

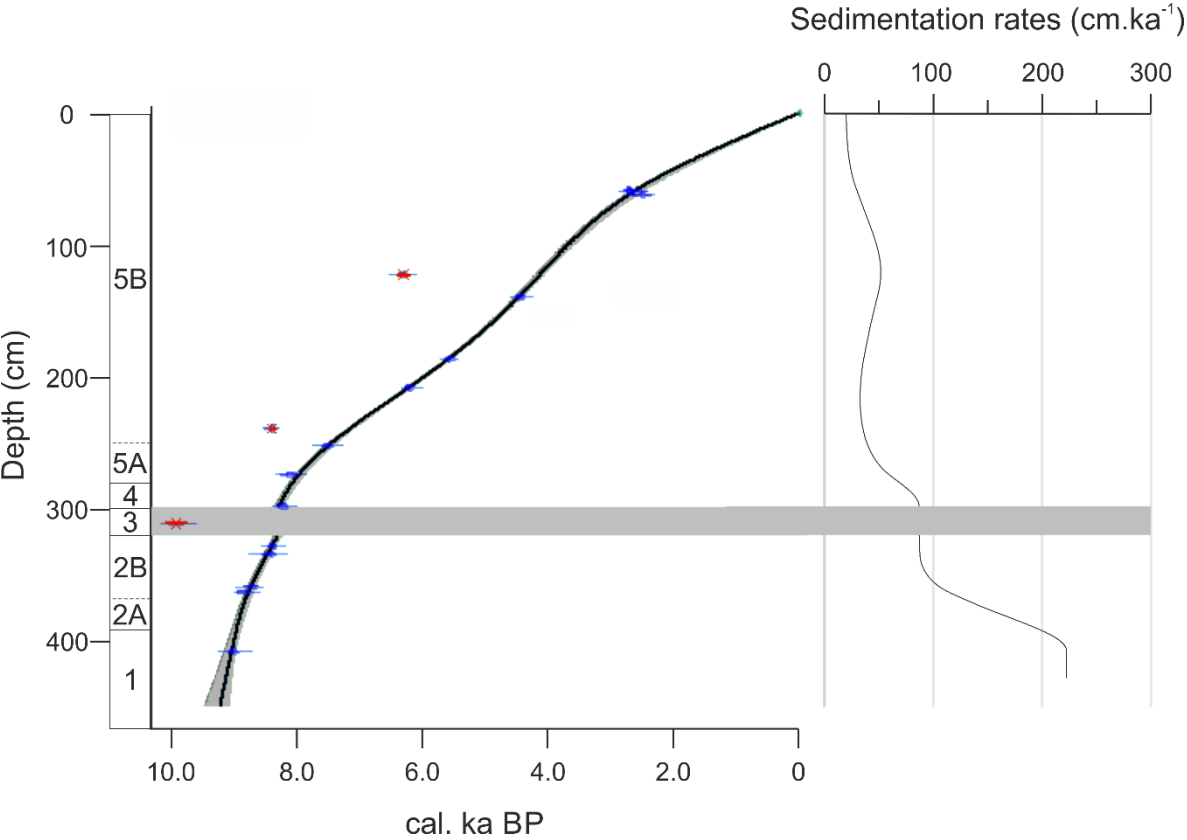


Figure 2.4: Core AMD14-Kane2b age model (a) and sedimentation rates (b). The age model is a smooth spline computed using CLAM 2.2 with a smoothing level of 0.4 based on selected radiocarbon dates presented in Table 2.1. 1σ uncertainty is shown in grey. ¹⁴C ages excluded from the age model (time reversals) are crossed out in red.

Table 2.1: AMS radiocarbon ages on selected carbonate material. Asterisks indicate data that were not used in the age model. MBF: mixed benthic foraminifera, Mollusc: unidentified mollusc shell.

Laboratory code	Dated material	Depth (cm)	¹⁴ C age (a BP) ±1σ	Calib 7.0 median probability age (cal. a BP) ΔR = 0	Calib 7.0 1 interval (cal a BP)	Calib 7.0 median probability age (cal. a BP) ΔR = 335	Calib 7.0 1 interval ΔR = 335 (cal. a BP)	Calib 7.0 median probability age (cal. a BP) ΔR = 240	Calib 7.0 1 interval ΔR = 240 (cal. a BP)
SacA-46000	Mollusc	58.5	3150+-35	2932	2869-2984	2576	2511 - 2659	2700	2673 - 2736
UGAMS-24304	Mollusc	59	3125+-25	2900	2854-2941	2542	2469 - 2611	2683	2655 - 2720
UGAMS-24305	Mollusc	62	3010+-25	2775	2739-2802	2362	2319 - 2396	2502	2428 - 2575
SacA-46003	MBF	122	6125+-45	6555	6494-6617	6216	6176 - 6265	6205	6259 - 6356
UGAMS-24308	Mollusc	139	3030+-25	2793	2754-2822	2385	2336 - 2420	2542	2469 - 2611
UCIAMS-173009	Mollusc	139	4540+-20	4760	4764-4809	4305	4253 - 4353	4427	4392 - 4453
UGAMS-24306	Mollusc	152	4190+-25	4283	4230-4339	3817	3766 - 3866	3937	3884 - 3978
UGAMS-24307	Mollusc	186	5445+-25	5823	5780-5876	5486	5445 - 5528	5572	5541 - 5602
UGAMS-24295	Mollusc	207.5	6005+-25	6417	6382-6458	6076	6012 - 6125	6005	6168 - 6240

UCIAMS-173006	Mollusc	238.5	8175+-20	8651	8595-8690	8317	8291 - 8348	8389	8363 - 8411
SacA-46002	MBF	251.5	7250+-60	7714	7649-7780	7426	7369 - 7486	7503	7451 - 7555
SacA-45999	MBF	273.5	7870+-50	8336	8290-8388	7992	7931 - 8039	7870	8026 - 8147
Beta-467584	MBF	297.5	7980+-30	8433	8388 - 8469	8100	8056 - 8151	8215	8167 - 8259
Beta-467583	MBF	310.5	9380+-30	10210	10180 - 10234	9735	9662 - 9809	9907	9821 - 10001
Beta-467583	MBF	327.5	8160+-30	8633	8577 - 8685	8298	8261 - 8347	8379	8347 - 8405
UGAMS-24294	Mollusc	301.5	43700+-225						
SacA-46001	MBF	333.5	8200+-60	8709	8587-8796	8329	8272 - 8395	8422	8358 - 8482
UCIAMS-173007	Mollusc	358.5	8450+-20	9050	9002-9080	8574	8538 - 8603	8703	8637 - 8752
UCIAMS-173008	Mollusc	362.5	8520+-20	9149	9094-9205	8665	8607 - 8708	8840	8773 - 8908
UGAMS-24296	Mollusc	407.5	8640+-30	9318	9272-9373	8882	8841 - 8955	8998	8968 - 9021

Laboratory code	Dated material	Depth (cm)	¹⁴ C age (a BP) ±1σ	Calib 7.0 median probability age (cal. a BP) ΔR = 0	Calib 7.0 1 interval (cal a BP)	Calib 7.0 1 median probability age (cal. a BP) ΔR = 335	Calib 7.0 1 interval ΔR = 335 (cal. a BP)	Calib 7.0 1 median probability age (cal. a BP) ΔR = 240	Calib 7.0 1 interval ΔR = 240 (cal. a BP)
-----------------	----------------	------------	--------------------------------	---	---------------------------------	---	---	---	---

1.6.3 Relationship between XRD data, grain size, and sediment sources

In modern sediments, the spatial variability of sediment geochemistry in Kane Basin is likely related to their provenance. Heavy crystalline minerals (e.g., garnet and orthopyroxene) occur in the eastern province of the basin with provenance from the Humboldt Glacier and Inglefield Land, whereas carbonates in its western sector are sourced from Ellesmere Island or from Washington Land in its northern sector (Figure 2.2, Kravitz, 1976). The geochemical composition of modern sediments varies likewise, with notably high concentrations of Fe and Zn in the eastern sector of Kane Basin (Kravitz and Siegel, 1994). Although the exact chemical variability of the source geological units is not known at present, we consider the sedimentary rocks from eastern Kane Basin and northern Nares Strait likely to be rich in Ca, whereas higher concentrations of Fe, Si, and K presumably characterise the crystalline rocks of the Ellesmere–Inglefield Precambrian Belt. We propose the use of Fe/Ca in our study to follow the potential erosion of rocks from under the Humboldt Glacier and Inglefield Land (presumably Fe-rich) and from Ellesmere Island (presumably Ca-rich). We then infer the position of the GIS and IIS in relation to the core site and the geological units. It can be noted, however, that a direct link between the XRF-derived elemental composition of the sediment and the nearby geological units can be compromised by the ubiquitous nature of certain elements in crystalline and sedimentary rocks, along with the sensitivity of elemental signals to grain size when using XRF core scanning. The interpretations of our XRF dataset in terms of sediment sources warrant confirmation by future research into the mineral associations in core AMD14-Kane2b (Caron et al., submitted). The inferred position of the GIS margin in Kane Basin exposed hereafter, however, is unlikely to be affected by the outcome of the latter study owing to our sedimentological and grain size studies that provide evidence for the distance of the ice margin to the coring site.

XRF counts in core AMD14-Kane2b are largely dominated by Ca and Fe, which are negatively correlated. Our records show a positive correlation between normalised K counts and clay content in the < 2 mm fraction (laser diffraction grain size data) with a correlation factor of $r^2 = 0.57$ that reaches $r^2 = 0.73$ by removing nine outlying data points from the total 150 samples analysed by laser diffraction (Figure 2.6; Figure 2.9 in the Supplement). Likewise, there is an excellent correlation between silt content and the Ti/K ratio from the XRF elemental composition data. The correlation factor between % silt and Ti/K is $r^2 = 0.35$, but rises to $r^2 = 0.84$ by removing nine outlying data points (seven of which are different to those removed to improve the correlation between K counts and % clay, mainly from lithological units 3A and 3C presented hereafter). The similar trends of normalised K counts and the Fe/Ca ratio in units 2, 3, 4, and 5 suggest that the clay content and sediment source may be linked or respond to the same controlling factor.

1.6.4 Lithological units and sedimentological processes

The chirp 3.5 kHz sub-bottom profile obtained prior to core recovery is shown in Figure 2.5. Given the good recovery of recent sediments at the top of core AMD14-Kane2b (Figure 2.3), we place the top of core AMD14-Kane2b at the sediment–water interface on this profile. Assuming an acoustic velocity of 1500 ms^{-1} , the base of

the core reached a coarse unit (unit 0) shown to continue below the retrieved sediment (Figure 2.5), which is likely to have stopped the penetration of the CASQ corer. The high level of backscatter, discontinuous reflectors, and lack of internal coherence in unit 0 are all discriminant acoustic characteristics of diamicton, which contains high amounts of unsorted clasts in a clay to silt matrix (Davies et al., 1984). We interpret this diamicton as being either subglacial till or the first glacial marine sediments deposited during the retreat of the marine-based ice sheet margin.

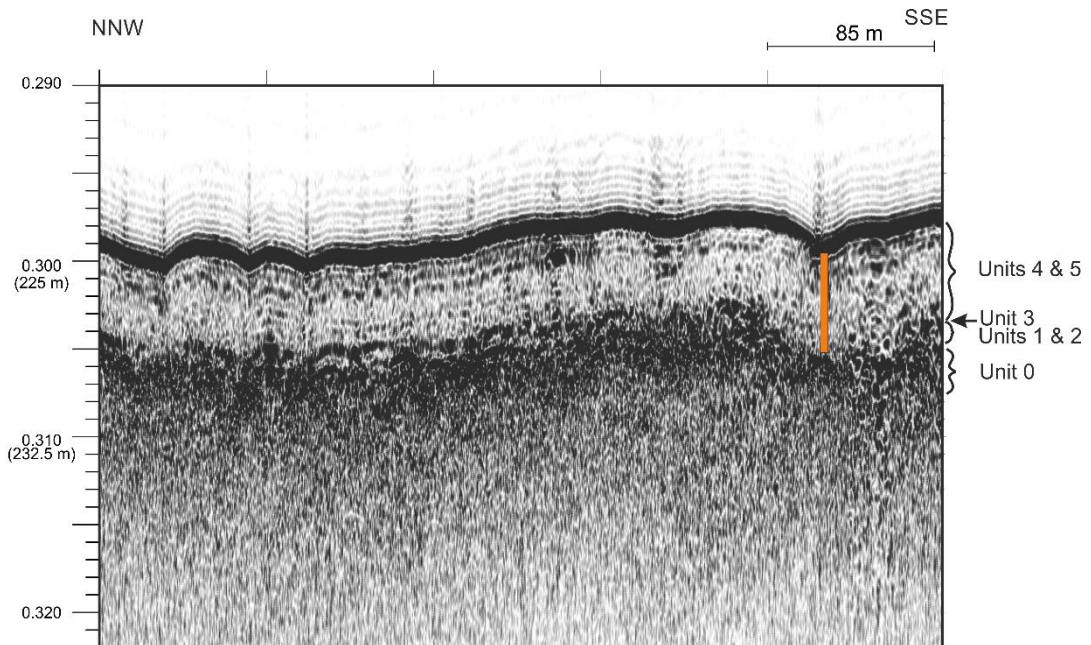


Figure 2.5: 3.5kHz chirp profile across the coring location. Core AMD14-Kane2b is represented by the orange line. Vertical scale in s (TWT) with depth conversion assuming 100 ms (TWT) = 75 m.

Based on CT scans and grain size records, five lithological units were defined for core AMD14-Kane2b, each corresponding to specific depositional environments (Figure 2.6, Table 2.2). The sedimentological processes at play will be examined here, while their environmental significance will be considered in the discussion section of this paper.

Unit 1 (425–394 cm, ca. 9.0 cal. kaBP) encompasses three subunits of distinct lithological nature.

Subunit 1A (425–416 cm) consists of high-density, occasionally sorted coarse sediment in a clayey matrix, interbedded with thinner layers of lower-density silty clay (Table 2.2). The base of the coarser laminations shows erosional contact with the underlying finer beds (thin sections in Table 2.2). Grain size analysis reveal large amounts of sand (26 % – 39 %) and silt (24 % – 32 %) in the < 2 mm fraction in this interval. The relative weight of the 125–800 μm and > 800 μm fractions also contributes considerably to the overall weight of the sediment (18 % and 11 %, respectively).

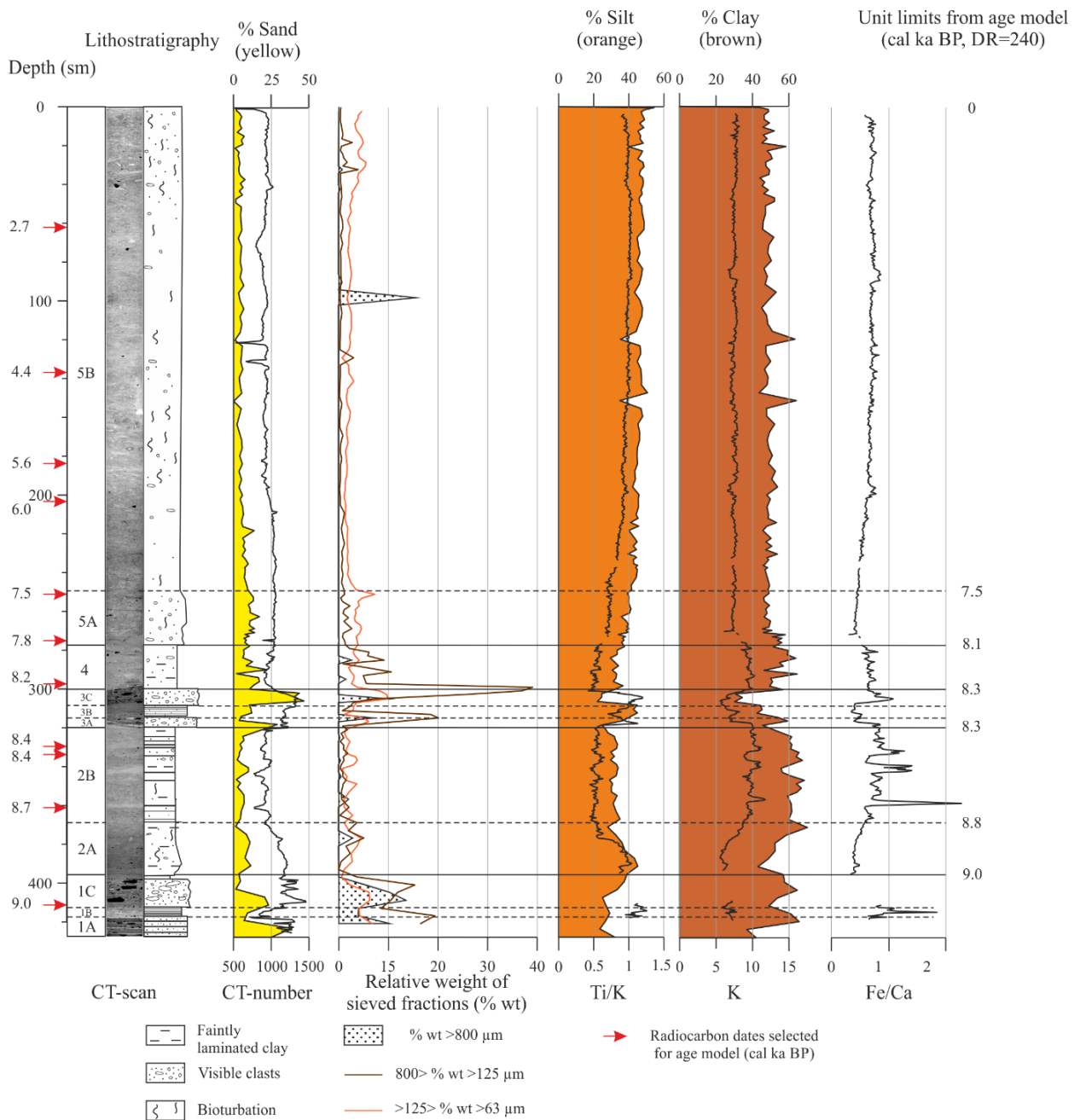


Figure 2.6: Sedimentological results and elemental signature of the detrital fraction of core AMD14-Kane2b. Laser diffraction grain size repartition (<2mm fraction) is shown as % sand, silt, and clay. Normalised Zr counts are not shown but their profile is similar to that of Ti.

Table 2.2: Details of CT scans and thin sections for each lithologic unit of core AMD14-Kane2b and summarised descriptions and interpretations. The paleo-environmental implications discussed in this study have been outlined here.

CT-scan	Lithostratigraphic representation	Thin sections	Unit	Description	Sedimentary process	Paleo-environmental implications
90 cm 100 cm			5B	Silty-clay matrix. Few limestones.	Hemipelagic sedimentation/ limited contribution of settling from meltwater plumes. Limited ice-rafting.	Glacial distal/hemipelagic sedimentation. Winnowing from strong subsurface currents. Moderate calving following the deceleration of glacial ice fluxes. Severe sea ice conditions.
250 cm 260 cm 270 cm			5A	Silty-clay matrix. Less frequent limestones in comparison to unit 4.	Less deposition from meltwater plumes. Less ice-rafting.	Greater distance of the ice margin to the core site (i. e. retreat of the GIS in eastern Kane Basin). Deceleration of glacial fluxes and/or increased sea ice.
280 cm 290 cm			4	Dominant clay. Frequent limestones.	Settling from meltwater plumes. Frequent ice-rafting	Distal glacial marine environment (O Cofaigh & Dowdeswell, 2001). Increased calving rates following the collapse of the glacial buttress in Kennedy Channel. Limited sea ice.
300 cm 310 cm 320 cm			3C 3B 3A	3C: Unsorted silt to gravel/ pebble in a clay matrix. Absence of grading 3B: Faintly laminated silty sediment. Limestones near-absent. 3A: Unsorted silt to gravel/ pebble in a clay matrix. Absence of grading	Iceberg-rafted sediment High energy water-transport predominant, minor ice-rafted debris Iceberg-rafted sediment	Increased calving rates resulting from accelerated glacial fluxes following the collapse of the glacial buttress in Kennedy Channel (MacGregor et al., 2016). Entrainment of sediment from northern Nares Strait associated to the establishment of the Hall Basin-Kane Basin connexion through Kennedy Channel. Collapse of the GIS/IIS ice saddle in Kennedy Channel.
340 cm 350 cm 360 cm			2B	Dominant clay, slightly laminated. Limestones less frequent in comparison to subunit 2A.	Settling from meltwater plumes. Ice-rafting less frequent.	Distal glacial marine environment (O Cofaigh & Dowdeswell, 2001). Increasing sea ice occurrence.
380 cm 370 cm			2A	Gradually finer material. Frequent limestones.	Settling from meltwater plumes. Occasional ice-rafting	Growing distance of the ice margin to the core site. Limited sea ice occurrence.
400 cm 410 cm 420 cm			1C 1B 1A	1C: Unsorted silt to gravel/ pebble in a clay matrix. Absence of grading 1B: Finely laminated sediment. Few or no limestones 1A: Interbedded coarse and fine laminae. Coarse laminations are occasionally graded	Iceberg-rafted sediment Settling of suspended sediment from meltwater plumes. Little to no ice-rafting. Meltwater plume deposits and small scale pro-glacial debris flows	Release of accumulated glacial ice flux following the breakup of sea ice and resulting in intense iceberg calving (Reeh et al., 2001). Proximal glacial marine environment under severe sea ice conditions (O Cofaigh & Dowdeswell, 2001) which may be related to the 9.3-9.2 cold event (Axford et al., 2009; Fisher et al., 2011) Ice marginal glacialmarine environment (O Cofaigh & Dowdeswell, 2001). GIS and/or IIS are close to/at the core site

These laminated deposits display all the characteristic of ice-proximal deposits (List, 1982; Ó Cofaigh and Dowdeswell, 2001). Unit 1A was most likely deposited at the ice sheet margin some *ca.* 9.0 cal. kyr ago, according to a dated mollusc shell at the base of unit 1C and given the very high sedimentation rates in ice-proximal environments.

Subunit 1B (416–410 cm) displays a sharp decrease in sediment density with the replacement of sand by finer material (60 % clay in the < 2 mm fraction; Figure 2.6, Table 2.2). While subunit 1B encompasses some clasts (CT scan in Table 2.2), the amount of sand and silt actually present in 1B may be lower than reflected by the laser diffraction and wet-sieving data, as the analysed samples likely included coarser material from the overlying and underlying subunits 1A and 1C. XRF data for subunit 1B show high Fe/Ca and Ti/Ca ratios and low Ca counts.

The finer grain size in this subunit is indicative of a change from an ice margin to an ice-proximal glacimarine environment in which suspended matter settling from turbid meltwater plumes is likely the main depositional process (Dowdeswell et al., 1998; Elverhøi et al., 1980; Hogan et al., 2016; Syvitski, 1991), although the limited thickness (4 cm) of subunit 1B is rather unusual for this process. The geochemical grain size tracers Ti/K and K show poor correlation with the relatively low silt and high clay content in subunit B2. While K counts are low, Ti/K ratios are high, which may suggest a high-energy environment, supporting the previous hypothesis of an ice-marginal environment in which meltwater pulses can transport relatively large particles. High Fe/Ca is evocative of an eastern origin of the sediments in subunit 1B, implying that the GIS was close to the core site.

Subunit 1C (410–394 cm) interrupts the fine-grained sedimentation with a sharp increase in the occurrence of oversized clasts. The coarser fractions account for a significant part of the sediment (up to 18 % for both the > 800 and 800–125 µm fractions) within a dominantly clayey matrix. Sediment density in subunit 1C increases to reach values similar to those observed in subunit 1A. However, unlike subunit 1A, subunit 1C is not laminated and clasts are larger (frequent gravel) and ungraded.

Given the high gravel content in subunit 1C, we consider the clasts to have been predominantly iceberg-rafted to the core location rather than sea-ice-rafted (Nürnberg et al., 1994; Pfirman et al., 1989). These large amounts of IRD among very poorly sorted material can be interpreted as (1) increased iceberg calving rates, (2) changes in the delivery of sediment by icebergs (increased melting of or dumping from icebergs), or (3) a severe decrease in the delivery of finer particles that increases the apparent contribution of clasts to the sediment (Hogan et al., 2016, and references therein).

Unit 2 (394–320 cm, 9.0–8.3 cal. ka BP) can be divided into two subunits based on grain size and density. The relative weight of the coarse fraction varies throughout unit 2 with a generally decreasing trend.

Subunit 2A (394–370 cm, 9.0–8.8 cal. ka BP) is composed of poorly sorted, bioturbated sediment (*ca.* 55 % clay and *ca.* 38 % silt in the < 2 mm fraction) with varying contributions of coarser material (between *ca.* 0 and 5 %) and occasional lonestones (Figure 2.6, Table 2.2). Sediment density is fairly high, but gradually decreases toward the

top of subunit 2A. Ti/K decreases gradually in this subunit, mirroring the decrease in density and opposing the increase in K counts. The Fe/Ca ratio is low at the base of subunit 2A before increasing upward in this subunit.

The dominance of fine particles in subunit 2A with occasional clasts points to a delivery by meltwater plumes and iceberg rafting. The decreasing Ti/K and silt content along with increasing K counts and clay suggests a growing distance of the ice margin from the core site since coarser silts and Ti-bearing minerals settle closer to the ice margin, while clay particles tend to sink in more ice-distal locations (Dowdeswell et al., 1998; Ó Cofaigh and Dowdeswell, 2001).

Increasing Fe/Ca in subunit 2A may indicate a growing contribution of Paleozoic carbonates on Ellesmere Island in western Kane Basin and/or Washington Land in northern Kane Basin (Figure 2.2).

The sediments of subunit 2B (370–320 cm, 8.9– 8.3 cal. ka BP) have a lower density and a lower sand and silt content than those of subunit 2A, while clay content reaches maximum values averaging 63 %. Scarce limestones occur in this subunit and the sediment appears to be faintly laminated. Four biogenic carbonate samples, both mollusc and mixed benthic foraminifera samples, were dated in subunit 2B, and high sedimentation rates of ca. 130 cm.ka⁻¹ decreasing upward to 90 cm.ka⁻¹ were calculated from the age model (Table 2.1, Figure 2.4). Subunit B2 is characterised by low Ti/K and high K and Fe/Ca.

These high sedimentation rates, substantial concentrations of clay, and the slightly laminated aspect of subunit 2B indicate that these sediments were mainly delivered by melt-water plumes in a more distal glacial setting (Ó Cofaigh and Dowdeswell, 2001). Relatively high Fe/Ca possibly reflects an increased contribution from eastern Kane Basin gneisses.

Unit 3 (320–300 cm, 8.3 cal. ka BP) stands out as a clast-rich interval. The high density of this unit is comparable to that of subunits 1A and 1C. CT scans and thin sections reveal the presence of a finer-grained horizon enclosed between coarser material, dividing this interval into three subunits (Table 2.2).

Subunit 3A (320–313 cm) corresponds to the lower clast-rich subunit. A significant portion of the bulk sediment is attributed to 800–125 µm sand (17 % wt) and > 800 µm sand (up to 7 % wt), while the clay matrix contributes to ca. 53 % of the < 2 mm fraction. Ti/K ratios are high, whereas Fe/Ca ratios and K have significantly decreased compared to the underlying subunit 2B (Figure 2.6).

The high clast content and absence of grading suggest that the sediments forming subunit 3A were ice-rafted and deposited at the core location (Ó Cofaigh and Dowdeswell 2001). The predominant carbonate (low Fe/Ca) material in this subunit likely originates from northern and/or western Kane Basin.

Faint laminations are visible on the CT scan images of subunit 3B (313–305 cm). The sediment of this subunit is composed essentially of clay and silt (47 % and 43 %, respectively) with a relatively low sand content (< 10 % in the < 2 mm fraction and each of the coarser fractions represents less than 3 % of the sediment weight). Ti/K ratios

have slightly decreased relative to 3A, but remain high and display a slightly increasing trend. K counts and Fe/Ca ratios remain low. Analysis of the sieved residues revealed the presence of benthic foraminifera in this subunit, which were picked and dated at ca. 9.4 ¹⁴CBP (9.9 cal. ka BP with $\Delta R = 240$; Table 2.1).

The poor sorting of sediments in subunit 3B could possibly indicate that they were ice-transported, but the near absence of clasts (e.g., in contrast to the overlying and underlying subunits of interval 3) contradicts this hypothesis. The modest contribution of clay along with the relatively high silt content rather points to the transport and deposition of these sediments by a high-velocity current. The elemental signature of this subunit (low Fe/Ca) denotes a probable northern and/or western Kane Basin origin. Concerning the old age yielded from the mixed benthic foraminifera picked in this subunit, the age model shows that these foraminifera were remobilised. It is possible that a small quantity of pre-Holocene foraminifera was mixed in with living fauna. This would imply that sediments predating the last glaciation (> 22 cal. ka BP) were preserved under the extended GIS and IIS in Nares Strait and were eroded and transported to the core site during the deposition of subunit 3B. An alternative explanation is that the sample is composed of postglacial specimens of a similar age which were eroded from the seabed and transported to the site.

Subunit 3C (305–300 cm) contains large amounts of coarse material with an average of 44 % sand and only 32 % clay in the < 2 mm fraction. The sand in this subunit is coarser than in 3A with the 800–125 μ m fraction contributing to ca. 34 % of the total sediment, while up to a further 10 % of the sediment weight is accounted for by the > 800 μ m fraction. Ti/K ratios (high) and K counts (low) are similar to subunit 3A, whereas Fe/Ca ratios are high in subunit 3C (Figure 2.5).

The very high clast content of subunit 3C along with high Ti/K ratios and the absence of grading are indicative of iceberg rafting and deposition. The shell fragment that was dated in the topmost horizon of this subunit (> 42 ¹⁴C BP) was clearly remobilised, likely by ice rafting. The sediment forming subunit 3C appears to originate from eastern Kane Basin (Figure 2.2) given the high Fe/Ca ratio. The age model points to rapid sedimentation of unit 3 with an age of 8.22 cal. ka BP on mixed benthic foraminifera picked from the horizon directly above unit 3, and an age of 8.38 cal. ka BP in a sample 7 cm below the base of unit 3 that extrapolates to ca. 8.29 cal. ka BP at 320 cm in the age model (Table 2.1, Figure 2.4).

Unit 4 (300–280 cm, 8.3–8.1 cal. ka BP) has a similar density and clay content (ca. 58 %) to subunit 2B. The contribution of sand in these sediments, however, is higher than in subunit 2B with ca. 6.5 % weight accounted for by > 125 μ m sand and ca. 14 % sand in the < 2 mm fraction. The elemental composition of unit 4 is also fairly similar to that of subunit 2B. Ti/K ratios are low, while K counts and Fe/Ca ratios are high (Figure 2.6).

The high clay content of unit 4 suggests that delivery from meltwater plumes was the dominant sedimentary process at play during this time interval. The substantial amount of sand in this unit indicates that a significant proportion of the sediment was also ice-rafted to the location. As previously mentioned, the increase in ice-rafted debris can indicate (1) increased calving rates when originating from iceberg rafting, (2) changes in iceberg delivery of

sediment (increased melting or dumping of icebergs), or (3) a decrease in the delivery of finer particles that increases the apparent contribution of clasts to the sediment (Hogan et al., 2016, and references therein). The high sedimentation rates (*ca.* 90 cm.ka⁻¹ from the age model and *ca.* 190 cm.ka⁻¹ from the linear interpolation between the dates at 297.5 cm (8.22 cal. ka BP) and 273.5 cm (8.09 cal. ka BP); Table 2.1, Figure 2.4) support this narrative of delivery by meltwater and ice rafting that are typically responsible for the transport and deposition of large quantities of sediment (Dowdeswell et al., 1998; Svendsen et al., 1992), while seemingly excluding the possibility of a significant decrease in the delivery of finer particles. High Fe/Ca values suggest that a notable portion of the sediments originates from the Precambrian gneisses of eastern Kane Basin, while the slightly decreasing trend displayed by this elemental ratio could potentially be linked to a progressive increase in the contribution of carbonate-rich formations from northern and/or western Kane Basin in this interval.

Unit 5 (280–0 cm, 8.1–0 cal. ka BP) clearly differs from underlying units with regard to the < 2 mm grain size fraction (Figure 2.6). The clay content drops to steady, lower values (49 % on average) and the CT scans show a generally homogenous sediment with frequent traces of bioturbation. Changes in grain size divide unit 5 into two subunits.

The sediments in subunit 5A (280–250 cm, 8.1–7.5 cal. ka BP) contain a relatively high proportion of sand peaking at 12 % in the < 2 mm fraction, while the combined contribution of the coarser fractions averages at *ca.* 5.5 % weight. Lonestones occur frequently and are visible in the CT scan images. K counts and Fe/Ca ratios drop sharply to lower values at the base of subunit 5A (Figure 2.6). Ti/K is low, but increases very discreetly toward the top of this subunit.

The significant decrease in clay particles in subunit 5A compared to units 4 and 2B suggests that delivery from meltwater plumes was reduced in this interval, either in relation to a decrease in glacial melting rates or to a more ice-distal setting. The sharp decrease in the Fe/Ca ratio between unit 4 and unit 5 is interpreted as a sudden reduction in the contribution of gneissic material in the sediments of core AMD14-Kane2b.

Subunit 5B (250–0 cm, 7.5–0 cal. ka BP) is generally homogenous with lonestones occurring sporadically throughout. The silt content increases gradually from *ca.* 40 to 47 % toward the top of the core. The contribution of the coarser fractions to the total sediment weight is fairly stable from the base to *ca.* 40 cm (1.9 cal. ka BP), where the 63–125 µm and > 125 µm fractions account for *ca.* 2 % and < 1 % of the total sediment weight, respectively. The relative weight of the 63–125 µm sand fraction doubles to *ca.* 4 % in the top 40 cm of the core (Figure 2.5). Both Fe/Ca and Ti/K ratios increase gradually until *ca.* 120 cm (*ca.* 4.1 cal. ka BP) after which they remain relatively high until the core top.

A sample of mixed benthic foraminifera yielded a radiocarbon age some 2 kyr older than expected at 238.5 cm. This sample probably contains a mixture of coeval and remobilised foraminifera (either by bioturbation or by water-ice transport from another location).

The overall limited contribution of the coarser fractions to the sediment of subunit 5B in comparison to the underlying

lithologic units indicates that ice delivery of sediment was reduced during this interval. Furthermore, the relatively low amounts of clay imply that meltwater delivery was also weakened. The sediments of subunit 5B were likely primarily water-transported to the core site (Gilbert, 1983; Hein and Syvitski, 1992). The increase in silt and Ti/K toward the top of the core suggests winnowing by an increase in bottom current (Bahr et al., 2014; Mulder et al., 2013). Relatively low sedimentation rates (20–50 cm.ka⁻¹) corroborate the narrative that delivery from meltwater plumes was limited in favour of a more hemipelagic sedimentation regime, also supported by the visible bioturbation in this subunit. The increase in fine sand in the most recent sediment may be due to a resumption of ice rafting over the last 1.9 cal. ka BP. The gradually increasing trend of Fe/Ca suggests that the contribution of carbonates from northern and/or western Kane Basin diminishes gradually between ca. 270 cm (ca. 7.9 cal. ka BP) in subunit 5A and ca. 120 cm (ca. 4.1 cal. ka BP) in subunit 5B after which it remains stable until the top of the core.

1.7 Discussion

Our study of core AMD14-Kane2b has enabled us to reconstruct a succession of depositional environments in Kane Basin following the retreat of the formerly coalescent GIS and IIS in Nares Strait (Figure 2.8). Here we discuss our reconstructions in light of other paleoceanographic and paleoclimatic studies to provide a broader view of the Holocene history of Nares Strait (Figures 2.6, 2.7, and 2.8, Table 2.2).

Previous studies have shown that the presence of erratic Greenland boulders on Ellesmere Island from Kennedy Channel to the northern entrance of Nares Strait attest to the coalescence of the IIS and GIS along the western side of northern Nares Strait during the Last Glacial Maximum (LGM) (e.g., England, 1999). The absence of such erratics along the western and southern coasts of Kane Basin implies that the confluence of the two ice sheets was further at sea in the southern half of the strait (England, 1999). Radiocarbon dating on samples from raised beaches provides minimum ages for marine ingress in Nares Strait. These ages are older in the northern and southern extremities of the strait, while only younger ages are yielded by samples in northern Kane Basin and Kennedy Channel, implying that a central (grounded) ice saddle persevered longer in the shallower sector of the strait (Bennike, 2002; England, 1999, and references therein). In addition to providing minimum ages for ice sheet retreat, ¹⁴C dating on marine-derived material in raised beaches enables one to identify the former shoreline and assess the glacio-isostatic readjustment of the continental crust. However, this approach can only provide minimum ages for (glacial ice-free) aquatic environments at a given place and time and does not necessarily correspond to the position of the ice margin, which can be several kilometres inland. Cosmogenic nuclide surface-exposure dating is an efficient method to temporally constrain inland ice sheet retreat. However, such investigations are scarce in Nares Strait: only two studies document the glacial retreat on Hans Island, off Greenland in Kennedy Channel (Zreda et al., 1999), and in Washington Land (Reusche et al., 2018). England's (1999) paleogeographical maps of ice sheet retreat in Nares Strait based on radiocarbon-dated molluscs were revised in Figure 2.8 in which offshore limits for the GIS and IIS are proposed based on our sedimentological and geochemical data from core AMD14-Kane2b. The continuous nature of our record also allows us to propose a more precise chronology of the deglaciation of central Nares Strait.

1.7.1 Ca. 9.0 cal. ka BP: ice sheet retreat in Kane Basin

Our archive demonstrates that marine sedimentation took place in Kane Basin as early as *ca.* 9.0 cal. ka BP. Grain size characteristics and sedimentary structures suggest that the laminated basal unit (1A) represents the topmost deposits in the ice-marginal environment shortly after ice sheet retreat at the core site (Figures 2.5 and 2.8-b, Table 2.2). The settling of meltwater plume sediments in the proximal glacial marine environment that followed (1B) is devoid of IRD and seems to have been interrupted by an iceberg-rafted interval (1C). The absence of molluscs predating 8.8 cal. ka BP in Kane Basin (England, 1999) likely indicates that following the deglaciation of Smith Sound *ca.* 9.9 cal. ka BP (Figure 2.8a–c, England, 1999), ice sheet retreat in Kane Basin occurred off the current coast where melting was potentially enhanced by the increasing influence of warmer Atlantic water from the West Greenland Current after 10.9 cal. ka BP, $\Delta R = 0$ (Funder, 1990; Kelly et al., 1999; Knudsen et al., 2008). Based on the sedimentary properties of subunit 1A, we propose that *ca.* 9.0 cal. ka BP, the GIS–IIS ice margin was located at the core site, completing the offshore area of England’s (1999) paleogeographical map for this period (Figure 2.8-b). The IRD-rich unit 1C, which appears to have been deposited by intense ice calving, could potentially mark the opening of Kennedy Channel. Our age of *ca.* 9.0 cal. ka BP for this unit agrees relatively well with the inferred age of an IRD-rich unit in a sediment core from Hall Basin that was interpreted as the opening of Kennedy Channel at *ca.* 8.6 cal. ka BP ($\Delta R = 240$) (Jennings et al., 2011). Alternatively, unit 1C could have been deposited during a readvance of the IIS–GIS in Kane Basin in relation to a cold event. Laurentide ice sheet readvances have been documented through the dating of end and lateral moraines on Baffin Island aged between 9 and 8 cal. ka BP (Andrews and Ives, 1978) and have been linked to colder periods. A particularly cold event *ca.* 9.2–9.3 cal. ka BP, which is reported in the regional literature from ice core (Fisher et al., 2012; Vinther et al., 2006) and lacustrine records (Axford et al., 2009), may be the source of the calving event in Kane Basin that led to the deposition of unit 1C. Reservoir ages in Kane Basin are likely to have been reduced prior to the collapse of the IIS–GIS ice saddle in Kennedy Channel and the arrival of poorly ventilated Arctic water. The age of unit 1 with $\Delta R = 0$ is 9.3 cal. ka BP, which suggests to us that subunit 1C could well have been deposited during the 9.2–9.3 cal. ka BP cold event.

1.7.2 Ca. 9.0–8.3 cal. ka BP: ice-proximal to ice-distal environment in Kane Basin

The increasingly finer particles that compose unit 2 suggest a growing distance between the core site and the ice margin. The dominant sedimentary process at play is settling from meltwater plumes, which is typically responsible for high sedimentation rates, along with frequent delivery of IRD (Table 2.2). The Early Holocene was characterised by high atmospheric temperatures during the Holocene Thermal Maximum (HTM) occasioned by greater solar insolation (Bradley, 1990). The HTM has been defined for the eastern sector of the CAA as the period between 10.7 and 7.8 cal. ka BP based on the Agassiz ice core record (Lecavalier et al., 2017). The high melting rates of the ice sheets during the HTM (Fisher et al., 2011) likely enhanced the delivery of particles by meltwater and contributed to the high sedimentation rates observed in our core. More distant glacial ice from the site is also in good agreement with the occurrence of molluscs dated between 8.8 and 8.4 cal. ka BP on Ellesmere Island and Northwest Greenland (Figure 2.8-c, England, 1999). The elemental signature of subunit 2B may suggest, however,

that the GIS was still present in eastern Kane Basin and delivered material derived from the gneiss basement to the core site. The volcanic clastics on Ellesmere Island may have also contributed to Fe counts in our geochemical record, but we consider their input marginal given the limited surface of this geological unit compared to the gneiss and crystalline basement, which outcrops in much of Inglefield Land and underlays Humboldt Glacier (Dawes and Garde, 2004). Furthermore, the IIS was a cold-base ice sheet (e.g., Dyke et al., 2002; Tushingham, 1991) and as such likely delivered overall less sediment from meltwater than the warm-based GIS. The occurrence of IRD in unit 2 may imply that relatively open water conditions occurred during this interval, enabling icebergs to drift in Kane Basin, although this may simply be a consequence of high calving rates as the GIS and IIS retreat. Reduced sea ice occurrence in Kane Basin during the Early Holocene would be in good agreement with low sea ice concentrations reported nearby in Lancaster Sound (from 10 to 6 cal. ka BP, $\Delta R = 290$ years, Vare et al., 2009; from ca. 10–7.8 cal. ka BP, $\Delta R = 335$, Pieńkowski et al., 2012). However, while the decreasing trend of the coarse fraction in unit 2 may indicate more stable sea ice conditions (or decreasing calving rates) toward the end of the interval, fluctuations in the coarse fractions in our record may also suggest that sea ice conditions were variable. This is in line with both decreasing atmospheric temperatures towards the end of the HTM (Lecavalier et al., 2017) and the Knudsen et al. (2008) observations of variable West Greenland Current influence and sea ice conditions between 9.5 and 8.2 cal. ka BP in northernmost Baffin Bay.

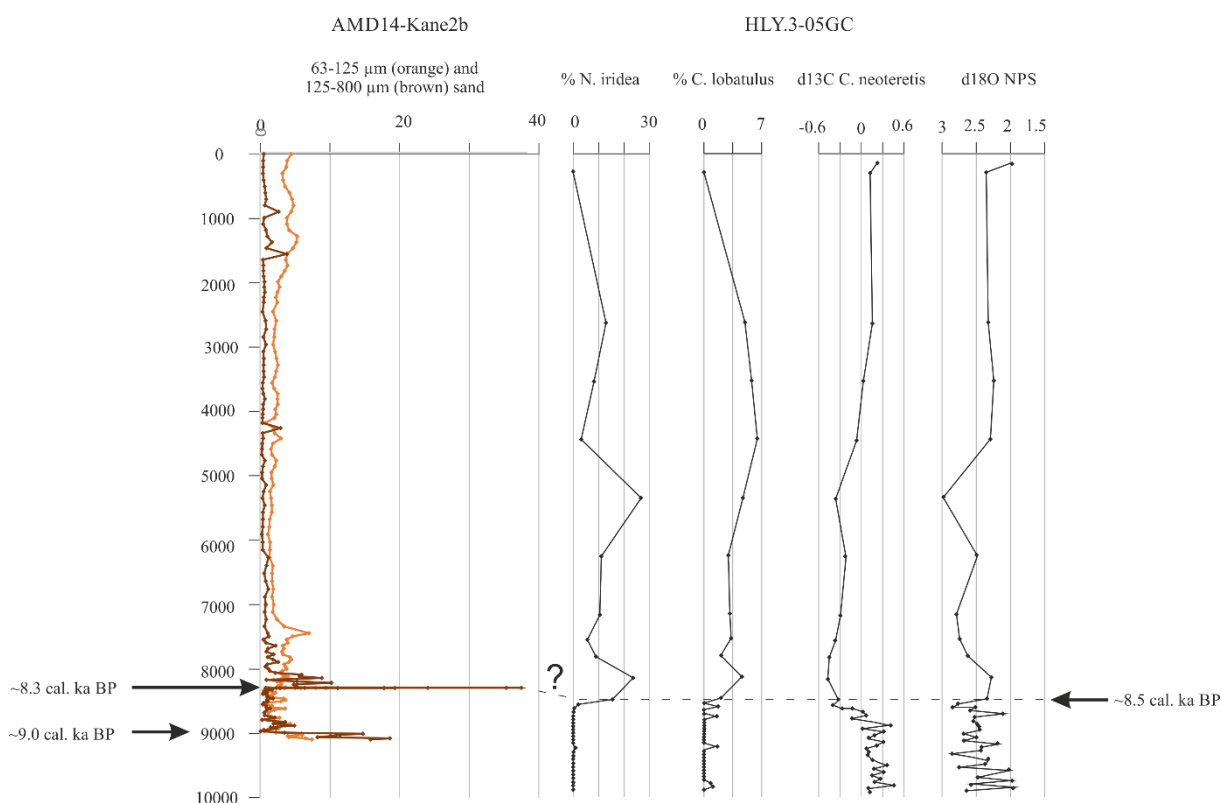


Figure 2.7: Comparison of sieved grain size data from AMD14-Kane2b and paleoceanographic proxies from HLY03-05CG in Hall Basin (Jennings et al., 2011). Radiocarbon ages presented in Jennings et al. (2011) were calibrated with $\Delta R = 240 \pm 51$ (Table 2.4 in the Supplement) years and the age model for core HLY03-05CG is a linear

interpolation between the calibrated ages.

1.7.3 Ca. 8.3 cal. ka BP: the opening of Kennedy Channel

Unit 3 appears to be primarily iceberg-rafted, with an inclusion of a finer, water-transported silty subunit (3B). A foraminifera-derived radiocarbon age obtained from subunit 3B (Table 2.1) suggests sediment remobilisation within this time interval. If we consider unit 3A to have been deposited by the passing over Kane Basin of glacial ice having broken up in Kennedy Channel, then a plausible origin for unit 3B could be the entrainment of sediment from northern Nares Strait associated with the discharge of large amounts of water as the connection was established. The absence of any molluscs in Kennedy Channel predating 8.1 cal. ka BP further suggests that Kennedy Channel was still blocked until then, although this method can only provide minimum ages for ice sheet retreat (Figure 2.8e–g). This proposed age for the opening of Kennedy Channel is only slightly younger than that proposed by Jennings et al. (2011), i.e. ca. 8.6 cal. ka BP ($\Delta R = 240$ years, Figure 2.7), based on the estimated age of an IRD event in Hall Basin, northern Nares Strait (core HLY0305GC). Both ages can be reconciled assuming that bottom waters in Hall Basin were probably poorly ventilated before the opening of the strait, inducing a higher reservoir age in the northern sector of Nares Strait. Furthermore, one might consider the possibility that the transitional IRD-rich unit in core HLY03-05GC that is interpreted by Jennings et al. (2011) as representing the opening of Kennedy Channel might in fact represent instabilities in the GIS–IIS prior to – and eventually leading to – the complete opening of the strait. If so, the transition from laminated to bioturbated mud in the Hall Basin sediment record which, according to X-radiography, CT scans, and the age model of core HLY0305GC, occurred close to 8.5 cal. ka BP, i.e. ca. 100 years after the deposition of the IRD-rich unit (Jennings et al., 2011), might in fact represent the true opening of Nares Strait (i.e. change from a rather confined Hall Basin to a ventilated environment under the influence of a strong southward current). Finally, we assume that the collapse of glacial ice in Kennedy Channel was more likely to have been recorded as an IRD-rich interval south of the channel (i.e. Kane Basin) in the direction of the presumable southward flow, rather than to the north.

It has recently been demonstrated that the Humboldt Glacier retreated from a previous position of stability ca. 8.3 ± 1.7 ka BP based on surface-exposure dating of an abandoned lateral moraine in Washington Land (Reusche et al., 2018). This instability in the Humboldt Glacier may have been linked to the break-up of glacial ice in Kennedy Channel. Furthermore, the onset of decreasing land-fast sea ice on the northern coast of Ellesmere Island and northern Greenland after 8.2 cal. ka BP (England et al., 2008; Funder et al., 2011) may have been associated with the flushing of ice through Nares Strait after the opening of Kennedy Channel. The local temperature drop recorded in the Agassiz ice core (Lecavalier et al., 2017) and, as suggested by Reusche et al. (2018), in Baffin Bay lacustrine records (Axford et al., 2009) may have been associated with oceanographic and atmospheric reorganisation resulting from the opening of Kennedy Channel, as well as the “8.2 event”. Given the excellent correspondence between the aforementioned evidence, we consider subunits 3A and 3B to have been deposited as the ice saddle in Kennedy Channel broke up. The high carbonate signal in the elemental data (Figure 2.6) also suggests that the sediments from subunits 3A and 3B originated from northern Nares Strait (Figure 2.2) rather than the Humboldt

Glacier alone.

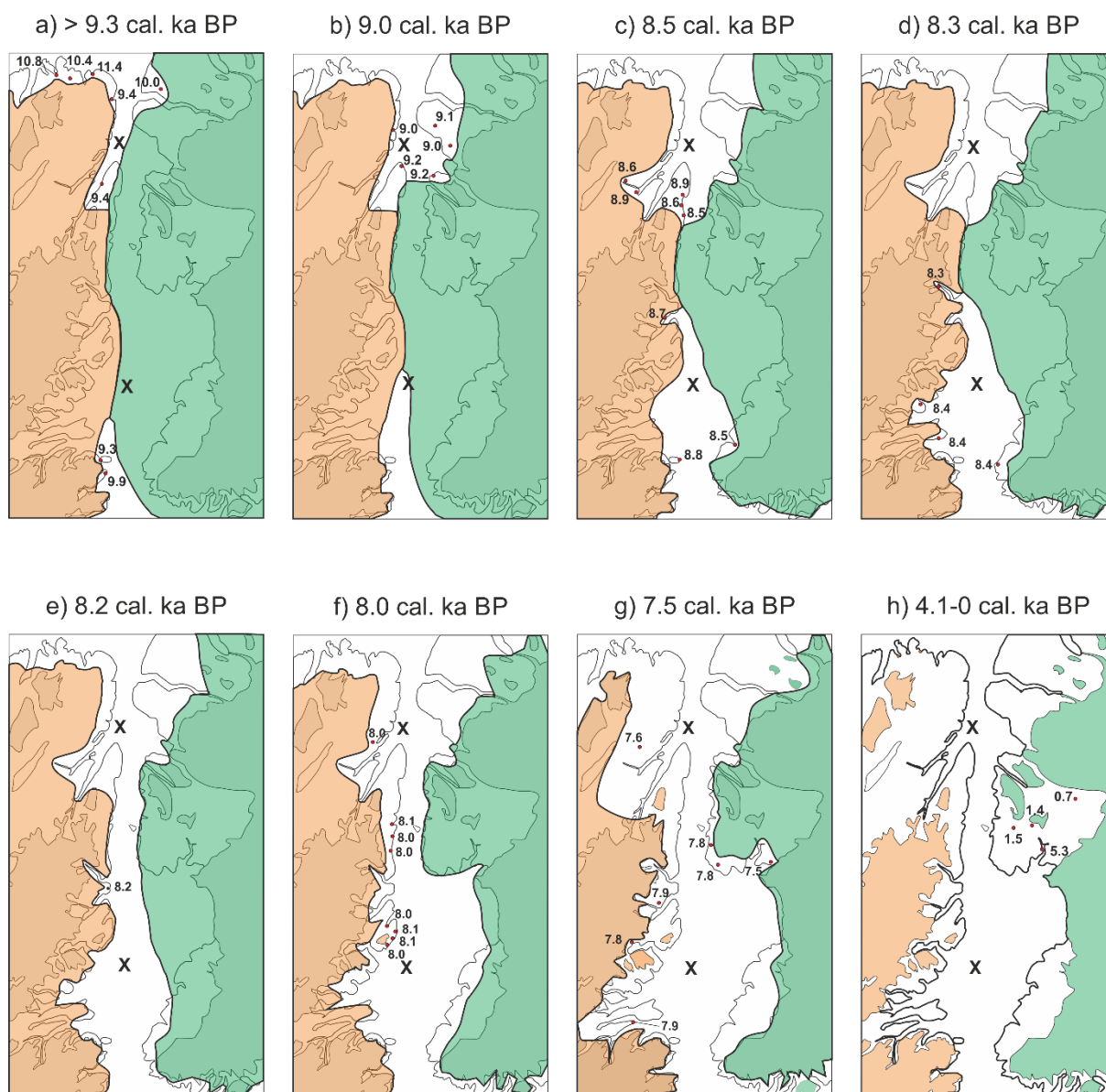


Figure 2.8: GIS and IIS retreat in Nares Strait. Adapted from England (1999) and including data from Bennike (2002) for Washington Land. Locations for core AMD14-Kane2b in Kane Basin and HLY03-05 (Jennings et al., 2011) in Hall Basin are marked by crosses. All mollusc ages from England (1999) were calibrated with $\Delta R = 240$ using Calib 7.1 (Stuiver et al., 2020) after first adding 410 years to the calibrated ages presented in England (1999) (Table 2.3 and Figure 2.10 in the Supplement). The position of the GIS and IIS margins offshore in Kane Basin are deduced from our sedimentological and geochemical data, while their locations in Hall Basin are deduced from the data presented in Jennings et al. (2011) and Jakobsson et al. (2018).

The dominant depositional process in subunit 3C is iceberg rafting based on the abundance of clasts in this interval. The elemental composition of subunit 3C suggests that the sedimentary material likely originates from the GIS in eastern Kane Basin (Figure 2.2). Investigations into the internal stratigraphy of the GIS and their comparison

to north Greenland ice cores have demonstrated that the collapse of the ice saddle in Kennedy Channel triggered the acceleration of glacial fluxes along Nares Strait (MacGregor et al., 2016). The destabilisation of the GIS following the collapse of the ice saddle may have provoked intense calving that led to the deposition of subunit 3C. In this regard, intense calving of the Humboldt Glacier as recently dated by Reusche et al. (2018) at 8.3 ± 1.7 ka BP might explain the observed elemental signature of the top part of unit 3.

However, the Reusche et al. (2018) findings also offer an alternative scenario for the deposition of unit 3. Intense calving of the Humboldt Glacier may have occurred as it retreated in eastern Kane Basin and abandoned a lateral moraine in Washington Land ca. 8.3 ± 1.7 ka BP (Reusche et al., 2018). This alternative scenario alludes to the possibility that the opening of Kennedy Channel may rather have occurred ca. 9.0 cal. ka BP (unit 1C). The elemental signature of subunit 3A and 3B does not, however, point to an eastern source and rather supports a northern–western origin of these sediments.

1.7.4 Ca. 8.3-8.1 cal. ka BP: increased iceberg delivery to Kane Basin

The abundance of iceberg-rafted debris has increased considerably in unit 4 compared to unit 2. This is possibly the result of the aforementioned acceleration of the GIS and IIS along Nares Strait following the collapse of the ice saddle in Kennedy Channel (MacGregor et al., 2016), as well as the arrival of icebergs from new sources to Kane Basin situated in northern Nares Strait. The retreating GIS in eastern Kane Basin was likely a primary source of icebergs during this period. However, the high clay content in our record implies that the GIS was still relatively close to the core site and had not yet fully retreated in eastern Kane Basin, contributing to the high sedimentation rates recorded in this unit (Figure 2.8-e).

1.7.5 Ca. 8.1-7.5 cal. ka BP: rapid retreat of the GIS in Kane Basin

The abrupt decrease in clay content and sedimentation rates at 280 cm in our record implies that the ice margin abruptly retreated ca. 8.1 cal. ka BP (Figure 2.6, Figure 2.8-f). The equal drop in Fe/Ca ratios suggests that it was probably the GIS that retreated rapidly in eastern Kane Basin. This abrupt retreat may have been initiated by the removal of the glacial buttress in Kennedy Channel (unit 3). The subsequent decrease in the $> 125 \mu\text{m}$ fraction may be associated with the onset of the deceleration of glacial fluxes along Nares Strait, as well as more distant glacial ice in eastern Kane Basin resulting from the retreat of the GIS. The timing of the retreat of the GIS in eastern Kane Basin corresponds remarkably well with the aforementioned abandonment of a lateral moraine by the Humboldt Glacier (Reusche et al., 2018). The authors in this recent study warn that two samples may be contaminated by previous exposure and that the age of abandonment of the moraine is likely to be younger than the proposed 8.3 ± 1.7 ka BP. Given the uncertainties in our radiocarbon dataset (analytical errors and ΔR uncertainties) and in the Reusche et al. (2018) surface-exposure dataset, both our dating of the opening of Kennedy Channel and the retreat of Humboldt Glacier are within the uncertainty range of the dating of the abandonment of the moraine by the Humboldt Glacier. It is thus difficult to distinguish whether this event was linked to the deglaciation of Kennedy Channel at ca. 8.3 cal. ka BP or whether it was delayed until ca. 8.1 cal. ka BP after the

cold “8.2 event” that may have brought a short period of stability to the GIS.

1.7.6 Ca. 7.5-0 cal. ka BP: deglaciation of Washington Land

The low Fe/Ca ratios at the beginning of this interval are likely related to the erosion and delivery of material from Washington Land and a decrease in the delivery of crystalline material by the GIS (Figure 2.6). The progressive increase in Fe/Ca between 7.5 and 4.1 cal. ka BP can be linked to the deglaciation of Washington Land. The oldest molluscs found on the southern coast of Washington Land are dated between 7.8 and 7.5 cal. ka BP, while specimens found in morainic deposits imply that the extent of the GIS reached a minimum between 4 and 0.7 cal. ka BP (Figure 2.7, Bennike, 2002). The decrease in the coarser fractions in our core after ca. 7.5 cal. ka BP may be the result of reduced marine termini of the GIS and hence less calving as the Greenland coast became deglaciated (Figure 2.8-g, Bennike, 2002). Increasing silt and Ti/K in our core suggest winnowing by stronger bottom water currents. We propose that as the glacio-isostatic rebound lifted the continental crust in Nares Strait, the seabed was progressively brought closer to the stronger subsurface currents. The isostatic rebound in Kane Basin has been estimated to be between 80 and 120 m (England, 1999, and references therein), which would have had considerable consequences on bottom water velocities. Interestingly, increased sedimentation rates in Kane Basin between ca. 4.5 and 2.8 cal. ka BP (Figure 2.3) coincide with a period of atmospheric warming recorded in the Agassiz ice core (Lecavalier et al., 2017). These higher sedimentation rates may have been associated with increased delivery of sediment by meltwater from the GIS and the residual ice caps on Ellesmere Island during a warmer period. The increase in the contribution of the coarse fraction in core AMD14-Kane2B over the last 1.9 kyr is suggestive of minimal seasonal sea ice and/or higher calving rates over the last 2 millennia in Kane Basin. This broadly coincides with low absolute diatom abundances in northernmost Baffin Bay, attesting to poor productivity rates after 2.0 cal. ka BP; $\Delta R = 0$ (Knudsen et al., 2008). The “bridge dipole” between Kane Basin and northernmost Baffin Bay entails the following: when sea ice conditions in Kane Basin are strong, surface conditions to the south of Smith Sound are largely open with the North Water polynya being productive and vice versa (Barber et al., 2001). This inverse relationship between sea ice conditions in Kane Basin and northernmost Baffin Bay has probably been true for at least the past ca. 2 kyr. Recent instabilities in the ice arch in Kane Basin that have led to increased sea ice export towards northernmost Baffin Bay have been observed by satellite imagery and hence are only documented for the past few decades. Together with the Knudsen et al. (2008) study in northern Baffin Bay, our results suggest that these instabilities may have begun as early as ca. 2 cal. ka BP. Late Holocene decreases in sea ice occurrence, indicative of milder conditions, were also documented in other sectors of the CAA such as in Barrow Strait between 2.0 and 1.5 cal. ka BP (Pienkowski et al., 2012) or in the adjacent Lancaster Sound between 1.2 and 0.8 cal. ka BP (Vare et al., 2009).

1.8 Conclusion

Our investigation of core AMD14-Kane2b has provided, for the first time, a paleoenvironmental reconstruction in Kane Basin over the last ca. 9.0 kyr. The confrontation of our dataset with both land-based (Bennike, 2002; England, 1999; Reusche et al., 2018) and marine (Jennings et al., 2011) evidence offers several alternative paleo-

environmental interpretations for our record. Of particular interest is the determination of which of the two IRD-rich units (unit 1C dated at ca. 9.0 cal. ka BP or unit 3 dated at ca. 8.3 cal. ka BP) in core AMD14-Kane2b might represent the opening of Kennedy Channel. We consider the evidence to be in favour of a later collapse of glacial ice in Kennedy Channel ca. 8.3 cal. ka BP that may have been linked to instabilities in the Humboldt Glacier ca. 8.3–8.1 cal. ka BP (Reusche et al., 2018). Our findings concerning the successive paleoenvironments in this central sector of Nares Strait following ice sheet retreat can be summarised as follows.

While evolving from a short-lived ice-proximal depositional environment at ca. 9.0 cal. ka BP to a rather secluded and narrow bay as the ice sheets retreated, compelling evidence indicates that Kane Basin was not connected to Hall Basin until the collapse of the GIS–IIS saddle in Kennedy Channel at ca. 8.3 cal. ka BP. The collapse of the glacial buttress in Kennedy Channel may have triggered the acceleration of glacial fluxes toward Nares Strait, increasing calving and iceberg-rafted debris in Kane Basin between 8.3 and 7.5 cal. ka BP. Instabilities in the GIS eventually resulted in the rapid retreat of glacial ice from eastern Kane Basin at 8.1 cal. ka BP. As the basin underwent shoaling induced by the glacio-isostatic rebound, the retreat of the GIS in Washington Land gradually reduced inputs of carbonate material to Kane Basin. A possible deterioration in sea ice conditions and/or increased iceberg release appear to have taken place over the last ca. 2 kyr and correspond with lower sea ice occurrence in other sectors of the CAA.

This archive provides a new viewpoint that has enabled us to propose a continuous timeline of the events related to the deglaciation of Kane Basin, which until now relied entirely on land-based studies. Our study suggests that the “bridge dipole” presented in Barber et al. (2001), in which warmer (colder) years exhibit more (less) sea ice in Smith Sound and less (more) ice in Nares Strait, may be extrapolated over the last 2 millennia. Future investigations into the Holocene variability of sea ice conditions in Kane Basin may provide a more comprehensive view on its controlling effect on the North Water polynya. High productivity rates in the North Water, however, are also fuelled by the throughflow of nutrient-rich Pacific water via Nares Strait, and further investigation into how oceanographic circulation responded to postglacial changes in Nares Strait will provide more insight into the Holocene evolution of this highly productive area of the Arctic. Other than emphasising the need for further research into local reservoir age corrections, our study is inclined to contribute to future work on the export of low salinity Arctic water and Holocene variations of deep water formation (Hoogakker et al., 2015; Moffa-Sánchez and Hall, 2017).

Acknowledgements: Eleanor Georgiadis’ studentship is funded by both the Initiative d’Excellence (IdEx) programme of the University of Bordeaux and the Natural Science and Engineering Research Council of Canada (NSERC). We would like to thank Anne Jennings, Sofia Ribeiro, Audrey Limoges, and Karen Luise Knudsen for constructive conversations on the history of the North Water Polynya and Benoit Lecavalier for having shared with us the much appreciated Agassiz ice core temperature record. We also extend our gratitude to Sebastien Zaragosi and Bernard Martin, who prepared and helped interpret thin sections, and Isabelle Billy, Pascal Lebleu, Olivier Ther, and Caroline Guilmette for analytical support. This work is supported by the Fondation Total, the French Agence

Nationale de la Recherche (GreenEdge project), the Network of Centres of Excellence ArcticNet, and the European Research Council (StG IceProxy). Finally, we wish to thank the CCGS *Amundsen* captain, officers, and crew for their support during the 2014 ArcticNet cruise.

Edited by: Ed Brook

Reviewed by: two anonymous referees

1.9 Supplements

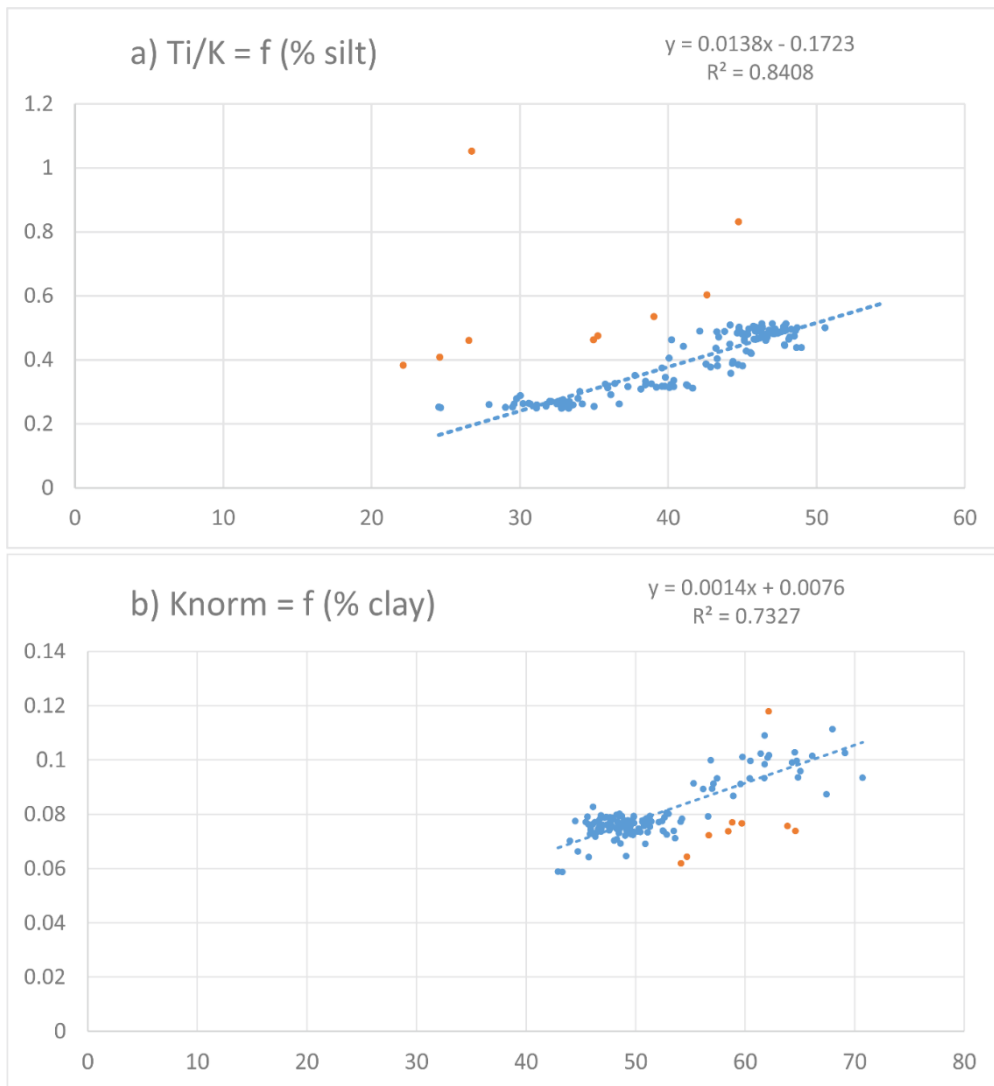


Figure 2.9: XRF data plotted against grain size data. a) $Ti/K = f(\% \text{ silt})$ shows a correlation factor $r^2=0.84$ when 9 outlying data points are omitted (shown in orange). b) $K_{norm} = f(\% \text{ clay})$ shows a correlation factor $r^2=0.73$ when 9 outlying data points are omitted (shown in orange).

Table 2.3: radiocarbon ages as reported in England (1999) and Bennike (2002) and calibrated with $\Delta R = 240 \pm 51$ years.

# on map	Laboratory dating number	age (yr BP)	¹⁴ C age	err	Lat	Long	Median age $\Delta R = 240 \pm 51$	$\sigma 1$	Original reference
1	GSC-1815	10100	10510	210	82°27	62°40	11386	11070 - 11740	England (1977, 1983)
2	S-1984	9825	10235	460	82°42	64°45	10781	10111 - 11378	England (1983)
3	GSC-3744	9580	9990	140	82°42	68°15	10668	10483 - 10867	England (1985)
4	S-1985	9270	9680	1055	82°30	64°15	10358	8991 - 11706	England (1983)
5	S-2307	9070	9480	150	81°49	58°40	10010	9807 - 10218	England (1985)
6a	TO-226	9010	9420	150	78°36	74°45	9938	9746 - 10159	Blake (1992)
6b	GSC-2516	8940	9350	100	78°36	74°45	9854	9683 - 10028	Blake (1992)
6c	TO-225	8840	9250	50	78°36	74°45	9681	9575 - 9759	Blake (1992)
7	TO-136	8520	8930	80	81°23	66°53	9352	9274 - 9450	England (1999)
8	SI-5551	8600	9010	90	82°08	62°03	9431	9345 - 9521	Retelle (1986)
9	GSC-3314	8470	8880	100	78°43	74°43	9291	9183 - 9427	Blake (1992)
10	DIC-737	8380	8790	105	81°33	64°30	9187	9036 - 9307	England (1985)
11a	SI-5855	8280	8690	90	81°35	60°55	9068	8963 - 9210	England (1985)
11b	S-2313	8295	8705	120	81°35	60°54	9082	8943 - 9270	England (1985)
12a	S-1990	8255	8665	215	81°53	63°20	9006	8723 - 9289	England (1985)
12b	GSC-3041	8050	8460	120	81°53	63°20	8746	8587 - 8918	England (1985)
13a	SI-5856	8230	8640	85	82°01	58°55	8994	8858 - 9124	England (1985)
13b	S-2309	8205	8615	135	82°01	58°55	8946	8730 - 9132	England (1985)
14	SI-5857	8225	8635	95	81°18	61°21	8984	8840 - 9128	England (1985)
15	DIC-549	8200	8610	260	81°15	65°45	8936	8604 - 9252	England (1983)
16	GSC-1775	8130	8540	200	81°32	68°58	8850	8573 - 9091	England (1983)
17	GSC-3286	8060	8470	70	78°41	74°07	8756	8626 - 8866	Blake (1992)
18	TO-3450	8050	8460	90	80°10	71°11	8744	8598 - 8870	England (1996)
19	GSC-2843	7960	8370	150	81°04	66°19	8643	8425 - 8803	England et al. (1981)
20	TO-434	7870	8280	90	81°03	66°38	8505	8394 - 8588	England (1996)
21	GSC-3179	7860	8270	270	81°41	69°08	8549	8233 - 8882	England (1983)
22a	S-2408	7825	8235	130	81°46	59°08	8472	8318 - 8604	England (1985)
22b	GSC-3693	7740	8150	90	81°46	59°08	8373	8283 - 8474	England (1985)
22c	S-2301	7965	8375	115	81°46	59°08	8638	8451 - 8775	England (1985)
23	L-1091E	7800	8210	200	~78°38	~71°00	8461	8194 - 8672	Nichols (1969)
24	TO-923	7780	8190	70	~78°39	71°01	8413	8342 - 8484	Blake et al. (1992)
25	TO-4192	7770	8180	70	79°30	74°59	8403	8332 - 8474	England (1996)
26	S-2109	7755	8165	125	81°40	65°20	8391	8266 - 8535	England (1983)
27	GSC-3710	7730	8140	120	79°04	75°30	8363	8233 - 8492	Blake (1987)
28a	TO-3778	7650	8060	60	80°30	70°43	8284	8218 - 8348	England (1996)
28b	TO-3464	7630	8040	60	80°30	70°43	8266	8199 - 8328	England (1996)
29	TO-3766	7540	7950	70	80°13	70°08	8176	8100 - 8278	England (1996)
30	TO-2919	7490	7900	60	80°47	67°55	8116	8032 - 8177	England (1996)
31	TO-4210	7480	7890	60	79°45	71°22	8106	8028 - 8168	Gualtieri and England 1977
32	S-2139	7385	7795	375	81°41	66°21	8042	7636 - 8389	England (1983)
33	TO-3765	7400	7810	70	80°37	69°15	8035	7955 - 8107	England (1996)
34a	TO-2922	7340	7750	70	80°42	68°29	7971	7892 - 8046	England (1996)

34b	TO-2925	7620	8030	600	80°42	68°29	8337	7664 - 8977	England (1996)
35a	TO-4200	7370	7780	70	79°53	71°34	8001	7925 - 8078	England (1996)
35b	GSC-5668	7320	7730	80	79°54	71°30	7950	7855 - 8025	England (1996)
36	TO-4214	7430	7840	70	79°49	71°07	8061	7987 - 8138	Gualtieri and England 1977
37	TO-4211	7390	7800	70	79°41	72°17	8022	7946 - 8098	Gualtieri and England 1977
38	TO-4198	7310	7720	70	80°10	71°28	7939	7859 - 8005	England (1996)
39	GSC-3700	7300	7710	140	79°06	76°05	7931	7782 - 8079	Blake (1988)
40	TO-4191	7190	7600	70	79°53	74°15	7822	7755 - 7909	England (1996)
41	S-2110	6995	7405	130	81°47	67°37	7643	7517 - 7764	England (1983)
42	SI-3300	6860	7270	70	81°17	69°25	7518	7454 - 7573	England (1983)
43	GSC-5670	6650	7060	190	80°04	72°19	7322	7151 - 7517	England (1996)
44	TO-3467	6500	6910	70	80°32	70°43	7199	7132 - 7284	England (1996)
45	TO-2918	6490	6900	90	80°55	67°54	7184	7082 - 7291	England (1996)
46	GSC-1614	6430		150	81°11	70°17		Driftwood	England (1977, 1983)
47	GSC-2370	6400	6810	100	79°54	63°58	7079	6966 - 7202	Blake (1987)
48	GSC-2334	5980	6390	70	81°04	63°35	6582	6490 - 6661	Blake (1987)
49	GSC-1755	6000		150	81°04	70°00		Driftwood	England (1977, 1983)
50a	Beta-91863	5920	6330	60	79°09	78°13	6517	6442 - 6594	England (1999)
50b	GSC-6088	5940	6350	90	79°09	78°13	6350	6433 - 6640	England (1999)
51	AAR-5768	8820	75	25	81°10.6	63°20.5	9225	9409 - 9539	Bennike 2002
52	AAR-5769	8010	75	25	81°10.1	63°04.9	8237	8389 - 8539	Bennike 2002
53	AAR-5766	6870	50	24	79°55.5	64°04.3	7162	7328 - 7427	Bennike 2002
54	AAR-5762	7240	65	23	79°56.5	64°17.1	7495	7636 - 7775	Bennike 2002
55	AAR-5755	6410	55	22	80°05.8	64°39.4	6605	6810 - 6961	Bennike 2002
56	AAR-5758	7090	80	21	80°24.0	66°58.2	7364	7496 - 7640	Bennike 2002
57	AAR-5757	7570	65	20	80°12.6	67°11.9	7793	7957 - 8102	Bennike 2002
58	AAR-5761	6890	60	19	80°21.5	67°18.7	7181	7338 - 7458	Bennike 2002
59	AAR-5760	7580	55	18	80°18.7	67°23.6	7803	7972 - 8103	Bennike 2002
60	AAR-5755	5165	55	19	80°08.8'	64°20.2'	5255	5470 - 5578	Bennike 2002
64	AAR-5772	1400	60	6	80°33.1'	67°11.1'	712	892 - 1027	Bennike 2002
61	K-7142	1310	35	15	80°09.4'	63°39.6'	638	609 - 672	Bennike 2002
62	K-7138	2170	55	38	80°23.9'	65°18.1'	1477	1693 - 1834	Bennike 2002
63	AAR-5531	2070	55	39	80°24.9'	64°20.0'	1376	1563 - 1706	Bennike 2002

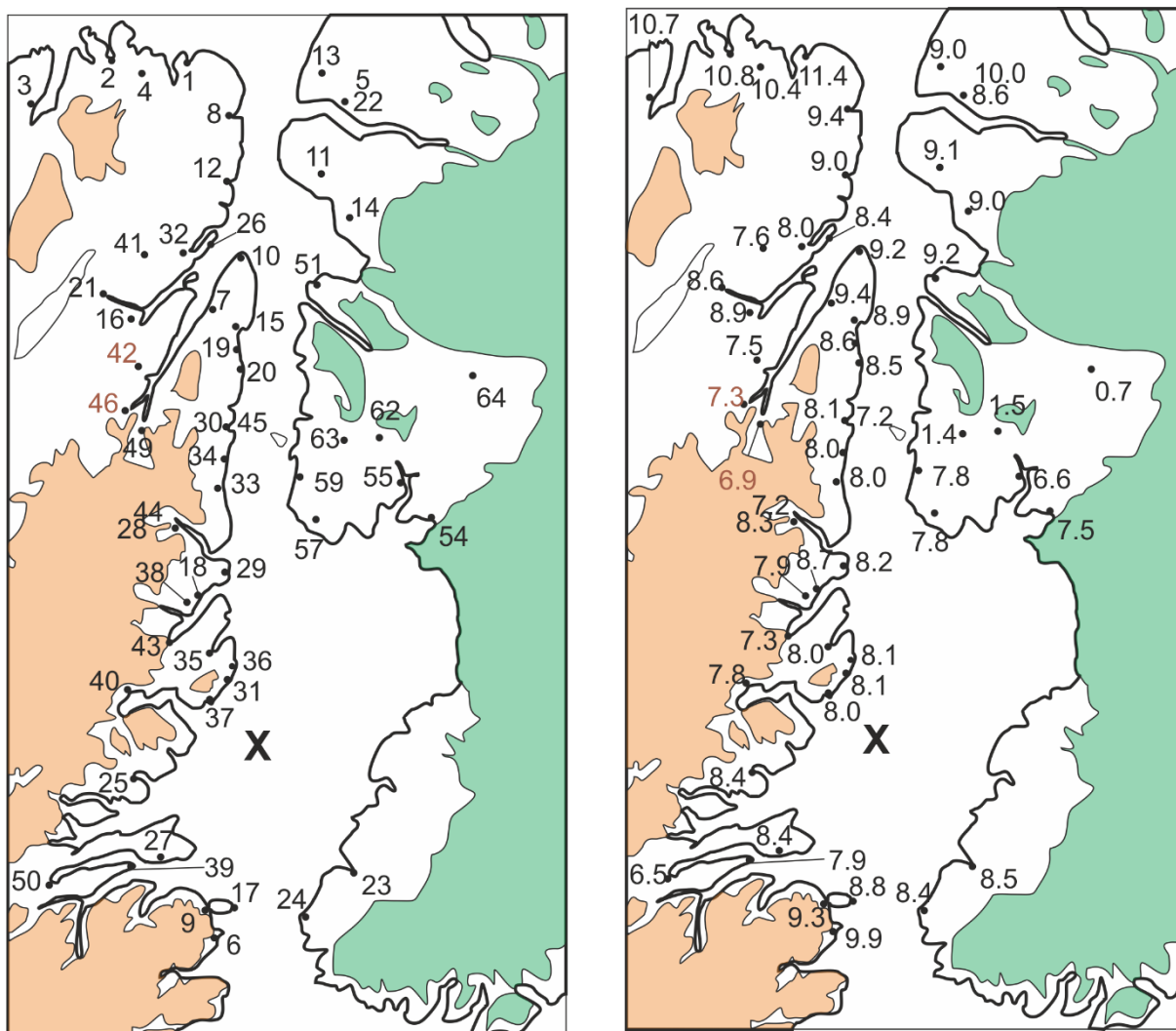


Figure 2.10: location of the radiocarbon ages in Nares Strait reported in England (1999) and Bennike (2002) and their calibrated with $\Delta R = 240 \pm 51$ years.

Table 2.4: Radiocarbon dated material from core HLY03-05CG (Jennings et al., 2011), calibrated with $\Delta R = 240 \pm 51$ years.

Depth in core (cm)	Laboratory number	¹⁴ C age	Material dated	Median age (ΔR=240)	1σ ΔR=240
0-2	AA-81309	530 ±53	<i>Bathyrca glacialis</i>	~290	
8-10	NOS -71686	3100 ±35	NPS	2636	2595 - 2709
28-30	NOS -71687	5040 ±40	NPS	5087	5010 - 5140
58-60	NOS -71688	6870 ±45	NPS	7164	7120 - 7234
68-70	AA-81310	7302 ±61	NPS	7543	7484 - 7596
69-98	NOS -72574	8290 ±50	NPS	8502	8439 - 8558
345-349	NOS -71689	9320 ±45	NPS and <i>C. neoteretis</i>	9794	9702 - 9882

AMD14-Kane2b is the first marine sediment core ever recovered from Kane Basin. The high sedimentation rates in the bottom 130 cm of the core (representing the 9.0-8.1 cal. ka BP interval) offer the opportunity to reconstruct at an exceptionally high resolution the postglacial retreat of ice-sheets over Kane Basin, completing former reconstructions based on land evidence. Our sedimentological and geochemical records indicate that:

- north-western Kane Basin was glacial ice-free by 9.0 cal. ka BP,
- the Kennedy ice saddle collapsed as early as 9.0 cal. ka BP, and as late as 8.3 cal. ka BP,
- Humboldt Glacier retreated in eastern Kane Basin around 8.1 cal. ka BP,
- the postglacial rebound may have been responsible for gradually increased bottom water velocities until *ca* 4.0 cal. ka BP,
- ice rafting in Kane Basin increased over the past *ca* 2.0 cal. ka BP.

While it seems likely that the opening of Nares Strait occurred closer to 8.3 cal. ka BP, our sedimentological and geochemical records alone cannot confirm this. In the next paper, based on a set of sedimentological, geochemical and mineralogical data from core AMD16-233 to the south of Nares Strait, we aim at complementing this first Kane Basin study, enabling us to describe Early Holocene ice sheet dynamics in the whole southern sector of Nares Strait.

Chapter 2 Holocene deglaciation of the southern sector of Nares Strait: insight from Talbot Fjord

2.1 Résumé

Une carotte de sédiments marins de 7,93 cm de long a été récupérée à l'entrée de Talbot Inlet, dans l'est de l'Arctique canadien, pour étudier la dynamique de la calotte glaciaire lors de la déglaciation et l'évolution holocène des environnements sédimentaires dans la partie nord de la baie de Baffin. La présence de laminines millimétrique à centimétriques sur un mètre (boue et sables interlaminés) à la base de l'enregistrement, ainsi qu'une surface globalement lisse confèrent à l'archive des qualités particulièrement propices à l'analyse de la composition chimique semi-quantitative (XRF core-scanning) haute résolution. Nous avons également effectué des mesures de minéralogie (q-XRD) discrètes. Sur cette base, un profil haute résolution de la provenance des sédiments a été obtenu. Les processus sédimentaires ont été évalués sur la base de mesures de la taille des grains, ainsi que sur l'inspection visuelle de photographies, d'images radiographiques/tomodensitométriques et de lames minces. Le cadre chronologique a été construit à partir de 20 âges radiocarbone. À la lumière de la littérature, nos enregistrements géochimiques et sédimentologiques sont interprétés en termes d'environnements sédimentaires liés à la configuration de la calotte glaciaire. Le faciès basal interlaminé a été déposé il y a plus de 9,8 ka à proximité d'une marge de calotte. Le retrait de la calotte glaciaire à l'entrée de Talbot Inlet a été suivi par la déglaciation du sud du bassin de Kane, probablement le long d'un axe au centre ou à l'ouest du bassin, entre > 9,8 et 9,1 cal. ka BP. Le retrait de la calotte glaciaire s'est poursuivie vers le nord et vers la côte, se terminant par l'ouverture complète du détroit de Nares reliant l'océan Arctique à la baie de Baffin ca. 8,5 cal ka BP. La chronologie des événements susmentionnés est en accord avec les travaux antérieurs dans la région du détroit de Nares. Un environnement sédimentaire glacio-distal relativement stable a été présent au site de carottage jusqu'à environ 2,0 cal ka BP, lorsqu'une augmentation des débris ice-raftés (IRD) indique un changement de l'activité des glaciers à terminaison marines dans Talbot Inlet.

2.2 Abstract

A 7.93 cm marine sediment core was retrieved at the entrance of Talbot Inlet, eastern Canadian Arctic, to investigate Early-Holocene ice sheet dynamics, and the Holocene evolution of sedimentary environments in northernmost Baffin Bay. One metre of sub-centimetre scale interlaminated mud and sand at the base of the record, and an overall smooth surface of the core were particularly well-suited for XRF analysis. Combined with discrete XRD measurements, a high resolution downcore profile of sediment provenance was achieved. Sedimentary processes were assessed based on grain size measurements, along with visual inspection of photographs, X-ray/CT-scan images and thin sections. The chronological frame was based on 20 radiocarbon dates. In light of the current literature, the geochemical and sedimentological proxy records are interpreted in terms of sedimentary environments linked to ice sheet configuration. The basal interlaminated mud and sand was deposited at a glacial ice margin >9.8 kyrs ago. The breakup and retreat of the ice sheet at the entrance of Talbot Inlet was followed by the deglaciation of southern Kane Basin, possibly along an offshore, western/central axis, between >9.8 and 9.1

cal ka BP. Ice sheet retreat continued northward and coastward, terminating by the complete opening of Nares Strait which connected the Arctic Ocean to northernmost Baffin Bay ca. 8.5 cal ka BP. The chronology of the aforementioned events is in keeping with previous work in the Nares Strait area. Our record indicates a relatively stable glacio-distal sedimentary environment until ca 2.0 cal ka BP, when increased ice-rafting debris was seemingly brought to the core site from the marine terminating glaciers in Talbot Fjord.

Eleanor Georgiadis^{1,2}, Jacques Giraudeau¹, Myriam Caron³, Jean-Carlos Montero-Serrano³, Sébastien Zaragosi¹, Guillaume Massé^{1,4}

¹Université de Bordeaux, CNRS, UMR 5805 EPOC, allée Geoffroy St-Hilaire, 33615 Pessac, France

²Université Laval, UMI 3376 TAKUVIK, 1045 avenue de la Médecine, G1V 0A6 Québec, QC, Canada

³ISMER, Université du Québec à Rimouski and GEOTOP Research Center, Rimouski, QC, Canada

⁴LOCEAN UMR 7159, CNRS, MNHN, IRD, Sorbonne-université, Station Marine de Concarneau, Concarneau, France

2.3 Introduction

The Canadian Arctic Archipelago (CAA) and northwest Greenland have undergone major geomorphologic reorganisation since the Last Glacial Maximum (England, 1999; England et al., 2006; Georgiadis et al., 2018; Jennings et al., 2011, 2019). The focus of the recently renewed interest in the Nares Strait deglacial to post-glacial history has been turned toward marine sediment cores, after pioneering research was based essentially on land-bound investigations (e.g., Blake Jr., 1992; Blake Jr. et al., 1992; Nichols, 1969; Retelle, 1986). Marine sediment cores are particularly well suited to investigate the temporal and spatial evolution of ice sheets, given their continuous nature (as opposed to discrete findings on land), their ability to record and discriminate a wide range of glacial-marine sedimentary processes (e.g. Dowdeswell, 1987), and the spatial integration of ice sheet dynamics by the material transported to the core site (e.g. Deschamps et al., 2018). The deglaciation of Nares Strait has been successfully constrained based on marine sediment core investigations in the north (Jennings et al., 2011; Reilly et al., 2019), and centre (Georgiadis et al., 2018) of the strait. However, marine Holocene reconstructions of ice sheet dynamics have been limited in the southern sector of Nares Strait and in northernmost Baffin Bay due to hiatuses due to the coring process, and/or low sedimentation rates (Jennings et al., 2019; Knudsen et al., 2008; Levac et al., 2001). The Prince of Wales Icefield (POW) sector of Ellesmere Island is particularly sensitive to recent environment change (Cook et al., 2019; Dalton et al., 2019; Mair et al., 2009; Van Wychen et al., 2016, 2014). Yet, with little pre-satellite observation, it has been difficult to properly assess the long-term response of the POW Icefield to climatic forcing on both Holocene and modern time-scales. The Trinity and Wykeham Glaciers, southern sector of the POW Icefield, drain into Talbot Inlet. They are the two fastest flowing tidewater glaciers of the CAA, their velocities having doubled over the past decade, and they now provide nearly 2/3 of icebergs originating from the CAA (Gardner et al., 2011; Van Wychen et al., 2016).

Here, we aspire to provide marine sediment core-based Holocene reconstructions of sedimentary environments at the entrance of Talbot Inlet, southern Ellesmere Island. Ice sheet dynamics will be investigated

based on a sedimentary study, while the provenance of the material will provide information regarding the spatial configuration of the ice sheets. The second objective of our work is to assess the applicability of high resolution XRF core-scanning in this High Arctic environment. Relatively few studies have used X-ray fluorescence (XRF) core-scanning at high latitudes, mainly due to the occurrence of coarse intervals which prevent measurements, and to the biases linked to the semi-quantitative nature of the elemental data generated. Yet, XRF core-scanning is a time-efficient, non-destructive, high-resolution (millimetre scale) method of measuring the elemental composition of the sediment. In this study, we attempt to identify elemental tracers of sediment provenance in our sediment core by combining discrete, quantitative mineralogical measurements and XRF-derived elemental composition, based on a statistical analysis of the geochemical datasets.

2.4 Study site

2.4.1 Holocene History and modern-day glacial activity

During the Last Glacial Maximum, the CAA was covered by the Innuitian Ice Sheet (Blake, 1977, 1972, 1970; Zreda et al., 1999) which coalesced with the Greenland Ice Sheet along Nares Strait (England, 1999; Retelle, 1986). Glacial ice flowed outward from a topographic central divide in Kane Basin, with northward-flowing ice in Kennedy Channel (England, 1999; Jakobsson et al., 2018), and southward-flowing ice in southern Kane Basin and Smith Sound (*cf.* Figure 3.1-a for locations; Blake Jr., 1992; Blake Jr. et al., 1992; Blake et al., 1996). The Smith Sound Ice Stream extended as far south as 76°35'N covering Carey Øer according to bathymetric and topographic features (Blake et al., 1996), overriding and depositing till at a nearby core site 2001LSSL-014 (Figure 3.1-a; Jennings et al., 2019). The retreat of the Smith Sound Ice Stream at site 2001LSSL-014 is dated *ca* 11.7-11.15 cal ka BP (Jennings et al. 2019), while site AMD14-Kane2b in Kane Basin was glacial ice-free *ca* 9 cal ka BP (Georgiadis et al., 2018). The collapse of the ice saddle in Kennedy Channel is thought to have occurred between 9 and 8.3 cal ka BP (Georgiadis et al., 2018; Jennings et al., 2011, 2019). Little is known about the Holocene history of the POW sector of Ellesmere Island, with only few mollusc shells found south of the area (Blake, 1981) and at Cape Hershel (Figure 3.1-b; Blake Jr., 1992), and low time resolution of the proxy records in core 2001LSSL-014PC during the Mid- and Late-Holocene (Jennings et al., 2019).

The modern activity of marine terminating glaciers in Ellesmere Island have received a relatively high amount of interest, with a number of studies highlighting their sensitivity to both atmospheric and oceanic warming (e.g. Dalton et al., 2019; Van Wychen et al., 2016; White and Copland, 2019 and reference therein). The POW Icefield in particular has been the focus of a number of studies aiming at monitoring its response to recent climate change. Talbot Inlet in south Ellesmere Island harbours several marine terminating glaciers of the POW Icefield, two of which (Trinity and Wykeham Glaciers) have proven to be particularly sensitive to recent environmental change in the Arctic (Figure 3.1-b; Cook et al., 2019; Dalton et al., 2019; Mair et al., 2009; Van Wychen et al., 2016). The Trinity and Wykeham Glaciers have evolved rapidly since the beginning of observational data in the late 1950s, and particularly since the early 2000s. The grounding line of Trinity Glacier has retreated ~8 km since 1959 (Sharp et al., 2014). The velocities of both glaciers have more than doubled during the second half of the 20th century, and they now provide ~62% of icebergs originating from the CAA, up from ~22% in 2000 (Sharp et al., 2014; Van

Wychen et al., 2016).

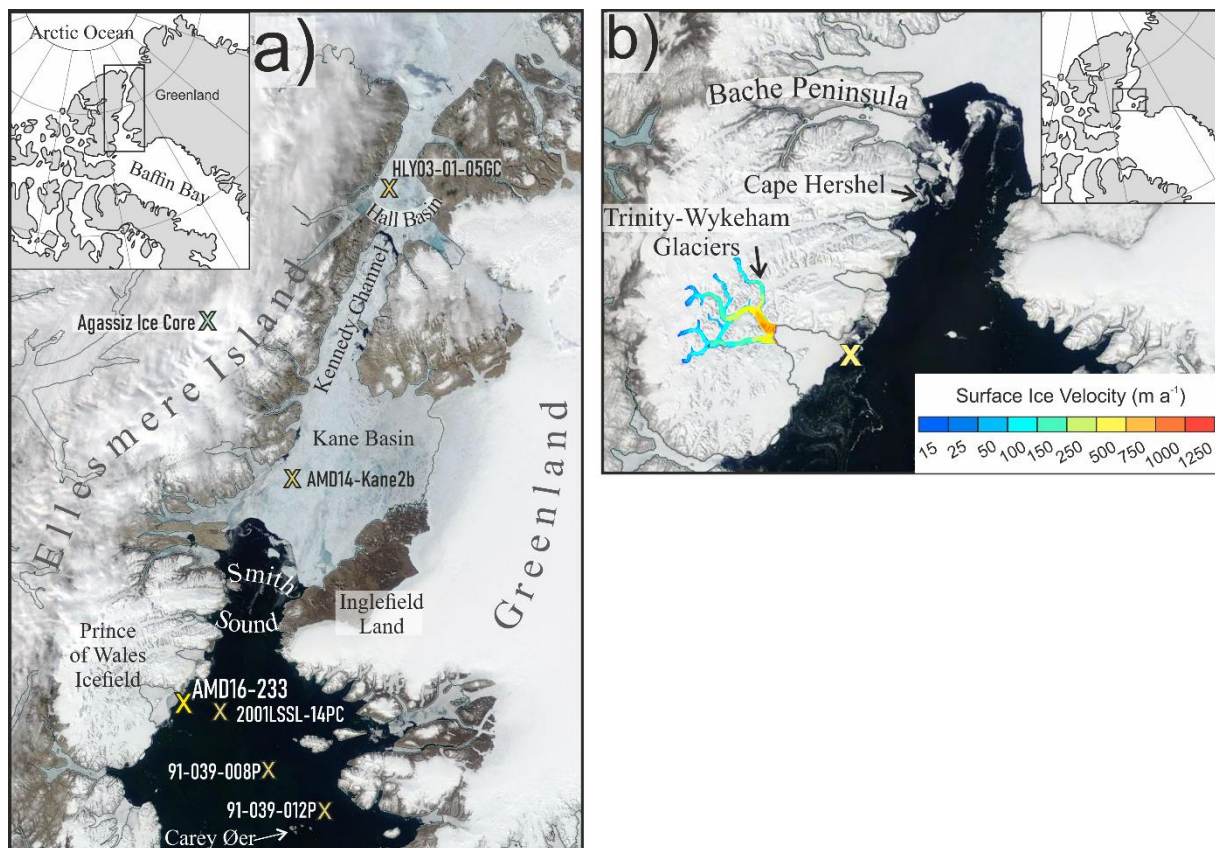


Figure 3.1: Study area in NW Greenland and location of core AMD16-233 shown on a MODIS satellite image (June 2016; <https://worldview.earthdata.nasa.gov/>). a) Nares Strait and locations of previously published marine core sites, with from north to south: HLY03-01-05GC (Jennings et al., 2011), AMD14-Kane2b (Georgiadis et al., 2018; in press.), 2001LSSL-14PC (Jennings et al., 2019), and 91-039-008P and 91-039-012P (Blake et al., 1996; Knudsen et al., 2008; Levac et al., 2001). Location of Agassiz Ice Core is also shown on Ellesmere Island. b) close-up of the Prince of Wales Icefield, with drainage basins and glacial velocities the Trinity and Wykeham Glaciers (Van Wychen et al., 2016).

The climate gradient between northern and southern Nares Strait is thought to be responsible for the accumulation of ice masses and the presence of numerous glaciers in the south relative to the north of the strait. The North Water polynya in northernmost Baffin Bay provides moisture to the area which records higher precipitations than the more arid northern Nares Strait (Maxwell, 1981). The relatively stable surface mass balance of the POW Icefield in modern times is linked to the proximity of this source of moisture (Mair et al., 2009). The Holocene history of the POW Icefield is thus likely connected to that of the North Water polynya. Furthermore, Holocene changes in sea ice cover in Talbot Fjord (and by extension, in the North Water) are likely to affect calving rates and POW Icefield mass balance as they do in modern times (Dalton et al., 2019; Van Wychen et al., 2014).

2.3.2 Regional geology and sediment sources

The geological setting of the Nares Strait region is summarized in Figure 3.2-a, with more detailed information

about local geology in Figure 3.2-b.

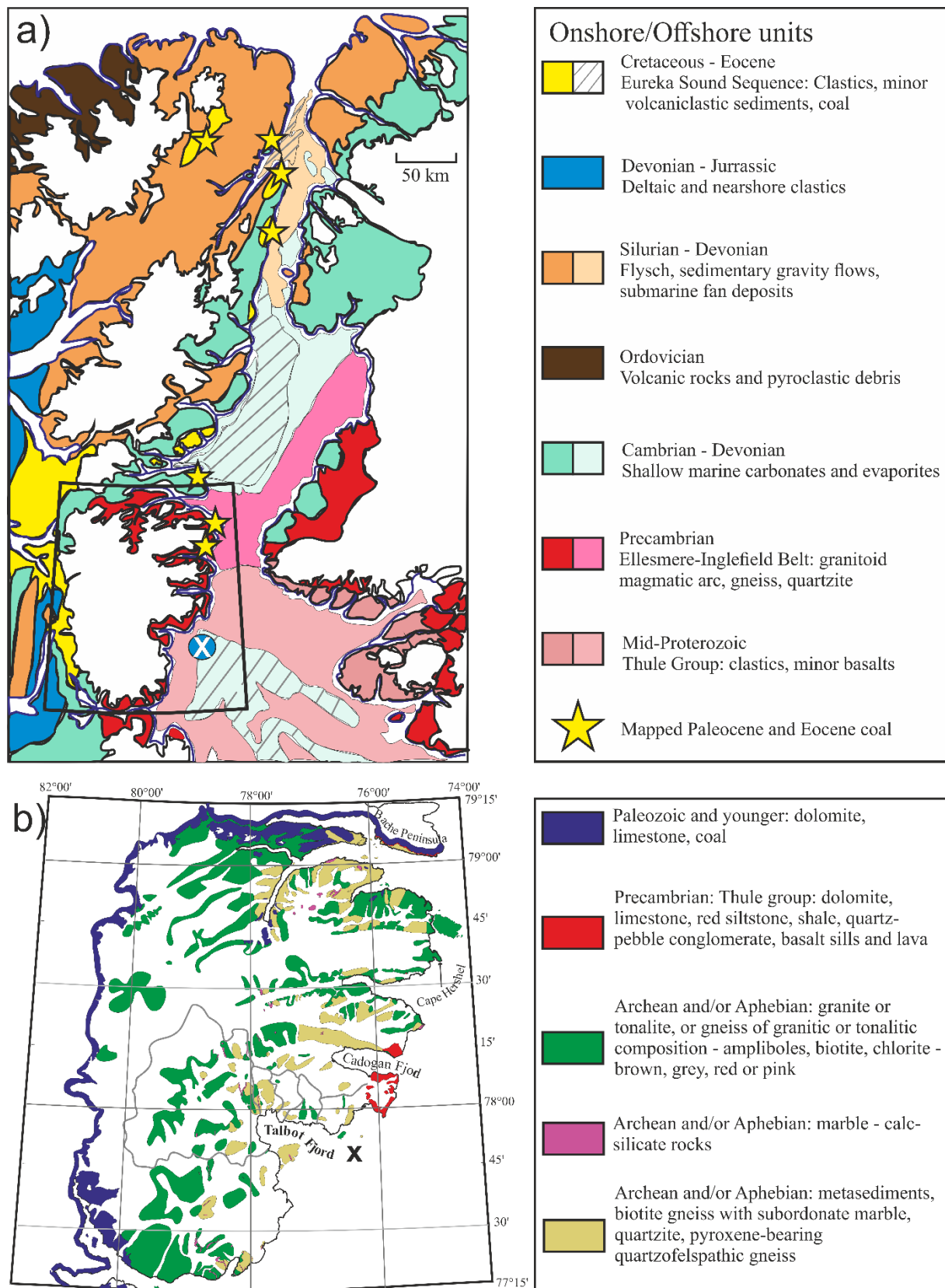


Figure 3.2: Synthetic geological map of the study area. a) simplified geological map of Nares Strait, adapted from Harrison et al. (2011) and Georgiadis et al. (2018). b) simplified geological map of the

Prince of Wales sector of Ellesmere Island (adapted from Frisch, 1984a, 1984b), with drainage basins for the glaciers terminating in Talbot Inlet shown in grey (Van Wychen et al., 2016).

The geological provinces in northern Nares Strait (both on Ellesmere Island and Greenland) and along the western coast of Kane Basin (Ellesmere Island) are represented by Paleozoic carbonates (Koch, 1929). Pockets of coal have been found associated to the Paleogene Eureka Sound sequence occurring in Ellesmere Island (Christie, 1974, 1964; Kerr, 1968, 1967; Miall, 1982), and in morainic deposits on Bache Peninsula and in the POW sector of Ellesmere Island (Fig. 2; Kalkreuth et al., 1993). In the south of Nares Strait, the Precambrian basement outcrops in Inglefield Land (Figure 3.2-a) and in the POW sector of Ellesmere Island as far north as the southern coast of Bache Peninsula (Figure 3.2-a-b). The Humboldt Glacial in western Kane Basin is also thought to overlay Precambrian bedrock based on surface sediments in Kane Basin (Kravitz, 1976). The Precambrian bedrock is constituted of metamorphic, crystalline rocks including gneissic and granitic material, as well as minor occurrences of marble (Dawes, 2004, 1997; Harrison, 2004; Jackson, 2000; Koch, 1933). Some Paleozoic carbonates overly the crystalline bedrock along the coast of Kane Basin in Inglefield Land (Figure 3.2-a; Koch, 1933). The majority of the POW sector of Ellesmere Island is represented by crystalline Precambrian bedrock (Figure 3.2-b). However, part of the Proterozoic Thule Group, which is predominantly present in Northwest Greenland (Figure 3.2-a), occurs in south-eastern Ellesmere Island between the north coast of Cardigan Fjord and north of Talbot Fjord (Figure 3.2-b). The Thule Group essentially contain unmetamorphosed continental to shallow marine sediments and red bed units (Dawes, 1997). This includes sandstone, dolostone, shale and basaltic rocks.

The on-land units continue offshore forming the bedrock geology of Kane Basin according to aeromagnetic data. A Cretaceous-Tertiary basin occurs in north-western and central Kane Basin forming a sill (Dawes, 2004; Harrison, 2004), while Precambrian bedrock underlays marine sediments along the eastern and southern edges of Kane Basin (Figure 3.2-a; Harrison et al., 2006; Hood et al., 1985; Oakey and Damaske, 2006; Okulitch et al., 1990).

According to Kravitz (1976), modern sediments in Kane Basin contain carbonates and clastics (including sandstone and shale), as well as igneous and metamorphic crystalline elements. The mineralogical study of nearby core 2001LSSL-014, to the east of site AMD16-233, demonstrated that on Holocene timescales sediments in the Smith Sound area can be separated into three main groups: (1) carbonate Paleozoic bedrock represented mainly by calcite, (2) a highly diverse group which was interpreted as representing sediment from the Thule Group, and (3) additional regional input which is not tied to a specific source (Jennings et al., 2019).

2.4 Material and Methods

2.4.1 Material: marine sediment core AMD16-233

Core AMD16-233 was retrieved at the entrance of Talbot Fjord in southern Ellesmere Island (77°47.751' N, 76°32.126' W), at 570 m water depth, and measures 7.93 m long (Figure 3.1). The core was photographed and X-rayed (SCOPIX) at UMR5105 EPOC (Université de Bordeaux, France). The bare visual inspection of the core

revealed several distinct lithofacies, the presence of which was confirmed with high-resolution X-rays. Core AMD16-233 is composed of one meter of laminated mud to fine sand at the base, which underlies approximately two meters of coarse sediment, while the top five meters of the core are essentially muddy, bioturbated sediments. The resolution of geochemical and sedimentological measurements in core AMD16-233 was chosen according to the various lithology of the horizons.

2.4.2 Chronology

One gastropod, 11 molluscs, and 13 benthic foraminifera samples (of which two mono-specific *Nonionellina labradorica* samples) from core AMD16-233 were radiocarbon dated by accelerator mass spectrometry (AMS) (Figure 2.1). Preliminary ^{210}Pb measurements at the core top indicated that modern sediments were retrieved, and that the core top was likely well preserved (S. Schmidt, *pers. comm.*). The ^{14}C ages of the dated material were generally in agreement, although three dates from the lower sections of the core were excluded from the age model as they were clearly outliers (Table 3.1; Figure 3.3). Carbonated material was absent in the basal laminated interval but abundant in the upper part of the coarse unit, particularly around 550 cm and 490 cm where several molluscs were found. In these intervals where benthic foraminiferal and mollusc material were dated at similar depths, the former demonstrated older ^{14}C ages than the later. This is again true at *ca* 240 cm where the benthic foraminifera sample yielded a slightly older age than the mollusc sample. The old benthic foraminifera ages (*ca* 12 and 15 cal ka BP) at the base of the coarse unit, are likely due to the presence of pre-Glacial benthic foraminifera in the sediment of core AMD16-233. The abundance of pre-Glacial foraminifera appears to decrease upcore as the difference in age between foraminiferal and mollusc samples is reduced at lower core depths (Table 3.1; Figure 3.3).

The reservoir age of bottom water at the core site is difficult to assess, since there are currently at least three sources for the water: (1) the Atlantic water from Baffin Bay which has been corrected with a ΔR of 0 or 140 years (Caron et al., 2019b; Knudsen et al., 2008; Lloyd et al., 2011), (2) Arctic water carried through Nares Strait – which presents sills of *ca* 200 m water depth – where calibration were made with a ΔR of approximately 240 or 260 years (Caron et al., 2019b; Georgiadis et al., 2018; Jakobsson et al., 2018), and (3) the locally formed brines produced in the North Water which increase the convection layer to *ca* 500 m (Sadler, 1976) and would significantly reduce the reservoir age of the water they mix with. Moreover, the reservoir age is likely to have changed through time due to an entirely different oceanographic circulation prior to the opening of Nares Strait (England, 1999; Georgiadis et al., 2018; Jennings et al., 2011; Zreda et al., 1999), and may also have varied depending on the strength of the West Greenland Current (WGC) (Perner et al., 2013) and brine production in the North Water polynya. Another challenge to correcting for reservoir ages in Smith Sound is the mismatch between the collection depth of the few living, pre-bomb molluscs retrieved in the area (0 to 85 m water depth, Table 3.4 in the Supplements; Coulthard et al., 2010; McNeely et al., 2006) and that of the core (570 m water depth). Facing these large uncertainties, we have chosen to apply the weighted mean of ΔR for the closest pre-bomb molluscs in the database, i.e. $\Delta R=264\pm 74$ years (Coulthard et al., 2010; McNeely et al., 2006), and to present the calibrated ages with $\Delta R=0$ and $\Delta R=335$ as an age envelope of the record according to Georgiadis et al. (2018) and Jennings et al. (2011, 2019). The age

model for core AMD16-233 was computed using CLAM 2.2 (Blaauw, 2010) as a smooth spline with a smoothing level of 0.4 from 0 to 550 cm, and as a linear interpolation between 550 and 615 cm. We assumed an age of 0 yr BP for the core top based on preliminary ^{210}Pb measurements, and did not extrapolate the age model beyond 615 cm due to the absence of reliable radiocarbon ages in the core below this depth. According to the age model, the sedimentation rates are maximal at the base of the coarse unit ($\sim 190 \text{ cm.k.a}^{-1}$ between 615 and 550 cm); they decrease to 50 cm.k.a^{-1} between 550 and 450 cm; they then increase to reach $\sim 100 \text{ cm.k.a}^{-1}$ at 200 cm, before decreasing to 20 cm.k.a^{-1} at the core top (Figure 3.3).

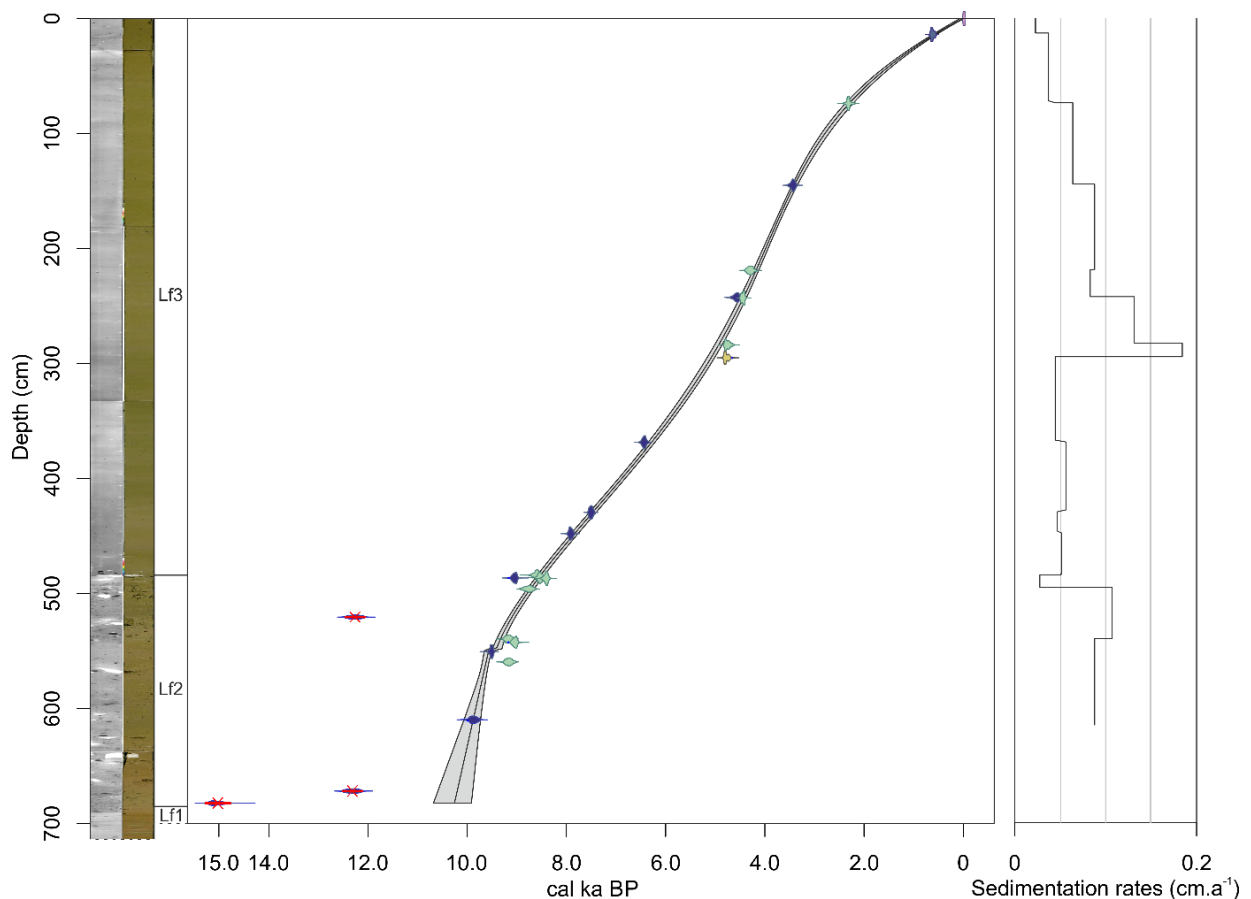


Figure 3.3: Age model and sedimentation rates of core AMD16-233. The gastropod age is plotted in yellow, mollusc ages in green, benthic foraminifera ages in blue, and excluded foraminifera ages are crossed out in red. X-ray images and photographs of the core, along with lithological units used in the sedimentological study are represented on the left.

Table 3.1: Radiocarbon dated material in core AMD16-233, and calibrated ages using $\Delta R = 0$, $\Delta R = 335$, and $\Delta R = 264 \pm 74$ years. * ^{14}C material excluded from age model

Radiocarbon lab number	Radiocarbon Lab	Depth from top (cm)	Material dated	14C age BP	Error	Calibrated ages $\Delta R = 0$			Calibrated ages $\Delta R = 335$			Calibrated ages $\Delta R = 264 \pm 74$		
						median	1 sigma	2 sigma	median	1 sigma	2 sigma	median	1 sigma	2 sigma
477769	BETA	683	MBF*	13290	60	15384	15251-15500	15170-15631	13290	14719-15060	14427-15140	14954	14774-15168	14424-15290
SacA49656	LMC14/ARTEMIS	672.5	MBF*	11045	40	12594	12551-12633	12508-12684	12111	11999-12209	11923-12378	12245	12083-12416	11950-12544
SacA49657	LMC14/ARTEMIS	610.5	MBF	9360	35	10197	10167-10224	10129-10266	9700	9614-9772	9556-9853	9831	9667-9959	9573-10111
SacA50434	LMC14/ARTEMIS	559.5	Mollusc (<i>M. calcarea?</i>)	8790	35	9461	9429-9491	9396-9520	9062	9001-9104	8975-9194	9160	9036-9258	8976-9384
SacA49658	LMC14/ARTEMIS	550.5	MBF	9125	35	9875	9767-9951	9713-10076	9461	9429-9491	9396-9520	9522	9433-9602	9351-9753
SacA50435	LMC14/ARTEMIS	542.5	Mollusc (<i>M. calcarea?</i>)	8695	35	9374	9325-9424	9273-9456	8951	8898-9003	8780-9035	9042	8944-9181	8770-9273
SacA50436	LMC14/ARTEMIS	539.5	Mollusc (<i>P. arctica?</i>)	8795	35	9464	9433-9495	9400-9522	9067	9005-9003	8979-9200	9166	9045-9268	8981-9386
SacA49659	LMC14/ARTEMIS	520.5	MBF*	11050	40	12597	12554-12636	12513-12687	12122	12006-12219	11937-12387	12252	12092-12423	11961-12548
SacA49660	LMC14/ARTEMIS	496	Mollusc (<i>M. calcarea?</i>)	8500	30	9118	9053-9185	9011-9237	8641	8582-8691	8542-8762	8764	8631-8889	8550-8982
SacA48018	LMC14/ARTEMIS	486.8	Mollusc (<i>M. calcarea?</i>)	8210	35	8711	8620-8772	8620-8772	8344	8312-8378	8250-8414	8410	8333-8498	8227-8583
SacA49661	LMC14/ARTEMIS	486.5	MBF	8700	35	9379	9330-9429	9278-9459	8958	8905-9008	8792-9057	9049	8951-9184	8776-9278
SacA48019	LMC14/ARTEMIS	486.3	Mollusc (<i>M. calcarea?</i>)	8335	35	8914	8861-8983	8763-9005	8454	8406-8497	8376-8540	8536	8418-8615	8355-8774
SacA49662	LMC14/ARTEMIS	484	Mollusc fragment (<i>M. calcarea?</i>)	8395	35	8994	8948-9040	8880-9111	8512	8462-8560	8413-8595	8617	8492-8735	8407-8887
SacA50431	LMC14/ARTEMIS	448.5	MBF	7715	30	8184	8140-8239	8069-8077	7850	7813-7900	7765-7927	7909	7827-7989	7732-8094
SacA50432	LMC14/ARTEMIS	429.5	<i>N. labradorica</i>	7270	30	7729	7683-7768	7654-7815	7444	7413-7470	7379-7512	7500	7430-7561	7363-7646
SacA49663	LMC14/ARTEMIS	368.5	MBF	6280	30	6732	6682-6774	6647-6829	6353	6310-6388	6281-6428	6436	6333-6522	6276-6622
SacA49664	LMC14/ARTEMIS	295	Gastropod	4825	30	5127	5053-5201	4999-5257	4694	4640-4773	4572-4799	4755	4639-4851	4524-4960
SacA48020	LMC14/ARTEMIS	283.8	Mollusc fragment	4905	30	5096	5024-5138	4964-5234	4663	4588-4719	4545-4786	4730	4627-4832	4511-4937
SacA49665	LMC14/ARTEMIS	243	Paired bivalve (<i>P. arctica?</i>)	4570	30	4795	4770-4836	4677-4855	4340	4293-4396	4229-4423	4432	4309-4541	4195-4685
SacA50433	LMC14/ARTEMIS	242.5	<i>N. labradorica</i>	4675	30	4894	4843-4932	4819-4989	4471	4422-4508	4391-4567	4580	4447-4689	4387-4805
SacA49666	LMC14/ARTEMIS	219	Mollusc (<i>P. arctica?</i>)	4460	30	4647	4567-4707	4531-4778	4184	4129-4238	4072-4298	4281	4174-4397	4061-4506
SacA49667	LMC14/ARTEMIS	145	MBF	3810	30	3757	3708-3811	3652-3853	3358	3319-3400	3259-3439	3438	3351-3538	3234-3631
SacA48021	LMC14/ARTEMIS	73.8	Mollusc (<i>M. calcarea?</i>)	2890	30	2684	2654-2727	2558-2742	2230	2185-2290	2136-2313	2313	2181-2412	2097-2574
476955	BETA	14	MBF	1320	30	864	825-908	778-931	576	540-609	517-634	624	548-676	501-759

2.5 Mineralogical and geochemical analyses

2.5.1 Quantitative bulk mineralogy

Quantitative X-ray diffraction (q-XRD) analyses were performed on the bulk fraction of 95 samples of sediment from core AMD16-233 at the Institut des sciences de la mer de Rimouski (Rimouski, Canada). The resolution was 6-16 cm for the upper *ca.* 700 cm, while 9 samples were collected in the bottommost meter of the core, selecting individual laminae of various grain size and colour when possible. The samples (1 g of bulk freeze-dried sediment) were prepared according to the methodology described in Eberl (2003) and Deschamps et al. (2018). The differential diffraction properties of minerals imply that X-rays are reflected with specific angles depending on the mineralogical suite present in a sample. The XRD results were converted to quantitative mineral weight percentages using the Excel macro-programme ROCKJOCK v11 (Eberl, 2003). The mineralogical results were processed with the nonlinear Excel macro-programme SedUnMixMC (Andrews et al., 2016, 2015; Andrews and Eberl, 2012) to assess the relative contribution of nearby sediment sources to the sedimentary material of core AMD16-233, usually summing up to 100%.

Based on surface sediment in Baffin Bay, Andrews and Eberl (2011) identified several provincial sediment sources for the Baffin Bay region. Nares Strait was considered essentially as a source of detrital carbonate. However, modern surface sediments in Kane Basin have shown that Nares Strait transports metamorphic crystalline elements, along with carbonates and clastics (of which sandstone and shale) (Kravitz, 1976), while Holocene sediments in the Smith Sound area include a diverse regional “background” component (Jennings et al., 2019). In the absence of fine tuning for sediment sources in Nares Strait, we use the wider Baffin Bay-scale sources from Andrews and Eberl (2011) to identify the contribution of potential sediment sources by the SedUnmix programme. Detrital carbonate likely originates from northern and west-central Nares Strait, while Precambrian bedrock is sourced from more local Inglefield Land and south-eastern Ellesmere Island (Figure 3.2). We include a source of weathered bedrock and shale to account for additional regional sediment input, and to enable a better estimation of the proportions of detrital carbonate vs. Precambrian bedrock in the sediments of core AMD16-233 by the SedUnmix programme (cf. Table 3.3 in the Supplements for the mineralogical assemblages of these sources). We acknowledge however that the mineralogical composition of weathered bedrock and Ordovician shale, which were determined on a wider, Baffin Bay scale (Andrews and Eberl, 2011), are not necessarily well suited for Nares Strait.

2.5.2 AVAATECH XRF-core scanning

Sediment core AMD16-233 was subjected to X-ray fluorescence (XRF) core-scanning at UMR5105 EPOC (Université de Bordeaux, France), with measurements performed at 5 mm resolution for the entire core, and additional measurements at 1 mm resolution for the lowermost meter of the core which presents some millimetre-scale laminae. The generator was set at 10, 30, and 50 kV in order to detect elements in the range of Al to Ba.

Core-scanning X-ray fluorescence spectroscopy is a time-efficient, near-autonomous method for acquiring high frequency semi-quantitative measurements of the elemental composition of sediment (e.g., 20 cm.h⁻¹ for a 5 mm

resolution, 3 cm.h⁻¹ for a 1 mm resolution, with generator settings of 10, 30 and 50 kV). The method is non-destructive, and only necessitates minor preparation of the sediment surface from a split core sections (i.e. the surface of the core must be smoothed and a protective Ultralene foil carefully applied to the sediment). The theoretical principle of XRF measurements warrants being presented here, so that precautions related to the exploitation of the dataset may be touched upon in this section. The core-scanner emits a primary X-ray beam which excites the elements at the surface of the sediment. Each element (atom) emits a secondary photon of a specific wave length. The number of photons of each energy level is counted by the scanner receptor. The semi-quantitative elemental composition of the sediment is then assessed through the processing of the spectra (number of photons of each wave length) yielded by the core-scanner receptor. If no calibrations are performed (i.e. several punctual XRF measurements on dry, homogenised sediment fused to glass beads or compressed to powder pellets), the results remain semi-quantitative and can be used to assess relative changes in elemental abundances downcore. The main setback of the method, however, is that downcore changes in elemental counts are not only dictated by the abundance of each element, but they are susceptible of being unpredictably influenced by sediment inhomogeneity, in particular, grain size and water content (e.g. Tjallingii et al., 2007). Horizons containing coarse material generally yield less elemental counts due to higher porosity and bad surface contact of the scanner (Lyle et al., 2012). The secondary photonic signal can also be attenuated by the absorption of energy by interstitial water between the sediment particles, or by the condensation of interstitial water between the sediment and the protective foil. Furthermore, the lower energy photons emitted by lighter elements are more likely to be absorbed before reaching the receptor, and it is estimated that up to 10% of the signal is lost for smaller atoms such as Al and Si (Tjallingii et al., 2007).

It is recommended that raw counts be normalised to limit the analytical biases linked to changes in grain size and water content. However, the normalisation correction itself is not devoid of bias. The most common approach is to use elemental ratios, often with terrigenous elements such as Al, Sr, K, Ti, Fe, and Zr as denominators to account for dilution by changes in fluxes of terrigenous input. It has been shown that elemental ratios should be used with caution, as inherent variations in the denominator element can introduce spurious correlations¹ between variables (cf. supplementary information), especially when the coefficient of variation of the denominator is larger than that of the nominator (Van der Weijden, 2002). The use of elemental ratios presents other limits in this study, since the aim of this work is to identify potential elemental tracers of sediment provenance (i.e. assessing changes in terrigenous material, not correcting for them). We thus apply a normalisation to the total number of counts received by the scanner (excluding Ag and Rh counts which are partly generated by the composites of the scanner itself). The normalisation to the total number of counts corrects to a certain extent for lower yields in coarse and/or water-rich intervals (Bahr et al., 2014). This allows us to produce a correlation matrix of all normalised elements and the relative contribution of geological sources (from the XRD dataset) to identify potential elemental tracers of sediment provenance.

¹ Spurious correlations appear to indicate a correlation where none exists between the original variables.

2.5.3 Statistical analysis of the geochemical dataset

A Pearson correlation matrix was plotted on transformed (log, centred and scaled) mineralogical and geochemical dataset in order to visualise the relationships between variables. This enables the potential identification of elements that can be used as tracers of the source of the sedimentary material, which in turn, would allow us to extrapolate the low resolution source data to the high resolution elemental data. Potential biases in the application of statistical analysis to geochemical datasets must however be acknowledged here. The exhaustive composition of a material must amount to 100% by definition, implying that as the abundance of one constituent increases, at least one other must decrease. Thus, each variable is negatively correlated to at least one other variable. This generates what is called a closed sum effect (Rollinson, 1993). While these negative correlations create somewhat artificial relationships between the variables, they can highlight potential dominant “competing” geological sources in the case of this study.

A stratigraphically constrained cluster analysis (CONISS, Grimm, 1987) was performed on the XRD-derived sediment source abundances, using the *vegan* (Oksanen et al., 2019), *mgcv* (Wood, 2019), and *grDevices* (R Core Team, 2017) packages in R, and plotted with the *Rioja* package (Juggins, 2019). This allows the identification of major changes in the origin of sediment composing core AMD16-233, which may be linked to glacial activity.

2.6 Sedimentological analyses

2.6.1 Thin sections

The visual inspection and high-resolution computed tomography (CT) images of core AMD16-233 revealed several distinct lithofacies. Intervals were chosen for thin section analysis in order to visualise the internal structure and the microscopic architecture of the sediment (773-783 cm, 733-769 cm, 708-718 cm, 688-698 cm). The high quality of thin section prepared at UMR5105 EPOC following the protocol described in Zaragosi et al. (2006), is particularly valuable in this study, since the microscopic layout and contact between particles carries discriminant information regarding the different sedimentation processes at play in glacial marine environments.

2.6.2 Grain size

One centimetre slices of sediment were wet sieved through 63 and 125 μm meshes in order to determine the relative weight of the coarser fractions of the sediment. A Malvern 2000 laser sizer was used to determine the relative contribution (expressed as % of particles) of clay and colloids (counted in the 0.04-4 μm interval due to overestimation of particle size by laser sizing), silt (4-63 μm), and sand (63-2000 μm) within the <2 mm fraction. The resolution of the grain size measurements was 8-10 cm in the upper ca. 700 cm, while individual laminae were selected in the bottommost meter of the core when possible. Several laser grain size measurements were performed on sufficiently thick individual laminae in order to evidence potential grading. Grain size analysis is used here as a means of assessing the contribution of various transport agents of the sedimentary material (e.g., subglacial outwash, meltwater plumes, icebergs, sea ice).

In core AMD16-233, the >125 μm weight fraction displayed the most variability in the coarser fraction. For clarity, the changes in relative weight of the 63-125 μm were not discussed in the result section of this paper, but

the trends follow those of the >125 µm fraction, only generally an order of magnitude lower (cf. Figure 3.5).

2.7 Results

2.7.1 Relationship between semi-quantitative elemental (XRF) and quantitative mineralogical (q-XRD) composition of sediment

The correlation matrix demonstrated a strong positive correlation between detrital carbonate and Ca (0.86), while they were both negatively correlated with all other sources and elements (Figure 3.4). Precambrian bedrock is positively correlated with most terrigenous elements, the strongest correlation being with Ba (0.83; Figure 3.4). Weathered bedrock showed weaker correlations with the elemental data, but was still positively correlated to most terrigenous elements, whereas Ordovician shale demonstrated very weak correlations with all other sources and elements. Ca was an obvious tracer for detrital carbonate given its strong positive correlation to this source, and negative or weak correlation with the other sources. The best tracer for Precambrian bedrock appeared to be Ba, since it was not only strongly and positively correlated to this source, but it is also negatively or weakly correlated to the other sources.

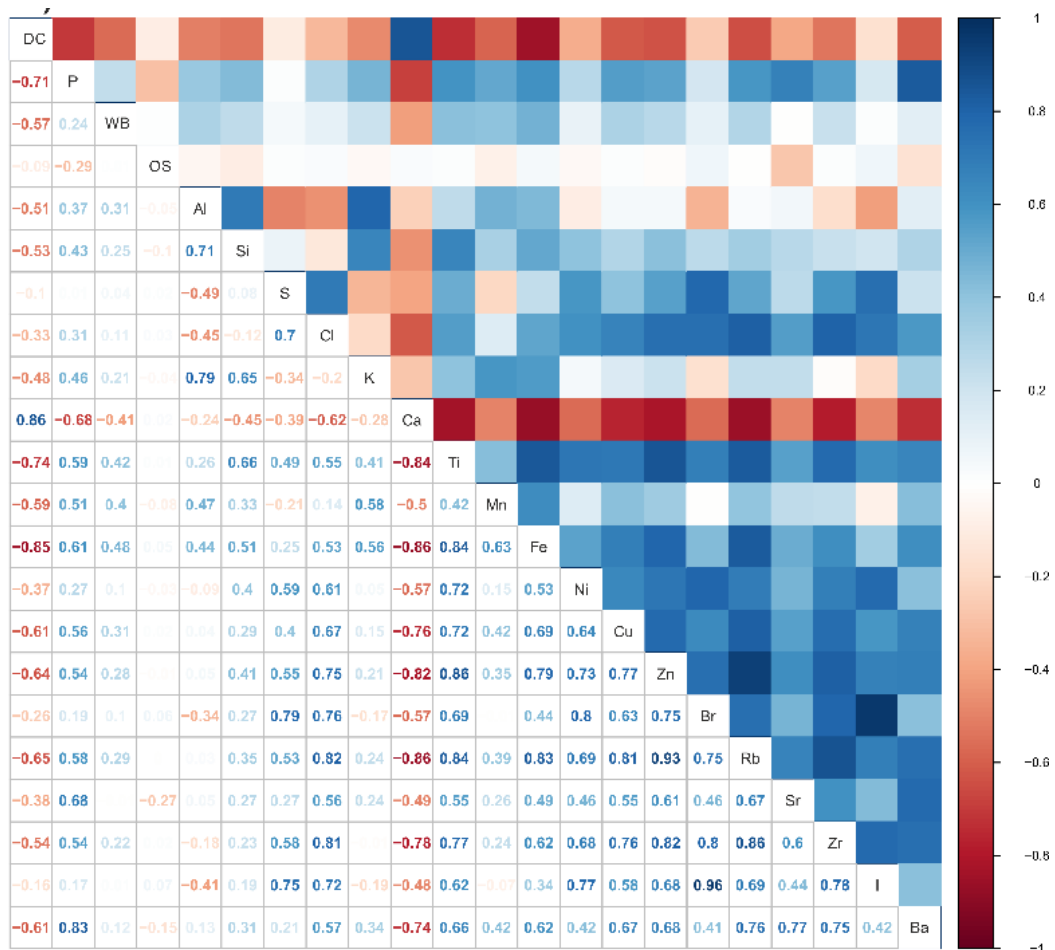


Figure 3.4: Correlation matrix of sediment provenance and normalised elemental counts. DC: detrital carbonate; P: Precambrian Bedrock; WB: weathered bedrock; OS: Ordovician Shale. Positive correlations are shown in blue, negative in red.

2.7.2 Lithofacies: sedimentological characteristics and source material

Three main units of distinct lithological nature were identified based on the bare visual inspection of core AMD16-233, along with X-ray images. These were: LF1, a laminated unit from 690 to 793 cm; LF2, a coarse interval from 690 to 485 cm; and LF3, a 5 m long interval of bioturbated mud from 485 to 0 cm (Figure 3.5). The boundaries between mineral clusters identified by the stratigraphically constrained cluster analysis on the XRD-derived relative abundance of sediment from each source generally corresponded to the visually identified lithological units. This suggests that changes in sediment provenance either occurred concurrently, or were linked to changes in sedimentation processes. The first mineral cluster corresponded to LF1, and was characterised by the predominance of Precambrian bedrock-sourced sediment (Figure 3.5). Three clusters fell within LF2, with limits generally corresponding to changes in grain size within LF2. The fifth cluster comprised the upper section of LF2 and lower section of LF3. These clusters demonstrated variable influences of Precambrian bedrock vs. detrital carbonate-sourced sediments. The final two clusters occurred within LF3, with a decreasing influence of detrital carbonate and increasing influence of Precambrian bedrock at the top of the core (Figure 3.5).

Following is a detailed description of each lithofacies and the subunits observed within, based on results presented in Table 3.2 and Figure 3.5.

Lithofacies LF1: laminated mud and sand

Lithofacies LF1 composed the bottommost meter of core AMD16-233 (693-793 cm from core top), presenting laminations of varying thickness, colour, and grain size. Laminations ranged from a few millimetres to several centimetres in thickness (Table 3.2). Generally, the laminations were thicker in the lower section of LF1, and became thinner upcore, with only sub-centimetre scale laminae above 720 cm. LF1 corresponds to the first mineral cluster where the major sediment source is the Precambrian basement (average of 53%), with a significant proportion of sediments represented by Ordovician shale-like sediment (average 47%). LF1 displayed the highest fraction of weathered bedrock in core AMD16-233, albeit at a relatively low content (< 15%). Sub-centimetre to centimetre scale offsets of laminae occurred along normal faults in LF1 (ca 744-750 cm, ca 733-740 cm, ca 703 to 710 cm, Table 2.2).

Three types of laminae made up LF1:

- Brown, coarser laminae (average of 32% sand, 29% silt and 39% clay in the <2 mm fraction). The thicker brown laminae displayed clear normal grading (e.g., from 767 to 764 cm, sand abundance decreased from 41 to 7% and clay increased from 27 to 53%, Table 2.2). High quartz (~40%) and carbonates (calcite + dolomite, ~13%) contents were measured in the mineralogical suite of the brown Laminae. The brown horizons were composed of the highest proportion of detrital carbonate-sourced sediment (average of 15%) within LF1, but were mainly derived from Precambrian basement (27%) with a considerable proportion of Ordovician shale-like sediments (50%).

- Grey, silty laminae (average of 60% clay and 30% silt² in the <2 mm fraction). The grey horizons were often the thinnest in LF1, and a single sample of “pure” grey sediment was subjected to XRD measurements. The q-XRD results suggested that approximately 49% of the sediment was sourced from Precambrian bedrock, 39% from Ordovician shale-like sediments, and 14% from weathered bedrock, with the most abundant minerals being quartz (~21%) and plagioclase (~22%) (Table 2.2).
- Red, clayey laminae (average of 65% clay and 25% silt³). The most abundant minerals in the red horizons were clays (total clays ~53%) and quartz (~14%) (Table 2.2). The red laminae were predominantly derived from Precambrian bedrock (average of 54%) and Ordovician shale-like sediments (average of 45%).

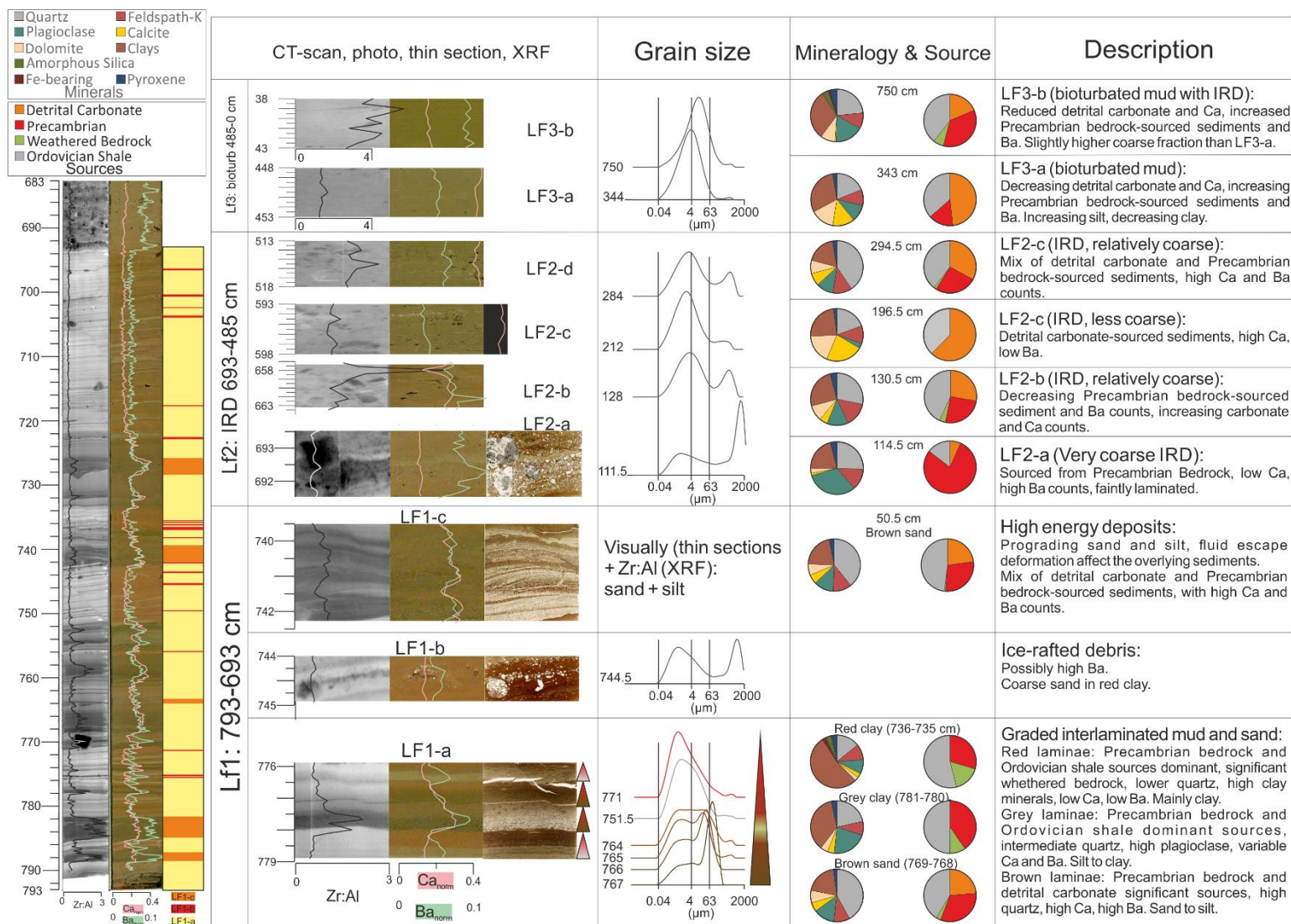
Three distinct lithological patterns were observed within LF1 (Table 2.2).

- The predominant form of laminae, LF1-a, were planar, with little mixing between colour and grain size. While the laminae transitioned gently between decreasing grain sizes (i.e. brown to grey to red, brown to red, or grey to red) the contact between the top of a finer and the base of a coarser horizon (i.e. brown or grey overlying red) was often sharp (Table 2.2, LF1-a). Occasional dropstones occur in LF1-a as visible in the X-ray images (e.g., 771 cm; Table 2.2).
- 16 layers of sand were counted in the clayey horizons of LF1, and made up LF1-b (Table 2.2).
- LF1-c consisted of high energy deposits. The five intervals of LF1-c (787-789 cm, 782-785 cm, 764-766 cm, 740-743 cm, and 727-729 cm) were affected by ripple cross bedding features, faintly visible in the X-ray, but clearly visible in the thin section. The thin section of LF1-c at 740-743 cm also displayed what appeared to be convolutes (cf. LF1-c, top of thin section in Table 2.2). The features of LF1-c were typical of “C layers” of Bouma sequences.

² Although the laminae were sampled with the greatest of care, contamination by over- and underlying brown horizons was likely responsible for the sand fraction measured in the grey and red laminae.

³

Table 3.2: Close-ups of X-rays, photographs and thin sections of the different lithofacies of core AMD16-233. Also shown is the XRD-derived Zr:Al ratio, normalised Ca and Ba counts, <2 mm fraction grain size, mineralogical composition, and sediment provenance of representative samples in each lithofacies.



Lithofacies LF2: coarse sediment

Lithofacies LF2 consisted of just over 2 m of coarse sediment between 693 and 485 cm. Overall, the <2 mm fraction was normally graded from 693 to 550 cm, and from 525 to 485 cm, with reverse grading occurring between 550 and 525 cm (Figure 3.5). The contribution of weathered bedrock to the sediments of LF2 was negligible, while detrital carbonate and Precambrian bedrock content demonstrated major variations. Four subunits in LF2 were delimited by the cluster analysis on sediment sources, with some grain size changes coinciding with cluster limits.

- LF2-a (693-672 cm) was the coarsest subunit in core AMD16-233. The grain size increased sharply between the top of LF1 and the base of LF2-a, with sand in the <2 mm fraction increasing from 10 to 68%, and the relative weight of the >125 μm fraction increasing from 6 to 50%. The sediment was normally graded between the base and the top of LF2-a, the sand content in the <2 mm fraction decreasing from 68% to 24%, while the clay content increased from 21 to 51%, and the >125 μm fraction was reduced from 50 to 19% of the weight (Figure 3.5). LF2-a displayed the highest abundance of Precambrian bedrock-sourced sediment (83%) in core AMD16-233 (Table 3.2). Faint laminae were visible in LF2-a.
- LF2-b (670-640 cm) was graded in the <2 mm fraction (26 to 16% sand, and 44 to 56% clay), while the coarser >125 μm fraction accounts for an average 29% of the weight. Within LF2-b, the proportion of sediment sourced from the Precambrian basement decreased from 42% at the base to 15% at the top, while that derived from detrital carbonate increased from 25 to 50% (Figure 3.5).
- LF2-c (640-525 cm) displayed high proportions of clay (average of 57%). The >125 μm fraction of the sediment accounted for an average 21% of the weight. Reverse grading was observed at the top of LF2-c, as the clay content decreased from 62 to 47%, while the weight of the >125 μm fraction increased from 7 to 37% (Figure 3.5). The dominant sediment source in LF2-c was detrital carbonate (55%), while the proportion of sediment derived from the Precambrian bedrock was negligible (4%) (Table 3.2).
- LF2-d (525-485 cm) was slightly coarser than LF2-c, with an average 52% clay and 19% sand in the <2 mm fraction, and an average 27% weight represented by the >125 μm fraction. No particular grading was observed in LF2-d. While detrital carbonate remained a dominant source of the sediment in LF2-d (43%), Precambrian bedrock accounted for a more significant portion compared to the previous subunit LF2-c (15%) (Table 3.2; Figure 3.5).

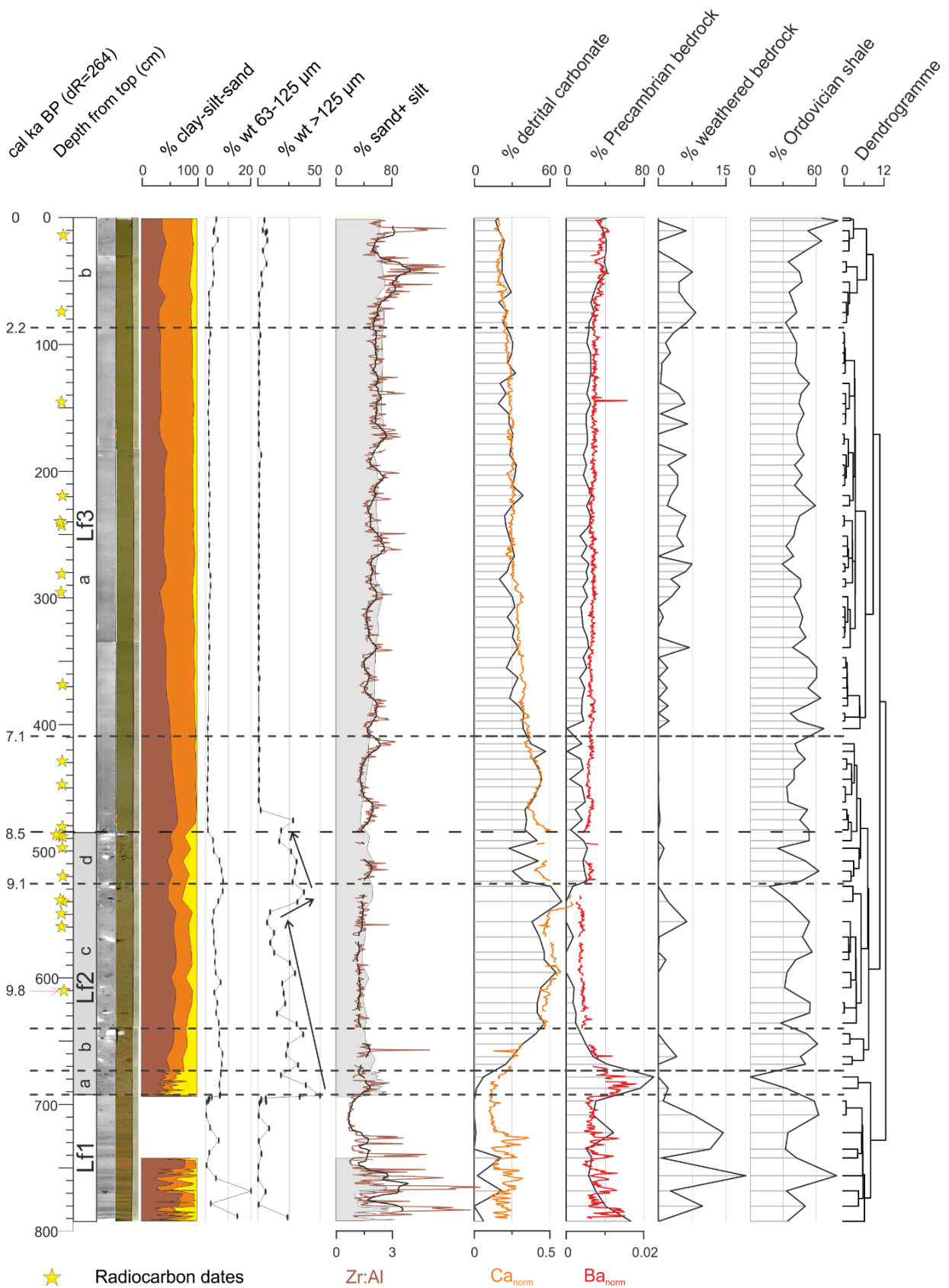


Figure 3.5: Sedimentological and geochemical data from core AMD16-233. Dashed lines represent the cluster limits from the stratigraphically constrained cluster analysis with the associated dendrogramme plotted on the right.

Lithofacies LF3: bioturbated mud

Lithofacies LF3 consisted of nearly 5 m of bioturbated mud, from 485 cm to the core top. Two subunits were identified in LF3 based on the cluster analysis on sediment source, and grain size changes.

- LF3-a (485-87 cm) was gradually, but clearly, graded in the <2 mm fraction. Starting with 65% at the base, clay content was progressively reduced to 34% at the top of LF3-a, while silt abundance increased from 32 to 57%, and sand abundance from 3 to 9% (Figure 3.5). The coarser fractions displayed little variability in LF3-a, hovering around 1% relative weight. The composition of the sediment gradually changed throughout LF3-a, as detrital carbonate-sourced sediment was reduced upward from ~50% to 28%, while Precambrian bedrock increased from 16 to 23%. Starting with near-nil values at the base of LF3-a, weathered bedrock content also increased upcore, but remained < 7% with an average of 2%.
- LF3-b (87-0 cm) was characterised by coarser sediment and a change in sediment composition relative to LF3-b. The relative weight of sediment >125 µm was an average 4%, and reaches a maximum of 8%. The proportion of sediment derived from Precambrian bedrock increased to an average of 34% in LF3-b, while detrital carbonate-sourced sediment accounted for only 23%. The weathered bedrock content doubles to reach an average 4%, with maxima of 8% (Table 3.2; Figure 3.4).

2.8 Discussion

2.8.1 Paleoenvironmental interpretation of XRF core scanning data

It is usually advised that discrete quantitative elemental measurements be used in conjunction with XRF core-scanning to validate downcore elemental trends derived from XRF core-scanning. The q-XRD measurements used in this study have allowed us to identify elemental tracers of sediment sources. The high resolution XRF measurements are particularly pertinent in the study of laminated sequences, where laminae thickness limits individual sampling for quantitative measurements.

While the high calcium carbonate content in carbonated rocks makes Ca the obvious tracer for detrital carbonate in core AMD16-233, the identification of Ba as a tracer for Precambrian bedrock was based entirely on the correlation matrix from the statistical analysis. Although Ba has been used as a paleoproductivity tracer (e.g. Ganeshram and Pedersen, 1998; Schmitz, 1987), the association of Ba to organic matter necessitates water depth of at least 1000 m to develop (Breyman et al., 1992). The major sources of barium to oceans is rivers (Martin and Meybeck, 1979), attesting to its terrigenous origin, and dissolved Ba concentrations in Arctic Ocean water are higher during deglacial meltwater events (Hall and Chan, 2004). In core AMD16-233, Ba content is likely brought to the core site by meltwater following glacial erosion of the crystalline basement in southern Nares Strait.

2.8.2 Reconstruction of sedimentary environments, and link with regional context

Based on sedimentological, mineralogical and geochemical data of core AMD16-233, we aim at

reconstructing sedimentary environments and glacial activity in Talbot Fjord, and will discuss their Holocene evolution in the light of the literature on environmental and climatic change in the area.

Previous studies have demonstrated that the extended Greenland and Inuitian Ice Sheets coalesced along Nares Strait during the Last Glacial Maximum (England, 1999; Jennings et al., 2011) flowing northward and southward from a central divide in Kennedy Channel (Blake et al., 1996; England, 1999; Jakobsson et al., 2018). The Smith Sound ice stream ran down southern Nares Strait as far as 76°35'N in northernmost Baffin Bay (Blake et al., 1996). The deglacial history of Smith Sound is dominantly based on onshore material (e.g., Blake Jr., 1992; Funder, 1990; Kelly et al., 1999). Little offshore evidence (seafloor profiles and marine sediment cores) exists regarding the retreat of the ice sheets and marine transgression into Smith Sound (Blake et al., 1996; Jennings et al., 2019; Knudsen et al., 2008). The marine sediment cores published in the area are affected by gaps between composite cores and/or very low sedimentation rates for the Mid- to Late-Holocene, making core AMD16-233 a valuable archive in the deglacial history of southern Nares Strait, and the first high resolution record of Holocene sedimentary environments in western Smith Sound. Radiocarbon dates reported in the literature were recalibrated by first adding 410 years when only the age corrected for $\delta^{13}\text{C}$ was published, before correcting for reservoir age and calibrating using CALIB 7.1 (Stuiver et al., 2020).

2.8.3 Ice proximal environment at the entrance of Talbot Fjord (>9.8 cal ka BP)

Lithofacies LF1, mainly consisting of LF1-a (graded sequences of coarser carbonates to fine, Precambrian bedrock-sourced clay), are similar to sediments found in glacial proximal environments (Dowdeswell et al., 2000). LF1 thus represents deposits from subglacial outwash at a glacial margin. The few punctual q-XRD measurements which were performed on sufficiently thick individual laminae (most of the 9 q-XRD samples from LF1 includes a mixture of the three laminae) reveal that brown, sandy or silty intervals are dominantly composed of carbonate (with high quartz and low clay content in the mineralogical suite); whereas the grey and red, silty or clayey intervals are essentially sourced from Precambrian bedrock (with lower quartz and higher clay minerals) (Table 3.2). However, the fact that Ba and Ca display similar profiles in LF1, when the glacial grounding line was close to the core site, and that the carbonate-rich brown laminae yielded high Ba counts, suggests that the carbonate in LF1 originates from the POW sector of Ellesmere Island. Carbonates are likely to be found in a number of local outcrops in the area (Figure 3.2). The red colour of the sediment in core AMD16-233, and particularly in LF1 is due to the red-beds and ferruginous clastic in the Thule Group that outcrop just north of Talbot Fjord (Dawes, 2009).

Horizons of coarse particles (LF1-b) occurring in LF1 are likely composed of ice-rafted debris (IRD) carried to the core site by either icebergs or sea ice. Since no datable material was retrieved in LF1, sedimentation rates for this unit are unknown. It is possible that the overall paucity of dropstones and IRDs between layers of LF1-b is due to land-fast sea ice at the core site, the seasonal breakup of which allowed the release of icebergs that deposited IRD layers (LF1-b). This infers that a seasonal character may be attributed to the occurrence of LF1-b horizons. Alternatively, continuous ice-rafting may have occurred if surface condition were predominantly open, but very high sedimentation rates associated to the subglacial outwash laminae caused the IRD to be visible only in

discrete intervals, during pauses in the subglacial efflux. It is thus impossible for us to confirm whether the core site was predominantly ice-free or ice-covered when the ice sheet margin was close to the core site. However, the occurrence of these IRD-rich intervals indicates that an ice-shelf was not present during the deglaciation of the core site. Overall very high sedimentation rates were likely in this glacial marginal environment given the high melting rate of the Ellesmere Ice Sheet during the Early Holocene (Fisher et al., 2012), regardless of the sea-ice regime at the time.

The five intervals of two to three centimetres of interlaminated silt and sand forming ripple cross bedding features and convolutes (cf. thin section of LF1-c in Table 3.2) are typical of the “C interval” of Bouma sequences, and are indicative of a high energy environment. LF1 is overall representative of proglacial turbidites linked to subglacial outwash and proglacial destabilisation. The faults visible in LF1 likely occur throughout the core, but are not visible in the units devoid of distinguishable horizontal features. These faults may have occurred during the coring process, or may be linked to seismic activity related to the postglacial isostatic rebound.

The absence of thicker, coarser laminae in the top 30 cm of LF1 (723-690 cm) suggests a retreat of the glacial margin, possibly during a significant calving event that generated high energy deposits (LF1-c) visible in the CT images (Table 3.2) from 729 to 723 cm.

No datable material was found in LF1, but the sediments are older than 9.8 cal ka BP ($\Delta R=264 \pm 74$ years) according to the radiocarbon age of a mixed benthic foraminiferal sample dated in the above-laying interval (LF2). Similar laminated deposits were found in a nearby core (2001LSSL-014PC) retrieved further offshore in Smith Sound, with an age >11.0 cal ka BP ($\Delta R=220 \pm 20$ years) (Jennings et al., 2019). Proglacial laminated sediment also occurs at the base of core 91039-012PC retrieved on the eastern side of northernmost Baffin Bay, yielding an age of *ca* 12.0 cal ka BP ($\Delta R=264 \pm 74$, from Blake et al., 1996; Knudsen et al., 2008). The nearest mollusc shell found south of the POW section of Ellesmere Island was dated at *ca* 10.7 cal ka BP ($\Delta R=264 \pm 74$ years; Blake, 1981), and the nearest mollusc to north, in Cape Hershel was dated at 9.9 cal ka BP ($\Delta R = 264 \pm 74$ years; Blake, 1992). Although the deglaciation pattern of the Smith Sound stream may have been complex, the glacial margin probably retreated the approximate 140 km northward from site 9103-012P to site 2001LSSL-014PC between 12.0 and *ca* 11 cal ka BP, and the approximate 35 km westward between site 2001LSSL-014PC and site AMD16-233 between *ca* 11.0 and *ca* 9.8 cal ka BP (Figure 3.6). The Ellesmere Island coast in the study area was progressively deglaciated from south (*ca* 10.7 cal ka BP) to north (*ca* 9.9 cal ka BP) according to landbased radiocarbon dating of molluscs (Blake, 1992, 1981). The rapid deglaciation of the Nares Strait area was initiated by the onset of the Holocene Thermal Maximum (HTM), induced by orbital forcing and starting *ca* 11 ka BP as evidenced by the $\delta^{18}\text{O}$ -derived atmospheric temperature record from the nearby Agassiz ice core (Lecavalier et al., 2017). Ice sheet retreat may have also been promoted by the increased strength of the West Greenland Current in Baffin Bay around 10 cal ka BP ($\Delta R=140 \pm 35$ years) (Weiser, *pers. comm.*), initiating ice sheet retreat on the eastern side of northernmost Baffin Bay.

Lf1 >9.8 cal. ka BP

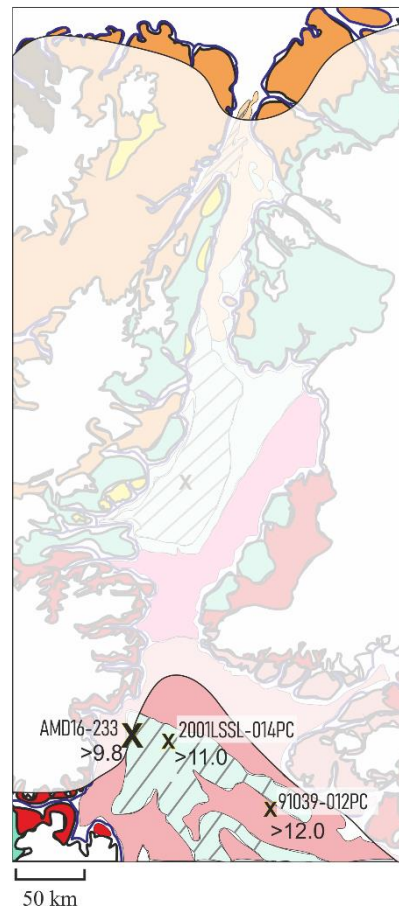


Figure 3.6: Schematic representation of ice sheet extent in Nares Strait, based on sedimentological, geochemical and mineralogical data from core AMD16-233, along with the minimal age of deglaciation of core sites from previously published records (cores 2001LSSL-014PC (Jennings et al., 2019) and 91039-012PC (Blake et al., 1996; Knudsen et al., 2008)).

2.8.4 Deglaciation of southern Nares Strait (>9.8-8.5 cal ka BP)

The cluster analysis showed that the IRD-rich unit LF2 is subdivided in four intervals of different sediment provenance. Starting at the base of LF2, the Ba and Ca counts diverge, where they were similar in LF1 (Table 3.2 and Figure 3.5). This suggests that the dominant Ca above the base of LF2 is no longer the local POW sector of the Ellesmere Island.

The first interval (LF2-a, 693-672 cm) is predominantly of Precambrian bedrock composition, with high Ba counts and low detrital carbonate content (Table 3.2 and Figure 3.5) and is likely sourced from the local crystalline basement of the POW sector of Ellesmere Island. The faint laminae indicate that turbid plumes still settled at the core site, but that ice-rafting transported much of the material to the core site. The sediments of LF2-a probably originate from the ice sheet retreating away from the core site over the local Precambrian bedrock, possibly opening part of Talbot Fjord (Figure 3.7).

Lf2-a >9.8 cal. ka BP

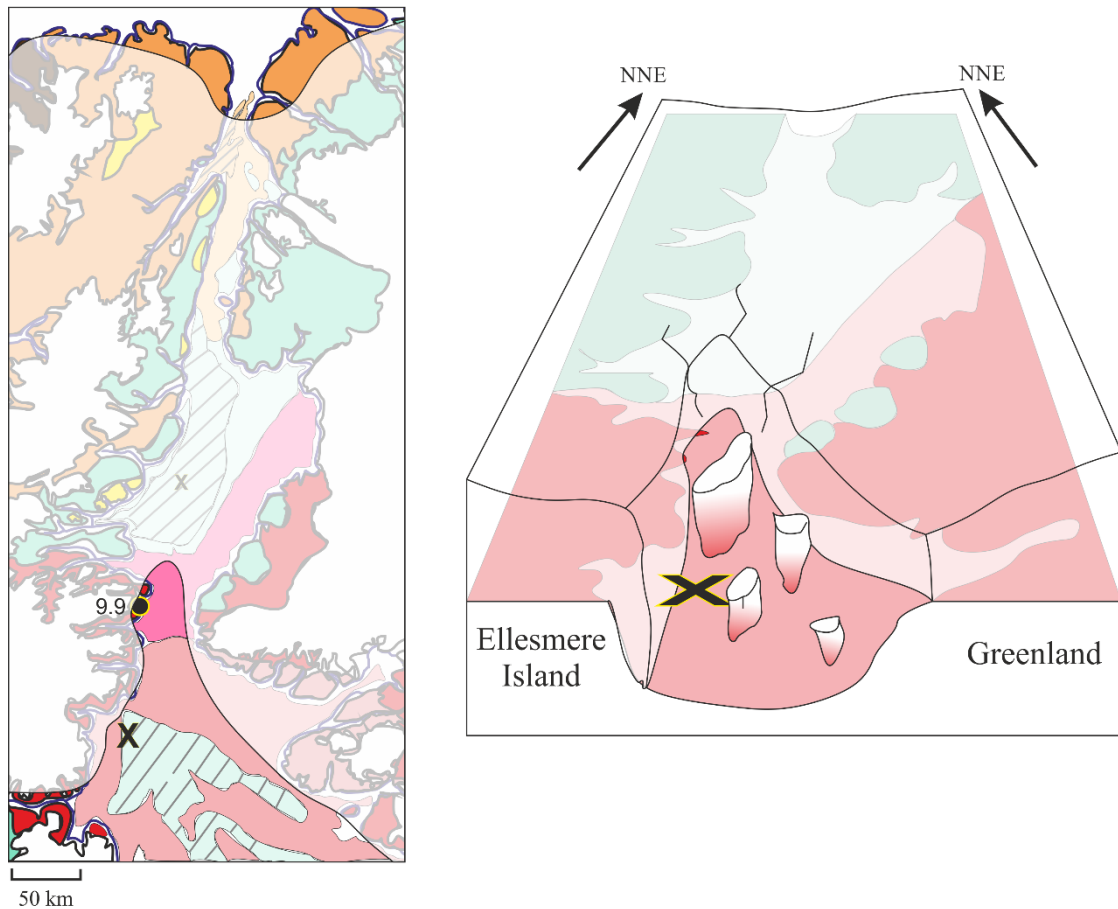


Figure 3.7: Retreat of Innuitian and Greenland Ice Sheets in southern Nares Strait before 9.8 cal. ka BP (corresponding to LF2-a in core AMD16-233), with ice sheet retreat on land at Cape Hershel evidenced a mollusc dated at 9.9 cal. ka BP (Blake, 1992). The dominance of Precambrian sediment in unit LF2-a suggests the material originates from the local Smith Sound area.

The second sub-unit (LF2-b, 672-640 cm) displays decreasing Precambrian bedrock and increased detrital carbonate-sourced sediments (Table 3.2 and Figure 3.5). The Precambrian component of the sediment is sourced locally from glacial retreat in Talbot Fjord, and/or from the deglaciation of southern Kane Basin. The detrital carbonate is likely sourced from west-central Kane Basin and brought to the core site by icebergs and turbid plumes from the Greenland and Innuitian Ice Sheets during their retreat in southern Nares Strait (Figure 3.8). The absence of molluscs older than 8.5 cal ka BP ($\Delta R=240\pm 51$) on the carbonate outcrops in southern Kane Basin (England, 1999) suggests that the coasts of Kane Basin were not yet deglaciated and that the carbonate in subunit LF2-b originated from offshore in Kane Basin.

Lf2-b >9.8 cal. ka BP

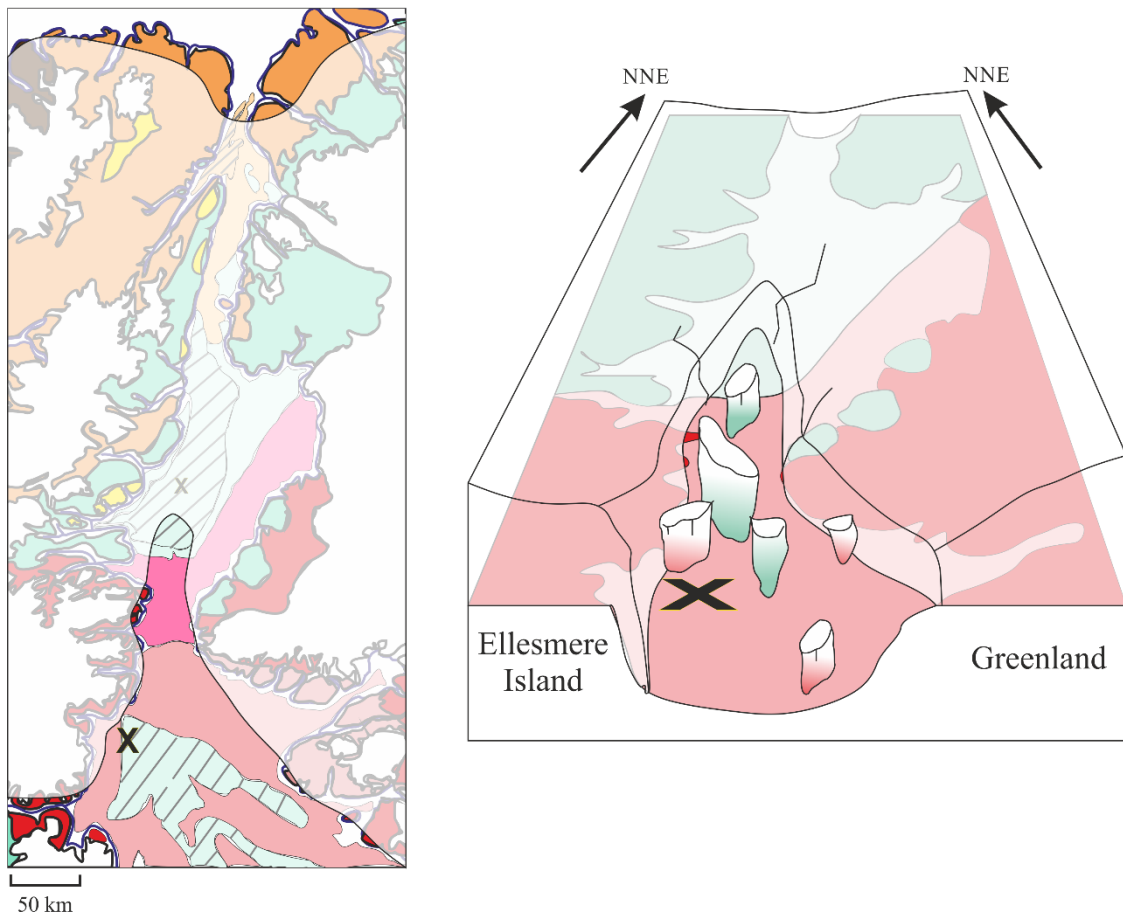


Figure 3.8: Ice sheet retreat in southern Nares Strait and along a west-central axis in Kane Basin. Decreasing Precambrian bedrock and increasing detrital carbonate in LF2-b indicates that a higher portion of the sediment originates from Kane Basin.

The third subunit (LF2-c, 640-525 cm) was predominantly sourced from detrital carbonate, and dated between >9.8 and 9.1 cal ka BP (Table 3.2 and Figure 3.5). This interval also predates the ages of molluscs found on Kane Basin's coasts (England, 1999), suggesting that the sediments of LF2-c originate from the deglaciation of offshore west-central Kane Basin (Figure 3.9). The age at the top of this subunit (tied to two radiocarbon samples within LF2-c, Table 3.1; Figure 3.3) corresponds to the age of glacio-proximal sediment at the base of core AMD14-Kane2B, retrieved in western Kane Basin (Figure 3.9; Georgiadis et al., 2018), also placing the grounding lines of the Inuitian and Greenland Ice sheets offshore in Kane Basin. It is possible that the basal age of subunit LF2-c is situated around 10.8 cal ka BP ($dR=220$) since a similar, radiocarbon-dated, carbonate-rich IRD interval was recorded in nearby core 2001LSSL-014PC, and interpreted as the retreat of the grounding line north of Bache Peninsula (i.e. north of the Precambrian bedrock) (Jennings et al., 2019).

Lf2-c >9.8-9.1 cal. ka BP

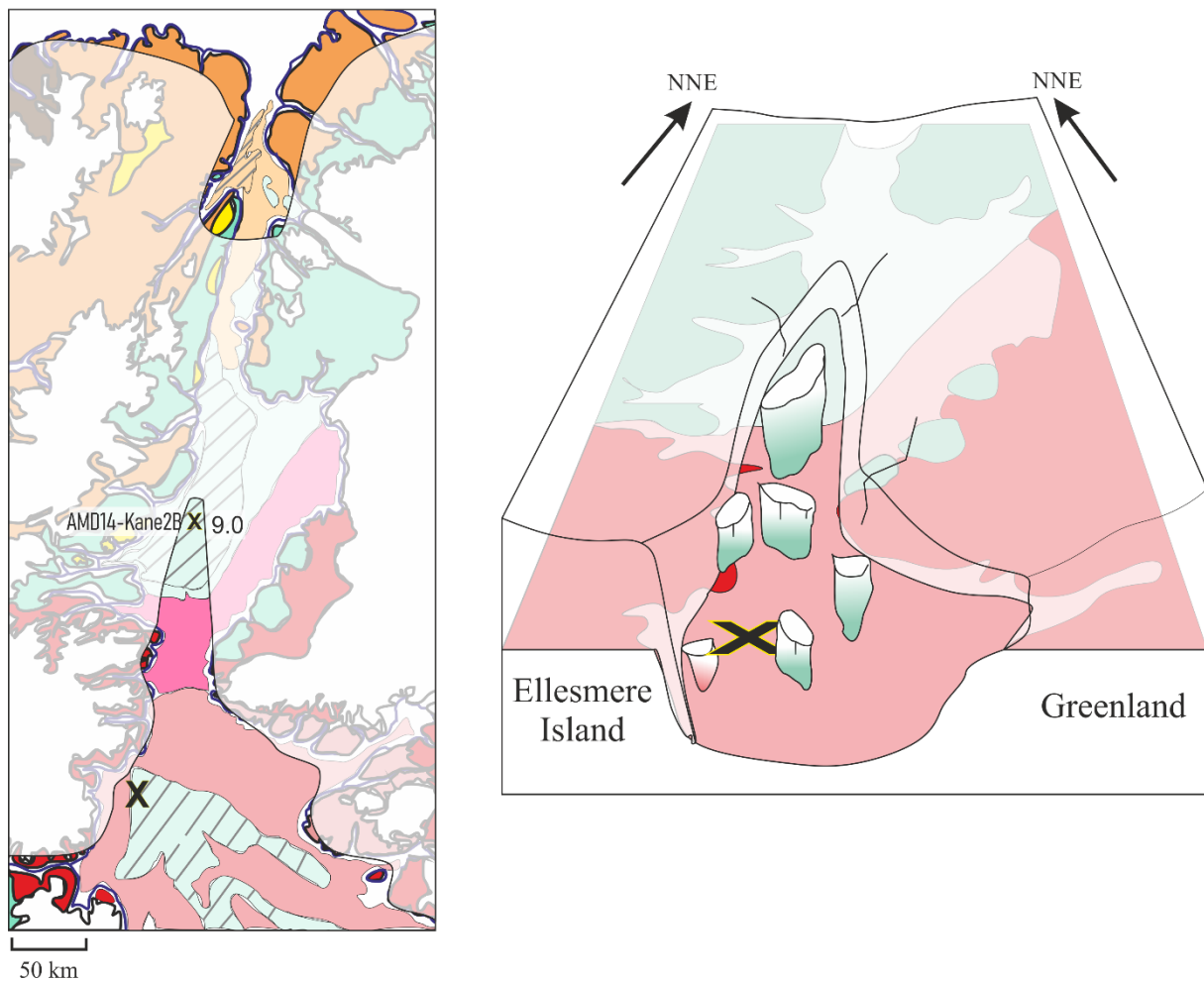


Figure 3.9: Further ice sheet retreat in southern Nares Strait and along the west-central axis in Kane Basin, reaching location AMD14-Kane2b around 9.0 cal. ka BP. The dominance of detrital carbonate in LF2-c infers that the material originates from east-central Kane Basin.

The fourth subunit (LF2-d, 525-482cm) is predominantly sourced from detrital carbonate, but a non-negligible fraction of the sediment is derived from Precambrian bedrock (Table 3.2 and Figure 3.5). The age of this interval is approximately 9.1 to 8.5 cal ka BP. These sediments are possibly derived from the deglaciation of carbonate and crystalline provinces in south-eastern Kane Basin where molluscs aged 8.4 and 8.5 cal ka BP were found (England, 1999), as well as from the carbonate outcrops in north-western Kane Basin where a mollusc was dated at 8.7 cal ka BP (England, 1999). It is possible that LF2-d terminates with the opening of Nares Strait since IRD become rare above LF2-d in core AMD16-233 (Figure 3.10). The sedimentological and geochemical evidence presented here suggest that southern Nares Strait transitioned from a calving bay to a channel connecting the Arctic Ocean and Baffin Bay around 8.5 cal ka BP. This chronology is slightly younger than possible evidence of the opening of Kennedy Channel as seen from nearby Smith Sound (*ca* 9 cal ka BP, $\Delta R=220\pm 20$; Jennings et al., 2019), slightly older than the timing of the event suggested by Georgiadis et al. (2018) as viewed from Kane Basin (8.3 cal ka BP, $\Delta R=240\pm 51$), and contemporaneous with that suggested by Jennings et al. (2011) as viewed from Hall Basin (8.5

cal ka BP, $\Delta R=240\pm 51$).

Lf2-d 9.1-8.5 cal. ka BP

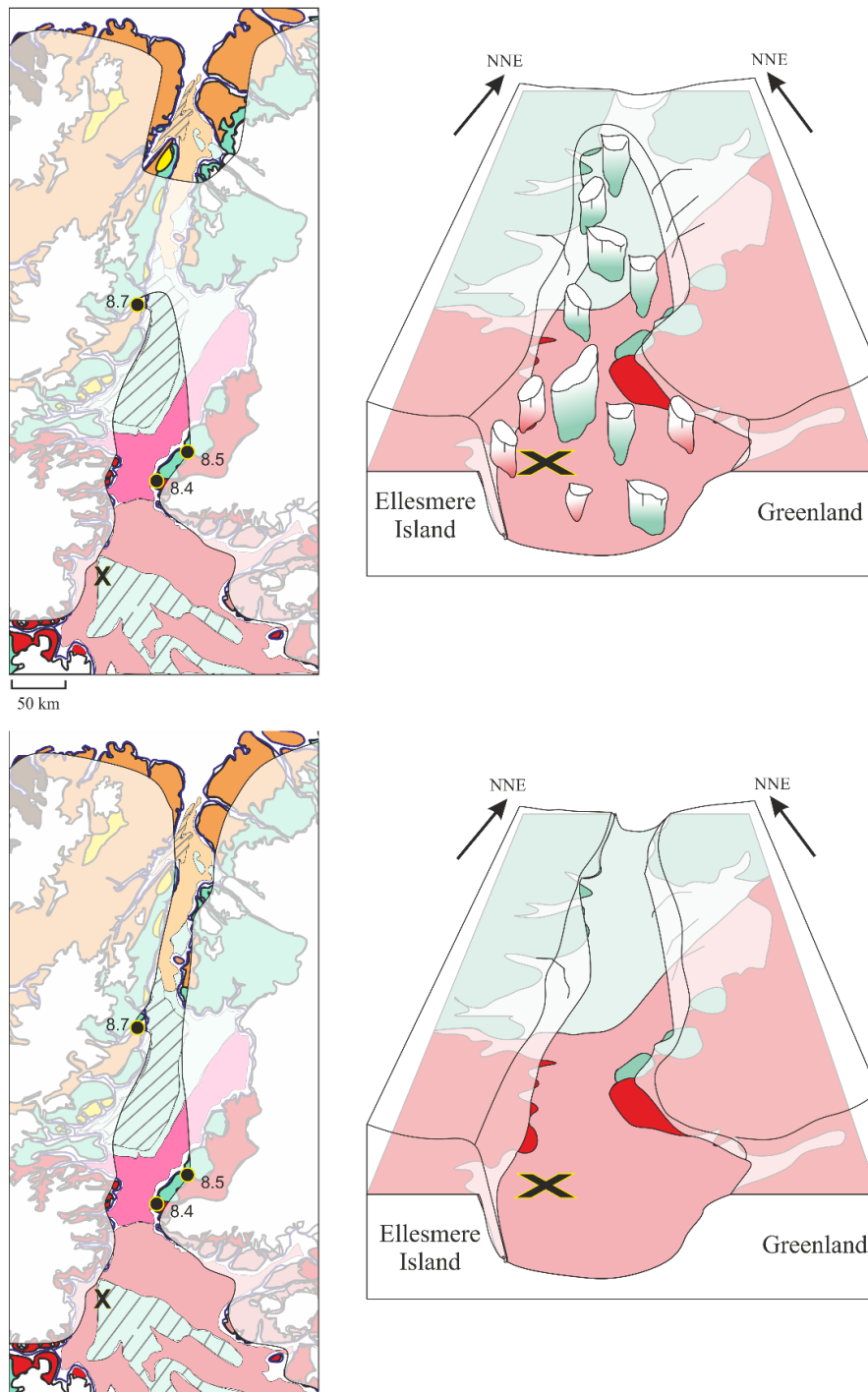


Figure 3.10: Further ice sheet retreat in northern Kane Basin, until the opening of Nares Strait was completed around 8.5 cal. ka BP. The dominance of detrital carbonate in LF2-c infers that the material originates from Kane Basin and northern Nares Strait in agreement with a mollusc dated at 8.7 cal. ka BP in northern Kane Basin, while molluscs dated at ca. 8.4-8.5 cal. ka BP on Inglefield Land suggest that the Greenland Ice Sheet has retreated coast-ward in eastern Kane Basin, which is supported by a slight increase in Precambrian bedrock in the sediments of LF2-d.

The changes in sediment provenance recorded in LF2 in core AMD16-233 are in keeping with land-based (Blake, 1992; Blake et al., 1992; England, 1996; Nichols, 1969) and offshore (Georgiadis et al., 2018) evidence of ice sheet retreat in Kane Basin. Given the spatial range of the four sediment cores (Georgiadis et al., 2018; Jennings et al., 2011, 2019; and this work) which cover approximately 500 km, and the uncertainties in the age models associated to these cores (including analytical error and reservoir ages uncertainties), the transition in core AMD16-233 corresponds remarkably well with these other records of the opening of Nares Strait.

2.8.5 Ice-distal environment (8.5-0 cal ka BP)

Few changes were reported in the sedimentological and geochemical records over the last 8.5 kyrs, demonstrating an apparent stability in the sedimentary environment at the entrance of Talbot Fjord despite significant changes in sea-ice cover and oceanic circulation in the area during the Mid- and Late-Holocene (Caron et al., 2019a; Georgiadis et al., 2020; Knudsen et al., 2008).

The decrease in clay and increase in silt between 8.5 and 2.5 cal ka BP (483-87 cm; Fig. 5) may be linked to an increase in velocity of bottom waters. In Kane Basin, the increase of silt was interpreted as being the result of the postglacial rebound, which brought the seafloor closer to the strong subsurface current in Nares Strait (Georgiadis et al., 2018). The southern sector of Ellesmere Island underwent a postglacial rebound of 80-100 m (England et al., 2006). The increase in bottom current at site AM16-233, may similarly be linked to isostatic adjustment that brought the seabed closer to the main subsurface Arctic outflow travelling along the western side of Nares Strait (Münchow et al., 2007). The decreasing portion of clay may also be linked to a decrease in glacial flour production as bedrock erosion by the ice sheets is reduced by both the extent and the thickness of the ice sheets, along with onshore retreat of the ice sheets. Detrital carbonate input to the core site was relatively high until *ca* 7.1 cal ka BP, when the cluster analysis delimitates the beginning of decreasing detrital carbonate and increasing Precambrian bedrock sediments at the core site (Figure 3.5). Similar trends of decreasing carbonate starting *ca* 7.5 cal ka BP were reported in Kane Basin (Georgiadis et al., 2018), and are thought to be linked to the onland retreat of the Innuitian and Greenland Ice Sheets according to the ages of molluscs found along the Nares Strait shorelines (England, 1999; Georgiadis et al., 2018).

The cluster analysis reveals a change in sediment source over the past *ca*. 2.5 kyrs, which becomes more evident at *ca* 2.0 cal ka BP (60 cm) as a marked increase in the coarser fractions of the sediment occurs (Figure 3.5). A similar increase in the coarse fractions of core AMD14-Kane2b was recorded over the past *ca*. 2 kyrs (Georgiadis et al., 2018) and was associated to a decrease in sea-ice cover in Kane Basin (Georgiadis et al., 2020). Decreasing atmospheric temperatures following the end of the HTM (*ca* 8.5 cal ka BP; Lecavalier et al., 2017) may have promoted a surge of the POW Icefield glaciers. Glacier readvance was evidenced by molluscs occurring in morainic deposits just south of Cape Hershel, which are situated 18 km from the present moraines, and dated *ca* 2.0 cal ka BP ($\Delta R=264\pm 74$; Blake, 1989). Such was also the case in nearby northwest Greenland where sectors of the Greenland Ice Sheet advanced between 3.2 and 2.1 ka BP during the Neoglacial cooling (Farnsworth et al., 2018). It is possible that the glacial surge inferred by land-based evidence on both sides of Smith Sound, was initiated by increased moisture produced by an active North Water polynya between 4.5 and 3 cal ka BP (Davidson

et al., 2018; Georgiadis et al., 2020). The North Water is an important source of moisture, and is responsible for the near-equilibrated surface mass balance of the POW Icefield in the modern times (Mair et al., 2009). Conversely, the subsequent retreat over the last two millennia (evidenced by land-bound studies) may have been enhanced by instabilities in the Nares Strait ice arch (Georgiadis et al., 2020), and in the North Water polynya formation (Davidson et al., 2018) beginning *ca.* 3 kyrs ago. The low sea-ice cover in the Nares Strait area after *ca.* 3 cal ka BP, presumably due to sea level pressure forcing in the Arctic (e.g., Arctic Oscillation; Georgiadis et al., 2020), could have reduced buttressing of the marine terminating glaciers in Talbot Fjord and promoted calving. It has been shown that calving rates of the Trinity and Wykham Glaciers in Talbot Inlet are presently closely linked to sea-ice cover both at a seasonal scale, and on a multi-annual basis as icebergs production has increased with decreasing sea-ice over the past two decades (Dalton et al., 2019; Van Wychen et al., 2014).

Our sedimentological and geochemical datasets suggests that mass loss in this sector of the POW icefield may have been predominantly due to surface melting when atmospheric temperatures were higher in the Mid-Holocene, and that, after 2.5 or 2.0 cal ka BP, calving may have acted more significantly as a component of mass loss. Sea ice cover, which may be linked to sea level pressure forcing (e.g., Arctic Oscillation) in the area (Georgiadis et al., 2020), may also have exerted a buttressing effect on tidewater glacier in Talbot Fjord during the Mid-Holocene. This hypothesis warrants further investigations of Holocene sea ice dynamics in Talboat Fjord.

2.9 Conclusion

The sedimentological and geochemical studies of core AMD16-233 bring new details on the deglaciation of southern Nares Strait, and contribute to mounting evidence that the complete opening of Nares Strait occurred *ca.* 8.5 kyrs ago (between *ca.* 9 and 8.3 cal ka BP). In this study, we have demonstrated that XRF core-scanning can be used to assess changes in sediment sources based on correlations with punctual XRD measurements. The high resolution measurements afforded by XRF core-scanning is particularly pertinent for the study of sub-centimetre scale laminated sequences. Downcore elemental profiles provided by this non-destructive method can be used as a basis for selecting horizons to sample for quantitative measurements, so as to ensure that changes in sediment composition are not missed.

Our findings concerning ice sheet retreat and Holocene paleoenvironments at the entrance of Talbot Fjord can be summarised as followed:

- An ice sheet margin was present at the core site prior to 9.8 cal ka BP.
- The breakup of this ice sheet brought large proportions of local, Precambrian-sourced material, during ice sheet retreat in Talbot Inlet and Smith Sound.
- As the ice sheets retreated northward along a west-central axis in Kane Basin between >9.8 and 9.1 cal ka BP, substantial amounts of carbonated sediment were brought to the core site from Nares Strait.
- The ice sheets then retreated eastward and further northward, eventually opening Nares Strait around 8.5 cal ka BP.

- A relatively stable environment in terms of sediment processes was recorded from *ca* 8.5 to 2.0 cal ka BP, and a decrease in carbonated material due to the onland retreat of the ice sheets in Nares Strait.
- Over the last *ca* 2.5 kyrs, ice-rafting increased in Talbot Fjord, bringing in higher proportions of local, Precambrian bedrock-sourced sediments, and may be linked to enhanced mobility of sea-ice cover in the Nares Strait area at the time.

Acknowledgments: This project received funding from the Initiative d'Excellence (IdEx) programme of the University of Bordeaux, and the Natural Science and Engineering Research Council of Canada (NSERC) for the studentship of EG. We are grateful to the captain, officers, crew and scientists on board the CCGS *Amundsen* during the 2016 ArcticNet expedition for the recovery of core AMD16-233. This study was supported by ArcticNet, the Natural Sciences and Engineering Research Council of Canada (NSERC) through Discovery Grants to JCMS, and GM. We thank Quentin Beauvais (ISMER) for technical support in the laboratory.

2.10 Supplements

Table 3.3: Mineralogical assemblages of the sources present in the Nares Strait area (Andrews and Eberl, 2011).

<u>Minerals present (%)</u>	<u>Source 1: Detrital carbonate</u>	<u>Source 2: Precambrian bedrock</u>	<u>Source 3: Cretaceous (weathered bedrock)</u>	<u>Source 4: Ordovician shale</u>
Quartz	14.9	23.0	16.2	20.4
Feldspath-K	17.8	10.0	11.1	5.3
Plagioclase	6.9	35.3	1.3	3.5
Calcite	10.6	0.7	0.3	9.1
Dolomite	26.1	0.6	19.6	3.1
Amphibole	0.7	5.8	0.3	0.1
Pyroxene	1.2	0.1	0.1	0.7
Fe-bearing	1.9	2.5	7.1	1.7
Amorphous Silica	8.3	14.3	12.9	18.7
Kaolinite	0.3	0.4	13.7	1.2
clays (non kaol.)	11.2	7.2	17.5	36.3
Smectites	2.0	1.3	5.6	10.3
Illites	4.6	3.3	3.6	10.7
Biotite&Chlorite	4.7	2.7	8.3	15.2

Table 3.4: ΔR of living, pre-bomb molluscs collected in or near to Smith Sound, and their distance to the core site.

Lat	Long	Depth (m)	ΔR	ΔR Err	Reference	Locality	Collection Year	Mollusc Species	Feeding	Habitat	distance (km)
76.67	-76.33	85	140	60	McNeely et al., 2006	Ellesmere Is., NU	1928	<i>Astarte montagui</i>	suspension	Infaunal	125
76.67	-76.33	85	270	70	McNeely et al., 2006	Ellesmere Is., NU	1928	<i>Balanus balanus</i>	suspension	Epifaunal	125
78.75	-74.92		228	70	Coulthard et al., 2010	Rice Strait, Smith Sound	1898	<i>Astarte bolearis</i>	suspension	Infaunal	112
78.76	-74.73	40	178	50	Coulthard et al., 2010	Rice Strait, NU	1898	<i>Balanus crenatus</i>	suspension	Epifaunal	115
78.76	-74.73	40	318	25	Coulthard et al., 2010	Rice Strait, NU	1898	<i>Astarte bolearis</i>	suspension	Infaunal	115
76.21	-81	0	193	80	Coulthard et al., 2010	Craig Hbr, NU	1953	<i>Astarte bolearis</i>	suspension	Infaunal	209

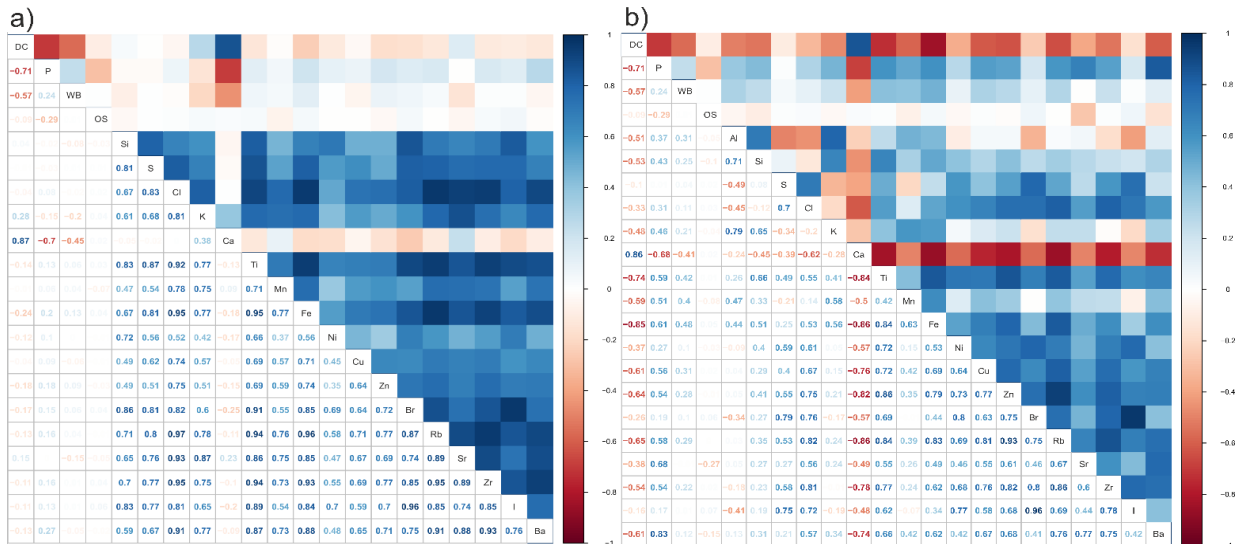


Figure 3.12: Correlation matrix of the XRD source data and Al-normalised XRF data, and b) correlation matrix of the XRD source data and XRF core-scanner data normalised to the sum of all counts used in the main text of this paper.

Using Al to normalise the XRF data results in high correlations between nearly all elemental counts, and virtually nil-correlations between Ca and the other elemental counts. The Al normalisation also leads to low correlations between the mineralogical sources and the XRF elemental counts, to the exception of Ca which remains highly correlated to detrital carbonate. These results are likely due to overwhelming trends in Al counts which appear in the other elemental counts when Al is used in their normalisation, hence inducing spurious correlations between nearly all elements.

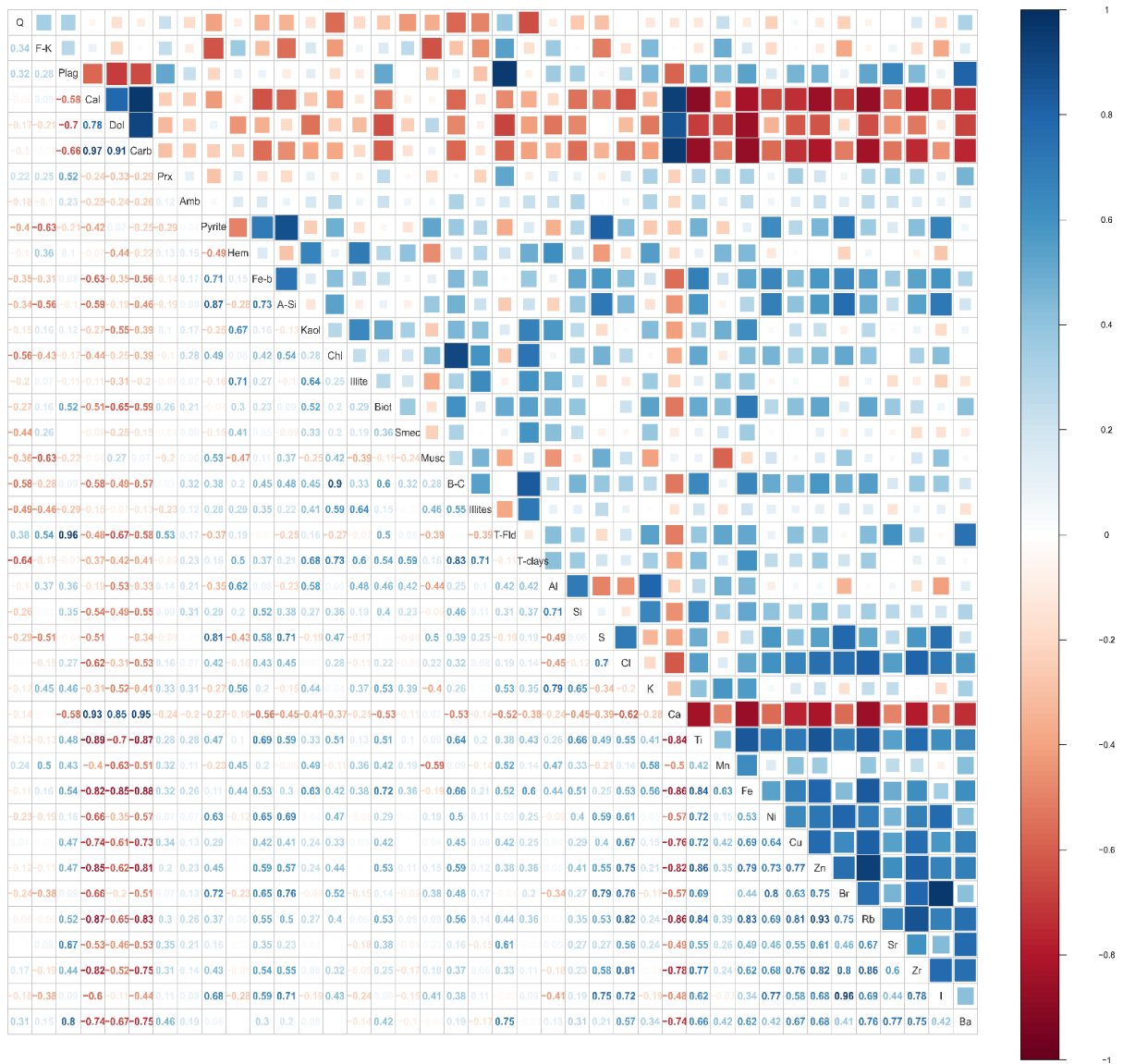


Figure 3.13: Correlation matrix of XRD-derived mineralogical data and normalised (sum) XRF-derived semi-quantitative elemental composition of the sediment of core AMD16-233. Blue squares indicate positive correlation, red squares negative correlations. The size of the square is proportionate to the correlation factor. Q: quartz; F-K: alkali feldspar; Plag: plagioclase; Cal: calcite; Dol: dolomite; Carb: carbonates (calcite + dolomite); Prx: pyroxene; Amb: amphibole; Hem: hematite; Fe-b: Fe-bearing minerals; A-Si: amorphous silica; Kaol: kaolinite; Chl: chlorite; Ill: illite; Biot: biotite; Smec: smectite; Musc: muscovite; B-C: biotite + chlorite; T-Fld: total feldspar; T-clays: total clays (kaolinite + chlorite + illite + biotite + smectite + muscovite).

Core AMD16-233 represents a unique, high resolution record of Holocene sedimentation at the entrance of Talbot Fjord, south of Nares Strait. High resolution (0.1 to 0.5 mm) semi-quantitative XRF core-scanner data were compared to low resolution mineralogical suites in order to identify suitable elemental markers for sediment provenance. Our sedimentological, geochemical and mineralogical datasets enable us to identify the provenance of the material involved in sedimentary processes, thus leading us to propose a detailed reconstruction of ice sheet retreat at the entrance of Talbot Fjord and southern Nares Strait. Key results of this study can be summarized as follows:

- a glacial margin existed at the core site prior to 9.8 cal. ka BP,
- ice sheet retreat in southern Nares Strait, possibly at the entrance of Talbot Fjord occurred before 9.8 cal. ka BP,
- Kane Basin became progressively glacial ice-free along an offshore, western/central axis from >9.8 to 9.1 cal. ka BP,
- deglaciation continued northward and coastward, eventually reaching the glacial saddle in Kennedy Channel, the collapse of which established the connection between the Arctic Ocean and northernmost Baffin Bay around 8.4 cal. ka BP, providing further evidence of a later date for the event,
- the sedimentary environment was relatively stable over the past 8.4 kyrs, with however increased delivery of local material and ice-rafted debris in the last 2.5/2.0 kyrs, perhaps associated with increased calving rates in Talbot Fjord.

The sedimentological, geochemical and mineralogical studies of cores AMD14-Kane2b and AMD16-233 enabled us to reconstruct geomorphological changes associated to ice sheet retreat in southern Nares Strait. The geomorphological setting having been defined in this first part of the project, the two cores may now be used to investigate the Holocene evolution of oceanic circulation and sea ice conditions in Kane Basin and in the North Water polynya.

Chapter 3 Local and regional controls on Holocene sea ice dynamics and oceanography in Nares Strait, Northwest Greenland

3.1 Résumé

Le détroit de Nares est l'un des trois détroits de l'archipel arctique canadien qui relie l'océan Arctique à la baie de Baffin. Des conditions de glace de mer uniques dans le détroit de Nares conduisent à la formation d'arcs de glace liées aux côtes (landfast ice) aux extrémités nord et sud du détroit. Ces arches de glace régulent l'export de glace de mer et d'eau douce en provenance de l'Arctique et favorisent l'ouverture de la polynie des eaux du Nord. Les enregistrements pré-satellites des conditions environnementales dans la région du détroit de Nares sont particulièrement peu nombreuses. La présente étude vise à reconstruire les conditions de la glace de mer et la circulation océanique holocène dans le détroit. L'archive centrale de l'étude est une carotte de sédiments marins stratégiquement récupérée sous l'arc de glace de mer actuelle dans le bassin de Kane au sud du détroit de Nares. La carotte fournit un enregistrement continu couvrant les 9 derniers mille ans. Nous utilisons des assemblages foraminifères benthiques et des biomarqueurs de la glace de mer pour identifier les changements dans la circulation océanique holocène et les conditions de la glace de mer dans le bassin de Kane. L'établissement de la circulation océanique moderne dans le bassin de Kane est lié au retrait de la calotte glaciaire et au rebond postglaciaire, tandis que les changements dans la couverture de glace de mer correspondent aux changements majeurs dans l'oscillation arctique (OA). Nos résultats suggèrent que la couverture de glace de mer dans le bassin de Kane était très variable entre ca. 9,0 et 8,3 cal. ka BP, avant d'augmenter, probablement en lien avec l'évènement froid de 8,2 cal. ka BP et l'ouverture du détroit de Nares. Une courte période de couverture de glace de mer minimale et d'influence maximale d'eau de fond provenant de l'Atlantique s'est produite entre ca. 8,1 et 7,5 cal. ka BP, lorsque le bassin de Kane était plus profond. Lorsque les températures atmosphériques chutent à la fin du maximum thermique holocène, la couverture de glace de mer s'est intensifiée dans le bassin de Kane entre ca. 7,5 et 5,5 cal. ka BP, mais des vents forts dans des conditions d'OA positives ont probablement empêché la formation d'arcs de glace dans le détroit de Nares. Pendant ce temps, nos données micropaléontologiques montrent que l'eau Atlantique a été progressivement exclue du bassin de Kane par le rebond isostatique postglaciaire. Des températures atmosphériques de plus en plus froides et des phases plus négatives de l'OA ont probablement favorisé l'établissement d'arcs de glace dans le détroit de Nares entre ca. 5,5 et 3,0 cal. ka BP. Des instabilités dans l'arc de glace du bassin de Kane situé ca. 3,0 cal. ka BP coïncident avec un changement vers des phases plus positives de l'OA, tandis qu'un brève rétablissement de l'arc de glace s'est produit lors de conditions plus négatives de l'OA entre ca. 1,2 et 0,2 cal. ka BP.

3.2 Abstract

Nares Strait is one of three channels that connect the Arctic Ocean to Baffin Bay. Unique sea ice conditions in the strait lead to the formation of land-fast ice arches at its northern and southern ends. These ice arches regulate Arctic sea ice and freshwater export through the strait and promote the opening of the North Water polynya. The

present study addresses the paucity of pre-satellite records of environmental conditions in the Nares Strait area, and aims at reconstructing Holocene sea ice conditions and ocean circulation in the strait. The investigation is based on a marine sediment core strategically retrieved from under the current ice arch in Kane Basin to the south of Nares Strait, and provides a continuous record spanning the past ca 9 kyr. We use benthic foraminiferal assemblages and sea ice biomarkers to infer changes in Holocene ocean circulation and sea ice conditions in Kane Basin. The establishment of the modern ocean circulation in Kane Basin is related to ice sheet retreat and postglacial rebound, while changes in sea ice cover concur with major shifts in the Arctic Oscillation (AO). Our results suggest that sea ice cover in Kane Basin was highly variable between ca. 9.0 and 8.3 cal. ka BP, before increasing, probably in link with the 8.2 cold event and the opening of Nares Strait. A short period of minimum sea ice cover and maximum Atlantic bottom water influence occurred between ca. 8.1 and 7.5 cal. ka BP, when Kane Basin was deeper than for the remaining of the Holocene. As atmospheric temperatures dropped, sea ice cover intensified in Kane Basin between ca. 7.5 and 5.5 cal. ka BP, but strong winds under prevailing positive-like AO conditions likely prevented the formation of ice arches in Nares Strait. During this time, our micropaleontological data show that Atlantic water was progressively excluded from Kane Basin by the postglacial isostatic rebound. Increasingly cooler atmospheric temperatures and a shift towards more negative phases of the AO may have promoted the establishment of ice arches in Nares Strait between ca. 5.5 and 3.0 cal. ka BP. Instabilities in the Kane Basin ice arch ca. 3.0 cal. ka BP coincide with a shift towards prevailing positive phases of the AO, while a brief recovery of the ice arch occurred during more negative-like AO conditions between ca. 1.2 and 0.2 cal. ka BP. Eleanor Georgiadis^{1,2}, Jacques Giraudeau¹, Anne Jennings³, Audrey Limoges⁴, Rebecca Jackson⁵, Sofia Ribeiro⁵, Guillaume Massé^{2,6}

¹Université de Bordeaux, CNRS, UMR 5805 EPOC, allée Geoffroy St-Hilaire, 33615 Pessac, France

²Université Laval, UMI 3376 TAKUVIK, 1045 avenue de la Médecine, G1V 0A6, Québec, QC, Canada

³INSTAAR, University of Colorado, Boulder, CO 80309-0450, USA

⁴Department of Earth Sciences, University of New Brunswick, 2 Bailey Drive, Fredericton, E3B 5A3, Canada

⁵Department of Glaciology and Climate, Geological Survey of Denmark and Greenland, Øster Voldgade 10, Copenhagen 1350, Denmark

⁶Université Sorbonne, CNRS, UMR 7159 LOCEAN, 4 place Jussieu, 7500 Paris Cedex, France

Marine Geology, 422, 2020 (<https://doi.org/10.1016/j.margeo.2020.106115>)

3.3 Introduction

Nares Strait, located between Greenland and Ellesmere Island, is one of three channels of the Canadian Arctic Archipelago (CAA) linking the Arctic Ocean to Baffin Bay (Figure 4.1). The strait is an important gateway for the export of water and sea ice from the Arctic Ocean towards the Atlantic Ocean, contributing to up to half of the volume of water transported through the CAA (McGeehan and Maslowski, 2012). The CAA is a major provider of freshwater to the Labrador Sea where it may influence deep water formation (Belkin et al., 1998). Regional ocean surface dynamics are partly regulated by the unique sea ice conditions in the strait. The export of Arctic sea ice

through Nares Strait ceases annually in the winter and spring, when land-fast ice covers the strait, and forms the Kane Basin ice arch (Figure 4.1-c; Barber et al., 2001). Fresh surface water export through Nares Strait is also reduced in the presence of this ice arch (Münchow, 2016). Furthermore, the Kane Basin ice arch is integral in maintaining the North Water polynya (Figure 4.1-b), as it prevents sea ice and icebergs from drifting into northern Baffin Bay, while northerly winds and ocean currents sweep away any newly formed sea ice in the polynya (Melling et al., 2001). The Kane Basin ice arch is formed by the congestion of multi-year sea ice from the Arctic Ocean and glacial ice calved from the Petermann and Humboldt Glaciers (Figure 4.1-b). The particular morphology of the strait promotes the build-up of ice in the southern part of the strait as (1) an anti-cyclonic gyre in the wider Kane Basin can slowdown and trap drift ice and icebergs (Nutt, 1966), and (2) the coastline forms a bottleneck on either side of Smith Sound and restricts the southern exit of Kane Basin. Another ice arch occasionally forms to the north of the strait along the Robeson Channel (Figure 4.1-e) by the convergence of thick multi-year ice in the Lincoln Sea (Kwok et al., 2010). A polynya in the south of the Lincoln Sea and in northern Nares Strait can be promoted by this northern ice arch, but it has been less studied than its southern counterpart (Kozo, 1991). Simulations have shown that the thickness of the ice forming these arches is a key factor in determining their resistance to the strong winds in Nares Strait (Dumont et al., 2009), suggesting that ice arch break-up is at least partly dictated by the effect of wind stress on thinning ice during the spring or summer. Locally, winds are orographically channelled by the steep coastal topography of Nares Strait, and their strength is correlated to the sea level pressure difference between northern and southern Nares Strait (Samelson and Barbour, 2008). While winds play a role in the predominantly south-ward flowing ocean surface current in Nares Strait, the main driver of this flow is considered to be the sea level difference between the Lincoln Sea and Baffin Bay (Münchow and Melling, 2008). The ingress of the West Greenland Current (WGC) into southern Nares Strait constitutes a counter-current of northward Atlantic-sourced water that runs through Smith Sound (Figure 4.1-b; Münchow et al., 2007), but the extent of its reach into Kane Basin is unclear. The water column in Nares Strait is stratified, with southward Arctic and Pacific water carried in the top 50 m, and a mix of Atlantic and Pacific water below this depth (Jones and Eert, 2004; Münchow et al., 2007). Most of the Atlantic water in Kane Basin is considered to enter via the north, from the Arctic Ocean (e.g., Münchow et al., 2011), although some may enter via the south, from Baffin Bay, in varying amounts (e.g., Sadler, 1976).

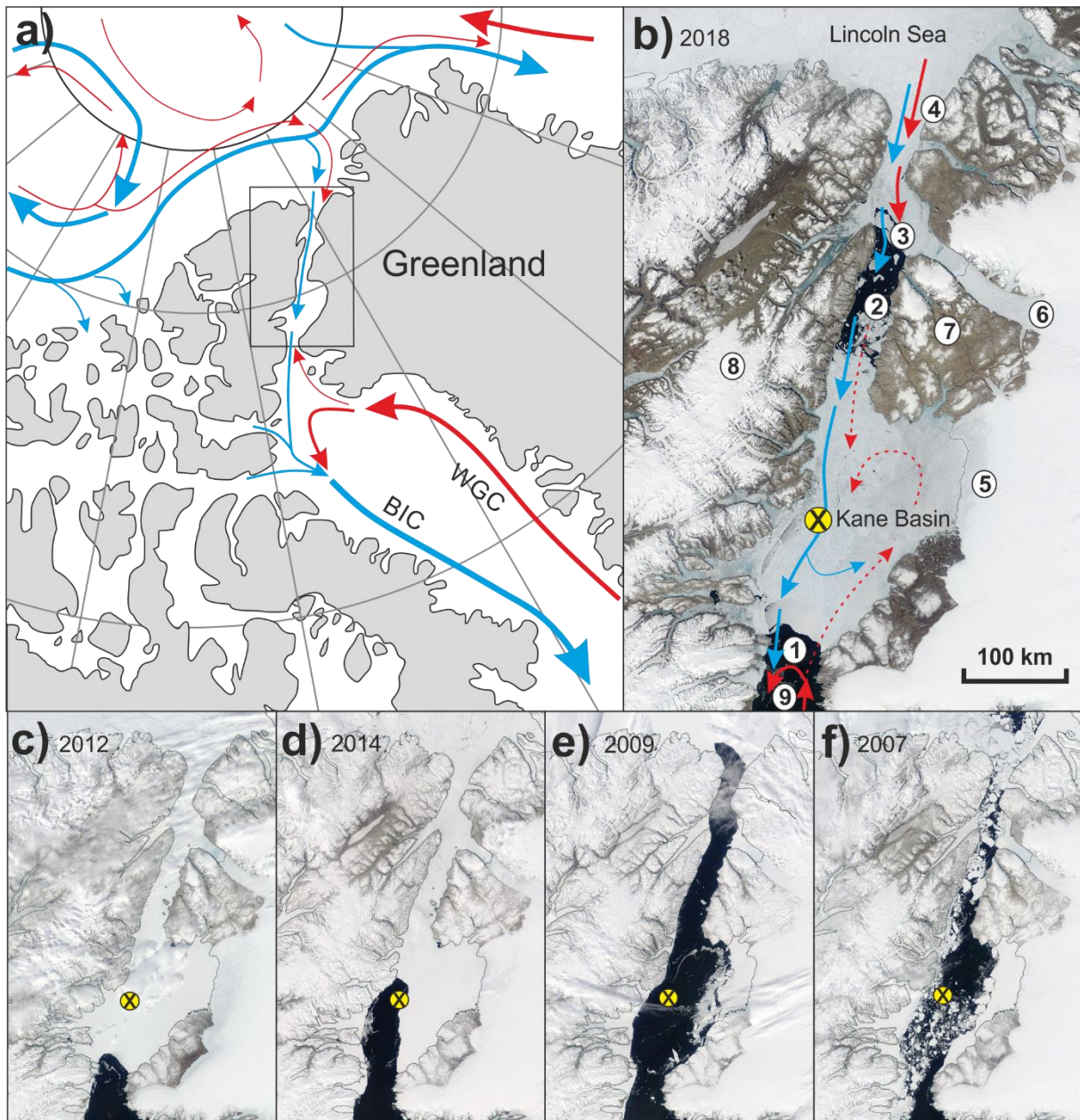


Figure 4.1: Schematic circulation in the Canadian and northern Greenland sectors of the Arctic Ocean and Baffin Bay (a) and within Nares Strait (b, snapshot from July 28th 2018), and inter-annual variations in sea ice cover in Nares Strait (c-f). The location of core AMD14-Kane2b is marked by a cross. Blue arrows represent Arctic (surface) water and red arrows deeper Atlantic water, red dashed arrows represent the potential circulation of Atlantic water in Nares Strait. WGC: West Greenland Current, BIC: Baffin Island Current. 1 - Smith Sound; 2 - Kennedy Channel; 3 - Hall Basin; 4 - Robeson Channel; 5 - Humboldt Glacier; 6 - Petermann Glacier; 7 - Washington Land; 8 - Agassiz Ice Cap; 9 - North Water polynya. Snapshots of satellite images from MODIS (500 m resolution) of Nares Strait during the first week of June in: c) 2012 (“typical” location of the southern ice arch), d) 2014 (northern migration of the southern ice arch – the NOW polynya extends to the core site), e) 2009 (northern ice arch in the Lincoln

Sea – the southern ice arch failed to form), and f) 2007 (year-round throughflow of ice – both ice arches failed to form). Satellite image source: <https://worldview.earthdata.nasa.gov/>.

Nares Strait has been the focus of a number of short-lived monitoring programs, and concerns have been raised regarding the future of the ice arches in the context of global warming. Some of the first documented observations of the North Water polynya in the literature report that the breakup of the southern ice arch usually occurred in late July or August in the 1960s, and as late as mid-August in 1967 (Dunbar, 1969). In the late 1990s and early 2000s, the ice arches typically collapsed in early July (Kwok et al., 2010). In the winter of 2006–2007, both ice arches failed to form for the first time in the satellite era (Kwok et al., 2010). Since then, a trend of late formation, early breakup or complete failure to form has been observed (Moore and McNeil, 2018; Münchow, 2016), and is associated with decreasing primary productivity in the North Water (Marchese et al., 2017). Those recent observations may suggest that the area is currently witnessing a rapid transition in sea ice dynamics (Moore and McNeil, 2018).

Long-term perspectives on sea ice dynamics in Nares Strait are essential to better understand their response to climatic forcing. Such records extending beyond the satellite era are however scarce in Nares Strait. Here, we present the first reconstruction of sea ice cover and oceanographic circulation in Kane Basin, based on the study of a 4.25 m long marine sediment core (AMD14-Kane2b) strategically retrieved from under the current southern ice arch that provides a continuous record of the past *ca* 9 cal. ka BP.

Nares Strait is situated along the former confluence of the Innuitian Ice Sheet (IIS) and the Greenland Ice Sheet (GIS), and was covered by glacial ice until *ca.* 9–8 cal. ka BP (e.g., England, 1999; Georgiadis et al., 2018; Jennings et al., 2011, 2019). In addition to the drastic climatic shift during the deglaciation (*ca.* 18–8 cal. ka BP), Nares Strait has undergone a major spatial reorganisation associated with ice sheet retreat and postglacial isostatic rebound during the Holocene (11.7–0 cal. ka BP). The opening of the Nares Strait also established a direct atmospheric channel between the polar vortex and Baffin Bay.

In this paper, we aspire to (1) reconstruct the Holocene environmental evolution of Kane Basin based on benthic foraminiferal assemblages and sea ice biomarkers (IP₂₅ and HBI III), and (2) establish possible links between sea ice dynamics and ocean circulation in the strait with local (geomorphologic) and regional (climatic) forcing. This work builds-on a previous sedimentological and geochemical study on the same core which laid the foundations for the post-glacial history of Nares Strait (Georgiadis et al., 2018).

3.4 Material and methods

3.4.1 Sediment core AMD14-Kane2b

The 4.25 m long marine sediment core AMD14-Kane2b (79°30' N 70°51' W, 220 m water depth) was retrieved in Kane Basin, the central basin of Nares Strait, with a CASQ – Calypso Square – corer during the 2014 ArcticNet cruise of CCGS *Amundsen*. A full description of sediment facies for this record is given in Georgiadis et al. (2018). Of particular interest are two units which are rich in ice-rafted debris (IRD) in the bottom half of the core dated at *ca* 9.0 cal. ka BP and 8.3 cal. ka BP, both of which fall within the time frame of the collapse of the glacial buttress in

Kennedy Channel based on previous datings of the event (England, 1999; Jennings et al., 2011, 2019). Georgiadis et al. (2018) argued that these lithofacies were likely linked to (1) a retreating ice- marginal environment ca. 9 cal. ka BP, and (2) the collapse of the glacial buttress in Kennedy Channel which established the connection of the Arctic Ocean to Baffin Bay through Nares Strait ca. 8.3 cal. ka BP.

The age model of core AMD14-Kane2b is presented in Caron et al., 2019 and Georgiadis et al. (2018). It is based on 14 AMS radiocarbon ages measured on benthic foraminifera and mollusc shells and corrected with $\Delta R = 240 \pm 55$ years. Sedimentation rates decrease from ~ 220 cm.ka⁻¹ at the very base of the core to ~ 30 – 50 cm.ka⁻¹ in the remaining 3.5 m of the core. ²¹⁰Pb measurements indicate that the core recovered modern sediments and suggests an average age for the core top of ~ 60 years (1955 CE) with low sedimentation rates of ~ 20 cm.ka⁻¹.

3.4.2 Sea ice biomarkers

The sea ice biomarkers used in this study are the Highly Branched Isoprenoids (HBI) IP₂₅ (Ice Proxy with 25 atoms of carbon) and HBI III (tri-unsaturated HBI). Their abundances were determined at a 1 to 4 cm resolution (10–160 years according to our age model) and following the protocol described by Belt and Müller (2013). Concentrations of IP₂₅ and HBI III are expressed in ng.g⁻¹ of dry sediment. In the absence of a pure HBI III standard, the concentrations of this biomarker are expressed in ng.g⁻¹ of internal standard equivalent.

Biomarker fluxes (concentration*density*sedimentation rate) were calculated using the CT-number as a proxy for sediment density, and are thus expressed in number/unit surface area/year (for additional information, the reader is referred to Georgiadis et al., 2018).

IP₂₅ is synthesised by spring, and, to a minor extent, summer sea ice dwelling diatoms *Haslea spicula*, *H. kjellmanii* and *Pleurosigma stuxbergii* var. *rhomboides* (Brown et al., 2014). IP₂₅ is considered as a proxy for seasonal sea ice cover. Its absence in sediment indicates either year- round ice-free (absence of habitat for sea ice diatoms) or permanently ice-covered (absence of detachment of the ice algae, and/or potential light limitation) waters (Belt and Müller, 2013). Freshwater input in coastal Arctic settings has been identified as being potentially detrimental to IP₂₅ production in sea ice, and changes in salinity should not be overlooked as a source of IP₂₅ variability (Ribeiro et al., 2017). HBI III has been found to be synthesized by the two sea ice margin diatom genera *Pleurosigma* and *Rhizosolenia* (Belt et al., 2010) generally associated with planktic ice-edge productivity and freshwater (Ribeiro et al., 2017).

The spatial variability of IP₂₅ and HBI III concentrations in Arctic regions causes difficulties in converting given biomarker concentrations into quantitative sea ice reconstructions. Biomarker abundances have been used in paleoceanographic studies as a means of reconstructing the changes in sea ice dynamics by observing the relative variations of biomarkers through time at a given location (e.g., Belt et al., 2010). Although in situ HBI measurements have not yet been carried out in Nares Strait, we assume that HBI III-producing diatoms may dwell in the ice-packed, fresher surface water following ice arch break-up. The irregular under-ice environment of the Kane Basin ice arch – made up of varying amounts of thick multi-year ice consolidated by thinner first year ice – and the continuous supply

of nutrients by the throughflow of Pacific-sourced Arctic water constitutes an ideal environment for IP₂₅-producing sea ice algae (Krembs et al., 2002).

3.4.3 Foraminifera

One centimetre-thick slices of approximately 25 cm³ of sediment were sampled and dried before wet sieving through 63 and 125 µm meshes. Benthic and planktic foraminifera census counts were performed on the oven-dried residue of each fraction every 4–16 cm throughout the core. This protocol (drying before and after sieving, and dry counting) has been a standard practice in micropaleontological studies including those conducted on marine sediments from the High Arctic, but this method is no longer recommended due to the loss of poorly cemented agglutinated and more fragile calcareous species (Sperling et al., 2002). Our foraminiferal assemblages were however diverse, and dominant taxa were similar to those found in nearby micropaleontological studies (Jennings et al., 2019; Knudsen et al., 2008). Concentrations of benthic and planktic foraminifera are expressed in number of individuals per gram of dry sediment, and fluxes (concentrations*density*sedimentation rates) are expressed in an arbitrary unit of number of individuals/unit surface area/year.

Table 4.1: List of foraminifera used to reconstruct paleoenvironments from core AMD14-Kane2b and their original references.

Benthic foraminifera:
<i>Brizalina pseudopunctata</i> (Höglund 1947)
<i>Buliminella elegantissima</i> (d'Orbigny 1839)
<i>Buccella frigida</i> (Cushman 1922)
<i>Cassidulina neoteretis</i> Seidenkrantz 1995
<i>Cassidulina reniforme</i> Norvan 1945
<i>Elphidium excavatum</i> forma <i>clavata</i> Cushman 1930
<i>Epistominella arctica</i> Green 1959
<i>Islandiella helenae</i> Feyling-Hanssen & Buzas 1976
<i>Islandiella norcrossi</i> (Cushman 1933)
<i>Nonionella iridea</i> Heron-Allen & Earland 1932
<i>Nonionellina labradorica</i> (Dawson 1860)
<i>Stainforthia feylingi</i> Knudsen & Seidenkrantz 1994
<i>Stainforthia fusiformis</i> (Williamson, 1848)

Planktic foraminifera:
<i>Neoglobobadrina pachyderma</i> (Ehrenberg 1861)

Foraminiferal assemblages offer detailed insight regarding past marine environmental conditions owing to the fossilisation potential of foraminifera tests and specific environmental preferences. Such information as the abundance of food supply, the occurrence of sea ice cover, and the presence of Atlantic water at the bottom can be provided by the specific composition of the assemblages. The benthic foraminifera used to reconstruct paleoenvironmental conditions in core AMD14-Kane2b are listed in Table 4.1 along with their original references.

A stratigraphically constrained cluster analysis (CONISS, Grimm, 1987) was performed on the relative abundance of calcareous benthic species using the *vegan* (Oksanen et al., 2019), *mgcv* (Wood, 2019) and *grDevices* (R Core Team, 2017) packages in R. The data and ecozones (i.e. clusters) were plotted using the *Rioja* package in R (Juggins, 2019). The broken sticks model indicated four main clusters.

3.5 Results and interpretations

3.5.1 Sea ice biomarkers

IP₂₅ was present in all samples analysed from core AMD14-Kane2b, attesting that Kane Basin was seasonally covered by sea ice during the last *ca.* 9 cal. ka BP (Figure 4.2). HBI III was detected in all but 6 samples, albeit at much lower concentrations than IP₂₅ (i.e. average [IP₂₅] = 57 ng.g⁻¹ sediment, average [HBI III] = 1 ng.g⁻¹ standard equivalent). Both biomarkers however displayed the same general trends in concentrations, with lower values below *ca.* 250 cm (*ca.* 7.2 cal. ka BP), higher values above this depth, and very high concentrations in the two IRD-rich intervals. Large sediment inputs at the base of our record, owing to the proximity of glacial ice (Georgiadis et al., 2018), were likely to have caused the lower concentrations in the bottom half of our record. We thus focus on biomarker fluxes rather than concentrations to interpret the record. The variations in biomarker fluxes were compared to the flux measured in the topmost sample of our core which is associated with modern conditions.

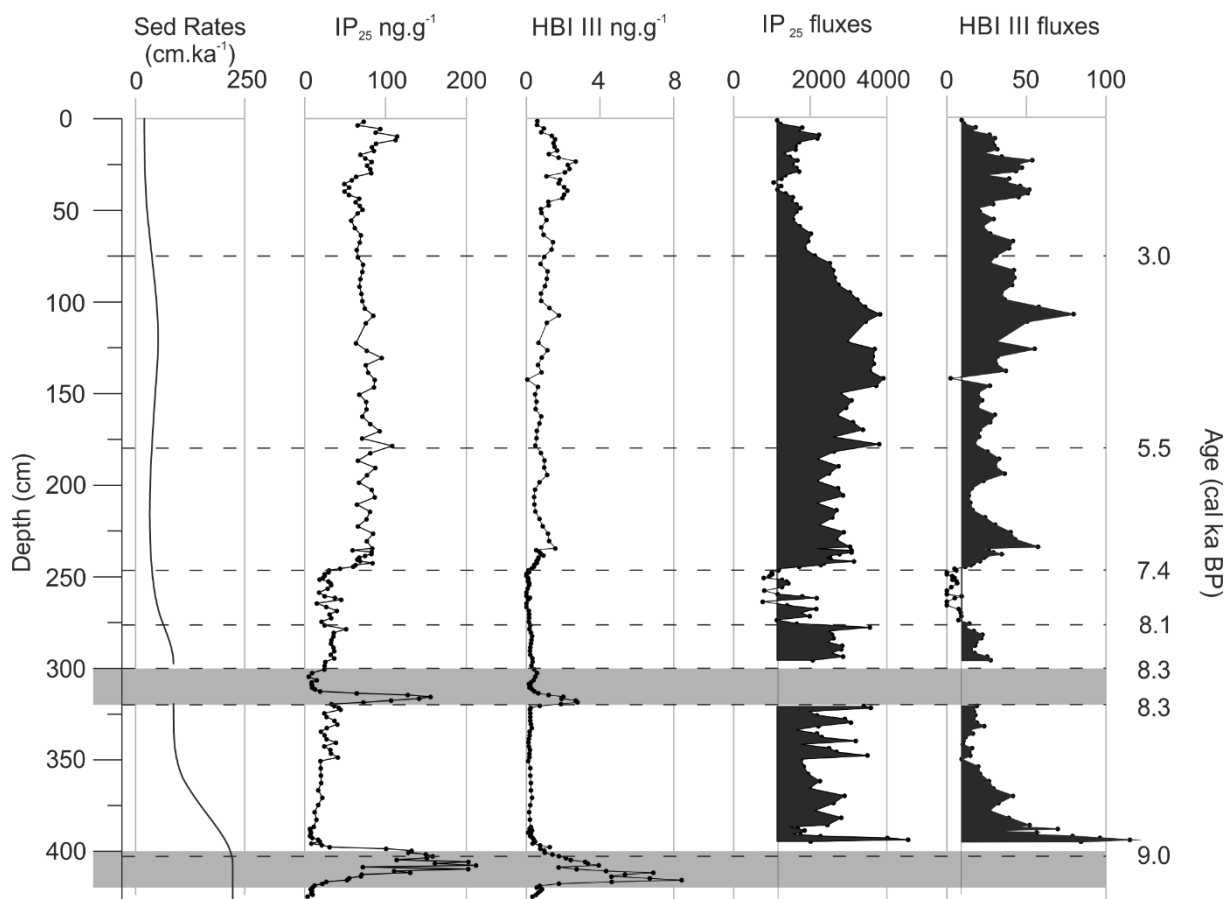


Figure 4.2: Sedimentation rates (from Georgiadis et al., 2018), HBI (IP_{25} and HBI III) concentrations and fluxes in core AMD14-Kane2b. The two IRD-rich units are highlighted by grey boxes. Fluxes were not calculated in these two IRD units owing to very high sedimentation rates in these intervals. Fluxes above the value measured at the core top are filled in black, those below appear white. Dashed lines indicate major changes in biomarker fluxes with corresponding ages on the right.

The two IRD-rich units at ca. 400–425 cm and ca. 300–320 cm, dated at ca. 9.0 and 8.3 cal. ka BP, were characterised by particularly high concentrations of IP_{25} and HBI III (Figure 4.2). Fluxes were not calculated in these two units due to the assumption that they were deposited very rapidly. High amplitude variations of IP_{25} fluxes occurred in the early part of the record from 400 to 320 cm (ca. 9.0 to 8.3 cal. ka BP). These oscillations may be due to the high temporal resolution owing to higher sedimentation rates (i.e. 1 cm represents an average of only 10 years of sedimentation in this interval) when the IIS and GIS were close to the core site (Georgiadis et al., 2018). Alternatively, or additionally, the proximity of the retreating ice sheets could have provided large amounts of freshwater that may have decreased IP_{25} production, even when seasonal sea ice was effectively present (Ribeiro et al., 2017). The high, but decreasing, HBI III fluxes from ca. 9.0 to 8.5 cal. ka BP also point to freshwater input during ice sheet retreat in Kane Basin, in line with the foraminiferal record. The high IP_{25} and HBI III concentrations measured at the base of the IRD-rich unit dated at ca. 8.3 cal. ka BP may have been associated to the breakup of glacial ice in Kennedy Channel (Georgiadis et al., 2018). The mechanical action of calving at an ice margin has been

reported to increase productivity (Shadwick et al., 2013) and may have contributed to the high biomarker concentrations. Recurrent seasonal sea ice between ca. 8.3 and 8.1 cal. ka BP is evidenced by the stable IP₂₅ fluxes. This period of sustained high IP₂₅ fluxes coincides in time with the 8.2 cal. ka BP cold event and may also have been promoted by the throughflow of cold and fresh Arctic water through Nares Strait. Biomarker fluxes clearly decreased between 8.1 and 7.4 cal. ka BP and were comparable to the low values at the top of our core. IP₂₅ fluxes increased sharply at ~250 cm (ca. 7.4 cal. ka BP) and remained high before beginning to decrease at 100 cm (ca. 3.5 cal. ka BP). A smaller increase occurred ~180 cm (ca. 5.5 cal. ka BP) and IP₂₅ fluxes were particularly high between ~150–110 cm (ca. 4.7 and 3.5 cal. ka BP). HBI III fluxes were variable between 250 and 140 cm (ca. 7.4 and 4.5 cal. ka BP), but remained relatively high in the top 140 cm of the core (past ca. 4.5 cal. ka BP). A minimum in IP₂₅ fluxes was reached around 35 cm (ca. 1.7 cal. ka BP), whereas HBI III fluxes were high during this time. This period centred around 1.7 cal. ka BP constitutes the second interval when IP₂₅ fluxes were similar to modern values, although HBI III fluxes were higher. A short recovery in IP₂₅ fluxes occurred around 10 cm (ca. 0.5 cal. ka BP), while HBI III fluxes decreased. Both IP₂₅ and HBI III fluxes decreased in the top 10 cm (over the past 500 years). The decrease in IP₂₅ over the past ca. 3 kyrs, culminating in lower IP₂₅ fluxes than present ca. 1.7 cal. ka BP, can either be interpreted as severe sea ice conditions (i.e. reduced light penetration in very thick sea ice), or as reduced sea ice cover. However, the reasonably high HBI III fluxes during the past 3 kyrs attest to at least occasional occurrence of open water in Kane Basin.

3.5.2 Foraminifera

Planktic foraminifera were represented exclusively by *Neogloboquadrina pachyderma* sinistral (NPS), a polar species usually the only (dominant) planktic foraminifera present in polar (subpolar) Atlantic water (e.g., Vilks, 1969). NPS concentrations varied between ca. 0 and 57 ind.g⁻¹ dry sediment (Figure 4.3). Their fluxes were higher in the earlier part of our record (425–240 cm, ca. 9.0 to 7.2 cal. ka BP), and decreased until 170 cm (ca. 5.5 cal. ka BP), after which the occurrence of NPS became rare (Figure 4.3).

The concentrations of benthic foraminifera varied between ~0 and 1300 ind.g⁻¹ dry sediment (Figure 4.3). The base of the core, which is IRD-rich, was barren of foraminifera until 401.5 cm when the abundance of coarse particles decreases (Georgiadis et al., 2018). Fluxes were highest between 280 and 240 cm (ca. 8.1 and 7.2 cal. ka BP), and were also relatively high between 401 and 280 cm (ca. 9.0 and 7.2 cal. ka BP), and between 150 and 60 cm (ca. 4.7 and 2.7 cal. ka BP).

The ecozones defined by the cluster analysis performed on the benthic assemblages were named E1 to E4, and their ages are shown in Figure 4.3.

The concentrations of benthic foraminifera varied between ~0 and 1300 ind.g⁻¹ dry sediment (Figure 4.3). The base of the core, which is IRD-rich, was barren of foraminifera until 401.5 cm when the abundance of coarse particles decreases (Georgiadis et al., 2018). Fluxes were highest between 280 and 240 cm (ca. 8.1 and 7.2 cal. ka BP), and were also relatively high between 401 and 280 cm (ca. 9.0 and 7.2 cal. ka BP), and between 150 and 60 cm (ca. 4.7 and 2.7 cal. ka BP).

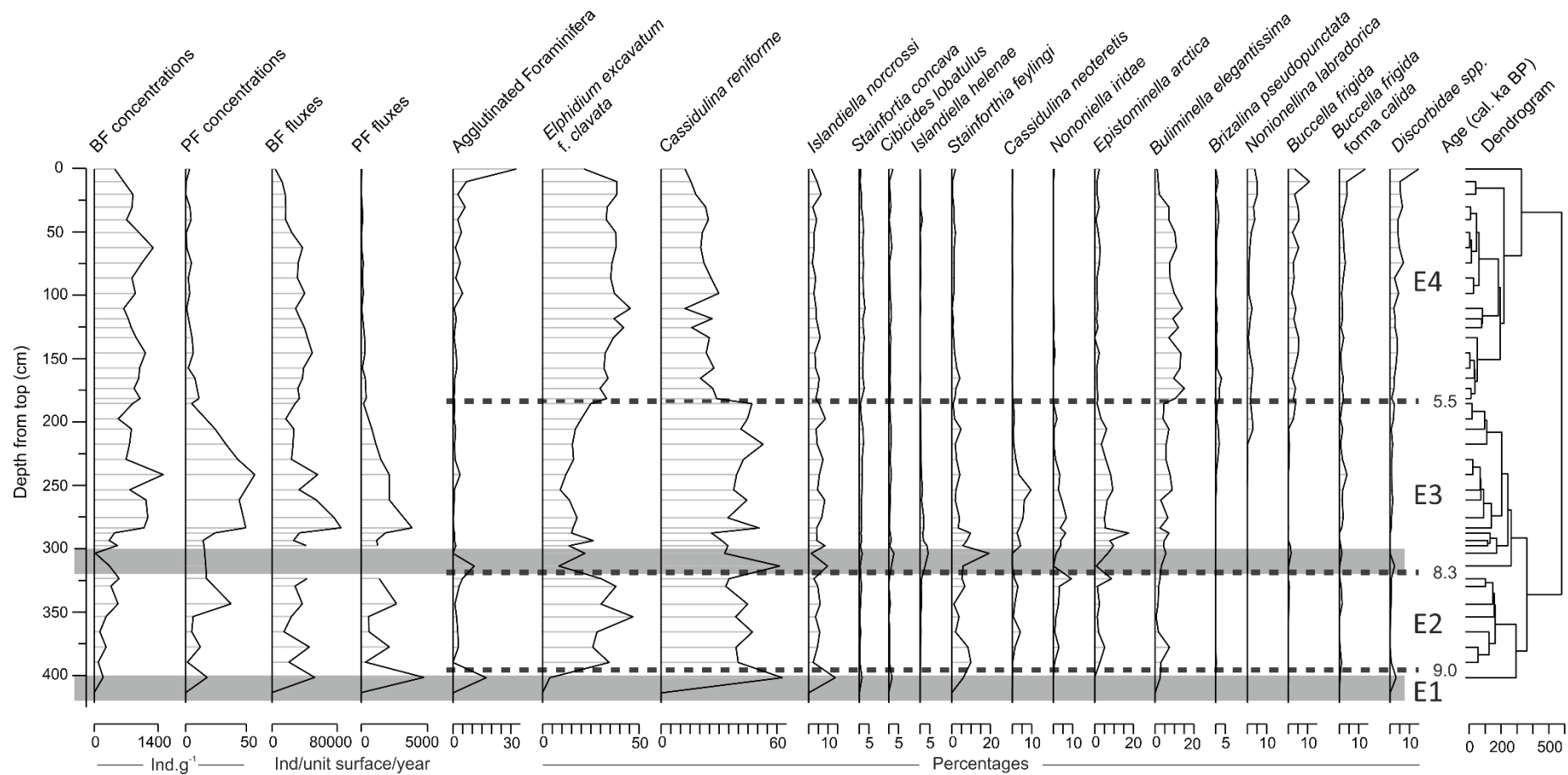


Figure 4.3: Benthic (BF) and planktic (PF) foraminifera concentrations and fluxes, percentages of agglutinated foraminifera, abundance of calcareous species in core AMD14-Kane2b, and the hierarchical clustering dendrogram of the distance matrix computed in R. The IRD-rich units are represented by a grey bar along the depth scale. Fluxes were not calculated in the two IRD units owing to very high sedimentation rates in these intervals (Georgiadis et al., 2018).

The ecozones defined by the cluster analysis performed on the benthic assemblages were named E1 to E4, and their ages are shown in Figure 4.3.

The assemblage composing E1, a single sample dated at ca. 9.0 cal. ka BP (401.5 cm), was largely dominated by *C. reniforme* (~63 %), with a subordinate contribution of *Islandiella norcrossi* (~14 %). High relative abundances of *C. reniforme* attest to the influence of bottom waters of Atlantic origin at the core site (e.g., Polyak et al., 2002), while *I. norcrossi* is indicative of stable salinity (Atlantic-sourced) water, possibly under seasonal sea ice (Steinsund and Hald, 1994). We also noted the particularly high abundance of agglutinated foraminifera in this sample (~17 % of the total amount of benthic foraminifera) – despite its older age and the method used for sample preparation.

The second assemblage E2 (389.5–323.5 cm, ca. 8.9–8.3 cal. ka BP) was co-dominated by *E. excavatum* forma *clavata* (~30 %) and *C. reniforme* (~40 %). Contributions of *I. norcrossi* were reduced in E2 and remain low throughout the rest of the core, while relative abundances of *Stainforthia feylingi* were notable at the base of this interval (up to 10%), and the abundances of *Nonionella iridea* increased up-core (up to 9 %). Although low percentages of *Cassidulina neoteritis* were found in E2, their presence was still noteworthy (average of ~2 %, with maxima of 4 %). The occurrence of the opportunistic species *E. excavatum* forma *clavata* is indicative of unstable environmental conditions and lower salinity (Hald et al., 1994). The presence of *S. feylingi* may also be associated with meltwater inputs in Kane Basin (Jennings et al., 2017). However, chilled Atlantic water was still present in the bottom waters at the core site according to the relatively high abundance of *C. reniforme* (Jennings et al., 2019; Knudsen et al., 2008; Polyak et al., 2002). A limited influence of relatively warmer Atlantic water was also hinted at by the presence of *C. neoteritis* (Jennings et al., 2004), albeit in low numbers. The subordinate contributions of *N. iridea* attest to the pulsed export of phytodetritus to the seabed (e.g., Gooday and Hughes, 2002). This assemblage is representative of a glacimarine environment, with a limited influence of Atlantic water at the bottom and reduced bottom water salinity, possibly due to meltwater inputs, and pulsed productivity related to seasonal sea ice cover.

The third ecozone E3 (313.5–181.5, ca. 8.3–5.5 cal. ka BP) was characterised by a sustained dominance of *C. reniforme* (~40 %), while contributions of *E. excavatum* forma *clavata* (~17 %) were reduced compared to E2. Subordinate species *S. feylingi*, *N. iridea*, *Epistominella arctica*, *Buliminella elegantissima*, and *Cassidulina neoteritis* each contributed to up to 7–19 % of the assemblage in E3. The increased contribution of *C. neoteritis* in E3 relative to E2 attests to a greater influence of warmer Atlantic water at the bottom of Kane Basin (Jennings et al., 2004), while the decreasing abundances of *E. excavatum* forma *clavata* and *S. feylingi* point to gradually reduced meltwater. The presence of *N. iridea*, *E. arctica*, and *B. elegantissima* indicate that the export of organic matter occurred in pulses and was related to seasonal sea ice cover (e.g., Gooday and Hughes, 2002). Ecozone E3 represents a more distal glacial marine environment with reduced meltwater input compared to E2, and maximal Atlantic influence in bottom water at the core site, under seasonal sea ice cover.

The assemblage of ecozone E4 (181.5–0 cm, ca. 5.5–0 cal. ka BP) was dominated by *E. excavatum* forma *clavata* (~36 %), with lower contribution of *C. reniforme* (~22 %). A number of subordinate species in E3 were replaced by *Nonionellina labradorica* (up to 5 %) and *Buccella frigida* (up to 11 %). The relative abundance of *B.*

elegantissima, however, increased to an average of 10 % in E4. The notable decrease in *C. reniforme* and *C. neoteretis* abundances compared to the previous ecozone points to a reduced influence of Atlantic bottom water at the core site from ca. 5.5 cal. ka BP, while increased contributions of *E. excavatum* forma *clavata* is indicative of fresh (possibly polar) water in Kane Basin. The occurrence of the high productivity species *N. labradorica* (Polyak et al., 2002), *B. frigida* (Steinsund and Hald, 1994) and *B. elegantissima* (Knudsen et al., 2008) are indicative of the export of phytodetritus to the seabed, although their individual relative abundances in E4 were on average < 5 %. While the decreased influence of Atlantic water in basal water is clear in E4, the precise significance of the replacement of two high productivity species by two others is more complex. It has been suggested that *N. labradorica* may be related to Arctic water masses (Racine, 2019), which supports the interpretation of reduced Atlantic water based on decreased contributions of *C. reniforme* and *C. neoteretis*, and increase fresh polar water based on *E. excavatum* forma *clavata* abundances. In addition, *N. labradorica* has been associated to fresh phytodetritus in polar fronts but not specifically to sea ice cover (Rytter et al., 2002), whereas *E. arctica* and *N. iridea* are known to withstand long periods of oligotrophic conditions (i.e. severe sea ice) and to reproduce very rapidly (i.e. more rapidly than other high productivity species) during very brief periods of food supply (e.g., Gooday and Hughes, 2002). Ecozone E4 is thus representative of reduced Atlantic influence and increased Arctic water in Kane Basin, under seasonal sea ice cover with significant periods of productivity. This suggests that the decrease in biomarker fluxes in the top part of our record should be interpreted as reduced sea ice, and not as severe sea-ice cover (cf. 3.1). The overall limited benthic foraminifera fluxes in this likely more productive interval may be due to (1) dissolution of the carbonated taxa, and/or (2) the loss of agglutinated taxa (possibly more competitive in corrosive Arctic waters; Aksu, 1983) caused by the sample preparation method.

3.6 Results and interpretations

The CAA has experienced major environmental changes since the last deglaciation (i.e. past ca 18 kyrs) in relation to climatic variability along with eustatic and glacio-isostatic sea-level change (e.g. England et al., 2006). The present study provides the first long-term proxy record of sea ice cover and oceanographic changes in Kane Basin. Both our micropaleontological and biogeochemical datasets suggest that Kane Basin was seasonally covered by sea ice during the last 9.0 kyrs. However, changes in biomarker fluxes and benthic foraminiferal assemblages suggest variability in sea ice dynamics and ocean circulation. Here, we discuss the history of paleoenvironmental conditions in Kane Basin in response to changing local geomorphology and regional climate during and following the deglaciation of Nares Strait.

3.6.1 Deglaciation of Kane Basin (ca. 9.0–8.3 cal. ka BP)

In line with sedimentological evidence previously shown by Georgiadis et al. (2018), a transition from an ice sheet-marginal to ice-distal environment was recorded by our micropaleontological and biomarker data from ca. 9.0 to 8.3 cal. ka BP. The co-dominance of *C. reniforme* and *E. excavatum* forma *clavata* attest to a glacial marine environment under the influence of Atlantic water in Kane Basin during this interval (Figure 4.4). The sediment at the base of our core displayed relatively high concentrations of sea ice biomarkers and were likely deposited close

to the ice margin. Ice marginal environments can be productive owing to the upwelling of nutrients through meltwater plumes, the stratification induced by meltwater inputs (e.g. Kanna et al., 2018), and the mechanically induced breakup of sea ice by calving (Shadwick et al., 2013). Both highly variable IP_{25} fluxes and high percentages of *E. excavatum* forma *clavata* suggest unstable salinity and likely variable sea ice cover in Kane Basin between ca. 9.0 and 8.3 cal. ka BP (Figure 4.4). These unstable conditions are possibly the result of freshwater input and a local cooling owing to the proximity of the GIS and IIS, and high atmospheric temperatures during the Holocene Thermal Maximum (HTM, Figure 4.5; Lecavalier et al., 2017). In Smith Sound, to the south of Nares Strait, benthic foraminiferal assemblages are indicative of a transition from harsh environmental conditions with a strongly stratified water column and severe sea ice cover, towards more seasonal sea ice and productive surface waters starting around 9 cal. ka BP (Jennings et al., 2019). This temporal disparity between the two core sites reflects the northward retreat of the IIS and the GIS in southern Nares Strait.

The IRD-rich unit dated at ca. 8.3 cal. ka BP in core AMD14-Kane2b has been interpreted to mark the opening of the Kennedy Channel (Georgiadis et al., 2018) and is characterised by high concentrations of sea ice biomarkers. High calving rates associated with the deglaciation of Kennedy Channel may have fuelled sea ice and ice margin productivity in Kane Basin by mechanically enhancing light availability due to sea ice break-up. Alternatively, this IRD-rich unit may have been deposited by the retreat of the Humboldt Glacier happening around this time (Reusche et al., 2018).

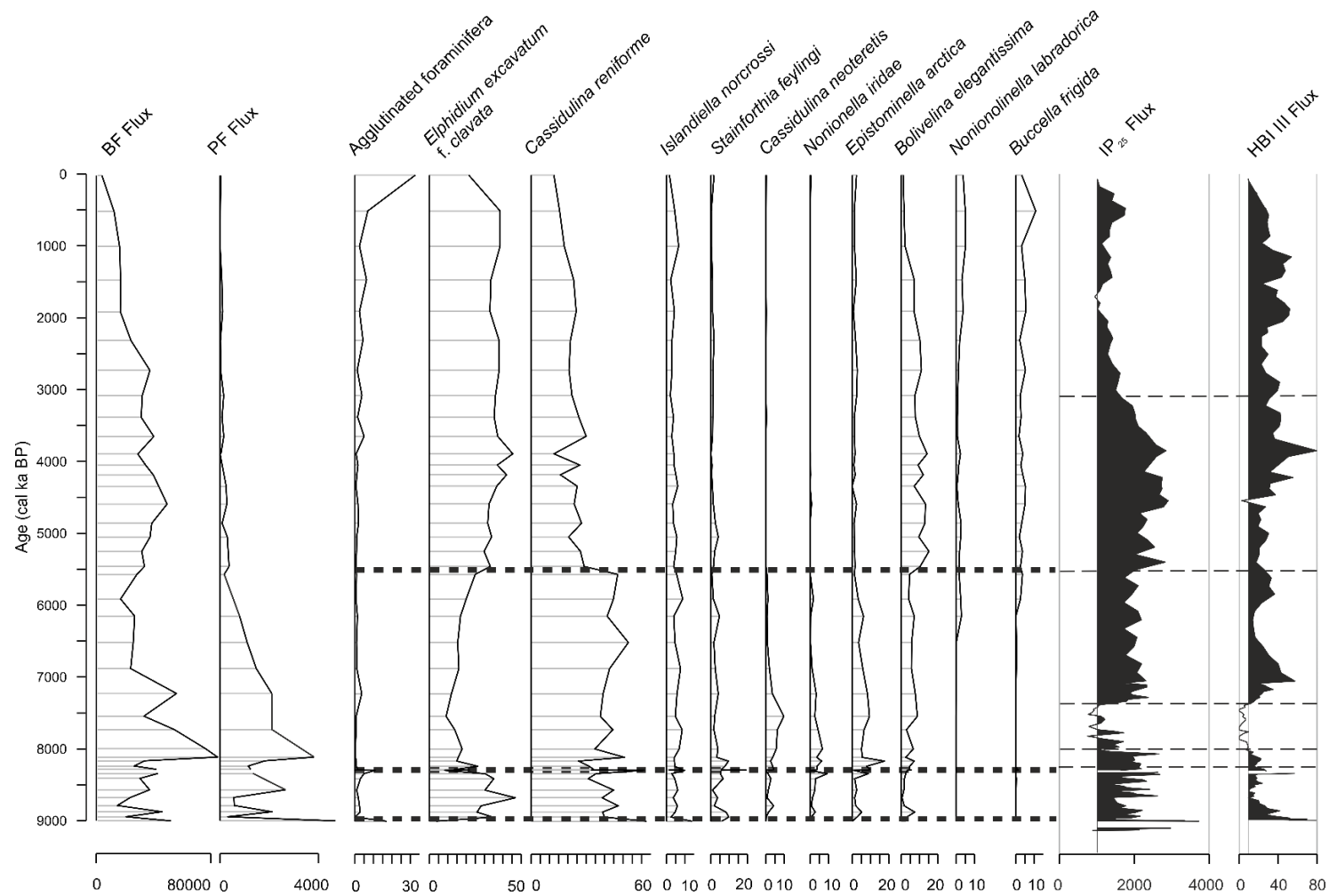


Figure 4.4: Benthic (BF) and planktic (PF) foraminifera fluxes, percentage of agglutinated foraminifera, and abundance of the benthic foraminifera species used to reconstruct paleoenvironment in Kane Basin, plotted next to IP_{25} and HBI III fluxes in core AMD14-Kane2b on an age scale. Thick dashed lines delimitate ecozones and thin dashed lines indicate changes in biomarker fluxes. The two IRD-rich units are represented by grey solid lines.

3.6.2 Maximum influence of Atlantic Water in Kane Basin (ca. 8.3-7.4 cal. ka BP)

The period between 8.3 and 7.4 cal. ka BP is marked by a maximum in Atlantic influence in the bottom water of Kane Basin as suggested by the dominance of *C. reniforme* and the presence of *C. neoteritis*. Biomarker fluxes are variable, indicating changes in sea ice cover during this interval. The ingress of Atlantic water into Kane Basin may have been facilitated by the greater water depth prior to the postglacial isostatic rebound (up to 120–140 m deeper; England et al., 2006). The modern Nares Strait bottom water characteristic implies that Arctic-sourced Atlantic Water lying at 350 m water depth must surpass a sill (300 m water depth) to enter Nares Strait from the north (Münchow et al., 2011), or face the upward sloping Kane Basin topography for Baffin Bay-sourced Atlantic water entering via the south (e.g., Münchow, 2016). Up to 120–140 m greater water depth in Nares Strait prior to the rebound would have facilitated the entrance of Atlantic water at depth, both through the north and the south. A short period (ca. 8.3–8.1 cal. ka BP) of high IP_{25} and relatively low HBI III fluxes follows the IRD-rich unit and coincides with the 8.2 event recorded in the nearby Agassiz ice core record (Figures 4.4 and 4.5; Lecavalier et al., 2017). This cold event is thought to have been triggered by the drainage of the proglacial Agassiz lakes (Barber et al., 1999). Locally, the cooling may have been accentuated by increased fluxes of freshwater and cold air through Nares Strait associated with the newly-established connection of the Arctic Ocean to Baffin Bay. The increased freshwater flux through the strait may have promoted recurrent (and possibly occasionally perennial) sea ice cover in Kane Basin during this cold period. Heavy sea ice cover is supported by the occurrence of *S. feylingi* and *E. arctica* (Figure 4.4). The link between the 8.2 event and extensive sea ice cover in Kane Basin may however be coincidental, since the error associated to our age model is approximately ± 200 years owing to reservoir age corrections alone (Georgiadis et al., 2018). Biomarker fluxes reach minimal values (some below those measured at the core top) between ca. 8.1 and 7.4 cal. ka BP, coinciding with persisting high atmospheric temperatures of the HTM in the region (Figure 4.5; Lecavalier et al., 2017). Low IP_{25} fluxes suggest that sea ice cover in Kane Basin was reduced during this time, possibly with a shorter sea ice season on a yearly basis. The maximum influence of (warmer) Atlantic water in Kane Basin at this time may have promoted more open water at the surface, along with more glacio-distal conditions as the GIS and IIS retreated. Alternatively, the throughflow of Arctic surface water through Nares Strait and increased meltwater input into Kane Basin during this warmer period could have been detrimental to IP_{25} -producing diatoms (Ribeiro et al., 2017). Dinocyst assemblages from core AMD14-Kane2b, which are largely dominated by heterotrophic taxa, display a short-lived increase of autotrophic species during this interval, supporting slightly warmer, more open-water conditions in Kane Basin (Caron et al., 2019). Nil to minimum HBI III fluxes suggest a reduced influence of marginal ice conditions at the core site between ca. 8.1 and 7.4 cal. ka BP. Both the decrease in HBI III and IP_{25} fluxes may have been caused by earlier spring melt of sea ice. An increase in seasonal open water conditions is also supported by the peak in both planktic and benthic foraminifera fluxes. In addition, it is worth noting that the occurrence of land-fast sea ice in the Lincoln Sea was scarce during the Early Holocene, according to driftwood records from northern Ellesmere Island (Figure 4.5; England et al., 2008). Our record of foraminifera and sea ice biomarker fluxes supports the fact that sea ice occurrence in the

Nares Strait area was relatively low between ca. 8.1 and 7.4 cal. ka BP, following a period of potentially sustained sea ice cover between 8.3 and 8.1 cal. ka BP (Figure 4.4).

3.6.3 Increased drift-ice and shallowing of Kane Basin (ca. 7.4-5.5 cal. ka BP)

The benthic foraminiferal assemblage in ecozone E3 and high planktic foraminifera fluxes are indicative of a strong influence of Atlantic water in Kane Basin between ca. 8.3 and 5.5 cal. ka BP and a gradual reduction of Atlantic water starting ca. 7.4 with decreasing numbers of *C. neoteretis* and planktic foraminifera (Figure 4.4). The post-glacial isostatic rebound likely began with the thinning of the GIS and IIS during the Early Holocene (Lecavalier et al., 2014), but the effects of the shallowing of Kane Basin are most apparent in our record between ca. 7.4 and 5.5 cal. ka BP. The decrease in warm Atlantic indicator species suggests a progressively reduced presence of Atlantic water associated with the shoaling of Nares Strait. Their replacement by *E. excavatum* forma *clavata* from ca. 5.5 cal. ka BP is indicative of fresher bottom water in Kane Basin, similar to the modern oceanographic circulation which is characterised by limited Atlantic water and pre-dominantly Arctic water masses.

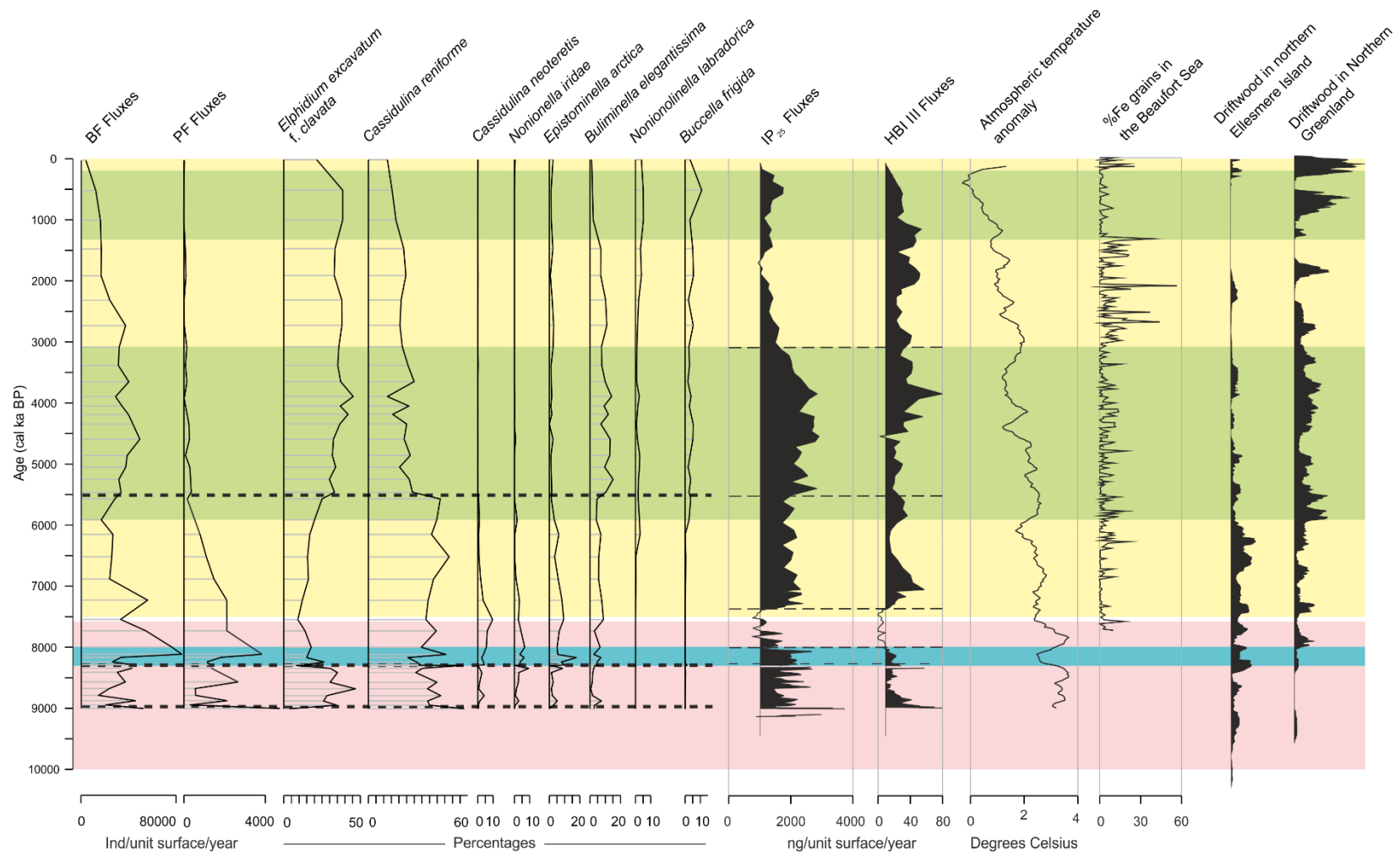


Figure 4.5: Comparison of benthic (BF) and planktic (PF) foraminifera fluxes, abundance of selected benthic foraminifera species, and IP_{25} and HBI III fluxes in AMD14-Kane2b with regional records, including the temperature anomaly ($^{\circ}C$, from $\delta^{18}O$) (Lecavalier et al., 2017), Siberian IRD in the Beaufort Gyre (Darby et al., 2012), cumulative probability distribution of calibrated ^{14}C ages of driftwood in northern Ellesmere Island (England et al., 2008) and north-eastern Greenland (Funder et al., 2011). The HTM is marked in red, and the 8.2 cold event in blue (based on the Agassiz temperature record). AO positive phases are represented in yellow, AO negative in green.

A pronounced increase in biomarker fluxes occurred ca. 7.4 cal. ka BP. The sustained high IP₂₅ fluxes indicate an increase in sea ice cover in Kane Basin between ca. 7.4 and 5.5 cal. ka BP. This coincides with a decrease in atmospheric temperatures ca. 7.5 cal. ka BP following the end of the HTM (Figure 4.5; Lecavalier et al., 2017). Interestingly, this also corresponds to a period of maximum driftwood deposition in northern Ellesmere Island (ca. 7.0–5.5 cal. ka BP; Figure 4.5; England et al., 2008), likely caused by enhanced sea ice in the Arctic Ocean as atmospheric temperatures dropped (Figure 4.5; Lecavalier et al., 2017). A marked decrease in July air temperatures is also inferred by chironomid assemblages recovered in sediments from a nearby lake (Axford et al., 2019). Although sea ice cover may have been present in Kane Basin during this time, we refrain from affirming that the ice arches existed in Nares Strait between ca. 7.5 and 5.5 cal. ka BP. This is based on the fact that there is no evidence to date of (1) the opening of a polynya in northernmost Baffin Bay during this interval (Davidson et al., 2018) nor (2) land-fast ice in northern Ellesmere Island that could have formed a recurrent northern ice arch (England et al., 2008). The relatively low abundances of sea ice diatoms in the North Water area between ca. 7.3 and 5.5 cal. ka BP (Knudsen et al., 2008) does not suggest that northernmost Baffin Bay was so severely ice-covered that the opening of the polynya may have been prevented by in situ sea ice formation were the Kane Basin ice arch indeed present. Instead, we propose that, although Arctic sea ice cover increased with lower atmospheric temperatures, winter atmospheric temperatures were not yet low enough to allow the formation of sufficiently thick ice in the Lincoln Sea and in Kane Basin to withstand the strong, along strait winds. Furthermore, according to the origin and the spatial distribution of driftwood between northern Ellesmere Island and Northern Greenland, positive phases of the Arctic Oscillation (AO) prevailed from ca. 8.5 and 6.0 cal. ka BP (Figure 4.5; Funder et al., 2011). During modern AO positive phases, the atmospheric Beaufort High likely extends over the Lincoln Sea (Steele et al., 2004), perhaps explaining the correlation between wind strength in Nares Strait and the AO index in modern times (Samelson and Barbour, 2008; Figure 4.6). The strong winds during this period of prevailing positive phases of the AO may have been unfavourable to ice arch formation (Dumont et al., 2009). The overall increase in HBI III fluxes between ca. 7.4–5.5 cal. ka BP suggests ice-loaded fresh surface water in Kane Basin. These surface conditions are consistent with high mobile sea ice and freshwater flux through Nares Strait in the absence of ice arches and under the influence of strong northerly winds.

3.6.4 Establishment of modern oceanography in Nares Strait and the inception of ice arches (ca. 5.5-3.0 cal. ka BP)

A further increase in IP₂₅ fluxes occurs ca. 5.5 cal. ka BP and coincides with a change in benthic foraminiferal assemblage (Figure 4.4). *E. excavatum* forma *clavata* replaces *C. reniforme* as the dominant species, attesting to a major shift in bottom water masses as they are represented by fresher water while the influence of Atlantic water is reduced following the shoaling of Kane Basin. The notable contributions of phytodetritus index species *N. labradorica*, *B. frigida*, and *B. elegantissima*, in the foraminiferal assemblage over the past 5.5 kyrs suggests the seasonal export of fresh organic matter related to ice-edge productivity in Kane Basin. Later sea ice retreat, in phase with the insolation maximum in the late spring or early summer, may have enhanced the export of organic matter since under-ice and ice-edge environments are more productive than open water (Mayot et al., 2018). Higher IP₂₅

fluxes are also suggestive of a longer sea ice productivity season (Belt and Müller, 2013). We propose that this later retreat of the sea ice in Kane Basin is likely linked to the onset of the recurrent, seasonal formation of a stable ice arch in Kane Basin. According to Funder et al. (2011), negative phases of the AO prevailed from ca. 6 cal. ka BP. Along with the Neoglacial cooling, negative phase of the AO could have promoted the formation of ice arches in Nares Strait through two main processes (Figure 4.6). Firstly, sea ice thickness in the Arctic Ocean is negatively correlated to the AO index due to the atmospheric control on sea ice circulation (Rigor et al., 2002). Secondly, weaker winds in Nares Strait during negative phases of the AO (Samelson and Barbour, 2008) are less likely to break-up land-fast ice (Dumont et al., 2009). Together, colder atmospheric temperatures, thicker sea ice, and weaker winds between ca. 5.5 and 3.0 cal. ka BP could have promoted ice arch formation in Nares Strait.

The changes observed in our Kane Basin proxy records at ca. 5.5 cal. ka BP are near synchronous with the development of ice shelves (Antoniades et al., 2011) and thick coastal ice (England et al., 2008) in northern Ellesmere Island. The development of these ice shelves may be linked to the establishment of the seasonal northern ice arch in Nares Strait. Benthic foraminiferal assemblages from the North Water display reduced abundances of *E. excavatum* forma *clavata* and increased contributions of *N. labradorica* ca. 5.2 cal. ka BP, suggesting a transition from harsh conditions towards a productive polar front with seasonal sea ice (Knudsen et al., 2008). This more productive environment could be linked to occasional openings of a polynya due to an infrequent ice arch in Kane Basin. However, according to Davidson et al. (2018) the inception of the North Water did not occur before ca. 4.5 cal. ka BP, which raises the question of whether the southern ice arch was firmly established between 5.5 and 4.5 cal. ka BP (Figure 4.5). Our biomarker records display a slight increase in IP₂₅ fluxes ca. 4.7 cal. ka BP, which may correspond to a more recurrent southern ice arch around the time of the inception of the North Water.

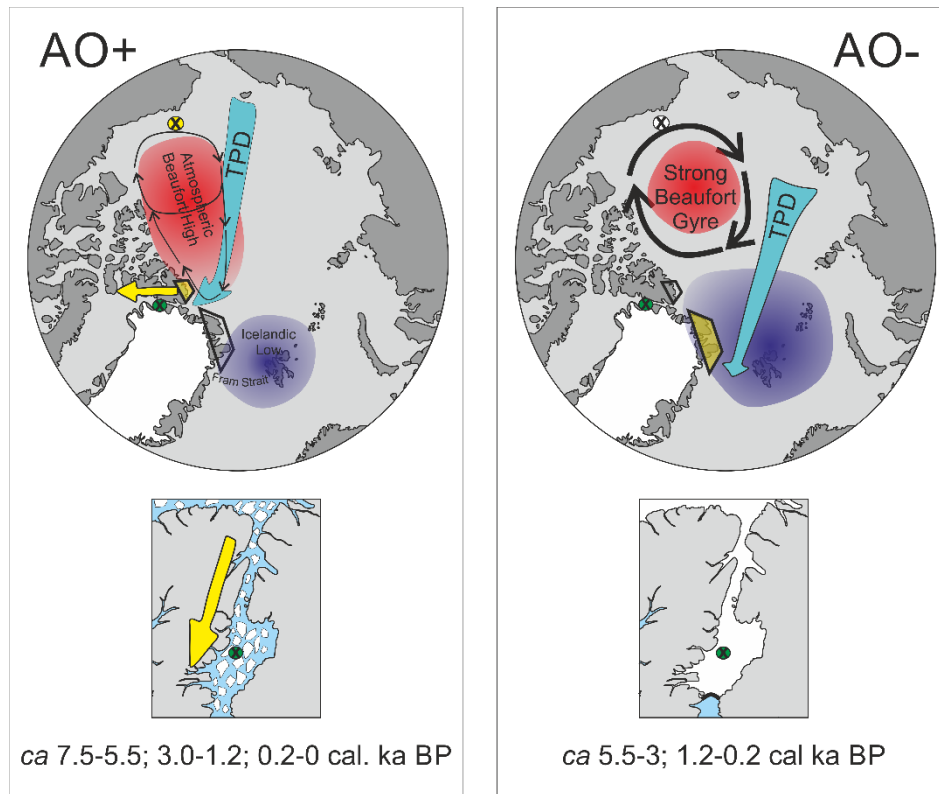


Figure 4.6: Schematic representation of positive (+) and negative (-) phases of the Arctic Oscillation (AO), and of sea ice conditions in Nares Strait, adapted from Steele et al. (2004). Location of core AMD14-Kane2b is marked by a cross in a green circle (this study), the record of IRD in the Beaufort Sea is marked by a cross in a yellow (AO+) or white (AO-) circle (Darby et al., 2012). The study area of driftwood occurrence in northern Ellesmere Island (England et al., 2008), and in Northern Greenland (Funder et al., 2011) are marked by trapezoids. In a positive phase of the AO, the Beaufort Gyre is weak (unfavourable to multi-year sea ice), the atmospheric Beaufort High (red) extends into the Lincoln Sea, and the transpolar drift (TPD, carrying Siberian IRD to the Beaufort Sea and driftwood to northern Ellesmere Island) originates in eastern Siberia and funnels ice towards Nares Strait. The pressure difference between northern and southern Nares Strait is strong during positive AO phases, leading to strong, along-strait winds (yellow arrow). Both thinner Arctic sea ice and strong winds are unfavourable to ice arch formation in Nares Strait under positive AO conditions. During a negative phase of the AO, a strong Beaufort gyre promotes multi-year sea ice, while the TPD takes a more direct route towards Fram Strait, and deposits driftwood in Northern Greenland. The extension of the Icelandic Low (blue) into the Arctic Ocean potentially creates low pressure in the Lincoln Sea, reducing the pressure gradient along Nares Strait. Thick multi-year sea ice and weaker winds promote the formation of ice arches in Nares Strait under negative AO phases.

3.6.5 Decline of sea ice cover in Kane Basin (ca. 3.0-0 cal. ka BP)

IP₂₅ fluxes in Kane Basin decrease after ca. 3.0 cal. ka BP indicating a decline in sea ice cover despite continued atmospheric cooling (Figure 4.5; Lecavalier et al., 2017). Darby et al. (2012) report strong positive phases of the AO starting ca. 3.0 cal. ka BP based on an IRD record in the Beaufort Sea (Figure 4.5). Prevailing positive AO phases are also supported by a decrease in driftwood occurrence in Northern Greenland (Funder et al., 2011). Stronger winds may have favoured the export of sea ice through Nares Strait and hindered the formation of the Kane Basin ice arch during this period, explaining the low IP₂₅ fluxes (Figure 4.6). The decay of Little Auk colonies in Thule after ca. 3.0 cal. ka BP is probably a result of an unstable southern ice arch in Kane Basin under these conditions. Lowest IP₂₅ fluxes occurred between ca. 2.2 and 1.1 cal. ka BP (Figure 4.5). IP₂₅ fluxes recover briefly around 0.5 cal. ka BP, as more negative phases of the AO are inferred by driftwood in Northern Greenland (Funder et al., 2011) and the IRD record in the Beaufort Sea (Darby et al., 2012). A decrease in IP₂₅ fluxes towards the core top coincides with increasing positive phases of the AO over the past two centuries (Darby et al., 2012), and warmer atmospheric temperatures (Lecavalier et al., 2017). We note that while the southern ice arch in Kane Basin appears to have been weaker over the past ca. 3 kyr than it was between 4.5 and 3.0 cal. ka BP, the northern ice arch was likely a recurrent feature in the Lincoln Sea during this time according to the paucity of driftwood in northern Ellesmere Island (England et al., 2008). The fact that the northern ice arch was present during this interval may explain the little change in our foraminiferal assemblages. The assemblage is similar to the previous interval, indicating a productive ice edge environment. The presence of the northern ice arch after 5.5 cal. ka BP likely limited the export of Arctic drift-ice through Nares Strait and promoted high productivity rates, as opposed to the interval between 7.4 and 5.5 cal. ka, when the northern ice arch was absent and productivity was hindered by the passing of drift-ice through Nares Strait. However, recent instabilities have also been recognised in the northern ice arch during the 20th century (England et al., 2008), and more recently since the early 2000s (Kwok et al., 2010; Moore and McNeil, 2018). This suggests that we may currently be witnessing a shift of surface conditions in Kane Basin towards those reported between 7.4 and 5.5 cal. ka BP (i.e. absence of both ice arches, increased sea ice export through Nares Strait, and decreased productivity under prevailing AO positive phases and warm atmospheric temperatures), or even towards HTM surface conditions reported between 8.1 and 7.5 cal. ka BP (i.e. very low sea ice cover, absence of ice arches, and limited productivity).

3.7 Conclusion

Our biomarker and foraminiferal datasets provide the first records of Holocene environmental conditions in Kane Basin related to ocean circulation and sea ice dynamics. Our results indicate that the establishment or the collapse of recurrent ice arches in Nares Strait throughout the last 9000 years are synchronous with major shifts in Arctic sea ice and atmospheric circulation patterns related to the Arctic Oscillation, while changes in ocean circulation in Kane Basin are likely linked to the postglacial rebound. Our reconstructions of surface conditions in Kane Basin and our hypothesis concerning the local and regional factors controlling sea ice dynamics and oceanographic circulation in Nares Strait can be summarised as follows:

- A glacial environment with highly variable sea ice cover persisted during ice sheet retreat in Kane Basin between ca. 9.0 and 8.3 cal. ka BP, and was influenced by warm atmospheric temperatures during the HTM and possibly by the local cooling effect of the IIS and GIS.
- Maximal influence of Atlantic water characterised the interval between ca. 8.3 and 7.5 cal. ka BP, when Kane Basin was deeper prior to the isostatic rebound. Minimal sea ice cover is inferred by low biomarker fluxes between ca. 8.1 and 7.4 cal. ka BP, during the end of the HTM and in a more glacio-distal environment.
- Mobile Arctic drift-ice likely passed through Nares Strait in the absence of the northern and southern ice arches during prevailing positive phases of the AO between ca. 7.5 and 5.5 cal. ka BP, hindering productivity, while Atlantic water was progressively excluded from Kane Basin by the postglacial uplift.
- Together with cooler atmospheric temperatures, a shift towards more negative phases of the AO may have favoured increased duration of sea ice occurrence and the establishment of ice arches in Nares Strait between ca. 5.5 (northern ice arch) or ca. 4.5 (southern ice arch) and 3.0 cal. ka BP.
- Prevailing positive phases of the AO starting ca. 3.0 cal. ka BP coincide with the beginning of recent instabilities in the Kane Basin ice arch, while a brief recovery of this southern ice arch occurred during more negative phases of the AO between ca. 1.2 and 0.2 cal. ka BP. Productivity in Kane Basin likely remained high owing to the presence of the northern ice arch during this time.

While we have focussed on shifts in the Arctic Oscillation to explain the changes in surface conditions in Kane Basin, it must be acknowledged that other secondary modes of sea level pressure variations (e.g., Barents Oscillation (Smedsrud et al., 2013), Dipole Anomaly (Wang et al., 2009)), along with thermodynamic factors (Kwok and Untersteiner, 2011), play significant roles in oceanic and atmospheric circulation in the Arctic Ocean and, in particular, sea ice export towards lower latitudes. However, the availability of records of the AO covering the Holocene, along with the potentially dominant role of the AO on longer time scales (e.g., build-up of sea ice in the Arctic Ocean which preconditions its response to secondary modes (Dumas et al., 2003)), justified the focus of our work on this index. The apparent link between the AO index and ice arch formation in Nares Strait implies that the recently observed instabilities of the ice arches are prone to continue with the predicted positive phases of the AO in the near-future (Rigor et al., 2002). These instabilities are likely to severely impact the North Water area (Marchese et al., 2017), and may influence convection patterns as far as the Labrador Sea (Belkin et al., 1998) as sea ice and freshwater export through Nares Strait increase in the absence of ice arches (Münchow, 2016).

Acknowledgements: Eleanor Georgiadis' studentship is funded by the Initiative d'Excellence (IdEx) programme of the University of Bordeaux, and the Natural Science and Engineering Research Council of Canada (NSERC). We warmly thank Benoit Lecavalier for constructive conversations, and for having shared with us the Agassiz ice core temperature record and simulations of sea level change in Nares Strait. Our gratitude is also extended to Naima El Bani Altuna, Frédérique Eynaud and Jérôme Bonnin for discussions concerning foraminifera,

and Caroline Guilmette for analytical support for HBI measurements. We thank the editor, Adina Paytan, for entrusting our original manuscript to both a paleoceanographer and a physical oceanographer in the reviewing process. The manuscript was greatly improved thanks to both reviewers' comments. This work is supported by the Fondation Total, the French Agence Nationale de la Recherche (GreenEdge project), the Network of Centres of Excellence ArcticNet, and the European Research Council (StG IceProxy). Finally, we wish to thank the CCGS *Amundsen* captain, officers and crew for their support during the 2014 ArcticNet cruise

Edited by: Shu Gao

Reviewed by: two anonymous referees

The micropaleontological (planktic and benthic foraminiferal assemblages) and biogeochemical (sea ice biomarkers IP₂₅ and HBI III) records obtained in core AMD14-Kane2b provide the first reconstruction of Holocene changes in ocean circulation and sea ice cover in Kane Basin. In an attempt to determine the controlling factors of sea ice conditions in Nares Strait, we hypothesize that the Arctic Oscillation (AO) may regulate ice arch formation in Kane Basin. Our reconstructions are as follows:

- environmental conditions were highly variable following deglaciation from ca 9.0 to 8.3 cal. ka BP, owing to both high atmospheric temperatures and meltwater input due to ice sheet retreat,
- sea ice cover reached minimal extent from ca 8.1 until 7.5 cal. ka BP, during the end of the Holocene Thermal Maximum, when Atlantic influence was enhanced at the core site,
- following this interval, Atlantic-sourced water still reached the core site, but its presence was reduced, especially after ca 5.5 cal. ka BP, when the postglacial rebound restricted the entrance of Atlantic-sourced bottom water at the core site, increasing Arctic influence,
- sea ice cover duration further increased starting at 5.5 cal. ka BP, with maximal values between 4.5 and 3.5/3.0 cal. ka BP, possibly indicating the inception of the Kane Basin ice arch in the spring and into the summer,
- sea ice cover was reduced over the past ca 3.0 kyrs, with a slight recovery from ca 1.2 to 0.2 cal. ka BP.

The reconstructions of sea ice conditions in Nares Strait evidence periods of stability and instability of the Kane Basin ice arch, which implies that the North Water polynya may have likewise experienced periods of high vs. low activity as a consequence of sea ice dynamics in Nares Strait. In the next paper, we use in sediments of core AMD16-233 the same set of proxies as in core AMD14-Kane2B, in order to reconstruct the Holocene history of the North Water polynya.

Chapter 4 Holocene dynamics of the North Water, northernmost Bafin Bay: a perspective from the western sector of the polynya

4.1 Résumé

Le détroit de Nares, dans le nord-ouest du Groenland, a montré des signes significatifs de sensibilité au changement climatique au cours des dernières décennies. La banquise qui recouvre le détroit de Nares produit un « arc de glace », au sud de laquelle s'ouvre la polynie des eaux du Nord, la plus grande polynie du domaine Arctique. Aujourd'hui, cette polynie entretient un ensemble d'espèces constituant un écosystème marin et terrestre unique. Cependant, une diminution de la couverture de glace de mer dans le détroit de Nares a entraîné une diminution de la productivité dans les eaux du Nord, et suggère qu'une transition du régime de surface dans la région a actuellement lieu. Dans ce travail, nous utilisons des enregistrements micropaléontologiques (assemblages foraminifères benthiques) et des mesures de biomarqueurs de la glace de mer (IP₂₅ et HBI III) pour reconstruire la dynamique holocène de la circulation océanique et des conditions de la glace de mer dans le secteur ouest de la polynie de l'eau du Nord, à l'entrée du fjord de Talbot. Nos résultats suggèrent qu'une couverture de glace de mer permanente était probablement présente avant ou pendant la déglaciation du site de carottage. L'influence d'eau Atlantique (relativement chaude) a possiblement favorisé le retrait de la calotte glaciaire. Cependant, la présence d'eau Atlantique a été écourtée au site d'étude à partir de 8,5 cal. ka BP du à l'ouverture du détroit de Nares qui a établi la connexion entre l'océan Arctique et la baie de Baffin. Nos enregistrements montrent que des conditions oligotrophes avaient lieu sous des températures atmosphériques plus chaudes jusqu'à environ 6,5 cal. ka BP. L'initiation d'une polynie latente est identifiée à environ 6,5 ou 5,5 cal. ka BP, avec la mise en place d'un arc de glace au sud du détroit de Nares. Les refroidissement néoglaciare ont probablement favorisé la production de glace de mer dans la polynie à partir de 4,5 cal. ka BP, et la convection d'eaux denses et salées (brines) ainsi que le pompage Ekman auraient induit un upwelling, conduisant à une polynie particulièrement productive (avec une composante de chaleur sensible). Nous faisons l'hypothèse qu'à partir de 3,7 cal. ka BP, l'absence de rupture de la glace de mer arctique dans le nord du détroit de Nares aurait potentiellement favorisé les conditions d'eau libre dans le détroit, résultant en une stratification accrue au le nord de la baie de Baffin. Un certain nombre de changements se produisent dans nos enregistrements autour de 1,9 cal. ka BP et semblent indiquer l'effondrement d'une plateforme de glace (ice shelf) dans le fjord de Talbot, qui pourrait avoir été déclenchée par la prévalence de l'eau libre dans la région. Dans cet article, nous discutons du forçage climatique et océanographique, ainsi que des mécanismes de rétroaction impliqués dans la dynamique holocène de la polynie des eaux du Nord et du détroit de Nares.

4.2 Abstract

Nares Strait in Northwest Greenland has shown significant signs of sensitivity to climate change over the last decades. Land-fast sea ice covering Nares Strait produces an "ice arch", to the south of which opens the North Water, the largest polynya in the Arctic. Today, the North Water sustains a unique marine and land-based ecosystem. However, a decreasing trend of both sea ice cover in Nares Strait and productivity in the North Water suggests that

we may currently be witnessing a transition in surface regime in the area. In this work, we use micropaleontological (benthic foraminiferal assemblages) and sea ice biomarker (IP₂₅ and HBI III) proxy records to reconstruct Holocene dynamics of ocean circulation and sea ice conditions in the western sector of the North Water polynya, at the entrance of Talbot Fjord. Our results suggest that permanent sea ice cover likely occurred prior to or during the deglaciation of the core site. Atlantic water influence may have promoted ice sheet retreat, but was cut-short at ca 8.4 cal. ka BP when glacial retreat in Nares Strait opened the connection between the Arctic Ocean and northernmost Baffin Bay. Oligotrophic conditions prevailed under warmer atmospheric temperatures until ca 6.5 cal. ka BP. Our records suggest initiation of a latent polynya starting at ca 6.5 or 5.5 cal. ka BP, with the establishment of an ice arch in the south of Nares Strait. We propose that when colder atmospheric temperatures enhanced sea ice production in the polynya after ca 4.5 cal. ka BP, brine convection and Ekman pumping caused upwelling, leading to a particularly productive polynya (with a sensible heat component). From 3.7 cal. ka BP, we hypothesise that the absence of breakup of Arctic sea ice in northern Nares Strait promoted open water conditions in the strait, and northern Baffin Bay became stratified. A number of changes occurring in our records round 1.9 cal. ka BP point to the collapse of an ice shelf in Talbot Fjord, which may have been triggered by the prevalence of open water in the area. In this paper, we discuss climatic and oceanographic forcing, as well as the feedback mechanisms involved in the Holocene dynamics of northernmost Baffin Bay and Nares Strait.

Eleanor Georgiadis^{1,2}, Jacques Giraudeau¹, Anne Jennings³, Jean Carlos Montero-serrano⁴, Audrey Limoges⁵, Sofia Ribeiro⁶, Guillaume Massé^{2,7}

¹Université de Bordeaux, CNRS, UMR 5805 EPOC, allée Geoffroy St-Hilaire, 33615 Pessac, France

²Université Laval, UMI 3376 TAKUVIK, 1045 avenue de la Médecine, G1V 0A6 Québec, QC, Canada

³INSTAAR, University of Colorado, Boulder, CO 80309-0450, USA

⁴ISMER, Université du Québec à Rimouski and GEOTOP Research Center, Rimouski, QC, Canada

⁵Department of Earth Sciences, University of New Brunswick, 2 Bailey Drive, Fredericton, E3B 5A3, Canada

⁶Department of Glaciology and Climate, Geological Survey of Denmark and Greenland, Øster Voldgade 10, Copenhagen 1350, Denmark

⁷LOCEAN UMR 7159, CNRS, MNHN, IRD, Sorbonne-université, Station Marine de Concarneau, Concarneau, France

4.3 Introduction

Ellesmere Island is the easternmost component of the Canadian Arctic Archipelago (CAA), and is separated from Greenland by Nares Strait (Figure 5.1). Nares Strait, like the other channels of the CAA, transports Arctic water towards Baffin Bay. The strong southward currents in Nares Strait are driven by the sea level pressure difference between the Lincoln Sea and Baffin Bay (Münchow and Melling, 2008), and by the strong northerly winds channelled by the steep coastal topography of the strait (Samelson et al., 2006). Ellesmere Island is covered by four main ice masses. The Prince of Wales (POW; Figure 5.1) Icefield in its south-eastern section hosts over 70 marine terminating glaciers. Maximal glacial fluxes are observed in Talbot Inlet, which forms a wide incision into

this sector of Ellesmere Island (Cook et al., 2019; Sharp et al., 2014; Van Wychen et al., 2016, 2014). Talbot Inlet harbours a total of six tidewater glaciers, and while the velocities of most glaciers in the CAA have decreased over the past decades, those of the Trinity and Wykeham glaciers in Talbot Fjord have accelerated (Van Wychen et al., 2016). Trinity and Wykeham produced 62% of icebergs from the CAA in 2015, up from 22% in 2000 (Van Wychen et al., 2016), with their fronts retreating 8 and 4 km, respectively, since the 1960s (Sharp et al., 2014). The reasons for their constant acceleration over the instrumental period appears complex (Van Wychen et al., 2016), although decreasing sea-ice cover may be one of the factors at play (Dalton et al., 2019). Land-fast sea ice typically covers Talbot Inlet from October or November to July or August (Dalton et al., 2019). Both calving rates and size of calving event increase during the open water season so that 44 and 56% of icebergs production by the Trinity and Wykeham Glaciers, respectively, occur during the ~2-3 months of open water in the Fjord (Dalton et al., 2019). No change in the length of the land-fast sea-ice season in Talbot Fjord over the study period evaluated by Dalton et al. (2019) (i.e. 1997-2015) was noted, although the authors emphasise that the first year of observation (1997) was marked by the absence of breakup of the land-fast ice, and an associated absence of iceberg calving that year. It is thus possible that the seasonal break-up of land-fast ice in Talbot Fjord is a relatively new event.

Despite the overall mass balance of the POW Icefield being negative (due largely to calving by the Trinity and Wykeham Glaciers), its surface mass balance was maintained between 1963 and 2003 owing to its close proximity to the moisture source that is the North Water polynya, in an otherwise ice-covered region (Mair et al., 2009). Satellite data shows that moisture flux is negatively correlated to sea ice concentration in the North Water, and positively correlated to its size (Boisvert et al., 2012). The polynya is also a heat source for the area, especially in the winter and spring (Marshall et al., 2007). The North Water is the largest polynya in the Arctic, and demonstrates characteristic of both latent and sensible polynyas. The opening of the North Water is conditioned by a land-fast ice arch which forms in southern Kane Basin (Figure 5.1; Figure 5.2) and prevents Arctic drift-ice and glacial ice from entering into northernmost Baffin Bay from Nares Strait (Barber et al., 2001; Dunbar, 1969). The ice arch typically forms in winter and holds through until summer, breaking up in late June or early July (Kwok, 2005). Predominantly southward-flowing ocean currents and northerly winds remove the newly formed ice. Latent heat is transferred to the surface through the continuous production of ice, and brines are released creating vertical advection (Melling et al., 2001). Relatively warmer Atlantic water is transported to northernmost Baffin Bay by the West Greenland Current (WGC), which upwells in the eastern sector of the NOW polynya due to wind-driven removal of surface layers and convection (Ekman pumping) (Dumont et al., 2010), and penetrative brine convection (Bâcle et al., 2002; Melling et al., 2001). The sensible heat provided by the upwelling of the WGC supplies approximately one third of the heat evacuated at the surface (Melling et al., 2001). The western sector of the North Water is dominated by the Arctic throughflow that is concentrated on the Ellesmere side of Nares Strait (Münchow et al., 2007).

The North Water is also a biological oasis, where the open water expands the primary productivity season to early spring, starting in April, while surrounding areas are still heavily ice-covered (Lovejoy et al., 2002). The physical processes occurring in the North Water influence the spatial and temporal characteristics of phytoplankton blooms and higher trophic levels (Vidussi et al., 2004). The western and eastern sectors of the North Water polynya are very different in terms of productivity, which is thought to be due mainly to a strong influence of the Nares Strait

outflow and downwelling motion in the west, and the upwelling of Atlantic-sourced water from Baffin Bay in the east (Lovejoy et al., 2002; Mei et al., 2002; J.-É. Tremblay et al., 2002; Vidussi et al., 2004). Blooms usually begin in April in the eastern sector of the North Water, where open water is found earlier in the year, and propagate towards the western sector in May when sea ice productivity slows down and more open water conditions occur (e.g. Lovejoy et al., 2002; Vidussi et al., 2004). Increased depth of the mixed layer, along with depleted nitrate in Pacific-sourced surface water in the west, lead to a higher contribution of autotrophic flagellates in phytoplankton communities, whereas the shallower mixed layer is more favourable to diatoms which dominate community assemblages in the east (Lovejoy et al., 2002; Mei et al., 2002; Vidussi et al., 2004). The productivity in the polynya is limited by nitrate, meaning that the upwelling of nitrate-rich, Atlantic-sourced water in the eastern North Water dictates the overall biomass produced during spring and summer (J.-É. Tremblay et al., 2002).

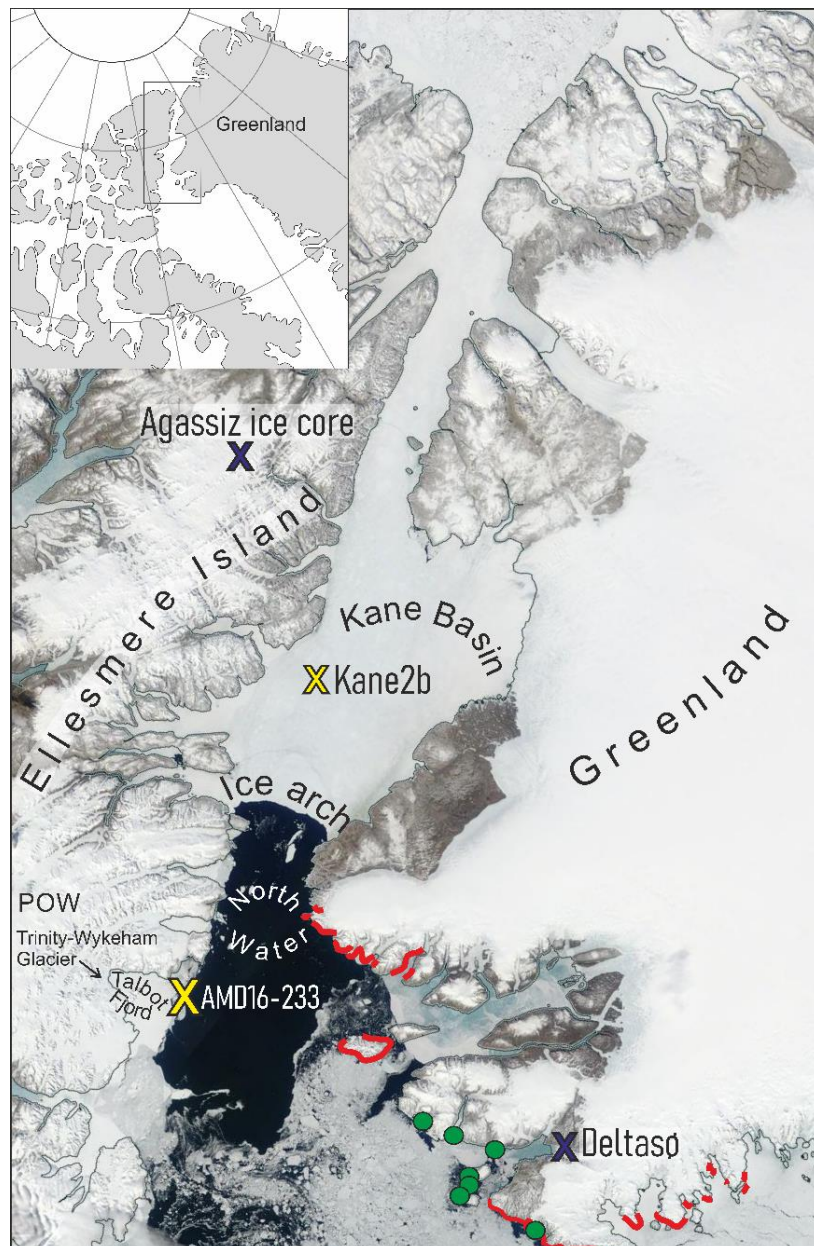


Figure 5.1: Study area, location of core AMD16-233 (Georgiadis et al., in prep.; this study), AMD14-Kane2b (Georgiadis et

al., 2018;2020), *Agassiz Ice core* (Lecavalier *et al.*, 2017), *Deltadø chironomid record* (Axford *et al.*, 2019); *Location of modern little auk colonies* (red), and *common eider and thick billed murre colonies* (green; Davidson *et al.*, 2018). *POW: Prince of Wales icefield*.

Recent instabilities in the ice arch, which has suffered from late formation, early collapse, or complete failure to form over the past decades (Vincent, 2019), pose a threat to this unique system consisting of the ice arch and the polynya (Figure 5.2). Since the beginning of scientific observations in the late 1960s (Dunbar, 1969), the seasonal duration of the ice arch has shortened over the years, culminating in the failure of the ice arches to form several times since 2007 (Münchow, 2016; Vincent, 2019). While a trend of decreasing productivity has been observed in the North Water since the 1990s (Marchese *et al.*, 2017), it has also been suggested that the absence of the Kane Basin ice arch does not necessarily prevent polynya formation, and can even lead to a larger polynya (Vincent, 2019). With a limited timeframe for satellite observation, and an even shorter time span for field data, long term trends in the dynamics of this intricately balanced system remain difficult to fully identify.

Pre-satellite archives in the area are rare. The only record of sea ice conditions in Nares Strait (Georgiadis *et al.*, 2020) reveals a possible link between the duration of sea ice cover in Kane Basin, and the presence of polynya-dependent Little Auk colonies in Northwest Greenland (Davidson *et al.*, 2018). Unfortunately, previously published marine sediment records from the North Water are affected by gaps between composite cores, or very low sedimentation rates in the Mid- to Late Holocene which hinder marine-based reconstructions of conditions in the North Water (Jennings *et al.*, 2019; Knudsen *et al.*, 2008; Levac *et al.*, 2001). In order to address the large uncertainties on the possible long-term dependency of the North Water towards the presence of the ice arch, we use biomarker measurements and benthic foraminiferal assemblages from sediment core AMD16-233, retrieved at the entrance of Talbot Fjord, to reconstruct surface condition and paleoceanographic circulation in the western sector of the North Water (Figure 5.1). Holocene dynamics of the Greenland and Inuitian Ice Sheets, as well as the POW Icefield have previously been reconstructed based on the same core (Georgiadis *et al.*, *in prep.*) The results presented here will be confronted to these reconstructions so as to explore possible links between (1) ocean circulation and surface conditions at the entrance of Talbot Fjord and in the wider North Water area, and (2) Holocene dynamics of the POW Icefield.

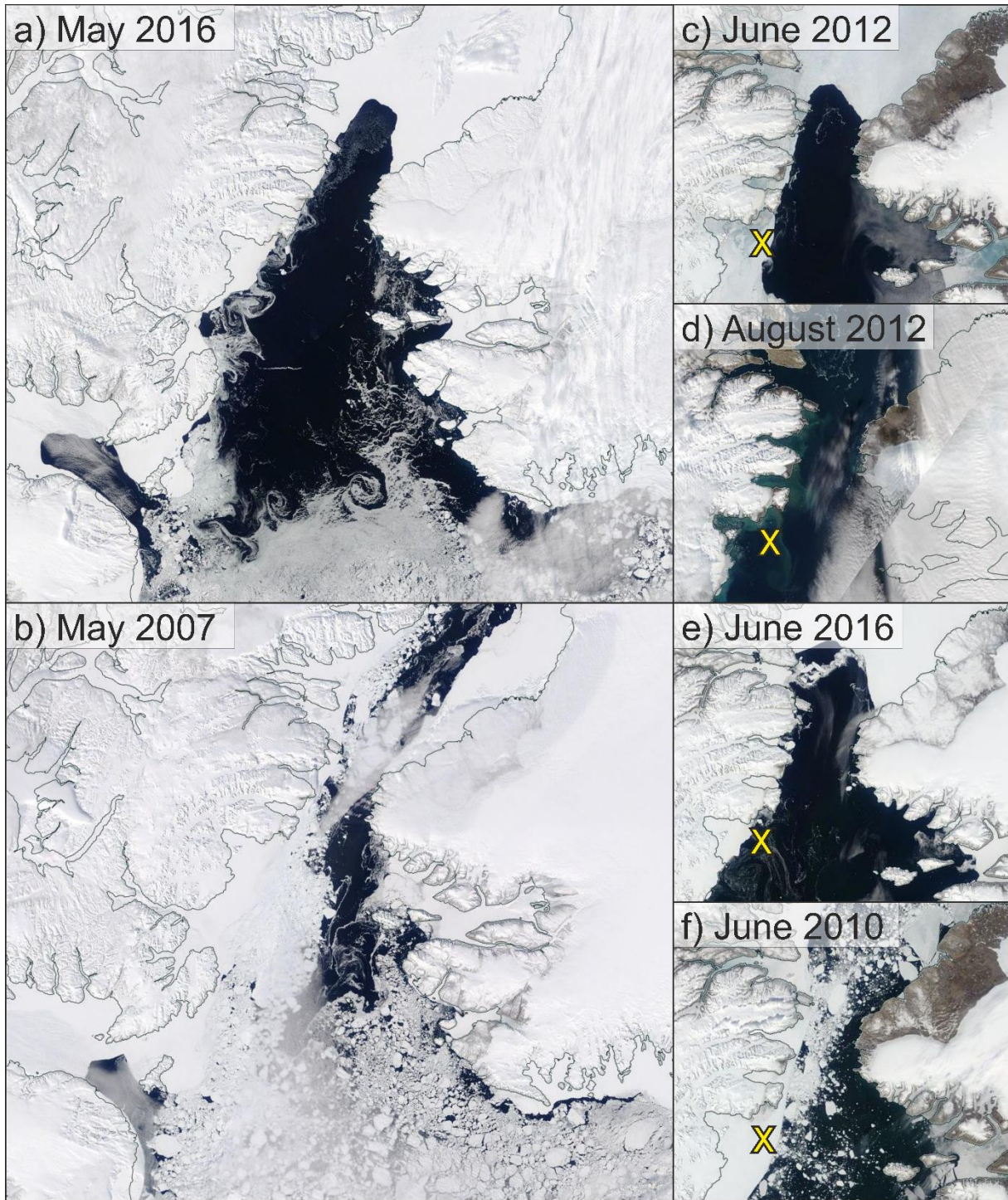


Figure 5.2: Variable surface conditions in the North Water related to the presence (a) and absence (b) of the Kane basin ice arch, and variable sea ice conditions at the core site: c) land-fast sea ice during most of spring 2012; d) open water conditions during summer 2012; e) open water conditions, polynya extended over core site during most of spring 2016; f) land-fast sea ice at the core site and drift ice in the polynya (source of satellite images: <https://worldview.earthdata.nasa.gov/>).

4.4 Material and Methods

4.4.1 Sediment core AMD16-233

Marine sediment core AMD16-233 (7.93 m) was retrieved at the entrance of Talbot Fjord (77°47.751' N, 76°32.126' W, 570 m water depth), in the western sector of the North Water during the 2016 ArcticNet cruise on the CCGS *Amundsen* (Figure 5.1). The location is situated at the edge of land-fast sea ice in the fjord, and the predominantly open waters of the polynya (Figure 5.2). The core itself consists of 1 m of laminated mud and sand at its base, overlaid by ca 2 m of ice rafted debris (IRD)-rich sediment, the rest of the core being composed of ca 5 m of bioturbated mud. These sediments represent, respectively, (1) ice sheet proximal sedimentation induced by glacial outwash (>9.8 cal. ka BP), (2) the deglaciation of southern Nares Strait (>9.8-8.5 cal ka BP), and (3) glacial-distal hemipelagic sedimentation (8.5-0 cal. ka BP) (Georgiadis et al., *in prep.*). The age model of core AMD16-233 was computed based on 22 radiocarbon dates and preliminary ^{210}Pb measurements at the core top, with an age reservoir of 264 ± 74 years.

For a full description of the lithofacies composing AMD16-233, as well as their interpretation in terms of ice sheet dynamics, and more details relevant to the age model, the reader is referred to Georgiadis et al. (*in prep.*).

4.4.2 Biomarker measurements

HBI (Highly Branched Isoprenoids) abundance was measured every 2-12 cm in core AMD16-233, by gas chromatography. Samples were prepared according to the protocol described in Belt and Müller (2013). A sample of “standard sediment” (surface sediment retrieved in large quantity and homogenised) was introduced at the end of each batch of samples to ensure that any deviation in concentration between batches may be detected. The concentrations were converted to fluxes (concentrations*density*sedimentation rate) using the computed tomography (CT) number which was processed according to Fortin et al. (2013). The use of the CT number for the calculations of fluxes entails that they are expressed in an arbitrary unit of ng/surface unit/year as in Georgiadis et al. (2020). The sedimentation rates used in this work are those derived from the polynomial age model which provided smoother transitions between radiocarbon samples.

The HBIs that are of interest in this study are IP₂₅ (Ice Proxy with 25 atoms of carbon) and HBI III (tri-unsaturated HBI). As summarised in the previous section of this chapter (Georgiadis et al., 2020), IP₂₅ is a mono-unsaturated HBI synthesised by spring and summer sea-ice diatoms, while HBI III is produced by ice-edge planktic diatoms (Brown et al., 2014). HBI III has been shown to be more abundant in inner-fjord environments, while IP₂₅ concentration increases seaward, suggesting, respectively, that HBI III-producing diatoms may thrive in freshwater, while decreased salinity in the pore water of sea ice may be detrimental to the development of IP₂₅-producing diatoms (Ribeiro et al., 2017). The diatom assemblages from a fjord in north-east Greenland also reflect this spatial repartition (Limoges et al., 2018).

Little is known about the current sympagic (i.e. sea-ice) and planktic microbial communities at the base of the food chain in both Nares Strait and the North Water. Attempts to characterise the modern compositions of assemblages have been challenged by high temporal variability, particularly in the western sector of the North

Water (Joli et al., 2018). A common observation arises from the scarce field work led in the area; is a clear taxonomical difference between the phytoplankton communities present in the western (Canadian) vs. eastern (Greenland) side of the North Water polynya, thought to be related to oceanographic distinctions (Joli et al., 2018; Lovejoy et al., 2002; Mei et al., 2002; Vidussi et al., 2004). Microbial communities also demonstrate a marked taxonomical difference between the North Water and Kane Basin (Kalenitchenko et al., 2019).

At site AMD16-233, it is likely that IP₂₅ essentially derives from sea ice produced in the outer fjord or in the seaward side of the site, rather than from sea ice within the fjord which certainly presents a high freshwater content. HBI-III is likely to originate within the fjord when surface conditions are open, while a minor fraction of the HBI III may derive from freshwater arriving from Nares Strait although the increased mixed layer associated with the inflow would probably limit diatom productivity compared to the sheltered inner fjord environment.

The strong currents in Nares Strait (up to 60 cm.s⁻¹, Münchow et al., 2007), however, necessarily induce particle transport over a wide distance, and it must be emphasised that HBI fluxes in the North Water, and particularly its western sector, might to a certain degree relate to biomarkers produced in Nares Strait.

4.4.3 Micropaleontological (foraminifera) assemblages

Benthic foraminifera were counted and identified every 4-35 cm in core AMD16-233. Between 0.6 and 7 g of wet sediment was sampled in order to obtain at least 300 individual foraminifera per sample. The samples were left to soak overnight in a buffered aqueous metaphosphate solution (9 g.L⁻¹), then carefully wet sieved at 63 µm. The > 63 µm fraction was preserved in a buffered alcoholic (30%) solution. Foraminifera were wet counted (in the storage solution) and identified according to the general classification of Loeblich and Tappan (1988). This protocol minimalizes the loss of agglutinated taxa and fragile calcareous species which are common in Arctic assemblages (Scott and Vilks, 1991; Sperling et al., 2002).

A stratigraphically constrained cluster analysis (CONISS, Grimm, 1987) was performed on the relative specific composition of the benthic foraminiferal assemblages, with the broken sticks model indicating eight main clusters.

Table 5.1: List of foraminifera taxa used to reconstruct paleoenvironmental conditions from core AMD16-233 and their original references.

Benthic foraminifera

Calcareous Taxa:

Brizalina pseudopunctata (Höglund 1947)

Buliminella elegantissima (d'Orbigny 1839)

Buccella frigida (Cushman 1922)

Cassidulina neoteretis Seidenkrantz 1995

Cassidulina reniforme Norvan 1945

Elphidium excavatum forma *clavata* Cushman 1930

Epistominella arctica Green 1959

Islandiella helenae Feyling-Hanssen & Buzas 1976

Islandiella norcrossi (Cushman 1933)

Nonionella iridea Heron-Allen & Earland 1932

Nonionellina labradorica (Dawson 1860)

Stainforthia feylingi Knudsen & Seidenkrantz 1994

Stetsonia horvathi Green 1960

Aglutinated taxa:

Adercotryma glomerata (Brady 1878)

Cuneata arctica (Brady 1881)

Eggerelloides advenus (Cushman, 1922)

Portotrochammina bipolaris Brönnimann & Whittaker 1980

Reophax catenata

Spiroplectamina biformis (Parker & Jones 1865)

Textularia torquata Parker 1952

Planktic foraminifera

Neogloboquadrina pachyderma (Ehrenberg 1861)

Foraminifera-based reconstructions provide a wide range of details with regards to environmental conditions (e.g. distance to glacial ice, dominant water masses, productivity regime, etc.; Georgiadis et al., 2020). In this paper, we use the combined sum of productivity-related species *Brizalina pseudopunctata* (Knudsen et al., 2008), *Buliminella elegantissima* (Harmon, 1972; Patterson et al., 2000; Snyder, 1990), *Eggerelloides advenus* (Schafer et al., 1991), and *Nonionellina labradorica* (Jennings et al., 2004; Polyak et al., 2002; Rytter et al., 2002) as an indication of the export of organic matter to the seabed. The taxa mentioned in the text, along with their original references are listed in Table 5.1. As opposed to HBIs that are produced at the surface, benthic foraminiferal assemblages are more likely to reflect in situ environmental conditions from a benthic point of view. Reworking of benthic foraminifera is a common occurrence in the lower part of core AMD16-233 as illustrated by the offset of the radiocarbon ages derived from foraminiferal and mollusc samples from the coarser interval which highlights the presence of Pre-Glacial foraminifera (Georgiadis et al., *in prep.*). The gradually reduced upcore difference in age of foraminifera vs. mollusc samples indicates that the abundance of Pre-Glacial foraminifera decreases with age in the core section.

4.4.3 XRD mineralogy

X-ray diffraction (XRD) measurements were performed on core AMD16-233 and previously discussed in Georgiadis et al. (*in prep.*). Here, we present the relative abundance of amorphous silica in the mineralogical suit of AMD16-233, as a proxy of biogenic silica. Downcore amorphous silica profiles measured by XRD, and biogenic silica profiles measured by wet-chemical leaching have been shown to be similar in High Arctic settings

(Deschamps et al., 2018).

4.5 Results and interpretations

4.5.1 General trends in the proxy records of core AMD16-233

General trends and changes in the proxy records of core AMD16-233 broadly coincided with the succession of lithofacies in the core. Biomarker abundances were close to zero in the laminated interval, before IP₂₅ significantly increased in the IRD-rich unit (Figure 5.3). Biomarker concentrations were relatively stable in the bioturbated mud, apart from brief increases in HBI III centred at 375 (6.4 cal. ka BP), 325 (5.5 cal. ka BP), 185 (4.5 cal. ka BP), and 165 cm (3.6 cal. ka BP). Fluxes, which were not calculated beyond the lowermost radiocarbon date (610 cm, 9.8 cal. ka BP), were more variable due to variations in sedimentation rates (Figure 5.3). The top half of the core was characterised by significant changes in biomarker concentrations and fluxes. Foraminifera were absent from the laminated unit at the base of core AMD16-233 (Figure 5.3). Benthic and planktic foraminiferal concentrations and fluxes were reduced in the IRD-rich interval, with maximal values at the base of the bioturbated mud. The planktic foraminiferal concentrations and fluxes gradually decreased upcore, as did the benthic foraminifera but to a lesser degree (Figure 5.3). The benthic foraminiferal assemblages in core AMD16-233 were diverse, but the planktic assemblage was entirely composed of *Neogloboquadrina pachyderma* sinistral (NPS), a species usually related to the Atlantic layer of High Arctic water masses (Hume, 1972; Husum and Hald, 2012; Vilks, 1969). While calcareous species were predominant in most of the core, the abundance of agglutinated taxa did reach over 50% in some samples, particularly in the top 384 cm (6.5 cal. ka BP; Figure 5.3). A number of observations pointed to enhanced preservation in the bottom section of the core, with fragile organisms such as pteropods (*Limacina helicina*) and the dissolution-sensitive morphotype of NPS (Vilks, 1969) found in samples below 384 cm (6.5 cal. ka BP). Foraminifera linings were only present above this depth (Figure 5.3). Biogenic silica was virtually absent in the lower sections of core AMD16-233, before increasing starting at 410 cm (ca 7.0 cal. ka BP), with highest content measured between 330 and 70 cm (ca 5.5 and 2.0 cal. ka BP; Figure 5.3).

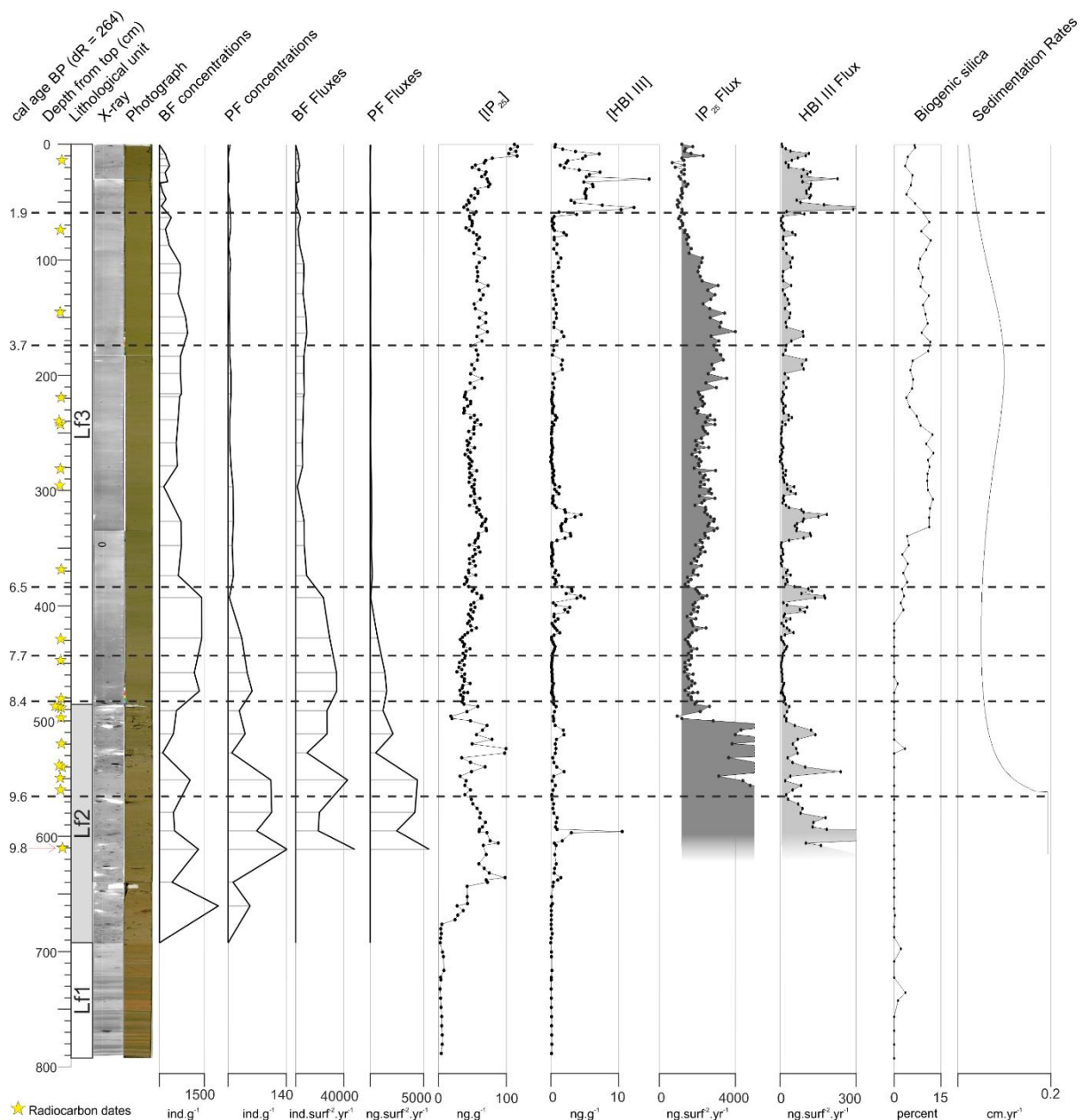


Figure 5.3: Depth scale of Benthic (BF) and planktic (PF) foraminiferal concentrations and fluxes, IP₂₅ and HBI III concentrations and fluxes, BSi content, sedimentation rates (from the polynomial age model). Lithological units, x-ray image and photograph were identified and discussed in Georgiadis et al. (in prep.).

Generally, the benthic foraminiferal ecozones do not mirror the clusters identified on the same core based on sedimentological and geochemical parameters (Figure 5.4 & Figure 5.5), hinting that the sediment provenance and the environmental conditions at the core site are not strictly linked. An exception to this observation being a change from a severely ice-covered environment (predominance of *S. horvathi*) with predominantly locally-derived sediment and intense ice-rafting, to less harsh conditions and more influence of Atlantic water as the dominant sediment source becomes more distant detrital carbonate (Figure 5.4). There was also a broad correspondence between a shift in the benthic assemblages ca. 1.9 cal. ka BP, and increased IRD and locally-sourced material over the past ca. 2.0 cal. ka BP evidenced in Georgiadis et al. (in prep.).

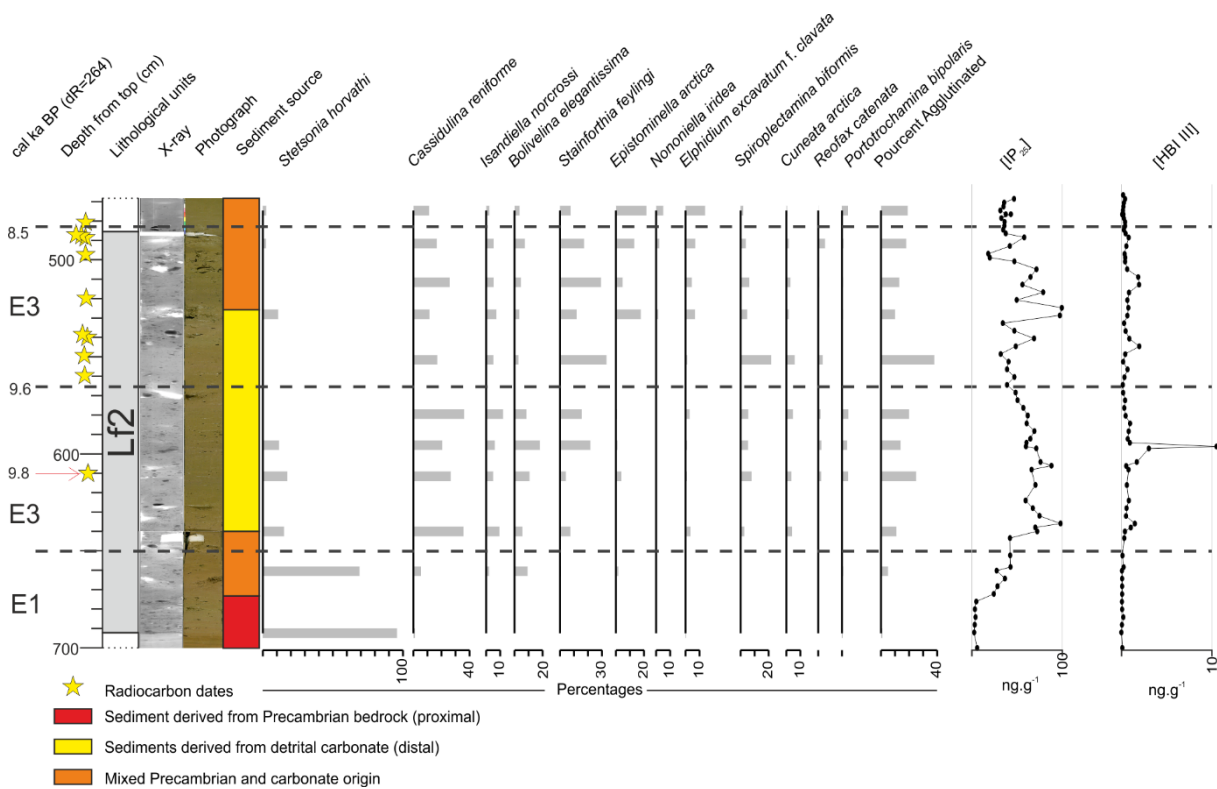


Figure 5.4: Close up of selected benthic foraminifera species, biomarker concentrations, and sediment provenance in the IRD-rich interval of core AMD16-233. Dashed lines represent ecozone boundaries defined the stratigraphically constrained cluster analysis. Precambrian bedrock is sourced locally from south-eastern Ellesmere Island, while carbonates originate predominantly from Nares Strait (Georgiadis et al., in prep.).

4.5.2 Environmental significance of the proxy records

In this section, the results from biomarker and biogenic silica analyses, along with the description of foraminiferal assemblages will be presented according to the eight ecozones identified by the stratigraphically constrained micropaleontological cluster analysis. Their significance in terms of sea surface conditions and oceanic circulation at the core site in the light of the sedimentological and geochemical data presented in Georgiadis et al. (in prep.).

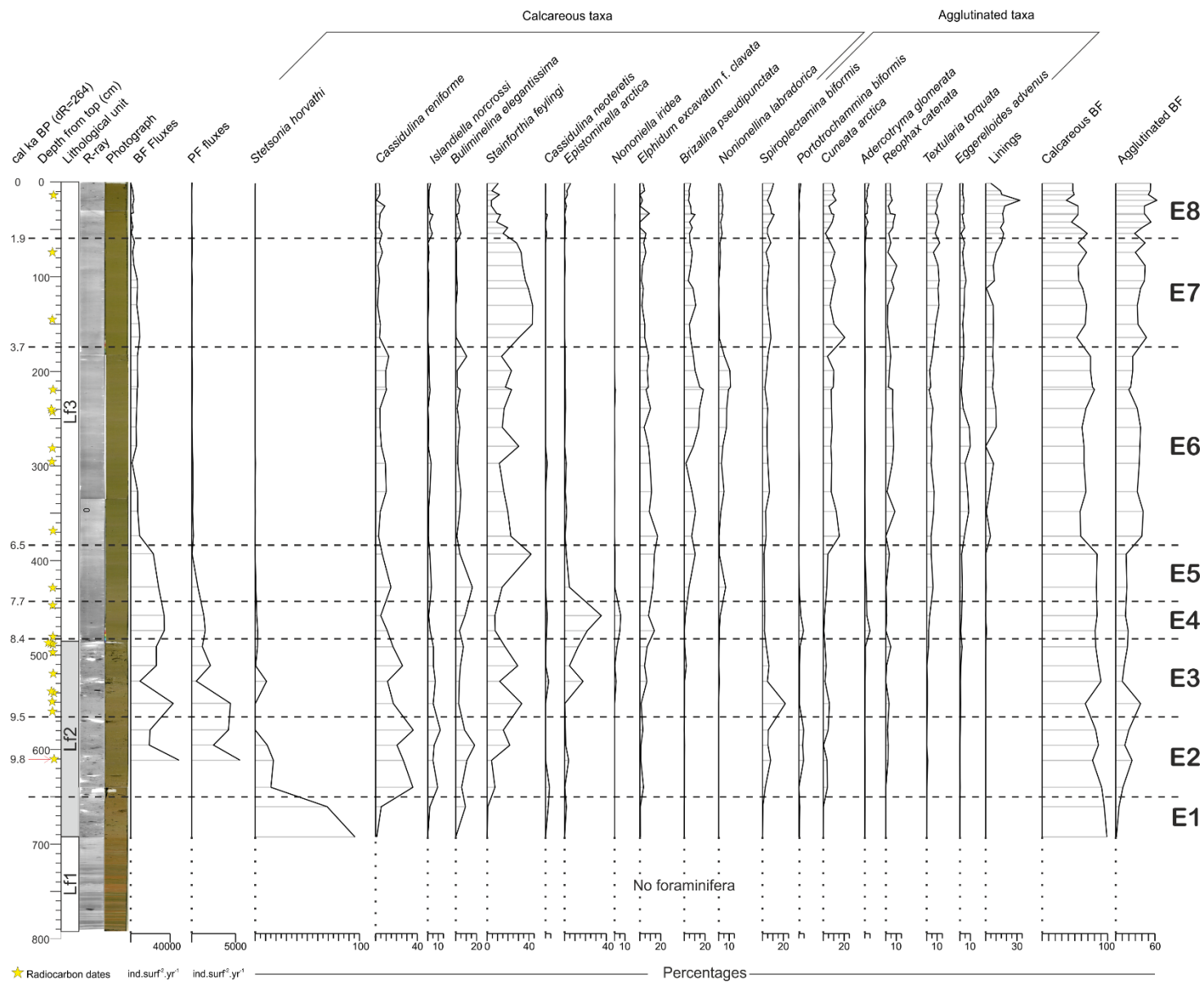


Figure 5.5: Depth scale of Benthic and planktic foraminiferal fluxes (expressed in ind/surface unit/year), major contributing species in the benthic foraminiferal assemblage, % linings (ratio of number of linings counted/number of tests counted in each sample), and relative contributions of calcareous and agglutinated taxa in the bulk assemblage of core AMD16-233. Dashed lines represent ecozone boundaries defined the stratigraphically constrained cluster analysis, with ages indicated in cal. ka BP corrected with $\Delta R = 264 \pm 74$ years..

The base of the core, consisting of interlaminated sand and mud (Georgiadis et al., 2020), was barren of foraminifera. HBI biomarkers are also either absent or in abundances close to nil (Figure 5.3 & Figure 5.4). This paucity of biological remains can be a result of either (1) extremely high sedimentation rates or (2) quasi-permanent sea ice cover at the core site, which would have induced an oligotrophic and poorly ventilated environment that did not allow the development of foraminifera. The presence of IRD in this laminated sediment indicates however that open water at the core site occurred at least occasionally (Georgiadis et al., *in prep.*). Thus, it is most probable that the laminated sediment at the base of core AMD16-233 was deposited very rapidly by glacial outwash, when the marine margin of the Innuitian Ice Sheet was located at the core site.

Three ecozones (E1, E2 and E3) were identified in the IRD-rich sediment (LF2), with the remaining five in the bioturbated mud (LF3) (Figure 5.4 & Figure 5.5).

The first ecozone (E1, 690-650 cm, >9.8 cal. ka BP) displayed relatively high concentrations of benthic foraminifera (913 ind.g⁻¹), while planktic foraminifera were considerably rarer (27 ind.g⁻¹). The benthic foraminiferal assemblage in E1 was nearly monospecific, clearly dominated by *Stetsonia horvathi* (Figure 5.4).

This species is usually linked to heavy, near perennial sea-ice cover (Wollenburg and Mackensen, 1998). This suggests that the coarse sediments composing E1 were deposited very rapidly during brief periods of open water (perhaps created by mobile icebergs calved from the ice margin in Talbot Fjord), in an otherwise heavily ice-covered environment. Biomarkers were absent until 670 cm likely due to quasi-permanent sea ice cover (Figure 5.4). The increase in IP₂₅ concentrations mirrors the decrease in *S. horvathi* abundances, indicated a gradually amelioration of surface conditions and the establishment of a more seasonal sea ice cover.

Foraminiferal species diversity was higher in the second ecozone (E2, 650-565 cm, ca >9.8-9.5 cal. ka BP) with a reduced abundance of *S. horvathi* (ca. 11%), and a higher contribution of *Cassidulina reniforme* which became the dominant species (ca. 30%). Accessory species included *Stainforthia feylingi* (12%), *Buliminellina elegantissima* (11%), and *Islandiella norcrossi* (8%) (Figure 5.4 & Figure 5.5). IP₂₅ concentrations were among the highest values measured in core AMD16-233, with an average of 66 ng.g⁻¹, despite high sedimentation rates (Figure 5.3 & Figure 5.4). HBI III concentration remained low, with the exception of a brief peak ca 600 cm (9.8 cal. ka BP). Both high IP₂₅ concentrations and a decrease in *S. horvathi* suggests seasonal break-up of sea ice leading to more open conditions at the entrance of Talbot Fjord. *C. reniforme* and *I. norcrossi* are two glacial marine species that attest, respectively, to the presence of chilled Atlantic-sourced water (e.g. Polyak et al., 2002), and stable salinity (Steinsund and Hald, 1994). The environmental significance of *B. elegantissima* and *S. feylingi* are less well constrained. *B. elegantissima* is associated to high organic matter content in modern sediments (Harmon, 1972; Patterson et al., 2000; Snyder, 1990) and usually occurs with high productivity species in paleo-records, indicating that it may be related to productive environments (e.g., Knudsen et al., 2008). *S. feylingi* is often referred to as part of the low-oxygen tolerant genus *Stainforthia* (Alve, 2003, 1994; Elberling et al., 2003; Patterson et al., 2000), but has also been associated with sea ice productivity (Seidenkrantz, 2013) and meltwater input (Jennings et al., 2017). The overall consensus on *S. feylingi* is that it is an opportunistic species which can tolerate low oxygen conditions at the seabed.

Ecozone E2 likely reflects a glacial environment influenced by chilled Atlantic-sourced water and some phytodetritus export related to seasonal sea-ice cover. This interval is characterised by the maximum influence of Atlantic water in our record. It is likely that large inputs of meltwater stratified the water column and occasionally led to more severe sea-ice condition and reduced ventilation of bottom water.

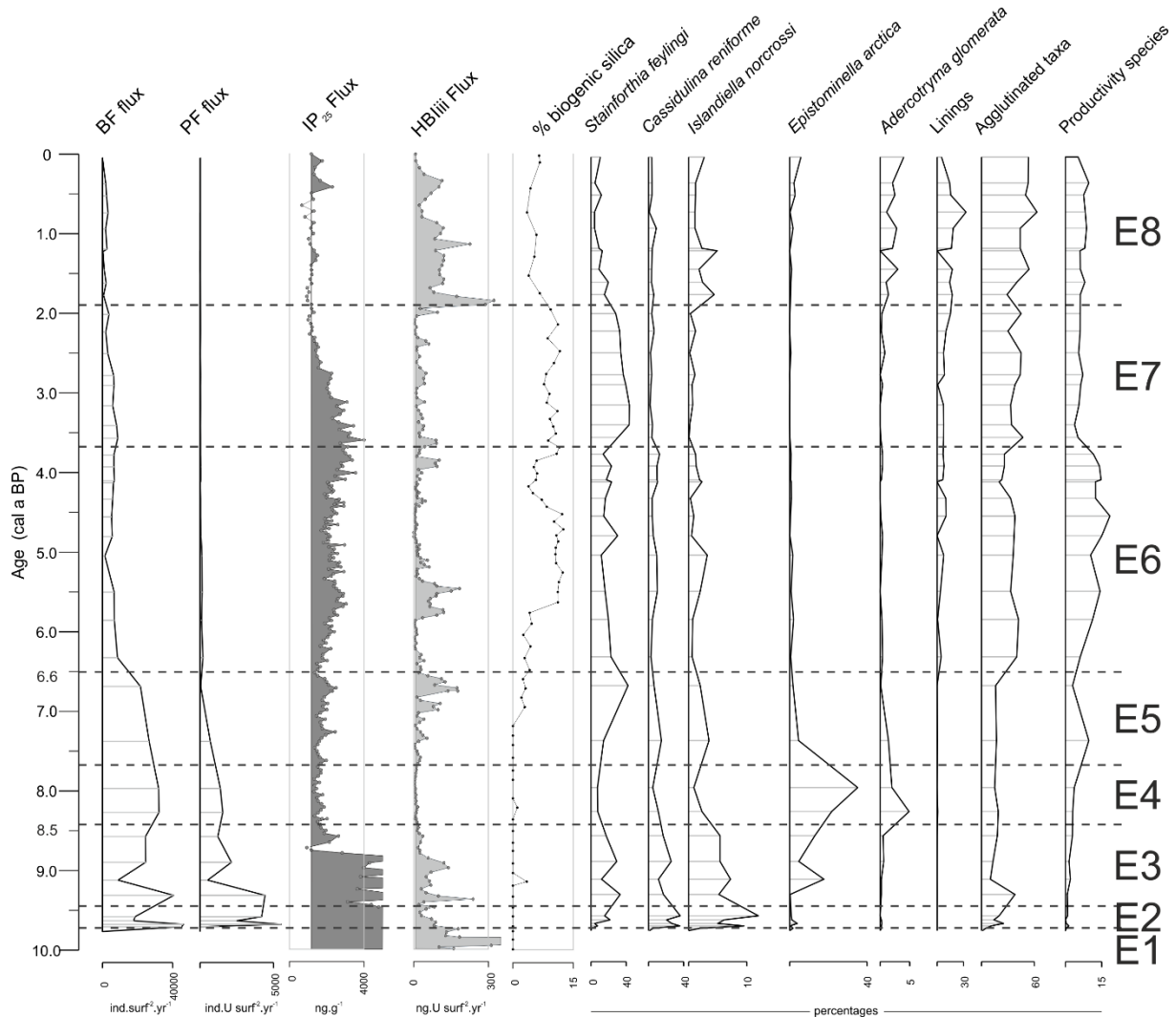


Figure 5.6: Time scale of benthic and planktic foraminifera fluxes, IP_{25} and HBI III fluxes, BSi content in the mineralogical suite, and relative abundance of selected benthic foraminifera species in core AMD16-233. Dashed lines represent boundaries between ecozones.

Ecozone E3 (565-483 cm, 9.5-8.4 cal. ka BP) featured a co-dominance of *S. feylingi* (23%) and *C. reniforme* (18%). *Epistominella arctica* and agglutinated species *Spiroplectamina biformis* each accounted for 9% of the assemblage (Figure 5.4 & Figure 5.5). Contributions of *I. norcrossi* decreased from 12 to 2%, while *Elphidium excavatum* forma *clavata* increased from 2 to 13% between the base and the top of E3 (Figure 5.4 & Figure 5.5). Although concentrations and fluxes of IP_{25} were relatively high overall, they displayed higher variability than E1 and E2 (Figure 5.3 & Figure 5.6).

While the presence of *C. reniforme* points to Atlantic-sourced bottom water, the occurrence of *S. biformis* attest to

the influence of glacial meltwater at the core site (Jennings and Helgadottir, 1994). High contributions of *S. feylingi* support a possible meltwater-induced stratification of the water column. The opposing abundance trends of the stable salinity indicator species *I. norcrossi* (decreasing) and *E. excavatum* f. *clavata* (increasing), a species associated to unstable environmental conditions and lower salinity (Hald et al., 1994), also illustrates the reduced influence of Atlantic-sourced water, and the presence of meltwater at the core site. Unstable environmental conditions during the time period represented by E3 are further inferred by the high variability in IP₂₅ concentrations and fluxes, as well highly variable total foraminiferal fluxes (Figure 5.3). The presence of *E. arctica* is indicative of oligotrophic conditions with pulsed input of organic matter (Wollenburg and Kuhnt, 2000).

Overall, ecozone E3 is indicative of more unstable hydrological conditions, including variations in bottom water salinity, sea ice cover – possibly as a result of increased meltwater influx – and is associated with limited productivity.

Ecozone 4 (E4, 483-443 cm, 8.4-7.7 cal. kaBP) was represented by *E. arctica* (28%) along with relatively high contribution of the accessory species *E. excavatum* f. *clavata* (11%), *S. feylingi* (8%), *C. reniforme* (8%), *B. elegantissima* (6%), and *N. iridea* (6%). Minor contributions of agglutinated species *A. glomerata* (<5%) are also noteworthy in this ecozone (Figure 5.5). Concentration and fluxes of IP₂₅ and HBI III were low in this interval (Figure 5.6).

Atlantic influence was limited, but still identifiable, according to the presence of *C. reniforme*. *E. excavatum* f. *clavata* points to unstable bottom water salinity, possibly in relation to meltwater input supported by the presence of *S. feylingi*. *B. elegantissima* attests to organic matter at the core site (Gooday and Hughes, 2002), but as in E3, the dominance of *E. arctica*, along with contributions of *N. iridea* (Duffield et al., 2015) indicates that the export of phytodetritus occurred as pulsed events in an environment marked by an overall scarcity of food. The presence of *A. glomerata* further supports extremely low food supply, possibly under occasionally permanent sea ice cover (Wollenburg and Kuhnt, 2000). Even if it is characterised by relatively low productivity, E4 displays overall higher benthic and planktic foraminiferal fluxes (Figure 5.5), suggesting that extremely hostile conditions did not occur during the entire time covered by E4. The low biomarker fluxes in this interval may be explained by multi-year land-fast sea ice in Talbot Fjord, with the foraminiferal record suggesting that the core site may have been at the edge this quasi-permanent ice cover.

Ecozone E4 represents an unstable environment similar to the previous ecozone E3, but with occasionally more severe sea ice conditions, the export of phytodetritus being limited to very brief outbursts in otherwise oligotrophic conditions. The core site was likely at the edge of multi-year land-fast sea ice in Talbot Fjord, and may have sometimes been covered by quasi-permanent sea-ice.

Ecozone 5 (E5, 443-384 cm, 7.7-6.5 cal. ka BP) is characterised by high relative abundances of *S. feylingi* (28%), along with secondary contributions of *E. excavatum* f. *clavata* (13%), *C. reniforme* 11%; *B. elegantissima* (11%), and *B. pseudopunctata* (8%) (Figure 5.5). Agglutinated taxa accounted for an average 17% of the bulk foraminiferal assemblages within E5, with *Textularia torquata* as the most abundant agglutinated species (ca. 5%). IP₂₅ concentrations and fluxes were slightly higher than in the previous ecozone, while HBI III concentration and flux profiles displayed distinctive peak values in the younger part of this interval (Figure 5.3 & Figure 5.6). Biogenic

silica (BSi) was present in the mineralogical suite of E5, albeit at low values of 1.5%, whereas it was virtually absent in sediments below this interval (Figure 5.6).

Although Atlantic-sourced bottom water is indicated by the presence of *C. reniforme*, much like in the previous ecozones, unstable bottom water salinity continues to increase as suggested by higher contributions of *E. excavatum* f. *clavata* in E5. The opportunistic species *S. feylingi* is indicative of occasionally sub-oxic conditions, related to sea ice cover and/or meltwater-induced stratification. Freshwater influence is also pointed at by higher HBI III fluxes. It is likely that Talbot Fjord was seasonally ice-free during the time period represented by E5, allowing the development of HBI III-producing diatoms in the fresher, open water of the fjord. The growth of IP₂₅-producing diatoms was likely still hindered in the freshwater sea ice of the fjord during the winter months. High contribution of agglutinated taxa to the bulk foraminiferal assemblage, of which *T. torquata* is the dominant species, suggests more Arctic water influence at the core site (Ishman and Foley, 1996). Finally, the replacement of *E. arctica* and *N. Iridea* by enhanced contributions of high productivity index species *B. elegantissima*, and *B. pseudopunctata* (Knudsen et al., 2008), along with the presence of BSi, are suggestive of a more productive environment than previously. Overall, E5 is marked by the influence of freshwater, possibly in link with meltwater input from a seasonally open Talbot Fjord, with higher exports of organic matter at the core site compared to previous intervals, but productivity was still relatively limited.

Ecozone 6 (E6, 384-175 cm, 6.5-3.7 cal. ka BP) featured a diverse assemblage, with dominant, albeit reduced, contributions of *S. feylingi* (19%). Accessory species were *B. pseudopunctata* (11%), *E. excavatum* f. *clavata* (9%), *C. reniforme* (8%), *Nonionellina labradorica* (6%), along with agglutinated species *Cuneata arctica* (9%), *Eggerelloides advenus* (5%), and *Reophax catenata* (5%) (Figure 5.5). The contribution of agglutinated taxa was persistently high throughout this interval (32%), while the number of linings equated to 5% of the number of tests counted. BSi content was on average higher in E6 (ca. 8% of the mineralogical suite) than in previous ecozones, with however lower values between 250 cm (4.5 cal. ka BP) and the top of E6. IP₂₅ concentration and fluxes increased until 333 cm (5.7 cal. ka BP), after which they remained relatively stable before increasing again at 200 cm (4.0 cal. ka BP) (Figure 5.6). HBI III concentrations and fluxes were very low, apart from a peak between 343 and 300 cm (5.8-5.1 cal. ka BP) and higher values above 200 cm (ca 4.0 cal. ka BP).

The benthic foraminiferal assemblage which characterizes E6 is indicative of environmental conditions similar to those described in previous intervals in terms of Atlantic-sourced bottom water and (meltwater-related) unstable salinity at the core site, as indicated by *C. reniforme* and *R. catenata* (Höglund, 1947), and *E. excavatum* f. *clavata*, respectively. The decreasing trend in *E. excavatum* f. *clavata* abundances is however indicative of gradually more stable bottom water conditions at the core site. Increased influence of more corrosive (polar?) water is suggested by the presence in E6 of linings which were previously absent. Polar influence is also supported by higher percentages of agglutinated taxa, of which *C. arctica* (Lloyd, 2006). It has recently been proposed in a discussion paper that agglutinated foraminifera may be related to locally formed corrosive brines (Fossile et al., 2019). Relatively high contributions of *B. pseudopunctata*, *N. labradorica*, a species associated to the export of fresh phytodetritus related to ice-edge blooms (Jennings et al., 2004; Polyak et al., 2002; Rytter et al., 2002), and *E.*

adventus, which is also associated to high organic content in modern assemblages (Schafer et al., 1991), along with high BSi content, are indicative of a productive environment. The highest contributions of phytodetritus-related species occurred between 260 and 200 cm (ca 4.7-4.0 cal. ka BP), making it the most productive interval in core AMD16-233 according to the benthic foraminiferal assemblages (Figure 5.6). Despite the high abundance of productivity-related species, the benthic foraminiferal flux is relatively low in this interval compared to those before 6.6 cal. ka BP (Figure 5.6). It is likely that most of the interval represented by E6 was characterised by multi-year, land-fast sea ice in Talbot Fjord, according to the very low HBI III fluxes between ca 5.1 and 4.0 cal. ka BP, while moderate fluxes of IP₂₅ correspond to seasonal sea-ice from outside the fjord (i.e. at or to the east of the core site) (Figure 5.3 & Figure 5.6). Relatively heavy sea-ice cover is also supported by the dominance, albeit limited, of *S. feylingi*. Brief periods of open water in Talbot Fjord may have occurred ca 5.8-5.1 cal. ka BP, and after 4.0 cal. ka BP, during peaks of HBI III fluxes. However, the relative abundances of meltwater-related benthic foraminiferal species displayed no significant changes when peaks in HBI III fluxes occurred in E6.

Ecozone E6 generally represents a productive environment, possibly in relation to seasonal sea ice at, or to the east of, the core site, with some meltwater influence, and increased polar water and/or brine production. Talbot Fjord was likely covered in multi-year land-fast ice between 5.1 and 4.0 cal. ka BP, and was possibly seasonally opened towards the beginning and end of the period represented by E6.

Ecozone 7 (E7, 175-60 cm, 3.7-1.9 cal ka BP) was characterized by maximal relative abundances of *S. feylingi* (36%), while contributions of productivity species were considerably reduced (*B. pseudopunctata* accounted for 7% of the assemblage, *E. adventus* 4%, and *N. labradorica* 1%) (Figure 5.5). Agglutinated taxa accounted for 40% of the assemblage, of which the most abundant species were *T. torquata* (10% of the total assemblage), *C. arctica* (11%) and *S. biformis* (6%). Post-mortem dissolution occurred according to the presence of linings in the samples (equivalent to 8% of the benthic foraminifera counted). While IP₂₅ concentrations remained high throughout E7, IP₂₅ fluxes were high at the base of E7, but decreased relatively sharply upcore (Figure 5.3 & Figure 5.6). HBI III concentrations and fluxes were moderately high compared to the underlying intervals. BSi content was stable throughout E7, with average values of 10% (Figure 5.3 & Figure 5.6).

High contributions of *S. feylingi* point to a stratified water column and very poorly oxygenated bottom water, possibly due to heavy sea ice cover. The high abundance of agglutinated foraminifera *T. torquata*, *C. arctica* and *S. biformis*, along with reduced contributions of *C. reniforme* (4%) and the presence of linings, are indicative of increased influence of polar water (Ishman and Foley, 1996; Lloyd, 2006) and/or brine production (Fossile et al., 2020) at the core site. Flickering HBI III fluxes suggest that short periods of occasional open water occurred in Talbot Fjord, and that multi-year sea-ice cover may have broken up slightly more often than previously. Decreasing IP₂₅ fluxes likely point to decreasing seasonal sea-ice cover at the core site.

Ecozone E7 represent an interval marked by Polar influence or brine production at the core site and decreased productivity relative to E6. The water column is poorly ventilated, and sea-ice cover appears to decrease upcore. Occasional open water conditions occur in Talbot Fjord, probably more consistently than previously.

Ecozone 8 (E8, 60-0 cm, 1.9-0 cal. ka BP) was highly diverse, and characterised by a lower contribution of *S.*

feylingi in the bulk foraminiferal assemblage (ca. 10%). Agglutinated taxa represented 48% of the assemblage, with considerable contributions of *T. torquata* (11%), *C. arctica* (8%) and *S. biformis* (8%) (Figure 5.5). Species which were absent from the assemblages since ca 7.0 cal. ka BP (410 cm), reappeared with minor contributions in E8 (Figure 5.6). Such is the case for *E. arctica* (up to 6%), and *Adercotryma glomerata* (up to 4%). Changes in biomarker fluxes were remarkable in E8, with a large increase in HBI III fluxes, and low IP₂₅ fluxes (Figure 5.3 & Figure 5.6). BSi content decreased to an average 6%.

The high abundance of agglutinated taxa along with high numbers of linings (equivalent to 15% of benthic foraminifera counted) point to the presence of corrosive water at the core site, related to increased inflow of Polar water or brine production. Reduced contributions of *S. feylingi* attest to a better ventilated water column. Sustained high HBI III fluxes together with minimal IP₂₅ fluxes, are indicative of increased open water conditions in Talbot Fjord, and either reduced sea ice cover, or the incorporation of more freshwater in seasonal sea ice at the core site. Low contributions of productivity index species are attest to a continued paucity of food, similar to E7. The reappearance of *E. arctica* in E8 further suggests an overall oligotrophic environment with pulsed export of phytodetritus. Minor contributions of *A. glomerata*, *A. catenata* (5%) and *C. reniforme* (4%) point to the presence of Atlantic-sourced bottom water at the core site, although its influence was limited compared to the polar inflow and/or brine influence. This interval broadly corresponds to the topmost cluster derived from the cluster analysis of the XRD dataset from core AMD16-233 (Georgiadis et al., *in prep.*) which was characterised by increased IRD and locally-sourced sedimentary material.

Overall, E8 represents a generally oligotrophic environment, with strong polar water or brine influence at the core site, relatively low seasonal sea-ice cover or enhanced incorporation of freshwater in sea ice, and a recurrence of seasonally opened water in Talbot Fjord.

4.6 Discussion

4.6.1 Heavy sea-ice cover during Early Holocene ice sheet retreat, and maximum Atlantic influence (>9.8-8.4 cal. ka BP)

Our multiproxy study of core AMD16-233, which includes sedimentological, geochemical (Georgiadis et al., *in prep.*), biogeochemical, and micropaleontological analyses, collectively points to rapid sedimentation of glacial ice-proximal material and local ice-rafted debris, most likely around, or shortly before, 9.8 cal. ka BP. Near-perennial sea-ice covered the area during ice sheet retreat away from the core site according to the dominance of *S. horvathi* in the sediments immediately above the laminated interval of core AMD16-233 (Figure 5.4). The IRD-rich sediments in which *S. horvathi* occurs were likely deposited very rapidly during brief openings in the sea-ice cover, possibly induced by calving. As the sediment provenance became more distant, attesting to ice sheet retreat from the core site (cf. Georgiadis et al., *in prep.*), higher diversity in the benthic foraminiferal assemblages suggest that conditions were more clement (Figure 4.3 & Figure 5.4). A shift from quasi-perennial to seasonal sea-ice cover is supported by both a decrease in *S. horvathi* and an increase of IP₂₅ abundances (Figure 5.4). The high contributions of *C. reniforme*, a glacial marine species associated to chilled Atlantic-sourced water, and *I. norcrossi*, indicative of stable bottom water salinity, suggests that the maximum influence of Atlantic water at the core site occurred

between >9.8 and 8.4 cal. ka BP. This time period also corresponds to enhanced strength of the West Greenland Current (WGC) in eastern Baffin Bay during the Early Holocene (Figure 5.7; Perner et al., 2013). Such a strengthened inflow of warm WGC may have promoted ice sheet retreat in northernmost Baffin Bay.

The maximum influence of Atlantic-sourced water at site AMD16-233 is short-lived compared to other areas of the North Water, echoing the same observation from nearby site 2001LSSL-014 made by Jennings et al. (2019). Relatively high abundances of Atlantic-related species in marine cores retrieved in the eastern sector of the North Water expand from the Early Holocene well into the Mid-Holocene (ca 5.8 cal. ka BP ($\Delta R = 140 \pm 60$) in AMD16-117Q, Jackson et al., submitted; and ca 3.0 cal ka BP ($\Delta R = 0$), Knudsen et al., 2008). The fact that the marine optimum was cut short at our core site is likely due to the establishment of modern circulation in Nares Strait following its opening ca 8.4 cal. ka BP. This opening, whose timing in our record corresponds to the end of the IRD-rich interval LF2, falls within previous dating of the event between 9.0 and 8.3 cal. ka BP (Georgiadis et al., 2018; Jennings et al., 2011, 2019). The event is likely to have had a greater influence on the western side of the North Water relative to the eastern side, since the Arctic outflow is concentrated on the western side of the strait (e.g. Münchow et al., 2007), hence explaining why both sectors of northernmost Baffin Bay behaved differently in terms of Holocene duration of maximum Atlantic-sourced water influence. Furthermore, our records suggest that northernmost Baffin Bay suffered from relatively harsh sea ice conditions during the Holocene Thermal Maximum (HTM), a period characterised by warm atmospheric temperatures (ca 2°C warmer than today; Figure 5.7; Lecavalier et al., 2017). This is likely due to increased meltwater supply, and the local cooling effect of nearby waning ice sheets. Higher sedimentation rates close to the core site may also have enhanced preservation of biomarker by rapidly burying the compounds and limiting their oxidation (e.g., Rontani et al., 2018) partly explaining the high values observed in the IRD-rich unit LF2.

4.6.2 Transition from multi-year to seasonal sea-ice cover, and from oligotrophic to more productive conditions at the core site, with reduced Atlantic influence (8.4-6.5 cal. ka BP)

The temporal resolution in this interval is low, owing to both lower sedimentation rates (Figure 5.3) and lower sampling resolution. Our micropaleontological record is marked by a decrease in the previously dominant *C. reniforme*, and the near disappearance of *I. norcrossi* at ca 8.4 cal. ka BP (Figure 5.6 & Figure 5.7). They are replaced by *E. excavatum* f. *clavata*, a species characteristic of unstable bottom water salinity. This specific shift is indicative of a restricted influence of Atlantic-sourced water and an enhanced influence of freshwater, likely in relation to the opening of Nares Strait.

A peak in *E. arctica*, a species found in modern assemblages under relatively heavy sea-ice cover where food is sparse and which reproduces rapidly during brief periods of phytodetritic export (Gooday and Hughes, 2002; Wollenburg and Mackensen, 1998), occurs between ca 8.3 and 8.0 cal. ka BP, and is indicative of overall oligotrophic conditions (Figure 5.6 and Figure 5.7). It is noteworthy that highest contributions of *E. arctica* (20-40%) occurred along with *A. glomerata* (albeit at low percentages <5%), between 8.3 and 8.0 cal. ka BP (Figure 5.5). *A. glomerata* has been shown to replace *E. arctica* when food supply shifts from episodic to extremely low, and both

species are able to survive under permanent ice-cover (Wollenburg and Kuhnt, 2000). Together with low IP₂₅ fluxes and extremely low HBI III fluxes, the specific assemblage of our benthic foraminiferal record suggests that the core site may have been under quasi-permanent sea-ice cover between ca 8.3 and 8.0 cal. ka BP. However, bulk benthic foraminiferal fluxes reach near maximal values during this period (Figure 5.5), indicating intense proliferation of opportunistic species (mainly *E. arctica* and *E. excavatum* f. *clavata*) during brief outburst of productivity. Small organisms, such as benthic foraminifera, may have thrived in the absence of competition and physical disturbance by macrofauna under near-perennial sea ice (Kröncke et al., 2000). This period of very harsh conditions at the core site corresponds to colder atmospheric temperatures recorded in the Agassiz ice core (Lecavalier et al., 2017) during the 8.2 event (Figure 5.7) which is thought to have been triggered by the drainage of proglacial Agassiz lakes (Barber et al., 1999). Georgiadis et al. (2020) suggested that the opening of Nares Strait may have locally accentuated the cooling, with enhanced sea-ice cover documented in Kane Basin.

A transition occurred some time between 8.0 and 7.4 cal. ka BP, with more a clement environment persisting until ca 6.5 cal. ka BP (Figure 5.7). Decreasing abundances of *E. arctica* and *A. glomerata*, along with an increase in HBI III fluxes point to seasonally open water at the core site, likely extending into Talbot Fjord. IP₂₅ fluxes barely increased suggesting that seasonal sea ice cover was reduced, or that IP₂₅-producing diatoms may have suffered from a higher freshwater content in the sea ice. A slight increase in BSi (1.5% of the mineralogical suite) also support a more productive environment and possibly open surface conditions. The abundance of productivity-related species remains however overall low (Figure 5.6 and Figure 5.7). This period corresponds to the end of the HTM which occurred around 7,800 years ago (Lecavalier et al., 2017), with high atmospheric temperatures persisting until ca 6.2 cal. ka BP according to temperature reconstructions based on chironomid assemblages from a nearby lake (Deltasø; Fig. 1) in northwest Greenland (Axford et al., 2019). The Kane Basin record shows variable conditions between ca 8.1 and 6.5 cal. ka BP (Figure 5.7; Caron et al., 2019; Georgiadis et al., 2020). Early sea ice melt and minimal sea-ice cover were recorded in Kane Basin between ca 8.1 and 7.5 cal. ka BP and was followed by an increase in seasonal sea-ice cover (Caron et al., 2019; Georgiadis et al., 2020), corresponding to the end of the HTM identified by Lecavalier et al. (2017) at ca 7.8 kyrs BP in the Agassiz Ice Core collected in north-eastern Nares Strait (Figure 5.1). Having recorded more open water conditions until ca 6.5 cal. ka BP (Figure 5.8-a), core AMD16-233 is in better agreement with the closer lacustrine record in which Axford et al. (2019) document sustained warm atmospheric temperatures until ca 6.1 cal. ka BP.

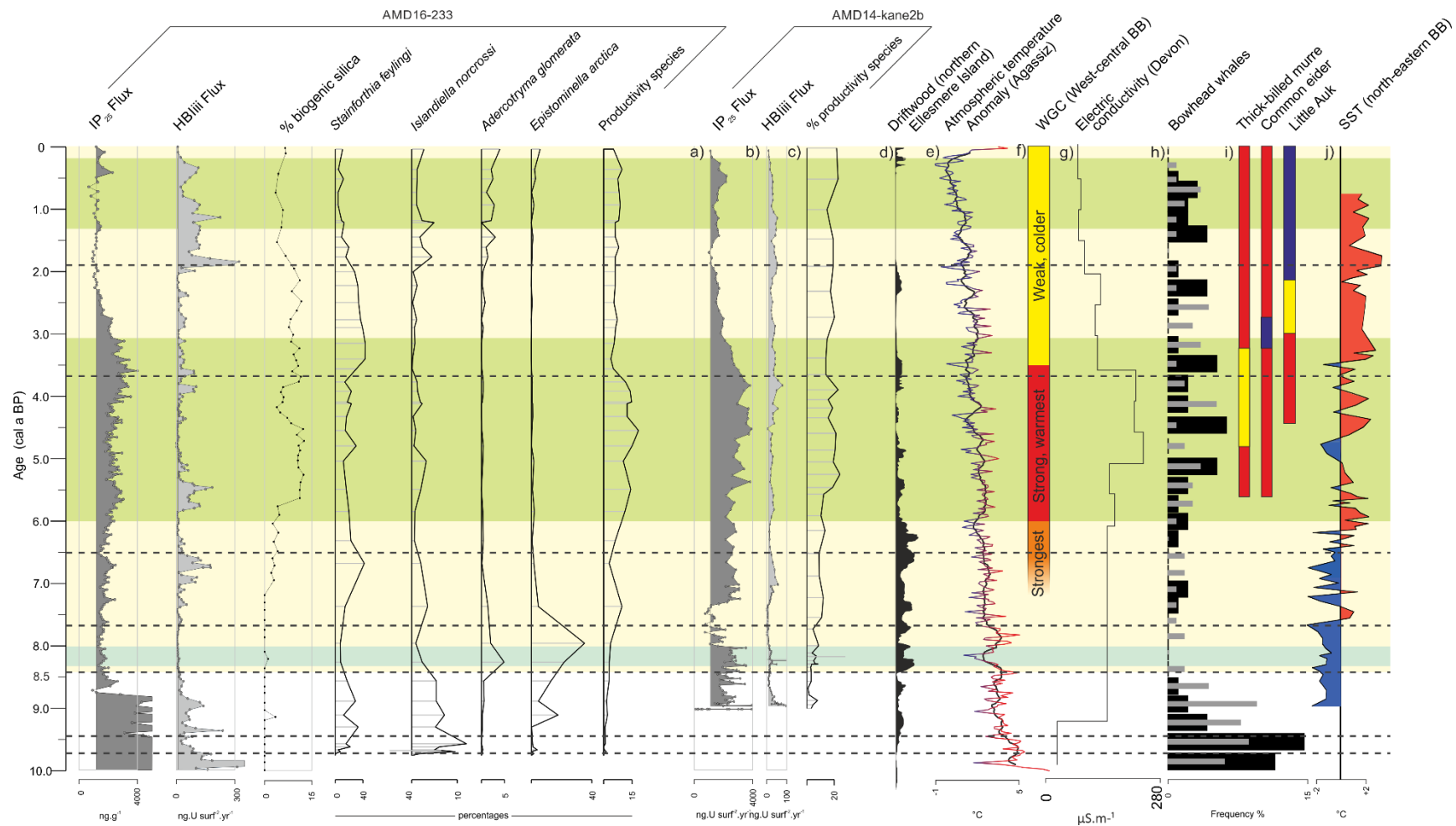


Figure 5.7: Same as figure 5.6 (dashed lines represent ecozone boundaries), but with a) IP_{25} and b) HBI III fluxes, and c) relative percentage of productivity species from core AMD14-Kane2b (Georgiadis et al., 2020); d) driftwood abundance in northern Ellesmere Island as an indication of landfast ice in northern Nares Strait (England et al., 2008); e) $\delta^{18}O$ -derived atmospheric temperature anomaly from Agassiz ice core (black: 200 year running average; Lecavalier et al., 2017); f) WGC current strength and temperature (Perner et al., 2013); g) electric conductivity in Devon Ice Core (Koerner, 1989); h) bowhead whale remains found in east-central CAA (Dyke et al., 1997, 1996, compiled by Lecavalier et al., 2017); i) bird abundance in NW Greenland (red: high numbers; yellow: variable number; blue: low numbers; Davidson et al., 2018); j) reconstructed sea surface temperatures (SST) in north-eastern Baffin Bay (Caron et al., 2019). Intervals characterised by predominantly positive (negative) phases of the AO are represented in yellow (green) (Darby et al., 2012; England et al., 2008; Funder et al., 2011), the blue interval represents the 8.2 cold event identified in the Agassiz Ice Core..

4.6.3 Enhanced productivity, and inception of the North Water polynya (6.5-3.7 cal. ka BP)

The interval between ca 6.5 and 3.7 cal. ka BP, particularly between ca 4.8 and 4.0 cal. ka BP, is characterised by the highest contributions of productivity-related species in the benthic foraminiferal assemblages, along with low abundances of oligotrophic species such as *E. arctica* (Figure 5.7). Benthic and planktic foraminiferal fluxes are however significantly reduced during this interval (Figure 5.6), which together with higher productivity, may indicate increased competition from macrofauna (Kröncke et al., 2000). Contribution of agglutinated are relatively high, possibly indicating increased brine production related to intense sea ice formation at the surface (Fossile et al., 2019). BSi remains low (~1.5%) until ca 5.6 cal. ka BP when it increases to maximal average values of ~10%, before decreasing again between ca 4.5 and 3.7 cal. ka BP. Since the increase in IP₂₅ flux in this interval coincides with an increase of IP₂₅ fluxes in Kane Basin (Figure 5.7), we cannot confirm that enhanced IP₂₅ at site AMD16-233 corresponds effectively to increased seasonal ice cover. It may in fact represent advection of enhanced IP₂₅ produced in Kane Basin.

The increase in BSi ca 5.6 cal. ka BP corresponds with enhanced IP₂₅ fluxes and high abundances of productivity-related species of benthic foraminifera in core AMD14-Kane2b, which was interpreted as possibly corresponding to the inception of the Kane Basin ice arch (Figure 5.7; Georgiadis et al., 2020). The ca 5.5-3.7 cal. ka BP interval also corresponds to maximal diatom abundances in a marine sediment core recovered in the central sector of the North Water covering the last ca 7.5 cal. ka BP, to the exception of the ca 2.5-1.0 cal. ka BP interval (Knudsen et al., 2008). Diatom productivity in the western sector of the North Water (at site AMD16-233) would have indeed been increased if the Kane Basin ice arch was present, preventing drift-ice from entering into Baffin Bay. Given the maximal values of BSi in core AMD16-233, it is likely that convection was limited and that the mixed layer was relatively shallower than it is at present (Lovejoy et al., 2002; Mei et al., 2002; Vidussi et al., 2004). This could have been promoted by (1) limited sea ice formation (and thus brine production) under warmer atmospheric temperatures, (2) a more linear shape of the ice arch in Kane Basin limiting Ekman-induced downwelling (Dumont et al., 2010), and/or (3) weaker winds along Nares Strait during predominantly negative phases of the Arctic Oscillation (AO) (Georgiadis et al., 2020; Samelson and Barbour, 2008).

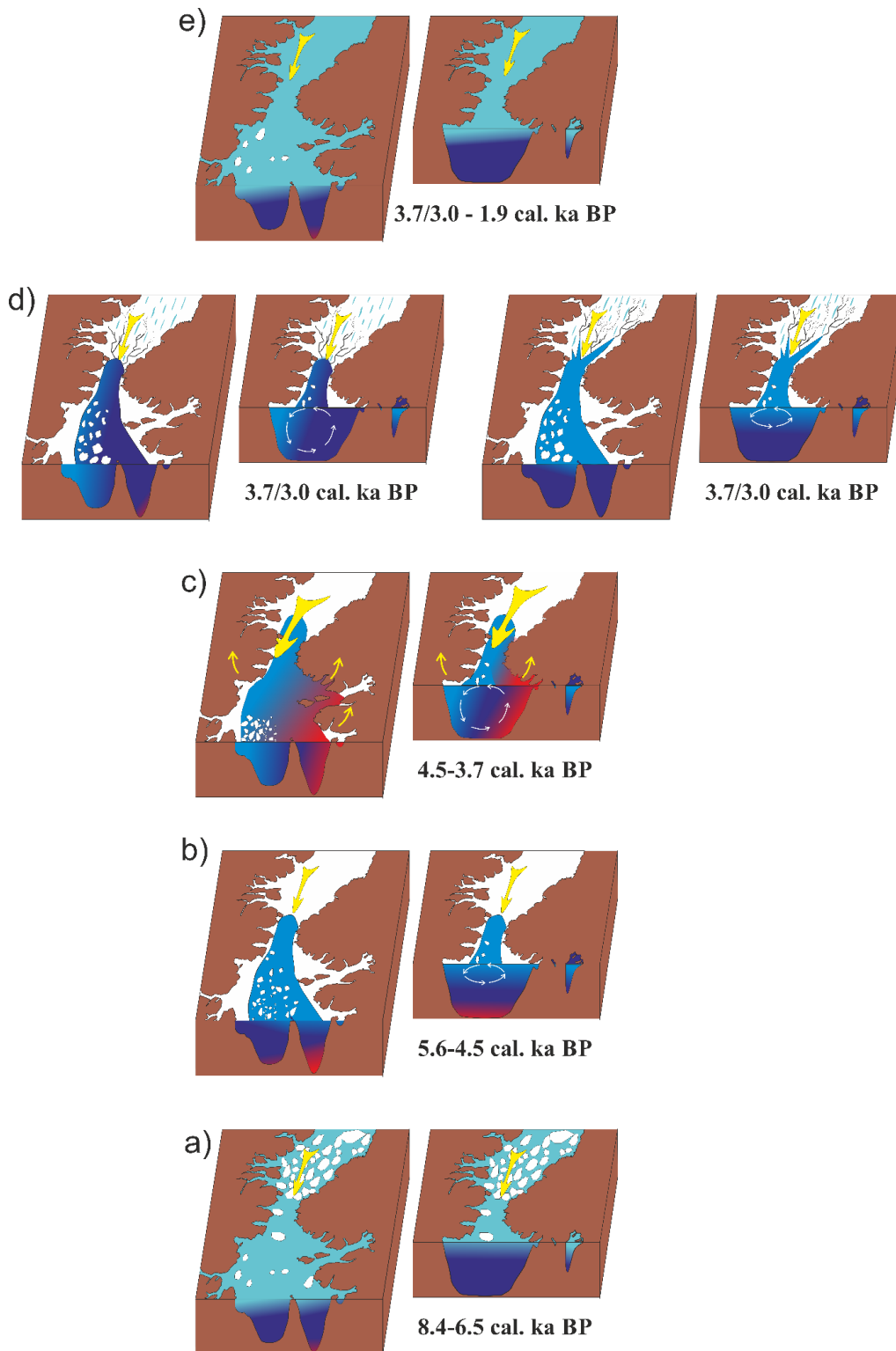


Figure 5.8: Schematic representation of surface conditions in Nares Strait and northernmost Baffin Bay and polynya dynamics, including wind-driven Ekman transport, brine convection, and upwelling. Light blue represents the surface mixed layer and red corresponds to warm Atlantic water. Yellow arrows over Kane Basin represent wind strength. Note that the upwelling of warm water in c) creates a local atmospheric low and increases wind strength.

Although the polynya had not reached its full potential in term of productivity, we note that the potential opening of a latent polynya near the core site corresponds to the arrival of thick-billed murres and common eiders in the area (Davidson et al., 2018). Both species were likely attracted to the more open water conditions occurring earlier

in the spring relative to the surrounding region. Thick-billed murre feeding predominantly on fish (Gaston and Hipfner, 2000), possibly profited from large supplies and more nutritious food under the warmer climate (Rose, 2005) at this time as suggested by Davidson et al. (2018). It has recently been shown that thick-billed murre reproductive success is dependent on sea-ice-derived productivity (Cusset et al., 2019), suggesting that the species may have profited from icier conditions (related from a restricted latent polynya) before the polynya opened to its full extent. The common eider, a benthic feeder foraging in water depth <10 m (Merkel et al., 2007), may have also profited of shallower coastal waters following the isostatic rebound. Models suggest that sea level along the NW Greenland was ca 20 m higher at 8 cal. ka BP compared to ca 4 cal. ka BP (Lecavalier et al., 2014), although more precise mapping on bathymetry in coastal areas would be needed to assess whether the rebound created shallower or deeper coastal waters.

Georgiadis et al. (2020) cautioned that the later arrival of little auk (a polynya-dependent migratory bird) at 4.4 cal. ka BP (Davidson et al., 2018) may indicate that the Kane Basin ice arch was not firmly established between ca 5.5 and 4.4 cal. ka BP. However, high BSi content in Core AMD16-233 supports the fact that the Kane Basin ice arch was present at this time. We propose that, while the Kane Basin ice arch was in fact firmly established by ca 5.5 cal. ka BP, limited convection in the western sector of the North Water was not strong enough to produce an upwelling in the eastern sector of the North Water (Figure 5.8-b). This age of the inception of Kane Basin ice arch corresponds with the general increase of multi-year land-fast sea ice in northern Greenland ca 6 cal. ka BP (Funder et al., 2011; Landvik et al., 2001). While convection and productivity in the North Water was likely limited in the Smith Sound area, the polynya may have reached as far as north-western Baffin Bay (Lancaster Sound), where a decrease in sea ice cover derived from dinocyst assemblages in suggests more open conditions starting at ca 5.5 cal. ka BP (Ledu et al., 2010). Maximum abundance of bowhead whale remains also occur between ca 5.5 and 3.0 cal. ka BP in the east-central CAA (Figure 5.7; Dyke et al., 1999, 1996), the species likely being attracted by the extended open water season in northern Baffin Bay, permitted by the presence of the ice arch.

As atmospheric temperatures continued to drop, it is likely that brine productivity increased in the western sector of the North Water, hindering diatom production as inferred by lower BSi content between ca 4.5 and 3.7 cal. ka BP. Penetrative convection may have been sufficient to produce some upwelling in the eastern sector of the North Water, in the same way that it has been suggested in the modern North Water (Bâcle et al., 2002). A tipping point may have occurred as the lower temperature allowed enough brine formation to induce upwelling. The polynya may have then become self-sustaining when sensible heat emission led to low atmospheric pressure, locally increasing wind strength and producing a positive feedback (Figure 5.8-c). Based on field data and model simulations, Marsden et al. (2004) suggest that this self-sustaining mechanisms may be an important physical process occurring in the modern North Water. An increase in the strength and temperature of the West Greenland Current (WGC) evidenced in eastern Baffin Bay in the Mid-Holocene, particularly between ca 5.5 and 3.5 cal. ka BP (Figure 5.7; Elnegaard Hansen et al., 2020; Jennings et al., 2014; Perner et al., 2013) may have aided the ingress of Atlantic water into northernmost Baffin Bay, but it is not likely to have effectively upwelled in the eastern sector of the North Water until convection was sufficient, around 4.5 cal. ka BP. Increased strength of the WGC may however have increased both the heat and nutrient content of the Atlantic-sourced water which was upwelled,

promoting the self-sustaining mechanism, and enhancing productivity, respectively.

Davidson et al. (2018) speculated that enhanced brine productivity linked to colder atmospheric temperatures after ca. 4.5 cal. ka BP may have been integral to the upwelling of nutrient-rich water and, thus, an extremely productive polynya between ca. 4.4 and 4.0 cal. ka BP, after which little auk numbers began being more variable. Our data fully support this claim. Furthermore, the self-sustaining atmospheric low above the North Water may have been a key factor in maintaining the polynya open by locally increasing wind strength, while the stability of the Kane Basin ice arch may have profited by overall weaker winds over Nares Strait during this interval of predominantly negative-like AO (Georgiadis et al., 2020; Samelson and Barbour, 2008).

4.6.4 Reduced productivity and enhanced stratification (3.7-1.9 cal. ka BP)

An increase in BSi coincides with a change of ecozone at ca 3.7 cal. ka BP (Figure 5.7). Higher contributions of *S. feylingi* in this interval compared to the previous period along with increased BSi are likely indicative of reduced brine convection and increased stratification. A decrease in productivity species in core AMD16-233 infers that the polynya is less productive. These observations all point to increased stratification and reduced upwelling. The oceanographic change coincides with reduced IP₂₅ fluxes in Kane Basin, suggesting that the Kane Basin ice arch may not be as stable as it was previously between ca 5.5 and 3.7 cal. ka BP (Figure 5.7). Although IP₂₅ fluxes are high at the beginning of this interval (ca 3.7-3.0 cal. ka BP), they then decrease until ca 1.9 cal. ka BP due probably to either progressively reduced *in situ* sea ice cover, or lower advection from Kane Basin, where IP₂₅ fluxes also decreased (Figure 5.7; Georgiadis et al., 2020.). Flickering HBI III fluxes suggest that Talbot Inlet may at least seasonally be ice free (Figure 5.7).

Two mechanisms may explain the changes observed in this interval, and may have worked in conjunction trigger in the downfall of the polynya's apogee:

- 1) Sea ice-related productivity (IP₂₅) in core AMD16-233 appears to reach maximal values since the end of deglaciation (8.4 cal. ka BP), peaking at 3.7 cal. ka BP, while the strength (and temperature) of the WGC begins to weaken in eastern Baffin Bay (Fig. 6; Perner et al., 2013). This may suggest that the self-sustaining mechanism may not have been as efficient as it was between 4.5 and 3.7 cal. ka BP (likely due to a colder WGC), and that sea ice eventually increased in the North Water, at least around 3.7 cal. ka BP (possibly from ca 3.7 to ca 3.0 cal. ka BP).
- 2) The beginning of this interval also corresponds to a complete absence of driftwood along the coast of northern Ellesmere Island between ca 3.5 and 2.8 cal. ka BP (England et al., 2008). It is possible that the Kane Basin ice arch became weaker starting at 3.5 cal. ka BP due to less inclusion of thicker Arctic sea ice when the northern ice arch was near-perennial.

The termination of the apogee of the North Water may thus have been related to (1) reduced self-sustainability, followed by (2) a weaker Kane Basin ice arch (Figure 5.8-d).

The previous period of ice arch stability in Nares Strait may have contributed to its weakening, and while there may

be a positive feedback between the Kane Basin ice arch stability and thickness of Arctic sea ice in the Lincoln Sea, it may eventually turn into a negative feedback. The build-up of sea ice in the Lincoln Sea likely resulted from millennia of reduced export due to (1) a stable ice arch in Kane Basin, and (2) prevailing negative phases of the AO from ca 6.0 cal. ka BP to ca 3.0 cal. ka BP (as evidenced by Kara Sea-sourced IRD in the Beaufort Sea; Darby et al., 2012) which are known today to promote sea ice build-up in the Lincoln Sea.

A shift towards more positive-like phases of the AO, occurs ca. 3.0 cal. ka BP (Darby et al., 2012), but is not met with any substantial change in our proxy records. The only significant change is decreased IP_{25} fluxes at the core site (Figure 5.7). We propose that the sea ice in the Lincoln Sea may have been sufficiently thick not to break up under positive AO forcing. The transition from a stable southern ice arch in Kane Basin towards a near-perennial ice arch in the Lincoln sea may have happened very rapidly (possibly a tipping point, occurring sometime between ca 3.7 and 3.0 cal. ka BP), and resulted in surface conditions similar to those observed in Nares Strait in 2009. In 2009, the Kane Basin ice arch did not form, but the northern ice arch persisted until late July. This resulted in open water in Nares Strait practically continuously between May and arch collapse, and anomalously high sea surface temperatures (ca 5° above normal) in the North Water and extending into Baffin Bay due to solar radiation and highly reduced sea ice cover, suggesting a highly stratified water column (Vincent, 2013). While sea ice occurred during winter, leading to some IP_{25} production at our core site between ca 3.0 and 1.9 cal. ka BP, the spring and summer was probably characterised by open water and strong stratification (Figure 5.8-e). Supporting this scenario, is a dinocyst archive from northeastern Baffin Bay (ca 73°N), which shows particularly warm and fresh surface water (Figure 5.8), typical of a stratified water column, after ca 3.4 cal. ka BP (Caron et al., 2019a). The surface temperatures and salinity reconstructions from Caron et al. (2019) originally appeared at odds with other regional records, which tend to show intense cooling, but it was most likely a local, northern Baffin Bay phenomenon due to a strong, near-perennial ice arch in northern Nares Strait at the time.

4.6.5 Collapse of the Trinity-Wykeham ice shelf limited recovery of North Water productivity (1.9 cal. ka BP-0)

A sharp increase in HBI III fluxes at ca 1.9 cal. ka BP coincides with a change of ecozone in the benthic foraminiferal assemblages (Figure 5.7). It also corresponds to an increase in IRD and a higher fraction of sediment coming from local sources (Georgiadis et al., *in prep*). Given the scarcity of IRD in the sediments since Early Holocene glacial retreat terminating around 8.4 cal. ka BP (Georgiadis et al., *in prep.*), we propose that an ice shelf may have been present in Talbot Fjord until ca 1.9 cal. ka BP. The presence of an ice shelf in Talbot Inlet is also supported by overall low HBI III fluxes in our record prior to 1.9 cal. ka BP, suggesting limited freshwater, fjord productivity. The sustained, high HBI III and low IP_{25} fluxes after ca 1.9 cal. ka BP suggest that freshwater fjord productivity was enhanced following the collapse of the ice shelf. Instabilities in the ice shelf may have been triggered by at least ca. 1.8 kyrs (i.e. previous interval 3.7-1.9 cal. ka BP) of predominantly open water (reducing or removing buttressing), and possibly increased temperature of the surface layer (enhanced melting) in the North Water. The collapse of the ice shelf may have further been promoted by advancing glacial ice as the Prince of Wales Icefield expanded during the Neoglacial cooling, leaving moraines dated at ca. 2.0 cal. ka BP 18 km beyond

the present margin in south-eastern Ellesmere Island (Blake, 1989). While Georgiadis et al. (*in prep.*) proposed that this advance may have been promoted by increased moisture provided by an active polynya between ca. 4.5 and 3.7 cal. ka BP, it appears that the predominantly open water conditions which followed (cf. Figure 5.8-e) eventually led to the collapse of an ice shelf in Talbot Fjord at ca 1.9 cal. ka BP, despite colder atmospheric temperatures. Iceshelf have been shown to buttress inland ice and reduce glacial discharge (Haseloff and Sergienko, 2018; Pegler, 2016). High IRD and locally-sourced sediment content in the last ca 2 cal. ka BP (Georgiadis et al., *in prep*) are thus consistent with accelerated glacial fluxes and calving of IRD-loaded icebergs following the collapse of an ice shelf.

A decrease in BSi content after ca 1.9 cal. ka BP (Fig. 6), may be due to perturbation of the surface layer by icebergs. However, decreasing abundances of *S. feylingi* attest to an amelioration of the ventilation of the seabed. A slight recovery of stable bottom water salinity species *I. norcrossi* occurs over the past 1.9 kyrs, and particularly between 1.8 and 1.2 cal. ka BP when its abundance reaches 5%. This may suggest that mass loss of the Prince of Wales Icefield was previously predominantly due to melting (particularly prior to the Neoglacial when atmospheric temperatures were warmer), and that meltwater influx was reduced in Talbot Fjord after 1.9 cal. ka BP, when calving became a more significant component of mass loss.

The absence of driftwood in northern Ellesmere Island between ca 1.7 and 0.2 cal. ka BP suggests that a near-perennial northern ice arch was present in Nares Strait during most of this interval (England et al., 2008). Minimal IP₂₅ fluxes in Kane Basin centred around 1.8 cal. ka BP likely point to significantly reduced sea ice in Nares Strait at the beginning of this interval, indicating that the open water conditions suggested for northernmost Baffin Bay in the previous interval (ca 3.7-1.9) may have extended into Nares Strait. It is possible that our records document a slight recovery of penetrative convection as the Kane Basin ice arch possibly reoccurs between ca 1.5 and 0.2 cal. ka BP (Figure 5.7; Georgiadis et al., 2020). Increased brine production may have hindered the development of *I. norcrossi* between 1.2 cal. ka BP and modern times, and ameliorated ventilation of the water column as inferred by reduced *S. feylingi* abundances (Figure 5.6; Figure 5.7). It is however difficult to assess whether the polynya activity was significant over the past 1.9 cal. ka BP, and the reappearance of oligotrophic species *A. glomerata* and *E. arctica* cast a doubt on how much organic matter effectively reached the entrance of Talbot Inlet if the North Water was active (Figure 5.7). Productivity in the polynya was possibly further reduced by decreased ingress of the WGC during the Late Holocene (Figure 5.7; Perner et al., 2013), limiting the amount of nutrients in Baffin Bay water even if upwelling in the eastern side of the North Water did occur.

4.7 Summary and conclusion

Our records of ocean circulation and sea-ice conditions at site AMD16-233, at the entrance of Talbot Inlet, attest to major Holocene environmental changes in the western sector of the North Water, northernmost Baffin Bay.

- Rapid sedimentation of barren interlaminated mud and sand occurred at a glacial margin just before 9.8 cal. ka BP.
- Severe sea ice cover – possibly perennial – was present during ice sheet retreat at the core site (ca. 9.8 cal. ka BP).

- Maximum influence of Atlantic water at the core site was facilitated by a closed Nares Strait, and may have promoted ice sheet retreat in southern Kane Basin from >9.8 to 8.4 cal. ka BP.
- Restricted influence of Atlantic water induced by the post-glacial opening of Nares Strait is dated at 8.4 cal. ka BP in core AMD16-233. The date of this event, which corresponds to the top of the IRD-rich unit in this core, agrees with previous dating of the initiation of the connection between the Arctic Ocean and Baffin Bay.
- An oligotrophic environment persisted until ca. 8.0 or 7.7 cal. ka BP with multi-year, land-fast ice in Talbot Inlet, before more clement conditions with seasonally opened water in the fjord occurred until 6.5 cal. ka BP.
- Productivity increased around 6.5 cal. ka BP, and was followed by the initiation of a more firmly established polynya at the core site with consolidation of the Kane Basin ice arch at ca 5.5 cal. ka BP. The polynya was a latent heat polynya, and limited sea ice production due to warmer temperatures likely reduced penetrative brine convection.
- Between ca 4.5 and 3.7 cal. ka BP, colder temperatures promoted intense brine production and increased convection. Strengthening of the West Greenland Current may have enhanced both the heat and nutrient content of the Atlantic-sourced water upwelled in the polynya at this time. Self-sustaining mechanisms (i.e. establishment of a local atmospheric low due to heat transfer to the atmosphere) were likely integral in promoting an extremely productive polynya.
- A quasi-permanent northern ice arch starting ca 3.7 cal. ka BP prevented multi-year Arctic sea ice from entering Nares Strait, ultimately resulting in open water conditions in Nares Strait and Baffin Bay and increased stratification at the core site. The high stability of the northern ice arch was probably due to previously (1) reduced sea ice export through Nares Strait due to the Kane Basin ice arch likely and (2) prevailing negative phases of the Arctic Oscillation which would have favoured the build-up of thick Arctic sea ice in the Lincoln Sea. Brine production and efficient Ekman pumping were hindered in the absence of the Kane Basin ice arch, and northernmost Baffin Bay was ice-free but severely stratified.
- Our records document several changes at ca 1.9 cal. ka BP compatible with the collapse of an ice shelf in Talbot Fjord, which may have been triggered by (1) glacial advance due to colder atmospheric temperature in the Neoglacial promoted by (2) increased accumulation due to enhanced moisture by the sensible component of the North Water during previous intervals, and (3) largely reduced sea ice cover and possibly increased surface temperatures in northernmost Baffin Bay due to the a quasi-perennial northern ice arch between ca 3.7 and 1.9 cal. ka BP.
- While a possible limited recovery of the Kane Basin ice arch centred around 0.5 cal. ka BP was suggested by Georgiadis et al. (2020), evidence of a recovery of the North Water is not convincing at our site in the western sector of the polynya. This may however be due to the change in glacial dynamics, with increased

iceberg production in Talbot Inlet in the absence of the ice shelf making it difficult to compare this interval with previous ones.

Our results demonstrate that the North Water and the Kane Basin ice arch constitute a complex tandem-system. While the Kane Basin ice arch may not be indispensable to create open water in northernmost Baffin Bay, it is integral in initiating and maintaining an *active* polynya, and high productivity rates. Our understanding is that enhanced activity of the North Water between ca 4.5 and 3.7 cal. ka BP was largely due to an increase in the sensible heat component in the polynya, and that self-sustaining mechanisms may have played an important part in maintaining a favourable environment for Ekman pumping south of the Kane Basin ice arch. The model used in Marsden et al. (2004) to evidence self-sustainability was limited by the non-inclusion of buoyancy flux, mixing and time dependency. Our results suggest that these may have been important parameters for a fully functioning North Water at its apogee, warranting further modelling of self-sufficiency of the polynya. Although the stability of the Kane Basin ice arch and the build-up and thickening of Arctic sea ice in the Lincoln Sea may promote each other through a positive feedback, our results suggest that the build-up of sea ice in the Lincoln Sea may come to a point where it is so stable and thick that it is no longer exported through Nares Strait, leading to an unstable or absent Kane Basin ice arch. To our knowledge, the interdependence of the southern and northern ice arches has not been explored in modelling or observational studies of the North Water/ice arch system. Our results along with those of Georgiadis et al. (2020) also warrant further investigation of the role of the Arctic Oscillation on the formation of ice arches.

A major result of our study is that productivity in the North Water appears to be significantly decreased in the Early Holocene, during warmer climatic conditions when neither of the ice arches were present in Nares Strait. The continued decrease in the duration of the Nares Strait ice arches over the instrumental period (Vincent, 2019), along with lower productivity in the North Water (Marchese et al., 2017) suggest that we may be returning to these conditions. Furthermore, the rate of change associated with this transition towards absence of land-fast ice in Nares Strait may be enhanced by a dwindling stock of thick Arctic sea ice due to the increased prevalence of positive phases of the Arctic Oscillation (Rigor et al., 2002).

Reconstructions of the Holocene activity of the North Water polynya based on the micropaleontological (planktic and benthic foraminiferal assemblages) and biogeochemical (sea ice biomarkers IP₂₅ and HBI III) investigation of marine sediment core AMD16-233 evidence various periods of contrasting environmental conditions in northernmost Baffin Bay:

- severe sea ice condition (near-perennial sea ice cover) occurred during the deglaciation of southernmost Nares Strait,
- maximal Atlantic influence at the core site from >9.8 to 8.4 cal. ka BP may have promoted ice sheet retreat in southern Nares Strait, while it was cut short by the inflow of Arctic water associated to the opening of Nares Strait ca 8.4 cal. ka BP,
- multi-year landfast sea ice was probably present at the entrance of Talbot Fjord, and may have been associated to oligotrophic conditions at the core site until 6.5 cal. ka BP, when seasonal sea ice provided fresh phytodetritus to the seabed,
- the consolidation of the Kane Basin ice arch around 5.5 cal. ka BP led to the establishment of a likely latent heat polynya between 5.5 and 4.5 cal. ka BP,
- decreasing atmospheric temperatures after 4.5 cal. ka BP enhanced brine production which may have led to increased convection. The upwelling of warm Atlantic water in eastern Kane Basin possibly established a self-sustained polynya associated to the enhanced sensible heat component of the polynya,
- near-perennial landfast sea ice in northern Nares Strait restricted the entrance of thick, multi-year sea ice into the strait starting around 3.7 cal. ka BP. This weakened the Kane Basin ice arch, eventually leading to reduced duration of sea ice cover in Kane Basin and an increased open water season,
- at 1.9 cal. ka BP, sustained high accumulation of freshwater biomarkers in the studied core, together with sedimentological and inorganic geochemical evidence suggest that an ice shelf may have collapsed in Talbot Fjord, increasing glacial fluxes and icebergs calving at the core site. The possible change in glacial regime hinders our reconstructions of the North Water activity over the past ca 1.9 kyrs.

This last work completes our study of the Holocene history of Nares Strait. The first part of this project documented ice sheet retreat in the area and the subsequent geomorphological reorganisation in Nares Strait. Once the geomorphological setting was established, our micropaleontological and biogeochemical datasets were interpreted in terms of changes in ocean circulation and sea ice conditions in Kane Basin

and in the North Water polynya. Our reconstructions were explored in the light of previous studies conducted on nearby marine and continental settings to help establish the local environmental conditions related to the Holocene dynamics of Nares Strait. In the final synthetic chapter of the present manuscript, our work will be contextualised in a wider perspective, by assessing the implication of Nares Strait dynamics on local and regional ocean, ice and climate dynamics.

Chapter 5 Nares Strait: a driver of local and regional ocean, ice and climate dynamics

5.1 Introduction

In this section, we consider larger scale or further-reached implications of postglacial geomorphological changes and sea ice dynamics in Nares Strait. Our work has shown that Nares Strait has undergone severe and rapid reorganisation linked to glacial retreat during the Early Holocene, with postglacial isostasy affecting the long-term morphological evolution of the strait, while ice arch-polynya dynamics may have varied to degrees not observed in modern times. We put our reconstructions in perspective by considering nearby and farther records which may have been influenced by Nares Strait Holocene dynamics.

5.2 Nares Strait environmental dynamics drive local change in the area

5.2.1 Ice shelf development in the northern Nares Strait area

We propose (Georgiadis et al., *in prep.*) that reduced sea ice cover in southern Nares Strait over the past ca 3 cal. ka BP may have promoted the break-up of a potential ice shelf in Talbot Fjord. Today, there are no ice shelves in southern Nares Strait. Floating ice shelves are a common feature in Antarctica, but the Arctic hosts only a few, most of them in northern Ellesmere Island, facing the Arctic Ocean. Sea ice is an essential component of ice shelves in the Arctic, as opposed to Antarctic ice shelves which are fed by glacial ice streams (e.g., Copland and Mueller, 2017; Jeffries, 1992). A number of studies have focused on the recent effect of a warming Arctic on the shrinking and disintegration of ice shelves in the Canadian Arctic Archipelago (CAA), and have proposed diminishing quantity and quality (e.g., thickness, incorporation of glacial ice) of marine ice cover as a major contributor to their decay, together with warmer atmospheric temperatures (e.g., Copland et al., 2007; Vincent et al., 2001; White and Copland, 2019). Considerably fewer studies exist on the Holocene dynamics of Arctic ice shelves.

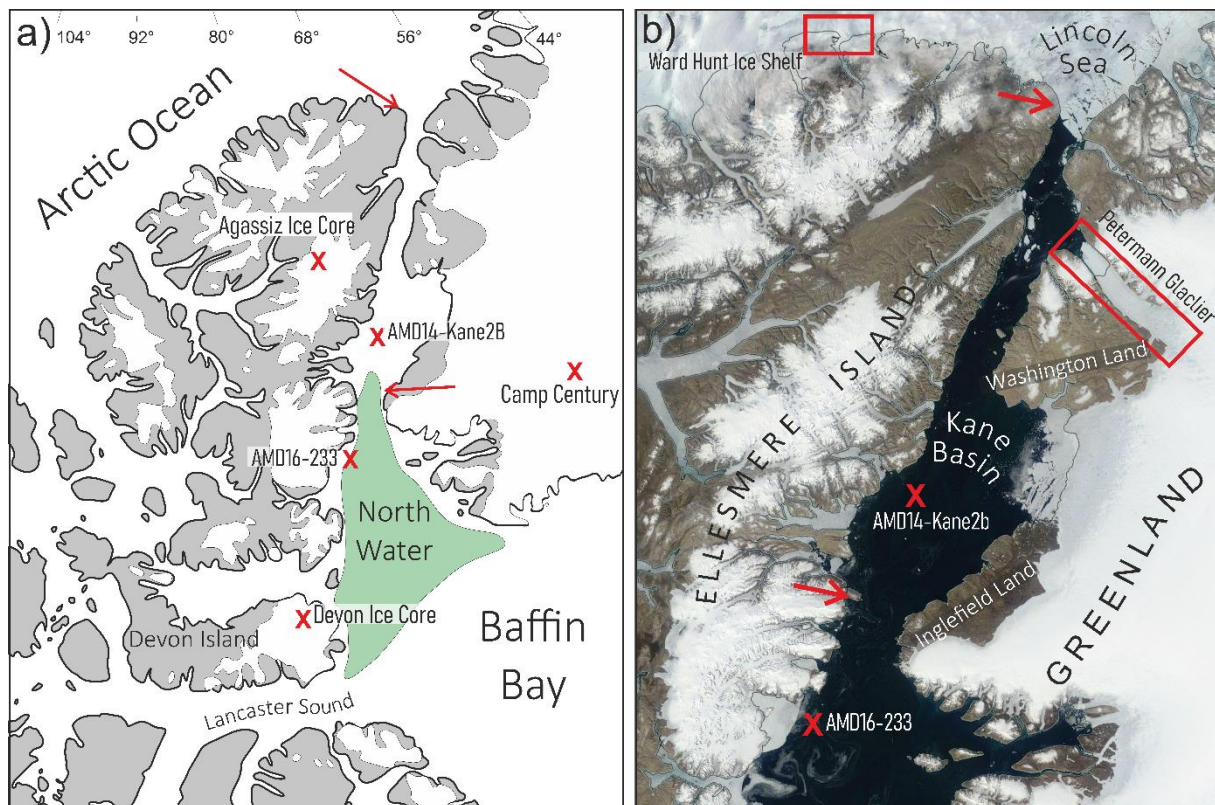


Figure 6.1: Study area with location of cores AMD14-Kane2B and AMD16-233, red arrows mark the general location of ice arches in Nares Strait. a) The modern extent of the North Water polynya, nearby ice cores are marked by a cross. b) red rectangles show the Ward Hunt and Petermann Glaciers and Ice Shelves.

The development of the Ward Hunt Ice Shelf in northern Ellesmere Island (Figure 6.1) has been dated at 4.0 cal. ka BP (Antoniades et al., 2011). The longer seasonal duration of sea ice in Nares Strait and the establishments of ice arches into the spring and summer ca 5.5 cal. ka BP (Georgiadis et al., 2020, *in prep.*) may have played a determinant role in promoting the formation of the Ward Hunt ice shelf by enhancing the build-up of Arctic sea ice in the Lincoln Sea.

A recent study documenting the Holocene dynamics of the Petermann Ice Shelf, in northern Nares Strait (Figure 6.1), demonstrates that the development of this Greenlandic ice shelf did not begin before ca 2.0 cal ka BP, with maximal extent reached between ca 0.6 cal. ka BP and modern times (Reilly et al., 2019). In fact, the ice shelf is thought to be completely absent when our reconstructions suggest maximal stability of the Kane Basin ice arch between ca. 5.5 and 3.7 cal. ka BP, with ice shelf development starting when our data suggest minimal sea ice cover in Kane Basin. In the modern era, an Atlantic vs. Pacific front is thought to exist in the Lincoln Sea. Negative (positive) phases of the Arctic Oscillation are linked to predominantly Atlantic (Pacific) water at the entrance of Nares Strait (Steele et al., 2004). It is possible that when AO negative-like phases are thought to have prevailed between ca 6.0 and 3.0 cal. ka BP (Darby et al., 2012; Funder et al., 2011), more Atlantic-sourced water entered into Nares Strait. Reilly et al. (2019) suggest that warmer atmospheric temperatures in the Mid-Holocene may have increased surface melting and subglacial run-off, preventing ice shelf development through the entrainment

of warmer oceanic water in meltwater plumes that, ultimately, promoted melting of the glacial front. The prevalence of warmer Atlantic-sourced water in Hall Basin between ca 5.5 and 3.0 cal. ka BP may have been particularly detrimental to ice shelf development. Conversely, between ca 3.0 and 1.3 cal. ka BP, prevailing positive phases of the AO (Darby et al., 2012) may have restricted the entrance of Atlantic-sourced water, while the northern Nares Strait ice arch may have led to local brine formation further decreasing oceanic temperatures in northern Nares Strait. Together with continued atmospheric cooling, this may have promoted the development of the Petermann Ice Shelf. The final stages of ice shelf formation resulting in its maximal extent ca 0.6 cal. ka BP, may have been promoted by the recovery of the Nares Strait ice arch around this time (Georgiadis et al., 2020, *in prep. a*), providing a buttressing effect on the glacial front. The comparison of the Kane Basin sea ice records and Petermann Ice Shelf reconstruction suggest that Holocene dynamics of the ice shelf were controlled primarily by oceanic and atmospheric temperatures, and that sea ice played a secondary role. This is supported by recent studies that have found that about 80% of glacial ablation of the Petermann Glacier occurs through basal melting (e.g., Rignot and Steffen, 2008). Since it is located south of the northern ice arch, the Petermann Glacier is bordered by less thick and more seasonal sea ice than the Canadian ice shelves in the Arctic Ocean, thus providing it with less stability and perhaps explaining its greater sensibility to ocean forcing compared with Canadian ice shelves. Further investigation into water characteristics in Hall Basin are however necessary to establish robust conclusions on the long-term sensitivity of the Petermann Ice Shelf to ocean forcing.

5.2.2 Mitigation of local climate, and influence on human dynamics

In addition to being oases in high latitude environments, polynyas dominate the heat budget in Arctic regions through several processes (Smith et al., 1990). The transfer of heat from the ocean towards the atmosphere can be enhanced by the release of latent heat through the freezing process of ice which is swept away by wind and ocean currents. Sensible heat can also be evacuated at the surface by the upwelling of warmer water. Furthermore, the low albedo of open water entails that solar radiation is absorbed by the surface water, providing additional heat to the system (Smith et al., 1990). Polynyas are also a source of moisture, as water is evaporated above open water when the temperature difference between the relatively warm ocean and the cold atmosphere is higher than 5°C (Saunders, 1964).

Today the North Water is both a source of heat and moisture for northern Baffin Bay. Land surrounding the polynya profit from a greater maritime character in their Arctic climate, due largely to the North Water (Maxwell, 1981). Evaporation above the North Water is manifested in the frequent occurrence of steam fog in the area (Dey, 1980), and moisture flux is proportional to the size of the polynya (Boisvert et al., 2012).

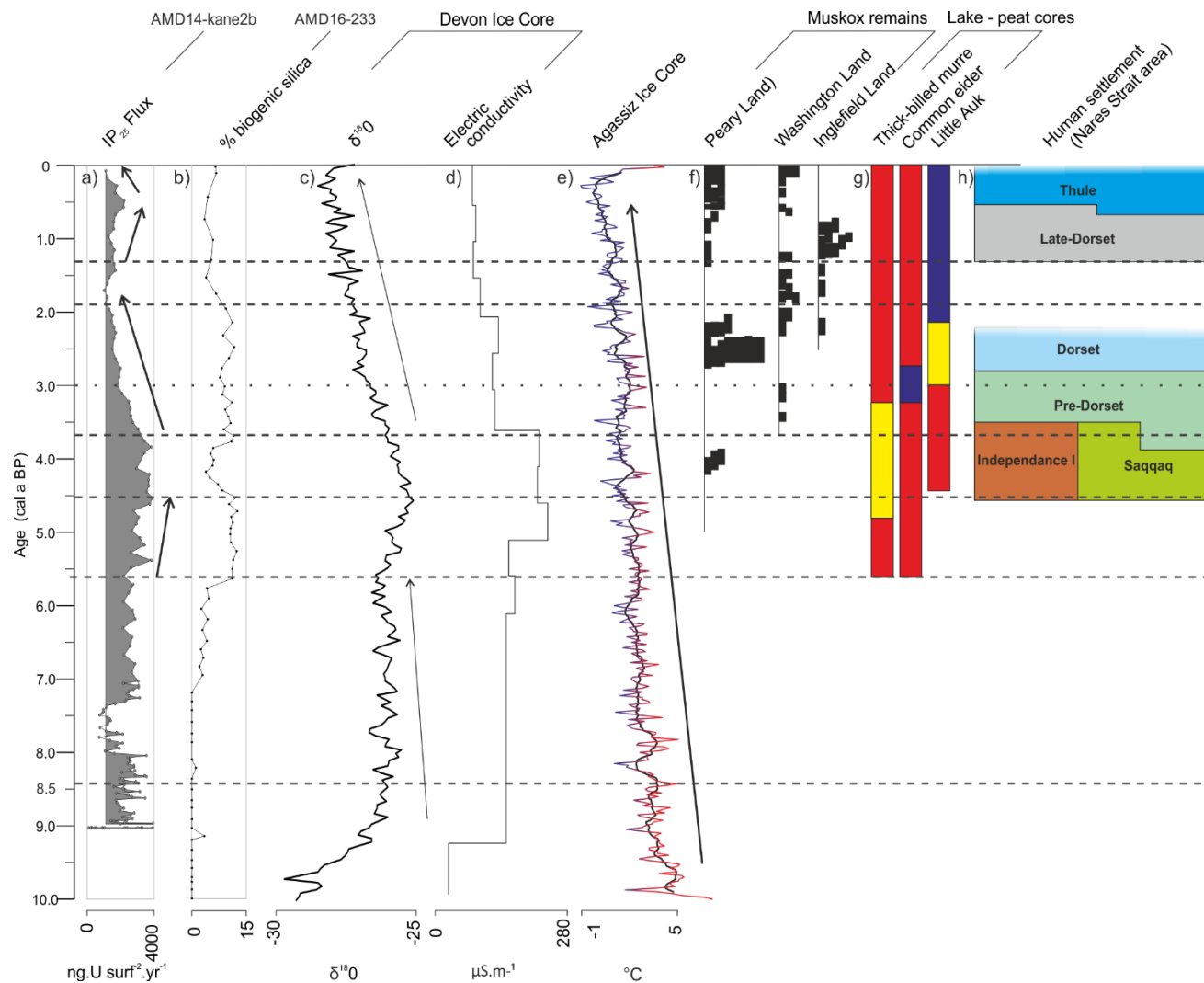


Figure 6.2: Comparison of data from cores AMD14-Kane2b and AMD16-233 with local records. a) IP_{25} fluxes in core AMD16-Kane2b; b) biogenic silica abundance in core AMD16-233; c) Devon Ice Core $\delta^{18}O$ and d) electric conductivity (Koerner, 1989); e) $\delta^{18}O$ -derived atmospheric temperature anomaly from the Agassiz Ice Core (Lecavalier et al., 2017); f) age range of radiocarbon dating of musk ox remains (Bennike, 2014, 2002; Bennike and Andreasen, 2005); g) bird abundance in NW Greenland (red: high numbers; yellow: variable number; blue: low numbers; Davidson et al., 2018); h) human settlement in the Nares Strait area (cf. references in main text).

Sensible heat was likely a greater component of the North Water during its apogee between ca 4.5 and 3.7 cal. ka BP (Georgiadis et al., *in prep.* a). The warmer WGC, as evidenced in central-eastern Baffin Bay (Perner et al., 2013), may have provided more heat which was upwelled to the surface in the North Water, and may have led to enhanced local warming. The Agassiz Ice Core recorded a gradual decrease in atmospheric temperatures over the Holocene (Figure 6.2-e; Lecavalier et al., 2017) and was overall unaffected by heat emission from the North Water. However, $\delta^{18}\text{O}$ values from the Devon Ice Core (Figure 6.2, Koerner, 1989), situated downwind from the North Water in the central-western CAA, displays a marked increase centred at ca 4.5 cal. ka BP suggesting a warming which interrupts the trend towards lower $\delta^{18}\text{O}$ values (Figure 6.2-c). The Devon Ice Core $\delta^{18}\text{O}$ record is not corrected for elevation change which can influence isotopic values, and thus this record must be interpreted with caution with respect to atmospheric temperatures and precipitations. However, higher conductivity in the ice layers representing this time period suggests elevated marine salt content coming from open water (Koerner, 1989; Figure 6.2-d). It is likely that the North Water was a major source of salt, and that high polynya activity at this time led to a slightly warmer climate with increased precipitations.

Through collaborative work, we have come to reflect on the role of the North Water polynya in human dynamics in the Nares Strait area. This work is led by Sofia Ribeiro at GEUS, Denmark (Ribeiro et al., *submitted*). Human settlement in the area began with the arrival of the first Paleo-Inuit (or Paleo-Eskimo) in Northwest Greenland and south-eastern Ellesmere Island ca 4.5 cal. ka BP (e.g., Schledermann, 1980), and is followed by a succession of cultures in the Nares Strait area. The arrival and abandonment of cultures correspond with changes in our records of the North Water polynya and sea ice dynamics (Figure 6.2-h). The establishment of ice arches in the CAA is thought to have been a determinant factor in the migration of Paleo-Inuit into northern Greenland (Helgason et al., 2006), as they followed musk oxen eastward over these stable bridges (McGhee, 1996). The presence of herbivores implies that vegetation was sufficient to sustain these herds. Thus, in addition to the establishment of ice bridges in the CAA channels, the deglaciation and ice sheet retreat on land was another physical element allowing a progressive eastern migration of the species. The Greenland Ice Sheet retreated beyond the modern coasts of Northwest Greenland and south-eastern Ellesmere Island shortly before the deglacial opening of Nares Strait, as attested by mollusc collections (Mörner and Funder, 1990; England, 1999 and references therein), while the postglacial rebound lowered relative sea level. In Inglefield Land, the Greenland Ice Sheet reached minimal extent around ca 4.7 cal. ka BP (Farnsworth et al., 2018) indicating that a large terrain of potential habitat was present by that time. A similar age has been proposed for maximal glacial retreat in north-eastern Greenland (e.g., Landvik et al., 2001). Meanwhile, the North Water would have acted towards sustaining vegetation growth on land through two processes: (1) by moisture evaporation leading to enhanced precipitation, and (2) by the ocean-to-land transfer of nutrients through little auk guano (Figure 6.2-g; González-Bergonzoni et al., 2017; Mosbech et al., 2018). The first evidence of human occupation in southern Kane Basin (Ellesmere Island coast and Inglefield Land) is dated at ca 4.5/4.6 cal. ka BP, with Saqqaq visiting

the area sporadically until ca 3.5 cal. ka BP, and Independence I likely settling during a pioneering phase until ca 4.2 cal. ka BP before visiting the area sporadically until 3.5 cal. ka BP (Figure 6.2-h; Grønnow and Sørensen, 2004; Schledermann, 1990). Starting around 3.5 cal. ka BP, Independence I, a culture known for its large use of land resources, and particularly the musk ox, travelled to north Greenland (Peary Land) where it established settlements until migrating further south in east Greenland (Figure 6.2-h). The Saqqaq were present in Inglefield Land and are known to exploit all available food resources, from birds to marine mammals (Grønnow, 1997; Meldgaard, 2004). Both these cultures regularly visited the North Water during its apogee (i.e. when the upwelling of Atlantic-sourced water was likely strongest; Georgiadis et al., *in prep.* a), and abandoned the area shortly after the sensible component of the polynya was diminished ca. 3.7 cal. ka BP. This suggests that the polynya has been a crucial land resources for these cultures via the transfer of marine-derived nutrients by little auk. Some evidence of sporadic Pre-Dorset settlements exists on south-eastern Ellesmere Island and has been dated between ca 3.9 and 2.8 cal. ka BP (Schledermann and McCullough, 2003), while Dorset seasonally occupied the area from 2.8 to 2.4 cal. ka BP (Figure 6.2-h; Schledermann, 1990). The disentanglement of the two cultures in archaeological findings is a complex matter, but there appears to be a transition from Pre-Dorset to Dorset in the Nares Strait area during the 3.9-2.4 cal. ka BP time interval (Grønnow and Sørensen, 2004). The main difference between the two cultures is a shift from land-sea dependence of resources towards more reliance on marine food (Taylor, 1968). This period corresponds to a transition in our record from a present, but less active North Water (from 3.7 to ca 3.0 cal. ka BP) towards a near-perennial northern ice arch and shorter sea ice season in Kane Basin (Georgiadis et al. *in prep.* a). The Pre-Dorset are likely to have relied on both marine resources hunted on the sea ice in Nares Strait, and polynya-dependent land-based resources such as the little auk, which was still abundant on the north-western coast of Greenland until ca 3.0 cal. ka BP (Figure 6.2-g; Davidson et al., 2018). The Dorset likely established more durable dwellings in the Nares Strait area, predominantly hunting walrus (Murray, 1999). However, IP_{25} fluxes in Kane Basin became minimal between 1.9 and 1.5 cal. ka BP, suggesting severely reduced seasonal sea ice season in Nares Strait, possibly due to a perennial northern ice arch (Georgiadis et al., *in prep.* a). The loss of their preferred hunting ground (i.e. sea ice) appears to have driven the Dorset to abandon the area. The next phase of human presence in the area is the Late Dorset, who were present from ca 1.3 to 0.7 cal. ka BP (Schledermann, 1990). The Late Dorset are thought to have become permanently established in the area, intensively hunting walrus (Appelt et al., 2016). This corresponds to the recovery of the Kane Basin ice arch (Georgiadis et al., 2020), which would have provided suitable grounds for walrus hunting. The final stages of human migration to the area are complex and involve periods of presence by the Thule culture with strong cross-cultural contact, intermittent with periods of isolation and abandonment (Hastrup et al., 2018; Schledermann and McCullough, 2003), however the resolution of our records do not permit to compare human and sea ice dynamics in historical times. The comparison of archaeological findings with our records illustrates that Paleo-Inuit and Inuit cultures have exploited the full

potential of resources offered in Nares Strait (i.e. prey, hunting grounds and transportation paths), with specific cultural adaptations ensuring the survival of successive communities in the area depending on sea ice and polynya conditions.

5.3 Further-reached implication of the Holocene history of Nares Strait

5.3.1 Silicate pump

While Pacific-sourced Arctic water entering Baffin Bay from the Canadian Arctic Archipelago (CAA), are typically enriched in silicate, a high drawdown of silica occurs today in northernmost Baffin Bay, particularly in the North Water. Tremblay et al. (2002) suggest that the North Water may presently work as a silicate trap based on nutrient measurements in the Smith Sound area. They show that, while surface waters entering through Nares Strait display excess silicate, sinking diatoms are dissolved in the in the deep water of the southern sector of the North Water, effectively removing silicate from surface waters.

Several marine sediment cores from western Baffin Bay covering the Late Pleistocene and the Holocene display similar patterns in terms of accumulation of diatom skeletons (Figure 6.3; Williams, 1990). Diatom productivity was shown to take place in the Early Holocene at core sites sufficiently far away from the Innuitian and Laurentide Ice Sheets at the eastern Canadian continental margin. The influence of the opening of the CAA, as a source of silicate, was not entirely clear in the records (Figure 6.3). Williams (1990) noted however that cores from southern Baffin Bay and Davis Strait are systematically barren of diatoms between ca 8000 and 3000 ¹⁴C BP (Figure 6.3), the exception being core HU78-029-024 (the northernmost of the cores studied by Williams, 1990) which displays high diatom fluxes in the Mid-Holocene (Figure 6.3). The author explains that this may be due to a meltwater cap preventing the upwelling of nutrients, and that, where other records report a marine optimum in Baffin Bay (e.g. Andrews, 1972; Miller, 1980), such was not the case for diatom productivity in the study area (southern Baffin Bay and Davis Strait). Diatom productivity was however reported in the central-eastern CAA with high values between ca 8.0 and 3.0 cal. ka BP (Finkelstein and Gajewski, 2008), and maximal accumulations of diatom skeletons occurred in a marine sediment core from the central sector of the North Water between ca 5.5 and 3.7 cal. ka BP (Knudsen et al., 2008). This suggests that silicate drawdown in the North Water may have been effective in the Mid-Holocene, when the polynya was most active. Some silicate may have reached site HU78-029-024, where it was entirely consumed, depriving the southernmost locations in Baffin Bay and Davis Strait from nutrients. Inversely, Late Holocene diatom productivity in Baffin Bay and Davis Strait (Figure 6.3) may have profited from limited drawdown when a northern ice arch in Nares Strait induced a highly stratified water column in northernmost Baffin Bay (Georgiadis et al., *in prep. a*).

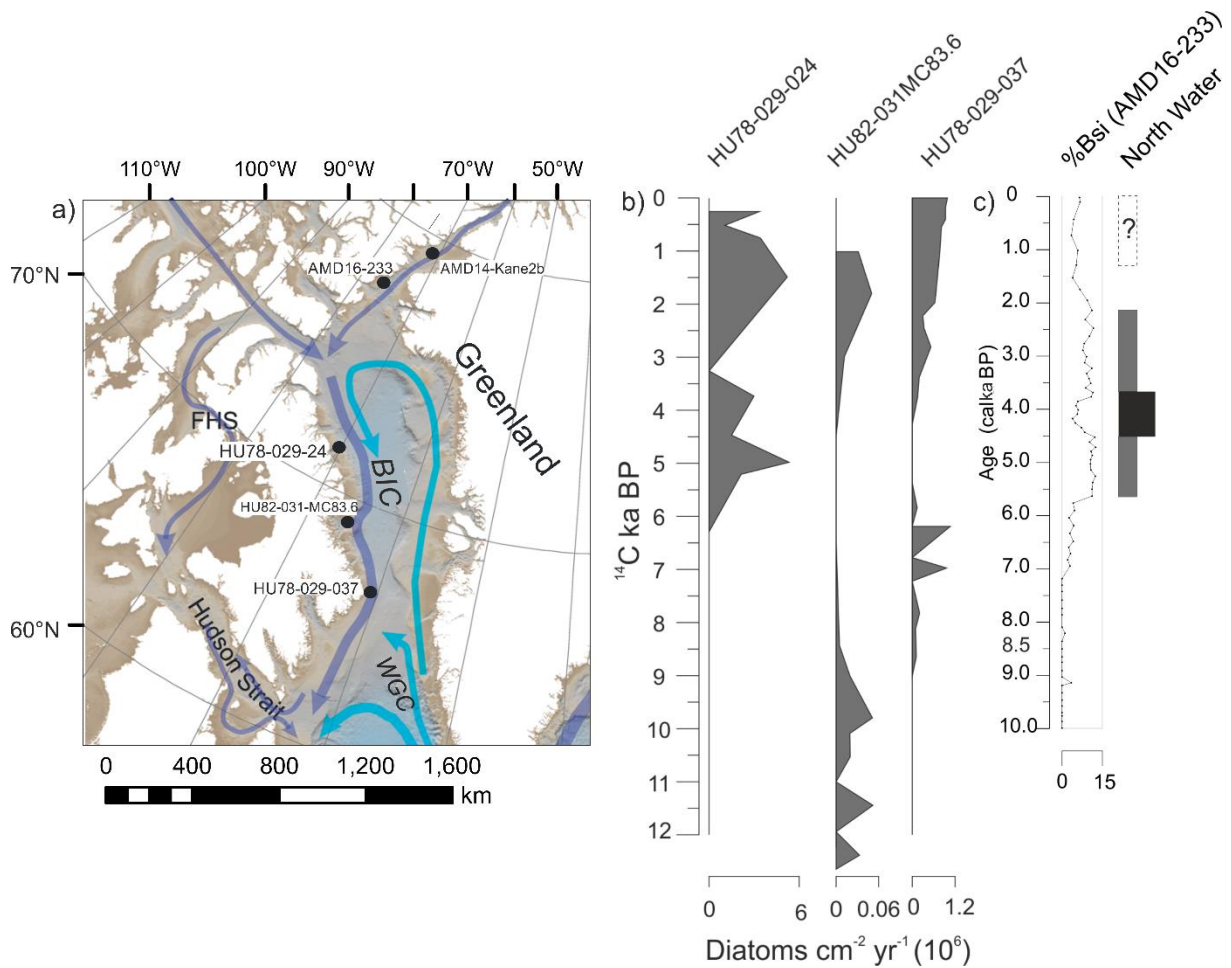


Figure 6.3: Comparison between diatom productivity-related proxies in Baffin Bay and our record of silicate drawdown in southern Nares Strait. a) location of cores; b) diatom fluxes from central and southern Baffin Bay and Davis Strait (Williams, 1990); c) Biogenic Silica (BSi) content in core AMD16-233 with representation of polynya activity. Latitudes of cores are: HU78-029-024: 71°N; HU82-031MC83.6: 69°N; HU78-029-037: 68°N. Note that data from Williams (1990) are presented according to their original age model derived from bulk organic matter.

5.3.2 Potential implications on North Atlantic Holocene circulation

Both major geomorphological changes during deglacial to post-glacial times, and the Holocene evolution of sea ice conditions in Nares Strait affected the local oceanography (Georgiadis et al., 2020), which in turn may have contributed to changes in the wider Baffin Bay ocean circulation.

In the Early Holocene, the outflow from the CAA was likely highly stratified, with a fresh, meltwater-rich surface layer (provided by retreating ice sheets) and more saline water masses below. The bottom water masses traveling through the CAA channels would have faced less obstruction along their way prior to the postglacial

isostatic rebound, when the channels were up to 180 m deeper (England et al., 2006), with deeper, more saline water entering Baffin Bay at depth. Over the course of the Holocene, the CAA throughflow was gradually restricted to fresher (less saline) waters in the top ca 200 m (Nares Strait, e.g. Münchow et al., 2007) or ca 130 m (eastern and central CAA, e.g. Jones and Coote, 1980), with possibly modern-like conditions of export achieved by ca 5 or 4 cal. ka BP (Georgiadis et al., 2020; Lecavalier et al., 2014; Pieńkowski et al., 2014). Other processes would have also played a role on the export of CAA water, particularly sea ice dynamics. The formation of the Kane Basin ice arch isolates the underlying water from wind mixing, producing a slightly more stratified water column at the exit of Nares Strait (e.g., Samelson et al., 2006). However, a northern ice arch in Nares Strait promotes open water conditions downstream in Nares Strait possibly increasing wind mixing, but promoting stratification in northernmost Baffin Bay due to the formation of a warm surface layer through solar radiation (Vincent, 2013). Furthermore, the export of Arctic sea ice and fresh surface water is highly reduced by the presence of these ice arches (Kwok, 2005), and is increased in their absence (Münchow, 2016). Water exiting Nares Strait is further modified by brine injection in Nares Strait during seasonal sea ice freezing, but also in the North Water, when continuous sea ice production leads to intense brine release (Bourke et al., 1989; Sadler, 1976).

Baffin Bay ocean circulation is characterised by the West Greenland Current (WGC) travelling up the Greenland side of Baffin Bay, and the Baffin Island Current (BIC) flowing southward along its Canadian side (Figure 6.4). The WGC is a mixture of fresh and colder polar East Greenland Current (EGC) water, and warmer and more saline Irminger Current water (IC). The CAA outflow mixes with warmer and saltier water transported via the WGC upon its entrance in Baffin Bay, forming the Baffin Island Current (BIC). The upper layer of the BIC, in western Baffin Bay, is thus fresher and cooler than the WGC circulating along the eastern side of Baffin Bay. Through brine convection, northernmost Baffin Bay is a source of cold, saline water. Bourke et al. (1989) propose that brines produced in the North Water mix with Nares Strait outflow and descend in plumes constituting an essential component of Baffin Bay Deep Water (BBDW), and contributing to the ventilation of Baffin Bay.

An additional role of sea ice dynamics in the Nares Strait region on local (and potentially regional) oceanography, is the role of brine produced in the North Water on steric height in Nares Strait. Although they did not investigate it, McGeehan and Maslowski (2012) mention that the convection of dense (cold and saline) water in southern Nares Strait is likely to accentuate the sea surface height gradient between northern and southern Nares Strait, thereby increasing the Nares Strait outflow.

Our Holocene reconstructions of (1) the restriction of Atlantic-sourced bottom water in Kane Basin by postglacial shoaling, (2) sea ice dynamics in Kane Basin (Georgiadis et al., 2020), and (3) convection in the western sector of the North Water (Georgiadis et al., *in prep.* a) have implications on the formation, ventilation and circulation of water masses in the wider Baffin Bay, and potentially on the freshwater flux towards the Labrador Sea. Our reconstructions suggest that:

- Following the opening of Nares Strait in the Eearly Holocene, deeper, more saline (and warm) Atlantic-sourced water likely entered Nares Strait from the north. We have found no evidence of the presence of an ice arch in the spring or summer during the Early Holocene (i.e. land-fast sea ice was limited to the winter months), meaning that the freshwater flux in the surface layer was likely high. The postglacial rebound gradually restricted Atlantic-sourced water from the outflow, making the outflow gradually less saline. The absence of ice arches infers that modern-like BBDW formation and ventilation was restricted (reduced brine convection), and may have been composed of a higher relatively warm and poorly ventilated Atlantic-sourced fraction having travelled through the deeper Nares Strait.
- The inception of ice arches decreased surface freshwater and sea ice export from *ca* 5.5 to 3.7 or 3.0 cal. ka BP. However, since the ice arches were not a perennial feature, freshwater flux through Nares Strait still occurred, and may have had an increased seasonal signal with reduced freshwater flux in the winter and spring, but export of thick, multi-year Arctic sea ice in the late summer. Modern quantification of the freshwater flux in Nares Strait in the presence vs. absence of ice arch however suggest that the overall freshwater flux is reduced in the presence of ice arches (e.g. Kwok, 2005; Münchow, 2016). Meanwhile, prevailing negative-like phases of the Arctic Oscillation (AO) may have increased Atlantic influence in the Lincoln sea, as it has been documented in the Modern (Steele et al., 2004), acting in conjunction with the Kane Basin ice arch to restrict fresher, Pacific-sourced outflow. The modern calculations of local salt injection in the deep water of Baffin Bay *via* the North Water are based on salt rejection during freezing of essentially Pacific-sourced surface water. However, if the Nares Strait outflow was constituted of a greater fraction of Atlantic-sourced water, the brine would likely have been considerably saltier. Hence, the overall contribution of Nares Strait to Baffin Bay was likely less freshwater export, increased salinity of the Nares outflow and potentially increased formation of cold and saline BBDW between *ca* 5.5 and 3.7 or 3.0 cal. ka BP.
- After 3.7 or 3.0 cal. ka BP, the northern ice arch in Nares Strait became near-perennial and the freshwater (liquid and solid) flux through Nares Strait would have been significantly reduced on a multi-year basis. The local convection centre may have migrated to northern Nares Strait at the ice arch margin. Since this configuration has no long-term modern analogue, it is difficult to assess the effect of brine convection in the Lincoln Sea on the local and regional oceanography of Nares Strait. If brine formation was significant in the Lincoln Sea, this may have reduced the sea surface height gradient along Nares Strait and reduced the overall inflow towards Baffin Bay. The Kane

Basin ice arch may have recovered around 0.5 cal. ka BP, perhaps increasing brine production in northernmost Baffin Bay, while seasonal export of Arctic sea ice resumed.

While some models have found the CAA to be an important source of freshwater susceptible of regulating convection in the Labrador Sea (e.g., Wadley and Bigg, 2002), others have found the contribution of the CAA to be negligible (Myers, 2005). Identifying the part played by the aforementioned geomorphologic and oceanographic dynamics in the wider Baffin Bay and in the Labrador Sea is likewise challenging. While we are not able to infer direct causal effect with the changes reported in our records, we suggest that the opening of Nares Strait and the establishment of ice arches may have participated in accentuating larger forcing trends.

Table 6.1: Marine sediment cores and studies used to compare with our records.

Marine Sediment core name	Reference
AMD14-Kane2b	This work
AMD16-233	This work
91-039-012P	<i>Knudsen et al., 2008</i>
AMD14-204	<i>Elnegaard et al., 2020</i>
HU78-029-24	<i>Williamson et al., 1990</i>
HU82-031-MC83.6	<i>Williamson et al., 1990</i>
HU78-29-037	<i>Williamson et al., 1990</i>
343310	<i>Perner et al., 2013</i>
343300	<i>Perner et al., 2013</i>
HU76-26	<i>Osterman & Nelson, 1989</i>
HU78-24	<i>Osterman & Nelson, 1989</i>
HU78-37	<i>Osterman & Nelson, 1989</i>
MSM45-19-2	<i>Lotche et al., 2019b</i>
Hu06-40	<i>Rashid et al., 2017</i>

Our dating of the opening of Nares Strait occurs synchronously with freshwater pulses related to the ice saddle collapse *ca* 8.5 cal. ka BP (Lochte et al., 2019a) and the drainage of Lake Agassiz (e.g., Jennings et al., 2015), and may have participated in increasing the freshwater flux through Davis Strait that has been reported in marine records from the Early Holocene until *ca* 7 cal. ka BP (e.g., Anderson et al., 2007; Sheldon et al., 2016). During the Early Holocene, Baffin Bay and the Labrador Sea regions are marked by lingering glacial to postglacial conditions in comparison to the larger North Atlantic due to the late retreat of the Laurentide Ice Sheet. Meltwater pulses in connection to the retreat of the Laurentide Ice Sheet in Hudson Bay (Jennings et al., 2015) are likely to have overshadowed the influence of the complete opening of the CAA channels and the connection between the Arctic Ocean and Baffin Bay. Furthermore, the asynchronous opening of the channels of the Canadian Arctic Archipelago (CAA) may have had a gradual effect on oceanographic and atmospheric

recirculation due to the pattern of deglaciation of the Innuitian Ice Sheet. The east-central CAA was open by ca 11.0 cal. ka BP (Pieńkowski et al., 2014), but Nares Strait opened considerably later, between 9.0 and 8.3 cal. ka BP (Georgiadis et al., 2018, *in prep.* b; Jennings et al., 2011, 2019), resulting in either a gradual or a stepwise increase of Arctic influx into Baffin Bay. We note that when the opening of Nares Strait has been taken into account in the literature, its opening has usually been placed at ca 10 cal. ka BP (e.g., Ledu et al., 2008), particularly in studies prior to the first published record of marine sedimentation in northern Nares Strait by Jennings et al. (2011).

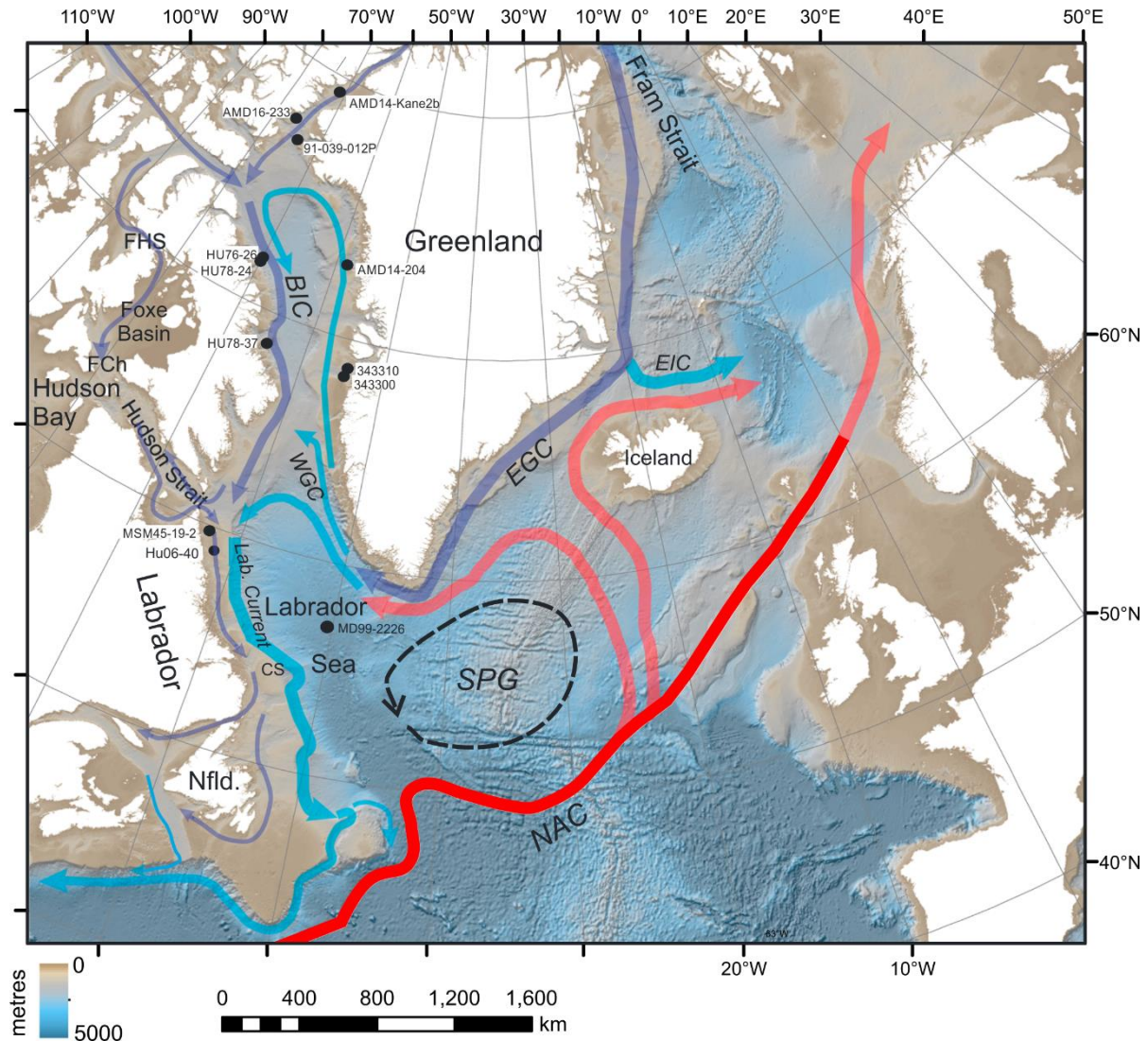


Figure 6.4: Map of the North Atlantic showing modern surface circulation (adapted from Rashid et al., 2017) and location of marine sediment cores (Nares Strait, Baffin Bay and Labrador Sea) discussed in the text and listed in Table 6.1.

Assessing changes relative to the freshwater outflow through Davis Strait in the Mid- to Late Holocene is

likewise challenging due to typically low Holocene sedimentation rates in the Labrador Sea since the disappearance of the Laurentide Ice Sheet no longer provided large sediment inputs. Following low convection in the Labrador Sea during the meltwater pulses of the Early Holocene, records show lower freshwater content at the surface and increased convection, with little variation in sea surface characteristics over the remainder of the Holocene (e.g., de Vernal et al., 2013; Gibb et al., 2015; Solignac et al., 2004). Shorter sea ice seasons are evidenced by benthic foraminiferal assemblages in the north-western Labrador Sea between *ca* 7 and 3 cal. ka BP (Figure 6.5-c-d-e; Lochte et al., 2019b). Interestingly, this record shows minimal relative abundances of Atlantic-related benthic foraminifera between *ca* 5 and 3.5 cal. ka BP (Figure 6.5-d), with slightly increased Arctic species (Figure 6.5-e). Although it may have only contributed to a minor extent, the initiation of ice arches in Nares Strait in the Mid-Holocene (*ca* 5.5 cal. ka BP; Figure 6.5-a-b) could have participated in the overall reduced freshwater flux through Davis Strait leading to reduced sea ice cover. Ice arch formation in Nares Strait and convection in the North Water would have increased brine production, and may have been partly responsible for a stronger (or at least colder) BIC, and thus a stronger Arctic signal in the north-western Labrador Sea benthic record. Benthic foraminiferal records from Baffin Bay exhibit a common feature that is a shift towards near-entirely agglutinated assemblages in the Mid- to Late Holocene, with cores on western Baffin Bay typically showing an earlier transition *ca* 6 cal. ka BP (Figure 6.5-h; Osterman and Nelson, 1989), and those on the eastern side of Baffin Bay transitioning later around 3 cal. ka BP (Figure 6.5-i; Elnegaard Hansen et al., 2020; Knudsen et al., 2008). It is possible that increased brine production following the initiation of ice arches participated in increasing the corrosiveness of bottom waters in Baffin Bay. A relatively strong and warm WGC between *ca* 6 and 3.5 cal. ka BP (Figure 6.5-g; Perner et al., 2013) may have buffered bottom water in the eastern Baffin Bay, while its reduced influence in the Late Holocene enabled a greater influence of corrosive brines in northernmost Baffin Bay (core 91-039-012P; Figure 6.5) and further penetration of brine-enriched bottom water towards north-eastern Baffin Bay (core AMD14-204; Figure 6.5).

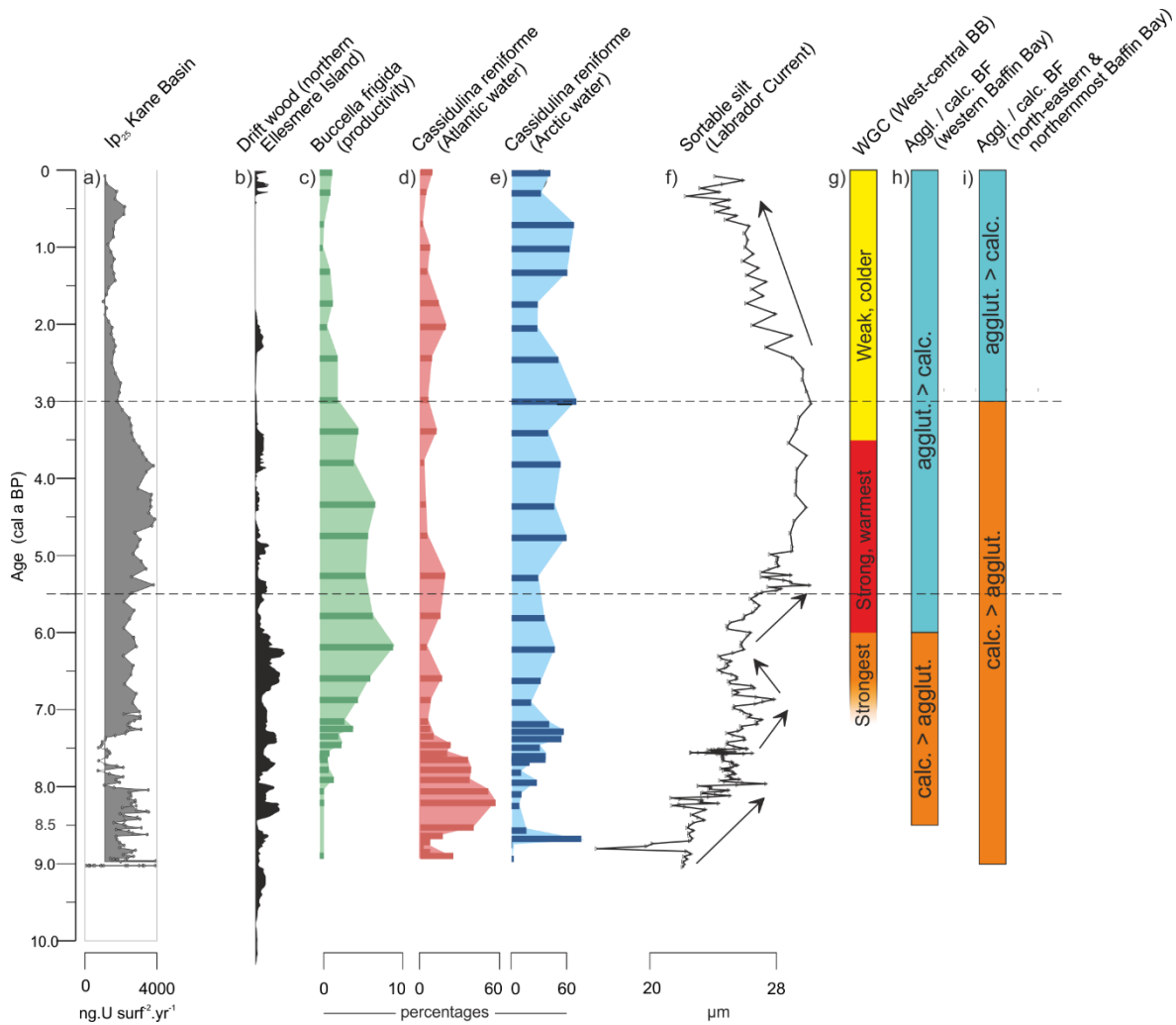


Figure 6.5: Comparison of sea ice dynamics in Nares Strait with oceanographic proxies in the Labrador Sea and Baffin Bay. a) IP_{25} fluxes in Kane Basin (AMD16-Kane2b, this study); b) driftwood in northern Ellesmere Island (England et al., 2008); c-d-f) benthic foraminiferal species abundances in the Labrador Sea (Lochte et al., 2019b); f) sortable silt in the Labrador Se (Rashid et al., 2017); g) strength and temperature of the WGC (Perner et al., 2013); h) agglutinated vs. calcareous benthic foraminiferal content in sediment cores of western Baffin Bay (Osterman & Nelson, 1989); i) agglutinated vs. calcareous benthic foraminiferal content in sediment cores of north-eastern (Elnegaard-Hansen et al., 2019) and northernmost Baffin Bay (Knudsen et al. 2008).

Paleoceanographic changes recorded off the coast of Newfoundland, display more Mid/Late Holocene variability than those from the Labrador Sea. Such is the case for a record of the Labrador Current strength with gradually increasing trends following the Early Holocene melt pulses, until maximum vigour is reached between ca 5 and 3 cal. ka BP, succeeded by a sharp decrease in current velocity (Figure 6.5-f; Rashid et al., 2017). The

authors propose that a strengthened Labrador Current corresponds to increased freshwater fluxes towards the Labrador Sea, and that the last Laurentide Ice Sheet melt pulse at 6.5 cal. ka BP may have enhanced the strength of the Labrador current in the Mid-Holocene, noting that this is in good agreement with slightly more saline surface water evidenced in a nearby core (Sheldon et al., 2016). However, no major salinity-related changes were apparent over the past *ca* 3 cal. ka BP, and the authors turn to the weakening of wind-stress to explain decreasing strength of the Labrador Current, which has been previously proposed by Thornalley et al. (2009) as a mechanism that may weaken the Subpolar Gyre. We propose that the CAA freshwater outflow, particularly related to sea ice dynamics and ice arch formation in the Nares Strait and North Water regions, may warrant further consideration in the context of freshwater export through Davis Strait. Our records suggest that a near-perennial northern ice arch may have been present in northern Nares Strait after 3.7 or 3.0 cal. ka BP, which only broke up occasionally on centennial time scales, effectively reducing the export of freshwater (liquid and solid) through Nares Strait (Georgiadis et al., *in prep.* a). Meanwhile, increased IP₂₅ fluxes in the eastern CAA starting *ca* 3 cal. ka BP suggest the possible inception of seasonal ice arches in Lancaster Sound (Belt et al., 2010). It is possible that ice arches in the CAA may have restricted freshwater flux through the CAA, ultimately lowering freshwater flux through Davis Strait. The two study sites (northernmost Baffin Bay and Newfoundland) are however considerably far apart, and further investigations are necessary to conclude on that matter.

5.4 Conclusion and implications of Nares Strait dynamics on modern and future ocean circulation and climate

Our reconstructions of the dynamics of the Nares Strait area in terms of geomorphology, oceanography, and sea ice conditions have enable us to propose new insight concerning the factors regulating local and regional climatic and oceanographic variability which had previously been undocumented. On Holocene timescales, local changes related to glacial dynamics, climate and human migrations were certainly influenced by geomorphology, surface conditions and physical processes occurring in Nares Strait. However, the further reached implications of our reconstructions on the larger circulation in Baffin Bay and the Labrador Sea warrant further investigation. In the same way, local effects of deteriorating sea ice and ice arch instabilities in Nares Strait in modern times have been evidenced, while regional oceanographic changes are harder to link to sea ice dynamics in the CAA.

The Petermann Glacier in northern Greenland (Figure 6.1) lost ~50% of its ice shelf during calving events in 2010-2012. Minimal sea ice cover is likely to have acted in conjunction with warmer water in Nares Strait to promote thinning and calving of this ice shelf (Münchow et al., 2014, 2011; Shroyer et al., 2017). As it has been in the past (Ribeiro et al., *submitted*), sea ice is a vital element in the subsistence of present-day local communities since it provides hunting grounds and stable transportation routes, while the North Water provides a winter refuge for many migratory and year round species, having historically insured ample resources for humans. Decreasing productivity in the North Water (Marchese et al., 2017), and reduced sea ice in the Nares Strait (Vincent, 2019) over the past decades have however threatened the subsistence of local communities

who have voiced their concerns for their future in the area (ICC, 2017). Our findings suggest that sea ice dynamics in Nares Strait have previously led to human abandonment of the area, although the incredible resilience of High Arctic cultures has enabled them to adapt to changing environment.

As opposed to the “great salinity anomaly” of the 1970s which is thought to be rooted in the North Atlantic to the east of Greenland (e.g., Dickson et al., 1988), the “great salinity anomaly” of the 1980s and another freshwater anomaly in the 1990s affected the Labrador Sea (Häkkinen, 2002). These anomalies occur predominantly during positive phases of the North Atlantic Oscillation (NAO), which correspond to positive phases of the Arctic Oscillation (AO), and have thus been linked to variability in the saline vs. fresh water masses entering the Labrador Sea from the North-east Atlantic and Davis Strait (Häkkinen, 2002). Belkin et al. (1998) however proposed that strong northerly winds associated with positive phases of the NAO may have increased freshwater flux through the CAA, while simulation by Myers (2005) tend to show that freshwater flux through Davis Strait have little influence on freshwater content in the Labrador Sea. A comparison of the duration of ice arches in Nares Strait (Vincent, 2019) with the prevailing winter AO, shows that the reduced ice arch durations during the 1990s was associated with a dominance of strong, positive winter AO phases (Figure 6.6). It is possible that the strong wind during the prevailing positive AO was responsible for (1) causing the early collapse of the Nares Strait ice arches, and (2) increasing freshwater (liquid and solid) through Nares Strait in the absence of ice arches. However, the impact on Labrador Sea freshening appears complex since ice arch duration was relatively long during the 1980s, while minimal ice arch duration in the late 2000s coincides with enhanced production of (saline) Labrador Sea Water in 2008 (Yashayaev and Loder, 2009). While our results suggest that long term variability in ice arch formation *may* have contributed to changes observed in the Labrador Sea (e.g., increased Arctic influence in the Labrador Sea when brine formation was likely maximal in Nares Strait, reduced strength of the Labrador Current with the establishment of a near-perennial ice arch in northern Nares Strait), our results warrant further investigations on whether ice arch dynamics may have had a significant effect on convection patterns in the Labrador Sea on shorter timescales in the modern era.

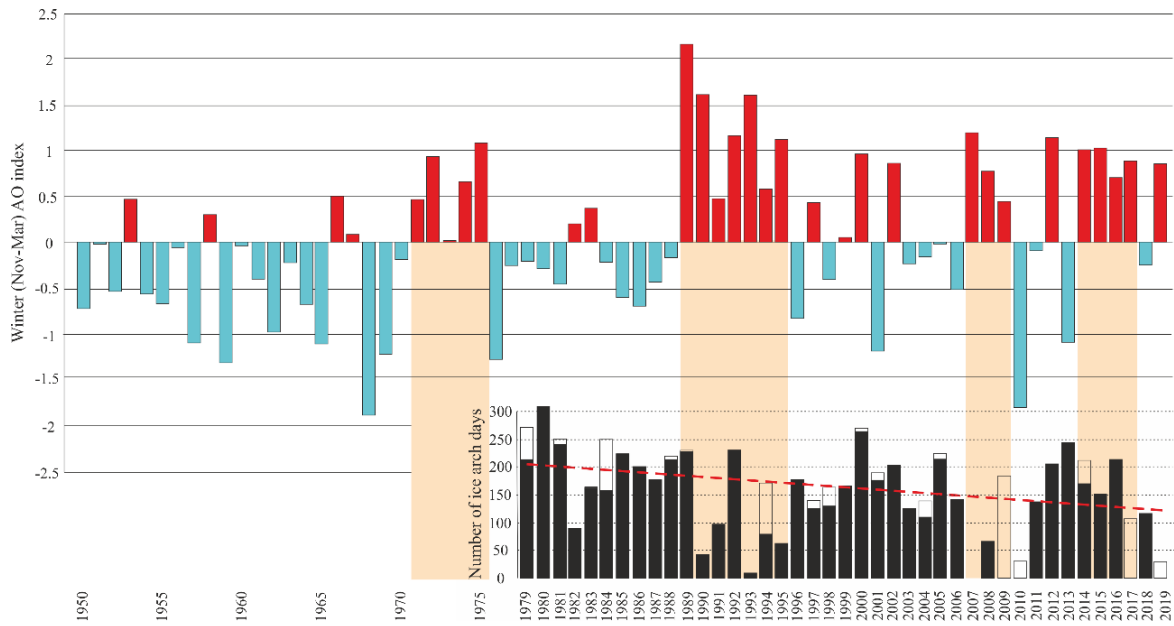


Figure 6.6: Comparison of the winter atmospheric Arctic Oscillation (AO) index (<https://www.pmel.noaa.gov/arctic-zone/detect>), with the seasonal duration of ice arches in Nares Strait (Vincent, 2019).

Conclusion and perspectives

This project on the recent history of Nares Strait, an Arctic Channel of which little is known concerning past, current and future dynamics, has enable us to document the Holocene dynamics of this gateway from the intrinsic perspective of Kane Basin, and from downstream northernmost Baffin Bay. Prior to this work, the crux of our knowledge regarding deglaciation and the establishment of modern oceanographic conditions in the study area relied on discrete land-based evidence and few, low resolution marine sediment records from the northern and southern sectors of the strait.

Based on our work, a number of new contributions were made concerning the postglacial geomorphologic evolution of Nares Strait during and following ice sheet retreat.

The sedimentological and geochemical records from core AMD14-Kane2b provide a new perspective of the deglaciation of Kane Basin and the opening of Nares Strait. They indicate that north-western Kane Basin was glacial ice-free by 9.0 cal. ka BP, and that the complete opening of Nares Strait occurred as early as 9.0 cal. ka BP or as late as 8.3 cal. ka BP, with ice-rafted debris intervals evidencing major stages of glacial retreat. A sudden change in sediment geochemistry, grain size and sedimentation rates were interpreted as evidence of the late retreat of Humboldt glacier in eastern Kane Basin *ca* 8.1 cal. ka BP. The onshore retreat of most of the Innuitian and Greenland Ice Sheet termini shortly after prevented the documentation of Mid- to Late Holocene ice sheet dynamics. Evidence of long-term geomorphological change is however shown in the gradually increasing silt content linked to the postglacial isostatic rebound which brought the seabed closer to the subsurface velocity maxima of the Nares Strait flow.

The sedimentological, geochemical and mineralogical datasets obtained from marine sediments in core AMD16-233, which was collected at the entrance of Talbot Fjord in southern Nares Strait, document both local (Smith Sound) and up-strait glacial retreat. One meter of millimetre to centimetre-scale laminated mud and sand at the base of the core indicate the proximity of a glacial margin prior to 9.8 cal. ka BP. The presence of ice-rafted debris within the laminated sequence attests to the absence of an ice shelf and to at least occasional breakup of land-fast sea ice. Glacial retreat in the area was recorded as two meters of ice-rafted debris-rich sediment. The collapse of the glacial margin proximal to the core site is evidenced by a local origin of the coarse sediment. An increasingly distant provenance in the ice-rafted unit traces the deglaciation of southern Nares Strait, starting in west-central Kane Basin between >9.8 and 9.1 cal. ka BP, before progressing further eastward and northward, resulting in the complete opening of Nares Strait around 8.4 cal. ka BP. No major changes of sediment processes or provenance at the entrance of Talbot Fjord were recorded during the Mid- to Late Holocene. However, over the last 2-2.5 kyrs, enhanced local sediment and ice-rated debris deliveries attest to increased glacial activity in Talbot Fjord.

Our micropaleontological and biogeochemical datasets from cores AMD14-Kane2b and AMD16-233

constitute the first high resolution, continuous Mid- to Late Holocene records of hydrological conditions in the area. They enabled us to constrain the establishment of the modern oceanography and the evolution of sea ice dynamics in Kane Basin and the North Water polynya.

Core AMD14-Kane2b evidences variable environmental conditions at the seabed and at the surface (i.e. sea ice) between *ca* 9.0 and 8.3 cal. ka BP in relation to initial glacial retreat in northern Kane Basin. According to our datasets on benthic foraminiferal assemblages, the early part of our record is marked by the presence of Atlantic-sourced waters in the bottom waters of Kane Basin from *ca* 9.0 to 5.5 cal. ka BP, with a maximum influence from 8.3 to 7.5 cal. ka BP. This pattern relates to a stronger West Greenland Current in Baffin Bay followed by gradual restriction of Atlantic-sourced bottom water in Nares Strait by the postglacial shoaling. According to our sea ice biomarker records, sea ice cover was reduced between 8.1 and 7.4 cal. ka BP before increasing with the onset of cooler atmospheric temperatures following the Holocene Thermal Maximum. Seasonal sea ice cover duration further increased around 5.5 cal. ka BP, according to both sea ice biomarkers and benthic foraminiferal assemblages, with maximal duration between *ca* 4.5 and 3.5/3.0 cal. ka BP. Sea ice biomarkers indicate reduced sea ice cover over the last 3.5/3.0 kyrs, while benthic foraminiferal assemblages display no changes, indicating that sea ice in Kane Basin may have been reduced, while productivity was potentially sustained by a northern ice arch allowing productive spring blooms. The seasonal duration of sea ice cover in Kane Basin may have recovered slightly between 1.2 and 0.2 cal. ka BP. In the light of nearby records, we were able to propose that maximal duration of sea ice cover in Kane Basin corresponds to the presence of the Kane Basin ice arch in the spring and into the summer, while restricted sea ice cover over the past 3.5/3.0 kyrs corresponds to the inception of a stable northern ice arch allowing open water in Kane Basin in the summer and possibly in the spring.

The micropaleontological (benthic foraminifera) and sea ice biomarker records from core AMD16-233 enabled us to document the consequences of Kane Basin sea ice dynamics on the evolution of the western sector south of Nares Strait where the North Water polynya is found today. Sea ice cover was near-perennial during initial ice sheet retreat prior to 9.8 cal. ka BP. Benthic foraminifera evidence a maximum influence of Atlantic-sourced water during the following stages of glacial retreat between >9.8 and 8.4 cal. ka BP. The reduced Atlantic influence after 8.4 cal. ka BP was a result of the opening of Nares Strait which connected the core site to the Arctic Ocean. Oligotrophic conditions in western Smith Sound were recorded from *ca* 8.0 to 7.7 cal. ka BP, when sea ice in Kane Basin was highly variable, and were followed by a more regular seasonal sea ice cover until 5.5 cal. ka BP. Our proxy records are consistent with the initiation of a latent heat polynya around 5.5 cal. ka BP, when the Kane Basin ice arch became firmly established. Reduced contents of biogenic silica from *ca* 4.5 to 3.7, while productivity-related benthic foraminifera are abundant, were interpreted as the result of increased convection in the polynya, with enhanced upwelling and a greater importance of the sensible character of the North Water. A return to more stratified conditions starting at *ca* 3.7 cal. ka BP indicate that the polynya

may have transitioned back to an essentially latent character. The reduced duration of the Kane Basin ice arch and prolonged duration of the northern ice arch in the Lincoln Sea may have led to a northward migration of the local convection centre. Enhanced productivity of freshwater diatoms is indicated by the biomarker record over the past 2 cal. ka BP. Together with the sedimentological and mineralogical datasets obtained on the same core, this indicates that an ice shelf may have collapsed in Talbot Fjord toward the end of the Holocene. The subsequent increased calving rates make it difficult to assess whether the enhanced water column mixing signal is due to increased convection coinciding with the recovery of the Kane Basin ice arch, or if it is a result of disturbance by icebergs.

A synthetic chapter was dedicated to putting our reconstruction of the geomorphological evolution and sea ice dynamics of Nares Strait in the context of other nearby and more distant studies to evaluate the part played by the Holocene dynamics of Nares Strait in the variability recorded in other locations. We find that both oceanography and sea ice conditions may have influenced the development of ice shelves in the area, and certainly were a driver of local climate and human dynamics. The further-reach implications of Nares Strait in the freshwater budget exiting Davis Strait were however unconvincing.

Earlier work in the Nares Strait area proposed that the strait was completely opened around 10 kyrs ago based on cosmogenic dating (Zreda et al., 1999). According to our study, we propose a considerably later opening date, between 9.0 and 8.3 cal. ka BP, with a more probable age around the later bracket of this timeframe. This date is fully consistent with the absence of mollusc older than 8.2 cal. ka BP in the central sector of Nares Strait (England, 1999). Our preferred age for the opening of Nares Strait slightly predates the one proposed by Jennings et al. (2011) who studied the first marine sediment core collected in Nares Strait, to the north of the glacial ice saddle that lingered in the central sector of the strait following the deglaciation of the north and south. The age of the opening viewed from northern Nares Strait was suggested as 9.0 cal. ka BP, although this age did not include an additional reservoir age (Jennings et al., 2011). When applying the same reservoir to cores from both Hall and Kane Basin, a later opening age of ca 8.5 cal. ka BP is more likely. Further, the transition between proglacial laminated mud to bioturbated mud in the northern core (Jennings et al., 2011) was likely influenced by the possible collapse of an ice shelf at the entrance of Petermann Fjord and possibly extending over the core site (Jakobsson et al., 2018). The lithofacies transition in the northern sediment core may have been influenced by this event in addition to the opening of Nares Strait.

Concerning the oceanographic evolution and sea ice dynamics in Kane Basin and the western sector of the North Water polynya, the paucity of such records in the area limit the scope of the critical comparison of our records. In the central and eastern sectors of the current North Water, previous studies have been hindered by sediment gaps between composite cores (Knudsen et al., 2008; Levac et al., 2001). Furthermore, the strong spatial disparities in productivity, ocean circulation, and physical processes in the eastern vs. western sector of the North Water introduces a mismatch between the records. For example, the marine sediment core in the

eastern sector of the North Water attests to a strong influence of Atlantic-sourced water until ca 3.0 cal. ka BP, and enhanced presence of corrosive water over the last 3 kyrs (Knudsen et al., 2008), whereas our western record displays a shorter Atlantic maximum. Jennings et al. (2019) found that Atlantic influence in the central-western sector of the North Water was reduced after ca 9.0 cal ka BP, but low sedimentation rates after ca 7 cal. ka BP provide little evidence for Mid-Late Holocene reconstructions. The opening of Nares Strait ca 8.4 cal. ka BP likely interrupted Atlantic water influence on the western side where the Nares Strait outflow is strongest, while the eastern side received more Atlantic-sourced water until the strength of the West Greenland Current decreased around 3.0 cal. ka BP, as suggested by records of bottom water masses further south in east-central Baffin Bay (Perner et al., 2013). Our records of sea ice dynamics, ice arch formation and polynya activity however complement land records (lake and peat cores) of bird arrival in the area in relation to anticipated marine productivity while surrounded areas are ice covered (Davidson et al., 2018). We were able to propose a continuous record of polynya dynamics which provided details of the Holocene evolution of the area in favour of the hypotheses advanced by Davidson et al. (2018) regarding polynya activity. In our synthetic chapter, we show that major changes in our record are remarkably well correlated to human dynamics in the area, demonstrating that Paleo-Inuit and Inuit cultures were able to exploit the resources offered by the Kane Basin ice arch and North Water polynya thanks to specific cultural adaptations which may have been driven by the evolution of the environment in the area.

While our work enabled us to provide new details concerning previously undocumented or under-documented environmental evolution of the Nares Strait area, it also highlights the limitations associated to our study. An obvious obstacle to providing accurate ages for changes occurring in the Nares Strait area was uncertainty concerning reservoir age correction. The bulk of geomorphological changes occurred within a limited timeframe of less than a millennium, while the age error associated to age reservoir uncertainty is several hundred years and was likely to have changed through time. Changes concerning sea ice and polynya dynamics also occur rapidly, and uncertainty concerning the ages of our reconstructions are attached to any comparison with other local and regional studies. Our attempts to accurately date the opening of Nares Strait were further overcast by doubt concerning which one of the two ice-rafted debris units in core AMD14-Kane2b represents the event. The lack of oceanographic proxies in our records, other than benthic foraminifera, has prevented us from drawing a definite conclusion on the matter. Unfortunately, limitations also arise from the methodology for foraminiferal sample preparations in sediments of core AMD14-Kane2b. The relative abundance of agglutinated species and the more fragile calcareous species are likely to be severely underestimated due to the drying of the samples prior to and post sieving. While our assemblages were represented by environmentally significant species, we must acknowledge that some information were lost and that our reconstructions may lack details carried by the more fragile taxa. We also have a significant amount of data which was not exploited to its full potential in this project. For example, bulk organic carbon content and stable isotope measurement were

performed, but their interpretation requires additional work due to the presence of considerable amounts of coal in the sediments. We were also limited by the overall paucity of records with which to confront our reconstructions and hypotheses. For example, the last ca 2 kyrs of our interpretations of the North Water activity are largely dependent on whether our hypotheses concerning a possible change in glacial regime associated to the collapse of an ice shelf in Talbot Fjord are true.

Our work has enable us to provide new details concerning previously undocumented or under-documented environmental evolution of the Nares Strait area. Our reconstructions are however limited on a larger scale, and additional working perspectives will need to be explored to extend further on the Holocene history of northern Baffin Bay.

Future work may include new preparation of foraminiferal samples on the material leftover from core AMD14-Kane2b, which would enable us to (1) confirm or deny our reconstructions as a whole, (2) explore the new assemblages for a possible oceanographic signal of the opening of Nares Strait, and (3) provide the first comparative study of how preparation techniques influence downcore profiles of foraminiferal assemblages. Elemental datasets on benthic and planktic foraminifera (trace elements) were performed at INSTAAR, USA in order to investigate a possible change of water mass present in Kane Basin following the opening of Nares Strait. These data were not part of this manuscript because of lack of time, but collaborative work with T. Marchitto is underway to fully explore them, and we are hopeful that they may provide further insight concerning the timing of the opening of Nares Strait.

Additional biogeochemical work on nutrient quality and quantity would provide more robustness to either confirming or denying certain of our hypotheses. For example, the presence of the Kane Basin ice arch in the Mid-Holocene, when regional records document a climatic optimum (warming), was largely based on increased IP₂₅ fluxes in core AMD14-Kane2b. However, one could argue that sea ice cover could have actually been reduced (due to warming) and that sea ice was in fact more productive because of a stronger WGC providing more nutrients. This may have effectively been the case when the WGC was strongest (ca 6-3.5 cal. ka BP) and the upwelling in the North Water was more active, bringing nutrients to the underside of the ice in Kane Basin. New biogeochemical analyses (trace element data on benthic and planktic foraminifera) would provide the opportunity to test the hypothesis of a shorter but more productive sea ice cover, vs. a longer (perhaps even near-perennial) sea ice cover which is supplied with fresh nutrients through upwelling of Atlantic-sourced water. The exploitation of oxygen-sensitive ratios in the XRF dataset may also provide more information concerning convection in the North Water.

While the Kane Basin archive may provide an accurate record of sea ice dynamics in Nares Strait, and particularly the establishment of the Kane Basin ice arch, further investigations of the dynamics associated to the northern ice arch are needed. This would offer the possibility to explore both the probable establishment of a near-perennial ice arch over the past ca three millennia, and the dynamics in the Lincoln Sea associated with

a possible latent polynya there.

Our reconstruction in the North Water are also limited to Smith Sound, and to the western sector of the polynya in Smith Sound. Additional work is underway to provide more insight into the eastern sector of the North Water on the basis of a continuous Holocene record there, and a high resolution record of the Late Holocene in the central sector of the polynya (Jackson et al., in prep.). The investigation of marine sediment cores from the far-western sector of the North Water in Lancaster sound or further to the south of Nares Strait in north-eastern Baffin Bay may offer a better view of the full extent of the polynya which will help understand the degree to which it was susceptible of influencing local and regional climate and ocean circulation.

Finally, Talbot Fjord has received some attention due to the incredible increase of icebergs production by the Trinity and Wykeham Glaciers which poses a threat to maritime routes. A number of recent projects have the ambition of mapping the bathymetry of this fjord, which we are hopeful will provide a possible answer concerning a previous position of stability of the grounding line and the evolution of the glacial regime.

References

- Aagaard, K., 1981. On the deep circulation in the Arctic Ocean. *Deep Sea Res. Part Oceanogr. Res. Pap.* 28, 251–268. [https://doi.org/10.1016/0198-0149\(81\)90066-2](https://doi.org/10.1016/0198-0149(81)90066-2)
- Aagaard, K., Carmack, E.C., 1989. The role of sea ice and other fresh water in the Arctic circulation. *J. Geophys. Res. Oceans* 94, 14485–14498. <https://doi.org/10.1029/JC094iC10p14485>
- Aagaard, K., Swift, J.H., Carmack, E.C., 1985. Thermohaline circulation in the Arctic Mediterranean Seas. *J. Geophys. Res. Oceans* 90, 4833–4846. <https://doi.org/10.1029/JC090iC03p04833>
- Alve, E., 2003. A common opportunistic foraminiferal species as an indicator of rapidly changing conditions in a range of environments. *Estuar. Coast. Shelf Sci.* 57, 501–514. [https://doi.org/10.1016/S0272-7714\(02\)00383-9](https://doi.org/10.1016/S0272-7714(02)00383-9)
- Alve, E., 1994. Opportunistic features of the foraminifer *Stainforthia fusiformis* (Williamson): evidence from Frerfjord, Norway. *J. Micropalaeontology* 13, 24–24.
- Anderson, T.W., Levac, E., Lewis, C.F.M., 2007. Cooling in the Gulf of St. Lawrence and estuary region at 9.7 to 7.2 14C ka (11.2–8.0 cal ka): Palynological response to the PBO and 8.2 cal ka cold events, Laurentide Ice Sheet air-mass circulation and enhanced freshwater runoff. *Palaeogeogr. Palaeoclimatol. Palaeoecol.* 246, 75–100. <https://doi.org/10.1016/j.palaeo.2006.10.028>
- Andrews, J., 1972. Recent and fossil growth rates of marine bivalves, Canadian Arctic, and Late-Quaternary Arctic marine environments. *Palaeogeogr. Palaeoclimatol. Palaeoecol.* 11, 157–176.
- Andrews, J.T., Bjork, A.A., Eberl, D.D., Jennings, A.E., Verplanck, E.P., 2015. Significant differences in late Quaternary bedrock erosion and transport: East versus West Greenland ~70°N – evidence from the mineralogy of offshore glacial marine sediments. *J. Quat. Sci.* 30, 452–463. <https://doi.org/10.1002/jqs.2787>
- Andrews, J.T., Eberl, D.D., 2012. Determination of sediment provenance by unmixing the mineralogy of source-area sediments: The “SedUnMix” program. *Mar. Geol.* 291–294, 24–33. <https://doi.org/10.1016/j.margeo.2011.10.007>
- Andrews, J.T., Eberl, D.D., 2011. Surface (sea floor) and near-surface (box cores) sediment mineralogy in Baffin Bay as a key to sediment provenance and ice sheet variations. *Can. J. Earth Sci.* 48, 1307–1328.
- Andrews, J.T., Ives, J.D., 1978. “Cockburn” Nomenclature and the Late Quaternary History of the Eastern Canadian Arctic. *Arct. Alp. Res.* 10, 617–633.
- Andrews, J.T., Stein, R., Moros, M., Perner, K., 2016. Late Quaternary changes in sediment composition on the NE Greenland margin (73° N) with a focus on the fjords and shelf. *Boreas* 45, 381–397. <https://doi.org/10.1111/bor.12169>
- Antoniades, D., Francus, P., Pienitz, R., St-Onge, G., Vincent, W.F., 2011. Holocene dynamics of the Arctic’s largest ice shelf. *Proc. Natl. Acad. Sci.* 201106378. <https://doi.org/10.1073/pnas.1106378108>
- Appelt, M., Damkjar, E., Friesen, M., 2016. Late Dorset, in: *The Oxford Handbook of the Prehistoric Arctic*.
- Axford, Y., Briner, J.P., Miller, G.H., Francis, D.R., 2009. Paleocological evidence for abrupt cold reversals during peak Holocene warmth on Baffin Island, Arctic Canada. *Quat. Res.* 71, 142–149. <https://doi.org/10.1016/j.yqres.2008.09.006>
- Axford, Y., Lasher, G.E., Kelly, M.A., Osterberg, E.C., Landis, J., Schellinger, G.C., Pfeiffer, A., Thompson, E., Francis, D.R., 2019. Holocene temperature history of northwest Greenland – With new ice cap constraints and chironomid assemblages from Deltasø. *Quat. Sci. Rev.* 215, 160–172. <https://doi.org/10.1016/j.quascirev.2019.05.011>
- Bâcle, J., Carmack, E.C., Ingram, R.G., 2002. Water column structure and circulation under the North Water during spring transition: April–July 1998. *Deep Sea Res. Part II Top. Stud. Oceanogr.* 49, 4907–4925. [https://doi.org/10.1016/S0967-0645\(02\)00170-4](https://doi.org/10.1016/S0967-0645(02)00170-4)
- Bahr, A., Jiménez-Espejo, F.J., Kolasinac, N., Grunert, P., Hernández-Molina, F.J., Röhl, U., Voelker, A.H.L., Escutia, C., Stow, D.A.V., Hodell, D., Alvarez-Zarikian, C.A., 2014. Deciphering bottom current velocity and paleoclimate signals from contourite deposits in the Gulf of Cádiz during the last 140 kyr: An inorganic geochemical approach. *Geochem. Geophys. Geosystems* 15, 3145–3160. <https://doi.org/10.1002/2014GC005356>

- Bailey, W.B., 1956. On the Origin of Deep Baffin Bay Water. *J. Fish. Res. Board Can.* 13, 303–308. <https://doi.org/10.1139/f56-020>
- Barber, D.C., Dyke, A., Hillaire-Marcel, C., Jennings, A.E., Andrews, J.T., Kerwin, M.W., Bilodeau, G., McNeely, R., Southon, J., Morehead, M.D., Gagnon, J.-M., 1999. Forcing of the cold event of 8,200 years ago by catastrophic drainage of Laurentide lakes. *Nature* 400, 344. <https://doi.org/10.1038/22504>
- Barber, D.G., Hanesiak, J.M., Chan, W., Piwowar, J., 2001. Sea-ice and meteorological conditions in Northern Baffin Bay and the North Water polynya between 1979 and 1996. *Atmosphere-Ocean* 39, 343–359. <https://doi.org/10.1080/07055900.2001.9649685>
- Belkin, I.M., Levitus, S., Antonov, J., Malmberg, S.-A., 1998. “Great Salinity Anomalies” in the North Atlantic. *Prog. Oceanogr.* 41, 1–68.
- Belt, S.T., Müller, J., 2013. The Arctic sea ice biomarker IP25: a review of current understanding, recommendations for future research and applications in palaeo sea ice reconstructions. *Quat. Sci. Rev.* 79, 9–25. <https://doi.org/10.1016/j.quascirev.2012.12.001>
- Belt, S.T., Vare, L.L., Massé, G., Manners, H.R., Price, J.C., MacLachlan, S.E., Andrews, J.T., Schmidt, S., 2010. Striking similarities in temporal changes to spring sea ice occurrence across the central Canadian Arctic Archipelago over the last 7000 years. *Quat. Sci. Rev.* 29, 3489–3504. <https://doi.org/10.1016/j.quascirev.2010.06.041>
- Bennike, O., 2014. Radiocarbon dating of musk-ox (*Ovibos moschatus*) bones from the Thule region, north-west Greenland. *Polar Rec.* 50, 113–118.
- Bennike, O., 2002. Late Quaternary history of Washington Land, North Greenland. *Boreas* 31, 260–272. <https://doi.org/10.1111/j.1502-3885.2002.tb01072.x>
- Bennike, O., Andreasen, C., 2005. Radiocarbon dating of musk-ox (*Ovibos moschatus*) remains from north-east Greenland. *Polar Rec.* 41, 305–310.
- Bennike, O., Dawes, P.R., Funder, S., Kelly, M., Weidick, A., 1987. The late Quaternary history of Hall Land, northwest Greenland: discussion. *Can. J. Earth Sci.* 24, 370–374.
- Bergeron, M., Tremblay, J.-É., 2014. Shifts in biological productivity inferred from nutrient drawdown in the southern Beaufort Sea (2003–2011) and northern Baffin Bay (1997–2011), Canadian Arctic. *Geophys. Res. Lett.* 41, 3979–3987. <https://doi.org/10.1002/2014GL059649>
- Bervid, H.D., Carlson, A.E., Hendy, I.L., Walczak, M., Stoner, J.S., 2016. Deglacial sea-surface temperature change and rapid response along the western margin of the northern and southern Cordilleran ice sheet, in: AGU Fall Meeting Abstracts.
- Beszczyńska-Möller, A., Woodgate, R., Lee, C., Melling, H., Karcher, M., 2011. A Synthesis of Exchanges Through the Main Oceanic Gateways to the Arctic Ocean. *Oceanography* 24, 82–99. <https://doi.org/10.5670/oceanog.2011.59>
- Biggs, N.R.T., Willmott, A.J., 2001. A steady-state coupled ocean-polynya flux model of the North Water, Baffin Bay. *Geophys. Astrophys. Fluid Dyn.* 95, 1–29. <https://doi.org/10.1080/03091920108203412>
- Blaauw, M., 2010. Methods and code for ‘classical’ age-modelling of radiocarbon sequences. *Quat. Geochronol.* 5, 512–518. <https://doi.org/10.1016/j.quageo.2010.01.002>
- Blake, W.J., 1992. Holocene emergence at Cape Herschel, east-central Ellesmere Island, Arctic Canada: implications for ice sheet configuration. *Can. J. Earth Sci.* 29, 1958–1980. <https://doi.org/10.1139/e92-153>
- Blake, W.J., 1989. Application of ¹⁴C AMS Dating to the Chronology of Holocene Glacier Fluctuations in the High Arctic, With Special Reference to Leffert Glacier, Ellesmere Island, Canada. *Radiocarbon* 31, 570–578. <https://doi.org/10.1017/S0033822200012157>
- Blake, W.J., 1981. Neoglacial Fluctuations of Glaciers, Southeastern Ellesmere Island, Canadian Arctic Archipelago. *Geogr. Ann. Ser. Phys. Geogr.* 63, 201. <https://doi.org/10.2307/520833>
- Blake, W.J., 1979. Age determinations on marine and terrestrial materials of Holocene age, southern Ellesmere Island, Arctic Archipelago. *Geol. Surv. Can. Pap.* 79, 105–109.
- Blake, W.J., 1977. Glacial sculpture along the east-central coast of Ellesmere Island, Arctic Archipelago Project 750063. *Rep. Act. Part C* 107–115.

- Blake, W.J., 1972. Climatic implications of radiocarbon-dated driftwood in the Queen Elizabeth Islands, Arctic Canada, in: Climatic Changes in Arctic Areas During the Last Ten-Thousand Years. Y. Vasari, H. Hyvairinen, and S. Hicks, pp. 77–104.
- Blake, W.J., 1970. Studies of glacial history in Arctic Canada. I. Pumice, radiocarbon dates, and differential postglacial uplift in the eastern Queen Elizabeth Islands. *Can. J. Earth Sci.* 7, 634–664. <https://doi.org/10.1139/e70-065>
- Blake, W.J., Boucherle, M.M., Fredskild, B., Janssens, J.A., Smol, J.P., 1992. The Geomorphological Setting, Glacial History and Holocene Development of “Kap Inglefield Sø”, Inglefield Land, North-West Greenland, by Weston Blake Jr., Mary M. Boucherle, Bent Fredskild, Jan A. Janssens and John P. Smol. *Geoscience* 27. <https://doi.org/10.14430/arctic1830>
- Blake, W.J., Jackson, H.R., Currie, C.G., 1996. Seafloor evidence for glaciation, northernmost Baffin Bay. *Bull. Geol. Soc. Den.* 43, 157–168.
- Boisvert, L.N., Markus, T., Parkinson, C.L., Vihma, T., 2012. Moisture fluxes derived from EOS aqua satellite data for the north water polynya over 2003-2009: MOISTURE FLUXES DERIVED FROM EOS AQUA. *J. Geophys. Res. Atmospheres* 117, n/a-n/a. <https://doi.org/10.1029/2011JD016949>
- Born, E.W., Teilmann, J., Acquarone, M., Riget, F.F., 2004. Habitat Use of Ringed Seals, *Phoca hispida*, in the North Water Area (North Baffin Bay). *Arctic* 57. <https://doi.org/10.14430/arctic490>
- Bourke, R.H., Addison, V.G., Paquette, R.G., 1989. Oceanography of Nares Strait and northern Baffin Bay in 1986 with emphasis on deep and bottom water formation. *J. Geophys. Res.* 94, 8289. <https://doi.org/10.1029/JC094iC06p08289>
- Bradley, R.S., 1990. Holocene paleoclimatology of the Queen Elizabeth islands, Canadian high arctic. *Quat. Sci. Rev.* 9, 365–384.
- Brakstad, A., Våge, K., Håvik, L., Moore, G.W.K., 2019. Water Mass Transformation in the Greenland Sea during the Period 1986–2016. *J. Phys. Oceanogr.* 49, 121–140. <https://doi.org/10.1175/JPO-D-17-0273.1>
- Breyman, M.T.V., Emeis, K.-C., Suess, E., 1992. Water depth and diagenetic constraints on the use of barium as a palaeoproductivity indicator. *Geol. Soc. Lond. Spec. Publ.* 64, 273–284. <https://doi.org/10.1144/GSL.SP.1992.064.01.18>
- Briner, J.P., McKay, N.P., Axford, Y., Bennike, O., Bradley, R.S., de Vernal, A., Fisher, D., Francus, P., Fréchette, B., Gajewski, K., Jennings, A., Kaufman, D.S., Miller, G., Rouston, C., Wagner, B., 2016. Holocene climate change in Arctic Canada and Greenland. *Quat. Sci. Rev.* 147, 340–364. <https://doi.org/10.1016/j.quascirev.2016.02.010>
- Brown, T.A., Belt, S.T., Tatarek, A., Mundy, C.J., 2014. Source identification of the Arctic sea ice proxy IP₂₅. *Nat. Commun.* 5, 4197. <https://doi.org/10.1038/ncomms5197>
- Caron, M., Montero-Serrano, J.-C., St-Onge, G., Rochon, A., submitted. Quantifying provenance and transport pathways of Holocene sediments from the northwestern Greenland margin.
- Caron, M., Rochon, A., Montero-Serrano, J., St-Onge, G., 2019a. Evolution of sea-surface conditions on the northwestern Greenland margin during the Holocene. *J. Quat. Sci.* 34, 569–580. <https://doi.org/10.1002/jqs.3146>
- Caron, M., St-Onge, G., Montero-Serrano, J.-C., Rochon, A., Georgiadis, E., Giraudeau, J., Massé, G., 2019b. Holocene chronostratigraphy of northeastern Baffin Bay based on radiocarbon and palaeomagnetic data. *Boreas* 48, 147–165. <https://doi.org/10.1111/bor.12346>
- Carr, J.R., Vieli, A., Stokes, C.R., Jamieson, S.S.R., Palmer, S.J., Christoffersen, P., Dowdeswell, J.A., Nick, F.M., Blankenship, D.D., Young, D.A., 2015. Basal topographic controls on rapid retreat of Humboldt Glacier, northern Greenland. *J. Glaciol.* 61, 137–150. <https://doi.org/10.3189/2015JoG14J128>
- Ceperley, E.G., Marcott, S.A., Reusche, M.M., Barth, A.M., Mix, A.C., Brook, E.J., Caffee, M., 2020. Widespread early Holocene deglaciation, Washington Land, northwest Greenland. *Quat. Sci. Rev.* 231, 106181. <https://doi.org/10.1016/j.quascirev.2020.106181>
- Christie, R.L., 1983. Lithological suites as glacial ‘tracers’, eastern Ellesmere Island, Arctic Archipelago. *Geol. Surv. Can. Pap.* 83—1A.
- Christie, R.L., 1974. Northeastern Ellesmere Island: Lake Hazen region and Judge Daly Promontory. *Pap Geol Surv Can* 74, 297–299.

- Christie, R.L., 1967. Reconnaissance of the Surficial Geology of Northeastern Ellesmere Island, Arctic Archipelago, by RL Christie. Queen's Printer.
- Christie, R.L., 1964. Geological reconnaissance of northeastern Ellesmere Island, District of Franklin (No. 331). <https://doi.org/10.4095/100555>
- Cook, A.J., Copland, L., Noël, B.P.Y., Stokes, C.R., Bentley, M.J., Sharp, M.J., Bingham, R.G., van den Broeke, M.R., 2019. Atmospheric forcing of rapid marine-terminating glacier retreat in the Canadian Arctic Archipelago. *Sci. Adv.* 5, 8507. <https://doi.org/10.1126/sciadv.aau8507>
- Copland, L., Mueller, D., 2017. Arctic ice shelves and ice islands. Springer.
- Copland, L., Mueller, D.R., Weir, L., 2007. Rapid loss of the Ayles ice shelf, Ellesmere Island, Canada. *Geophys. Res. Lett.* 34.
- Coulthard, R.D., Furze, M.F.A., Pieńkowski, A.J., Chantel Nixon, F., England, J.H., 2010. New marine ΔR values for Arctic Canada. *Quat. Geochronol.* 5, 419–434. <https://doi.org/10.1016/j.quageo.2010.03.002>
- Cusset, F., Fort, J., Mallory, M., Braune, B., Massicotte, P., Massé, G., 2019. Arctic seabirds and shrinking sea ice: egg analyses reveal the importance of ice-derived resources. *Sci. Rep.* 9. <https://doi.org/10.1038/s41598-019-51788-4>
- Dalton, A., Copland, L., Tivy, A., Van Wychen, W., Cook, A., 2019. Iceberg production and characteristics around the Prince of Wales Icefield, Ellesmere Island, 1997–2015. *Arct. Antarct. Alp. Res.* 51, 412–427. <https://doi.org/10.1080/15230430.2019.1634442>
- Darby, D.A., Ortiz, J.D., Grosch, C.E., Lund, S.P., 2012. 1,500-year cycle in the Arctic Oscillation identified in Holocene Arctic sea-ice drift. *Nat. Geosci.* 5, 897–900. <https://doi.org/10.1038/ngeo1629>
- Darby, M.S., Willmott, A.J., Somerville, T.A., 1995. On the influence of coastline orientation on the steady state width of a latent heat polynya. *J. Geophys. Res. Oceans* 100, 13625–13633. <https://doi.org/10.1029/95JC01024>
- Davidson, T.A., Wetterich, S., Johansen, K.L., Grønnow, B., Windirsch, T., Jeppesen, E., Syväranta, J., Olsen, J., González-Bergonzoni, I., Strunk, A., Larsen, N.K., Meyer, H., Søndergaard, J., Dietz, R., Eulears, I., Mosbech, A., 2018. The history of seabird colonies and the North Water ecosystem: Contributions from palaeoecological and archaeological evidence. *Ambio* 47, 175–192. <https://doi.org/10.1007/s13280-018-1031-1>
- Davies, H.C., Dobson, M.R., Whittington, R.J., 1984. A revised seismic stratigraphy for Quaternary deposits on the inner continental shelf west of Scotland between 55° 30 'N and 57° 30'N. *Boreas* 13, 49–66.
- Dawes, P.R., 2009. Precambrian-Palaeozoic geology of Smith Sound, Canada and Greenland: key constraint to palaeogeographic reconstructions of northern Laurentia and the North Atlantic region. *Terra Nova* 21, 1–13. <https://doi.org/10.1111/j.1365-3121.2008.00845.x>
- Dawes, P.R., 2004. Explanatory notes to the geological map of Greenland, 1:500 000, Humboldt Gletscher, Sheet 6, Geological Survey of Denmark and Greenland map series. GEUS, Copenhagen.
- Dawes, P.R., 1997. The Proterozoic Thule Supergroup, Greenland and Canada: history, lithostratigraphy, and development, *Geology of Greenland survey bulletin*. Geological Survey of Denmark and Greenland, Ministry of Environment and Energy, Copenhagen, Denmark.
- Dawes, P.R., Garde, A.A., 2004. Geological map of Greenland 1: 500 000, Humboldt Gletscher, sheet 6. *Geol. Surv. Den. Greenl. Cph. Den.*
- de Vernal, A., Hillaire-Marcel, C., Rochon, A., Fréchette, B., Henry, M., Solignac, S., Bonnet, S., 2013. Dinosaur-based reconstructions of sea ice cover concentration during the Holocene in the Arctic Ocean, the northern North Atlantic Ocean and its adjacent seas. *Quat. Sci. Rev.* 79, 111–121. <https://doi.org/10.1016/j.quascirev.2013.07.006>
- Deming, J.W., Fortier, L., Fukuchi, M., 2002. The International North Water Polynya Study (NOW): a brief overview. *Deep Sea Res. Part II Top. Stud. Oceanogr.* 49, 4887–4892. [https://doi.org/10.1016/S0967-0645\(02\)00168-6](https://doi.org/10.1016/S0967-0645(02)00168-6)
- Deschamps, C.-E., Montero-Serrano, J.-C., St-Onge, G., 2018. Sediment Provenance Changes in the Western Arctic Ocean in Response to Ice Rafting, Sea Level, and Oceanic Circulation Variations Since the Last Deglaciation. *Geochem. Geophys. Geosystems* 19, 2147–2165. <https://doi.org/10.1029/2017GC007411>

- Dick, L., 2001. *Muskox Land: Ellesmere Island in the Age of Contact*. University of Calgary Press.
- Dickson, R.R., Meincke, J., Malmberg, S.-A., Lee, A.J., 1988. The “great salinity anomaly” in the northern North Atlantic 1968–1982. *Prog. Oceanogr.* 20, 103–151.
- Dietz, R., Mosbech, A., Flora, J., Eulaers, I., 2018. Interactions of climate, socio-economics, and global mercury pollution in the North Water. *Ambio* 47, 281–295. <https://doi.org/10.1007/s13280-018-1033-z>
- Dowdeswell, J.A., 1987. Processes of glacial marine sedimentation. *Prog. Phys. Geogr. Earth Environ.* 11, 52–90. <https://doi.org/10.1177/030913338701100103>
- Dowdeswell, J.A., Elverhfi, A., Spielhagen, R., 1998. Glacial marine sedimentary processes and facies on the Polar North Atlantic margins. *Quat. Sci. Rev.* 17, 243–272.
- Dowdeswell, Whittington, Jennings, Andrews, Mackensen, Marienfeld, 2000. An origin for laminated glacial marine sediments through sea-ice build-up and suppressed iceberg rafting: An origin for laminated glacial marine sediments. *Sedimentology* 47, 557–576. <https://doi.org/10.1046/j.1365-3091.2000.00306.x>
- Duffield, C.J., Hess, S., Norling, K., Alve, E., 2015. The response of *Nonionella iridea* and other benthic foraminifera to “fresh” organic matter enrichment and physical disturbance. *Mar. Micropaleontol.* 120, 20–30. <https://doi.org/10.1016/j.marmicro.2015.08.002>
- Dumas, J.A., Flato, G.M., Weaver, A.J., 2003. The impact of varying atmospheric forcing on the thickness of arctic multi-year sea ice. *Geophys. Res. Lett.* 30. <https://doi.org/10.1029/2003GL017433>
- Dumont, D., Gratton, Y., Arbetter, T.E., 2010. Modeling Wind-Driven Circulation and Landfast Ice-Edge Processes during Polynya Events in Northern Baffin Bay. *J. Phys. Oceanogr.* 40, 1356–1372. <https://doi.org/10.1175/2010JPO4292.1>
- Dumont, D., Gratton, Y., Arbetter, T.E., 2009. Modeling the Dynamics of the North Water Polynya Ice Bridge. *J. Phys. Oceanogr.* 39, 1448–1461. <https://doi.org/10.1175/2008JPO3965.1>
- Dunbar, M., 1979. Fall Ice Drift in Nares Strait, as Observed by Sideways-Looking Airborne Radar. *Arctic* 32, 283–307. <https://doi.org/10.14430/arctic2629>
- Dunbar, M., 1975. Interpretation of SLAR imagery of sea ice in Nares Strait and the Arctic Ocean. *J. Glaciol.* 15, 193–213.
- Dunbar, M., 1973. Ice Regime and Ice Transport in Nares Strait. *ARCTIC* 26, 282–291. <https://doi.org/10.14430/arctic2927>
- Dunbar, M., 1969. The Geographical Position of the North Water. *Arctic* 22, 438–441.
- Dunbar, M., Dunbar, M.J., 1972. The History of the North Water. *Proc. R. Soc. Edinb. Sect. B Biol.* 72, 231–241. <https://doi.org/10.1017/S0080455X00001788>
- Dunbar, M.J., 1951. Eastern arctic waters: a summary of our present knowledge of the physical oceanography of the eastern arctic area, from Hudson Bay to Cape Farewell and from Belle Isle to Smith Sound. Fisheries Research Board of Canada.
- Dyke, A.S., Andrews, J.T., Clark, P.U., England, J.H., Miller, G.H., Shaw, J., Veillette, J.J., 2002. The Laurentide and Innuitian ice sheets during the last glacial maximum. *Quat. Sci. Rev.* 21, 9–31.
- Dyke, A.S., Hooper, J., Harington, C.R., Savelle, J.M., 1999. The Late Wisconsinan and Holocene record of walrus (*Odobenus rosmarus*) from North America: a review with new data from Arctic and Atlantic Canada. *Arctic* 160–181.
- Dyke, A.S., Hooper, J., Savelle, J.M., 1997. A history of sea ice in the Canadian Arctic Archipelago based on postglacial remains of the bowhead whale (*Balaena mysticetus*). *Oceanogr. Lit. Rev.* 4, 330.
- Dyke, A.S., Hooper, J., Savelle, J.M., 1996. A history of sea ice in the Canadian Arctic Archipelago based on postglacial remains of the bowhead whale (*Balaena mysticetus*). *Arctic* 235–255.
- Eberl, D.D., 2003. User guide to RockJock-A program for determining quantitative mineralogy from X-ray diffraction data. US Geological Survey.
- Elberling, B., Luise Knudsen, K., Kristensen, P.H., Asmund, G., 2003. Applying foraminiferal stratigraphy as a biomarker for heavy metal contamination and mining impact in a fiord in West Greenland. *Mar. Environ. Res.* 55, 235–256. [https://doi.org/10.1016/S0141-1136\(02\)00219-2](https://doi.org/10.1016/S0141-1136(02)00219-2)
- Elnegaard Hansen, K., Giraudeau, J., Wacker, L., Pearce, C., Seidenkrantz, M.-S., 2020. Reconstruction of Holocene oceanographic conditions in the Northeastern Baffin Bay. *Clim. Past.* <https://doi.org/10.5194/cp-2019-152>

- Elverhøi, A., Liestøl, O., Nagy, J., 1980. Glacial erosion, sedimentation and microfauna in the inner part of Kongsfjorden, Spitsbergen. *Nor. Polarinst. Skr.* 172, 33–58.
- England, J., 1999. Coalescent Greenland and Inuitian ice during the Last Glacial Maximum: revising the Quaternary of the Canadian High Arctic. *Quat. Sci. Rev.* 18, 421–456. [https://doi.org/10.1016/S0277-3791\(98\)00070-5](https://doi.org/10.1016/S0277-3791(98)00070-5)
- England, J., 1996. Glacier dynamics and paleoclimatic change during the last glaciation of eastern Ellesmere Island, Canada. *Can. J. Earth Sci.* 33, 779–799.
- England, J., 1976. Late Quaternary glaciation of the eastern Queen Elizabeth Islands, NWT, Canada: alternative models. *Quat. Res.* 6, 185–202.
- England, J., Atkinson, N., Bednarski, J., Dyke, A.S., Hodgson, D.A., Ó Cofaigh, C., 2006. The Inuitian Ice Sheet: configuration, dynamics and chronology. *Quat. Sci. Rev.* 25, 689–703. <https://doi.org/10.1016/j.quascirev.2005.08.007>
- England, J., Dyke, A.S., Coulthard, R.D., Mcneely, R., Aitken, A., 2013. The exaggerated radiocarbon age of deposit-feeding molluscs in calcareous environments: Exaggerated radiocarbon ages of molluscs. *Boreas* 42, 362–373. <https://doi.org/10.1111/j.1502-3885.2012.00256.x>
- England, J.H., Lakeman, T.R., Lemmen, D.S., Bednarski, J.M., Stewart, T.G., Evans, D.J.A., 2008. A millennial-scale record of Arctic Ocean sea ice variability and the demise of the Ellesmere Island ice shelves. *Geophys. Res. Lett.* 35. <https://doi.org/10.1029/2008GL034470>
- Farnsworth, L.B., Kelly, M.A., Bromley, G.R.M., Axford, Y., Osterberg, E.C., Howley, J.A., Jackson, M.S., Zimmerman, S.R., 2018. Holocene history of the Greenland Ice-Sheet margin in Northern Nunatarssuaq, Northwest Greenland. *arktos* 4. <https://doi.org/10.1007/s41063-018-0044-0>
- Finkelstein, S.A., Gajewski, K., 2008. Responses of Fragilarioid-dominated diatom assemblages in a small Arctic lake to Holocene climatic changes, Russell Island, Nunavut, Canada. *J. Paleolimnol.* 40, 1079–1095. <https://doi.org/10.1007/s10933-008-9215-5>
- Fisher, D., Zheng, J., Burgess, D., Zdanowicz, C., Kinnard, C., Sharp, M., Bourgeois, J., 2012. Recent melt rates of Canadian arctic ice caps are the highest in four millennia. *Glob. Planet. Change, Perspectives on Climate in Medieval Time 84–85*, 3–7. <https://doi.org/10.1016/j.gloplacha.2011.06.005>
- Fortin, D., Francus, P., Gebhardt, A.C., Hahn, A., Kliem, P., Lisé-Pronovost, A., Roychowdhury, R., Labrie, J., St-Onge, G., 2013. Destructive and non-destructive density determination: method comparison and evaluation from the Laguna Potrok Aike sedimentary record. *Quat. Sci. Rev.* 71, 147–153. <https://doi.org/10.1016/j.quascirev.2012.08.024>
- Fossile, E., Nardelli, M.P., Jouini, A., Lansard, B., Pusceddu, A., Moccia, D., Michel, E., Péron, O., Howa, H., Mojtahid, M., 2019. Benthic foraminifera as tracers of brine production in Storfjorden sea ice factory (preprint). <https://doi.org/10.5194/bg-2019-405>
- Franceschetti, A.P., 1964. Oceanographic Observations: Kennedy Channel, Kane Basin, Smith Sound and Baffin Bay, Summer 1963. Coast Guard.
- Frisch, T., 1984a. Geology, Prince of Wales Mountains, District of Franklin, Northwest Territories; Geological Survey of Canada, Map 1573 A, scale 1:250 000.
- Frisch, T., 1984b. Geology, Makinson Inlet, District of Franklin, Northwest Territories; Geological Survey of Canada, Map 1573 A, scale 1:250 000.
- Funder, S., 1990. Late Quaternary Stratigraphy and Glaciology in the Thule Area, Northwest Greenland. Museum Tusulanum Press.
- Funder, S., Goosse, H., Jepsen, H., Kaas, E., Kjær, K.H., Korsgaard, N.J., Larsen, N.K., Linderson, H., Lyså, A., Möller, P., Olsen, J., Willerslev, E., 2011. A 10,000-Year Record of Arctic Ocean Sea-Ice Variability—View from the Beach. *Science* 333, 747–750. <https://doi.org/10.1126/science.1202760>
- Ganeshram, R.S., Pedersen, T.F., 1998. Glacial-interglacial variability in upwelling and bioproductivity off NW Mexico: Implications for Quaternary paleoclimate. *Paleoceanography* 13, 634–645. <https://doi.org/10.1029/98PA02508>
- Gardner, A.S., Moholdt, G., Wouters, B., Wolken, G.J., Burgess, D.O., Sharp, M.J., Cogley, J.G., Braun, C., Labine, C., 2011. Sharply increased mass loss from glaciers and ice caps in the Canadian Arctic Archipelago. *Nature* 473, 357–360. <https://doi.org/10.1038/nature10089>

- Gaston, A.J., Hipfner, J.M., 2000. Thick-billed Murre: *Uria lomvia*. Birds of North America.
- Georgiadis, E., Giraudeau, J., Jennings, A., Limoges, A., Jackson, R., Ribeiro, S., Massé, G., 2020. Local and regional controls on Holocene sea ice dynamics and oceanography in Nares Strait, Northwest Greenland. *Mar. Geol.* 422, 106115. <https://doi.org/10.1016/j.margeo.2020.106115>
- Georgiadis, E., Giraudeau, J., Jennings, A.E., Montero-Serrano, J.-C., Limoges, A., Ribeiro, S., Massé, G., in prep. a. Holocene dynamics of the North Water, northernmost Baffin Bay, view from the western sector of the polynya.
- Georgiadis, E., Giraudeau, J., Martinez, P., Lajeunesse, P., St-Onge, G., Schmidt, S., Massé, G., 2018. Deglacial to postglacial history of Nares Strait, Northwest Greenland: a marine perspective from Kane Basin. *Clim. Past* 14, 1991–2010. <https://doi.org/10.5194/cp-14-1991-2018>
- Georgiadis, E., Giraudeau, J., Montero-Serrano, J.-C., Zaragosi, S., Massé, G., in prep. b. Holocene deglaciation of northernmost Baffin Bay and southern Nares Strait: sedimentological study of a High-Arctic marine sediment core.
- Gibb, O.T., Steinhauer, S., Fréchette, B., de Vernal, A., Hillaire-Marcel, C., 2015. Diachronous evolution of sea surface conditions in the Labrador Sea and Baffin Bay since the last deglaciation. *The Holocene* 25, 1882–1897. <https://doi.org/10.1177/0959683615591352>
- Gilbert, R., 1983. Sedimentary processes of Canadian Arctic fjords. *Sediment. Geol.* 36, 147–175.
- González-Bergonzoni, I., Johansen, K.L., Mosbech, A., Landkildehus, F., Jeppesen, E., Davidson, T.A., 2017. Small birds, big effects: the little auk (*Alle alle*) transforms high Arctic ecosystems. *Proc. R. Soc. B Biol. Sci.* 284, 20162572. <https://doi.org/10.1098/rspb.2016.2572>
- Gooday, A.J., Hughes, J.A., 2002. Foraminifera associated with phytodetritus deposits at a bathyal site in the northern Rockall Trough (NE Atlantic): seasonal contrasts and a comparison of stained and dead assemblages. *Mar. Micropaleontol.* 46, 83–110. [https://doi.org/10.1016/S0377-8398\(02\)00050-6](https://doi.org/10.1016/S0377-8398(02)00050-6)
- Goffredsen, A.B., Appelt, M., Hastrup, K., 2018. Walrus history around the North Water: Human–animal relations in a long-term perspective. *Ambio* 47, 193–212. <https://doi.org/10.1007/s13280-018-1027-x>
- Grimm, E.C., 1987. CONISS: a FORTRAN 77 program for stratigraphically constrained cluster analysis by the method of incremental sum of squares - ScienceDirect [WWW Document]. URL <https://www.sciencedirect.com.docelec.u-bordeaux.fr/science/article/pii/0098300487900227> (accessed 4.22.19).
- Grønnow, B., 1997. The Saqqaq Harpoon: An Analysis of Early Paleo-Eskimo Harpoon Heads from Qeqertasussuk, West Greenland, in: *Fifty Years of Arctic Research. Anthropological Studies From Greenland To Siberia*. Department of Ethnography. Nationalmuseet, pp. 119–130.
- Grønnow, B., Sørensen, M., 2004. Palaeo-eskimo migrations into Greenland: the Canadian connection. *Dyn. North. Soc.* 59–74.
- Guyard, H., Chapron, E., St-Onge, G., Labrie, J., 2013. Late-Holocene NAO and oceanic forcing on high-altitude proglacial sedimentation (Lake Bramant, Western French Alps). *The Holocene* 23, 1163–1172.
- Haas, C., Hendricks, S., Doble, M., 2006. Comparison of the Sea-ice thickness distribution in the Lincoln Sea and adjacent Arctic Ocean in 2004 and 2005. *Ann. Glaciol.* 44, 247–252. <https://doi.org/10.3189/172756406781811781>
- Häkkinen, S., 2002. Freshening of the Labrador Sea surface waters in the 1990s: Another great salinity anomaly? *Geophys. Res. Lett.* 29, 85-1-85–4.
- Hald, M., Steinsund, P.I., Korsun, S., Polyak, L., Aspeli, R., 1994. Recent and Late Quaternary distribution of *Elphidium excavatum* f. *clavatum* in Arctic seas. *Cushman Found. Spec. Publ.* 32, 53.
- Hall, J.M., Chan, L.-H., 2004. Ba/Ca in *Neogloboquadrina pachyderma* as an indicator of deglacial meltwater discharge into the western Arctic Ocean: Foraminiferal Ba/Ca as meltwater proxy. *Paleoceanography* 19, n/a-n/a. <https://doi.org/10.1029/2003PA000910>
- Harmon, R.A., 1972. The distribution of microbiogenic sediment near the mouth of the Columbia River. *Columbia River Estuary Adjac. Ocean Waters Univ. Wash. Press Seattle* 265–277.
- Harrison, J.C., 2004. In Search of the Wegener Fault: Re-Evaluation of Strike-Slip Displacements Along and Bordering Nares Strait. *Polarforschung* 73, 129–160.
- Harrison, J.C., Brent, T.A., Oakey, G.N., 2006. Bedrock Geology of the Nares Strait Region of the Arctic Canada and Greenland, with Explanatory Text and GIS Content. Geological Survey of Canada.

- Jackson, G.D., 2000. Geology of the Clyde-Cockburn Land map area, north-central Baffin Island, Nunavut. Geological Survey of Canada, Ottawa.
- Jackson, J.M., Lique, C., Alkire, M., Steele, M., Lee, C.M., Smethie, W.M., Schlosser, P., 2014. On the waters upstream of Nares Strait, Arctic Ocean, from 1991 to 2012. *Cont. Shelf Res.* 73, 83–96. <https://doi.org/10.1016/j.csr.2013.11.025>
- Jakobsson, M., Hogan, K.A., Mayer, L.A., Mix, A., Jennings, A., Stoner, J., Eriksson, B., Jerram, K., Mohammad, R., Pearce, C., Reilly, B., Stranne, C., 2018. The Holocene retreat dynamics and stability of Petermann Glacier in northwest Greenland. *Nat. Commun.* 9. <https://doi.org/10.1038/s41467-018-04573-2>
- Jeffries, M.O., 1992. Arctic ice shelves and ice islands: Origin, growth and disintegration, physical characteristics, structural-stratigraphic variability, and dynamics. *Rev. Geophys.* 30, 245–267. <https://doi.org/10.1029/92RG00956>
- Jennings, A., Andrews, J., Pearce, C., Wilson, L., Ólafsdóttir, S., 2015. Detrital carbonate peaks on the Labrador shelf, a 13-7ka template for freshwater forcing from the Hudson Strait outlet of the Laurentide Ice Sheet into the subpolar gyre. *Quat. Sci. Rev.* 107, 62–80. <https://doi.org/10.1016/j.quascirev.2014.10.022>
- Jennings, A., Sheldon, C., Cronin, T., Francus, P., Stoner, J., Andrews, J., 2011. The Holocene History of Nares Strait: Transition from Glacial Bay to Arctic-Atlantic Throughflow. *Oceanography* 24, 26–41. <https://doi.org/10.5670/oceanog.2011.52>
- Jennings, A.E., Andrews, J.T., Ó Cofaigh, C., Onge, G.St., Sheldon, C., Belt, S.T., Cabedo-Sanz, P., Hillaire-Marcel, C., 2017. Ocean forcing of Ice Sheet retreat in central west Greenland from LGM to the early Holocene. *Earth Planet. Sci. Lett.* 472, 1–13. <https://doi.org/10.1016/j.epsl.2017.05.007>
- Jennings, A.E., Andrews, J.T., Oliver, B., Walczak, M., Mix, A., 2019. Retreat of the Smith Sound Ice Stream in the Early Holocene. *Boreas*. <https://doi.org/10.1111/bor.12391>
- Jennings, A.E., Helgadottir, G., 1994. Foraminifer assemblages from the fjords and shelf of eastern Greenland. *J. Foraminifer. Res.* 24, 123–144. <https://doi.org/10.2113/gsjfr.24.2.123>
- Jennings, A.E., Walton, M.E., Ó Cofaigh, C., Kilfeather, A., Andrews, J.T., Ortiz, J.D., De Vernal, A., Dowdeswell, J.A., 2014. Paleoenvironments during Younger Dryas-Early Holocene retreat of the Greenland Ice Sheet from outer Disko Trough, central west Greenland. *J. Quat. Sci.* 29, 27–40.
- Jennings, A.E., Weiner, N.J., Helgadottir, G., Andrews, J.T., 2004. Modern foraminiferal faunas of the southwestern to northern Iceland Shelf: Oceanographic and environmental controls. *J. Foraminifer. Res.* 34, 180–207. <https://doi.org/10.2113/34.3.180>
- Jeppesen, E., Appelt, M., Hastrup, K., Grønnow, B., Mosbech, A., Smol, J.P., Davidson, T.A., 2018. Living in an oasis: Rapid transformations, resilience, and resistance in the North Water Area societies and ecosystems. *Ambio* 47, 296–309. <https://doi.org/10.1007/s13280-018-1034-y>
- Joli, N., Gosselin, M., Ardyna, M., Babin, M., Onda, D.F., Tremblay, J.-É., Lovejoy, C., 2018. Need for focus on microbial species following ice melt and changing freshwater regimes in a Janus Arctic Gateway. *Sci. Rep.* 8, 1–11. <https://doi.org/10.1038/s41598-018-27705-6>
- Jones, E.P., 2003. Tracing Pacific water in the North Atlantic Ocean. *J. Geophys. Res.* 108. <https://doi.org/10.1029/2001JC001141>
- Jones, E.P., 2001. Circulation in the Arctic Ocean. *Polar Res.* 20, 139–146. <https://doi.org/10.3402/polar.v20i2.6510>
- Jones, E.P., Coote, A.R., 1980. Nutrient Distributions in the Canadian Archipelago: Indicators of Summer Water Mass and Flow Characteristics. *Can. J. Fish. Aquat. Sci.* 37, 589–599. <https://doi.org/10.1139/f80-075>
- Jones, E.P., Eert, A.J., 2004. Waters of Nares Strait in 2001. *Polarforschung* 73, 185–189.
- Juggins, S., 2019. rioja: Analysis of Quaternary Science Data.
- Kalenitchenko, D., Joli, N., Potvin, M., Tremblay, J.-É., Lovejoy, C., 2019. Biodiversity and Species Change in the Arctic Ocean: A View Through the Lens of Nares Strait. *Front. Mar. Sci.* 6. <https://doi.org/10.3389/fmars.2019.00479>

- Kalkreuth, W.D., McCullough, K.M., Richardson, R.J.H., 1993. Geological, Archaeological, and Historical Occurrences of Coal, East-central Ellesmere Island, Arctic Canada. *Arct. Alp. Res.* 25, 277–307.
- Kelly, M., Bennike, O., 1992. Quaternary geology of western and central North Greenland. *Rapp. Grøn. Geol. Undersøgelse* 153, 34.
- Kelly, M., Funder, S., Houmark-nielsen, M., Knudsen, K.L., Kronborg, C., Landvik, J., Sorby, L., 1999. Quaternary glacial and marine environmental history of northwest Greenland: a review and reappraisal. *Quat. Sci. Rev.* 18, 373–392. [https://doi.org/10.1016/S0277-3791\(98\)00004-3](https://doi.org/10.1016/S0277-3791(98)00004-3)
- Kerr, J.W., 1968. Stratigraphy of Central and Eastern Ellesmere Island, Arctic Canada, Part II, Ordovician. Queen's Printer.
- Kerr, J.W., 1967. Stratigraphy of central and eastern Ellesmere Island, Arctic Canada. Queen's Printer.
- Kliem, N., Greenberg, D.A., 2003. Diagnostic simulations of the summer circulation in the Canadian arctic archipelago. *Atmosphere-Ocean* 41, 273–289. <https://doi.org/10.3137/ao.410402>
- Knudsen, K.L., Stabell, B., Seidenkrantz, M.-S., Eiríksson, J., Blake, W., 2008b. Deglacial and Holocene conditions in northernmost Baffin Bay: sediments, foraminifera, diatoms and stable isotopes. *Boreas* 37, 346–376. <https://doi.org/10.1111/j.1502-3885.2008.00035.x>
- Koch, L., 1933. The geology of Inglefield Land. *Meddeleser Om Grøn.* 73.
- Koch, L., 1929. Stratigraphy of Greenland. *Meddeleser Om Grøn.* 73, 205–320.
- Koerner, R.M., 1989. Queen Elizabeth Islands glaciers. *Quat. Geol. Can. Greenl. Geol. Surv. Can. Geol. Can.* 1, 464–473.
- Kozo, T.L., 1991. The hybrid polynya at the northern end of Nares Strait. *Geophys. Res. Lett.* 18, 2059–2062. <https://doi.org/10.1029/91GL02574>
- Kravitz, J.H., 1976. Textural and mineralogical characteristics of the surficial sediments of Kane Basin. *J. Sediment. Res.* 46, 710–725.
- Kravitz, J.H., Siegel, F.R., 1994. Chemical element distribution in the surface sediments of Kane basin. *J. Coast. Res.* 101–112.
- Kröncke, I., Vanreusel, A., Vincx, M., Wollenburg, J., Mackensen, A., Liebezeit, G., Behrends, B., 2000. Different benthic size-compartments and their relationship to sediment chemistry in the deep Eurasian Arctic Ocean. *Mar. Ecol. Prog. Ser.* 199, 31–41. <https://doi.org/10.3354/meps199031>
- Kwok, R., 2006. Exchange of sea ice between the Arctic Ocean and the Canadian Arctic Archipelago. *Geophys. Res. Lett.* 33. <https://doi.org/10.1029/2006GL027094>
- Kwok, R., 2005. Variability of Nares Strait ice flux. *Geophys. Res. Lett.* 32. <https://doi.org/10.1029/2005GL024768>
- Kwok, R., 2000. Recent changes in Arctic Ocean sea ice motion associated with the North Atlantic Oscillation. *Geophys. Res. Lett.* 27, 775–778. <https://doi.org/10.1029/1999GL002382>
- Kwok, R., Toudal Pedersen, L., Gudmandsen, P., Pang, S.S., 2010. Large sea ice outflow into the Nares Strait in 2007: Nares Strait sea ice outflow. *Geophys. Res. Lett.* 37. <https://doi.org/10.1029/2009GL041872>
- Kwok, R., Untersteiner, N., 2011. The thinning of Arctic sea ice. *Phys. Today* 64, 36–41. <https://doi.org/10.1063/1.3580491>
- Landvik, J.Y., Weidick, A., Hansen, A., 2001. The glacial history of the Hans Tausen Iskappe and the last glaciation of Peary Land, North Greenland. *Hans Tausen Ice Cap Glaciol. Glacial Geol. Meddelelser Om Grøn. Geosci.* 39, 27–44.
- Lecavalier, B.S., Fisher, D.A., Milne, G.A., Vinther, B.M., Tarasov, L., Huybrechts, P., Lacelle, D., Main, B., Zheng, J., Bourgeois, J., Dyke, A.S., 2017. High Arctic Holocene temperature record from the Agassiz ice cap and Greenland ice sheet evolution. *Proc. Natl. Acad. Sci.* 201616287. <https://doi.org/10.1073/pnas.1616287114>
- Lecavalier, B.S., Milne, G.A., Simpson, M.J.R., Wake, L., Huybrechts, P., Tarasov, L., Kjeldsen, K.K., Funder, S., Long, A.J., Woodroffe, S., Dyke, A.S., Larsen, N.K., 2014. A model of Greenland ice sheet deglaciation constrained by observations of relative sea level and ice extent. *Quat. Sci. Rev.* 102, 54–84. <https://doi.org/10.1016/j.quascirev.2014.07.018>

- Ledu, D., Rochon, A., de Vernal, A., St-Onge, G., 2008. Palynological evidence of Holocene climate change in the eastern Arctic: a possible shift in the Arctic oscillation at the millennial time scale. *Can. J. Earth Sci.* 45, 1363–1375. <https://doi.org/10.1139/E08-043>
- Ledu, D., Rochon, A., Vernal, A. de, Barletta, F., St-Onge, G., 2010. Holocene sea ice history and climate variability along the main axis of the Northwest Passage, Canadian Arctic. *Paleoceanography* 25. <https://doi.org/10.1029/2009PA001817>
- Levac, E., Vernal, A.D., Jr, W.B., 2001. Sea-surface conditions in northernmost Baffin Bay during the Holocene: palynological evidence. *J. Quat. Sci.* 16, 353–363. <https://doi.org/10.1002/jqs.614>
- Lewis, L.E., Ponton, D., Legendre, L., Leblanc, B., 1996. Springtime sensible heat, nutrients and phytoplankton in the Northwater Polynya, Canadian Arctic. *Cont. Shelf Res.* 16, 1775–1792. [https://doi.org/10.1016/0278-4343\(96\)00015-5](https://doi.org/10.1016/0278-4343(96)00015-5)
- Limoges, A., Massé, G., Weckström, K., Poulin, M., Ellegaard, M., Heikkilä, M., Geilfus, N.-X., Sejr, M.K., Rysgaard, S., Ribeiro, S., 2018. Spring Succession and Vertical Export of Diatoms and IP25 in a Seasonally Ice-Covered High Arctic Fjord. *Front. Earth Sci.* 6. <https://doi.org/10.3389/feart.2018.00226>
- List, E.J., 1982. Turbulent jets and plumes. *Annu. Rev. Fluid Mech.* 14, 189–212.
- Lloyd, J., Moros, M., Perner, K., Telford, R.J., Kuijpers, A., Jansen, E., McCarthy, D., 2011. A 100 yr record of ocean temperature control on the stability of Jakobshavn Isbrae, West Greenland. *Geology* 39, 867–870. <https://doi.org/10.1130/G32076.1>
- Lloyd, J.M., 2006. Modern distribution of benthic foraminifera from Disko Bugt, West Greenland. *J. Foraminif. Res.* 36, 315–331. <https://doi.org/10.2113/gsjfr.36.4.315>
- Lochte, A.A., Repschläger, J., Kienast, M., Garbe-Schönberg, D., Andersen, N., Hamann, C., Schneider, R., 2019a. Labrador Sea freshening at 8.5 ka BP caused by Hudson Bay Ice Saddle collapse. *Nat. Commun.* 10. <https://doi.org/10.1038/s41467-019-08408-6>
- Lochte, A.A., Repschläger, J., Seidenkrantz, M.-S., Kienast, M., Blanz, T., Schneider, R.R., 2019b. Holocene water mass changes in the Labrador Current. *The Holocene* 29, 676–690. <https://doi.org/10.1177/0959683618824752>
- Loeblich, A.R., Jr, Tappan, H., 1988. *Foraminiferal Genera and Their Classification*. Springer US. <https://doi.org/10.1007/978-1-4899-5760-3>
- Lovejoy, C., Legendre, L., Martineau, M.-J., Bâcle, J., von Quillfeldt, C.H., 2002. Distribution of phytoplankton and other protists in the North Water. *Deep Sea Res. Part II Top. Stud. Oceanogr.* 49, 5027–5047. [https://doi.org/10.1016/S0967-0645\(02\)00176-5](https://doi.org/10.1016/S0967-0645(02)00176-5)
- Lyle, M.W., Olivarez Lyle, A., Gorgas, T.J., Holbourn, A.E.L., Westerhold, T., Hathorne, E.C., Kimoto, K., Yamamoto, S., 2012. Data report: raw and normalized elemental data along the Site U1338 splice from X-ray fluorescence scanning, in: Pälike, H., Lyle, M., Nishi, H., Raffi, I., Gamage, K., Klaus, A., Expedition 320/321 Scientists (Eds.), *Proc. IODP, 320/321. Integrated Ocean Drilling Program Management International, Inc., Tokyo*. <https://doi.org/10.2204/iodp.proc.320321.203.2012>
- MacDonald, G.M., 2010. Some Holocene palaeoclimatic and palaeoenvironmental perspectives on Arctic/Subarctic climate warming and the IPCC 4th Assessment Report. *J. Quat. Sci.* 25, 39–47. <https://doi.org/10.1002/jqs.1307>
- MacGregor, J.A., Colgan, W.T., Fahnestock, M.A., Morlighem, M., Catania, G.A., Paden, J.D., Gogineni, S.P., 2016. Holocene deceleration of the Greenland ice sheet. *Science* 351, 590–593.
- Mair, D., Burgess, D., Sharp, M., Dowdeswell, J.A., Benham, T., Marshall, S., Cawkwell, F., 2009. Mass balance of the Prince of Wales Icefield, Ellesmere Island, Nunavut, Canada. *J. Geophys. Res.* 114. <https://doi.org/10.1029/2008JF001082>
- Marchese, C., Albouy, C., Tremblay, J.-É., Dumont, D., D'Ortenzio, F., Vissault, S., Bélanger, S., 2017. Changes in phytoplankton bloom phenology over the North Water (NOW) polynya: a response to changing environmental conditions. *Polar Biol.* 40, 1721–1737. <https://doi.org/10.1007/s00300-017-2095-2>
- Marsden, R.F., Serdula, J., Key, E., Minnett, P.J., 2004. Are polynyas self-sustaining? *Atmosphere-Ocean* 42, 251–265. <https://doi.org/10.3137/ao.420403>

- Marshall, S.J., Sharp, M.J., Burgess, D.O., Anslow, F.S., 2007. Near-surface-temperature lapse rates on the Prince of Wales Icefield, Ellesmere Island, Canada: implications for regional downscaling of temperature. *Int. J. Climatol.* 27, 385–398. <https://doi.org/10.1002/joc.1396>
- Martin, J.-M., Meybeck, M., 1979. Elemental mass-balance of material carried by major world rivers. *Mar. Chem.* 7, 173–206. [https://doi.org/10.1016/0304-4203\(79\)90039-2](https://doi.org/10.1016/0304-4203(79)90039-2)
- Maxwell, J.B., 1981. Climatic Regions of the Canadian Arctic Islands. *Arctic* 34. <https://doi.org/10.14430/arctic2525>
- Mayot, N., Matrai, P., Ellingsen, I.H., Steele, M., Johnson, K., Riser, S.C., Swift, D., 2018. Assessing Phytoplankton Activities in the Seasonal Ice Zone of the Greenland Sea Over an Annual Cycle. *J. Geophys. Res. Oceans* 123, 8004–8025. <https://doi.org/10.1029/2018JC014271>
- McGeehan, T., Maslowski, W., 2012. Evaluation and control mechanisms of volume and freshwater export through the Canadian Arctic Archipelago in a high-resolution pan-Arctic ice-ocean model. *J. Geophys. Res. Oceans* 117. <https://doi.org/10.1029/2011JC007261>
- McGhee, R., 1996. *Ancient people of the Arctic*. Vancouver. British Columbia: UBC Press.
- McLaughlin, F.A., Carmack, E.C., Macdonald, R.W., Bishop, J.K.B., 1996. Physical and geochemical properties across the Atlantic/Pacific water mass front in the southern Canadian Basin. *J. Geophys. Res. Oceans* 101, 1183–1197. <https://doi.org/10.1029/95JC02634>
- McNeely, R., Dyke, A.S., Southon, J.R., 2006. Canadian marine reservoir ages, preliminary data assessment (No. 5049). <https://doi.org/10.4095/221564>
- Mei, Z.-P., Legendre, L., Gratton, Y., Tremblay, J.-É., LeBlanc, B., Mundy, C.J., Klein, B., Gosselin, M., Larouche, P., Papakyriakou, T.N., Lovejoy, C., von Quillfeldt, C.H., 2002. Physical control of spring–summer phytoplankton dynamics in the North Water, April–July 1998. *Deep Sea Res. Part II Top. Stud. Oceanogr.* 49, 4959–4982. [https://doi.org/10.1016/S0967-0645\(02\)00173-X](https://doi.org/10.1016/S0967-0645(02)00173-X)
- Meldgaard, M., 2004. *Ancient harp seal hunters of Disko Bay*. Museum Tusulanum Press.
- Melling, H., 2000. Exchanges of Freshwater through the Shallow Straits of the North American Arctic, in: Lewis, E.L., Jones, E.P., Lemke, P., Prowse, T.D., Wadhams, P. (Eds.), *The Freshwater Budget of the Arctic Ocean*, NATO Science Series. Springer Netherlands, Dordrecht, pp. 479–502. https://doi.org/10.1007/978-94-011-4132-1_20
- Melling, H., Gratton, Y., Ingram, G., 2001. Ocean circulation within the North Water polynya of Baffin Bay. *Atmosphere–Ocean* 39, 301–325. <https://doi.org/10.1080/07055900.2001.9649683>
- Merkel, F.R., Jamieson, S.E., Falk, K., Mosbech, A., 2007. The diet of common eiders wintering in Nuuk, Southwest Greenland. *Polar Biol.* 30, 227–234.
- Miall, A.D., 1982. Tertiary sedimentation and tectonics in the Judge Daly Basin, northeast Ellesmere Island, Arctic Canada. *Energy, Mines, and Resources Canada*.
- Miller, G.H., 1980. Late foxe glaciation of southern Baffin Island, NWT, Canada. *Geol. Soc. Am. Bull.* 91, 399–405.
- Moffa-Sánchez, P., Hall, I.R., 2017. North Atlantic variability and its links to European climate over the last 3000 years. *Nat. Commun.* 8, 1–9.
- Møller, H.S., Jensen, K.G., Kuijpers, A., Aagaard-Sørensen, S., Seidenkrantz, M.-S., Prins, M., Endler, R., Mikkelsen, N., 2006. Late-Holocene environment and climatic changes in Ameralik Fjord, southwest Greenland: evidence from the sedimentary record. *The Holocene* 16, 685–695.
- Moore, G.W.K., McNeil, K., 2018. The Early Collapse of the 2017 Lincoln Sea Ice Arch in Response to Anomalous Sea Ice and Wind Forcing. *Geophys. Res. Lett.* 45, 8343–8351. <https://doi.org/10.1029/2018GL078428>
- Mörner, N.-A., Funder, S.V., 1990. C-14 dating of samples collected during the NORDQUA 86 expedition, and notes on the marine reservoir effect, in: *Late Quaternary Stratigraphy and Glaciology in the Thule Area, Northwest Greenland*. Kommiss. f Vidensk. Unders. i Grønland, pp. 57–59.
- Mosbech, A., Johansen, K.L., Davidson, T.A., Appelt, M., Grønnow, B., Cuyler, C., Lyngs, P., Flora, J., 2018. On the crucial importance of a small bird: The ecosystem services of the little auk (*Alle alle*) population in Northwest Greenland in a long-term perspective. *Ambio* 47, 226–243. <https://doi.org/10.1007/s13280-018-1035-x>

- Moynihan, M.J., 1971. Oceanographic observations in Kane Basin, September 1968 and July, September 1969 84.
- Mudie, P.J., Rochon, A., Prins, M.A., Soenarjo, D., Troelstra, S.R., Levac, E., Scott, D.B., Roncaglia, L., Kuijpers, A., 2006. Late Pleistocene-Holocene marine geology of Nares Strait region: palaeoceanography from foraminifera and dinoflagellate cysts, sedimentology and stable isotopes. *Polarforschung* 74, 169–183.
- Muench, R.D., 1971. Oceanographic conditions at a fixed location in western Kane Basin, May 1969. US Coast Guard Oceanographic Report N°44. Oceanographic Observations in Kane Basin and Baffin Bay in May and August-Oct.1996.
- Mulder, T., Hassan, R., Ducassou, E., Zaragosi, S., Gonthier, E., Hanquiez, V., Marchès, E., Toucanne, S., 2013. Contourites in the Gulf of Cadiz: a cautionary note on potentially ambiguous indicators of bottom current velocity. *Geo-Mar. Lett.* 33, 357–367.
- Münchow, A., 2016. Volume and Freshwater Flux Observations from Nares Strait to the West of Greenland at Daily Time Scales from 2003 to 2009. *J. Phys. Oceanogr.* 46, 141–157. <https://doi.org/10.1175/JPO-D-15-0093.1>
- Münchow, A., Falkner, K.K., Melling, H., 2007. Spatial continuity of measured seawater and tracer fluxes through Nares Strait, a dynamically wide channel bordering the Canadian Archipelago. *J. Mar. Res.* 65, 759–788. <https://doi.org/10.1357/002224007784219048>
- Münchow, A., Falkner, K.K., Melling, H., Rabe, B., Johnson, H.L., 2011. Ocean Warming and Freshening of Nares Strait Bottom Waters off NW Greenland 2003-09 14.
- Münchow, A., Melling, H., 2008. Ocean current observations from Nares Strait to the west of Greenland: Interannual to tidal variability and forcing. *J. Mar. Res.* 66, 801–833. <https://doi.org/10.1357/002224008788064612>
- Münchow, A., Melling, H., Falkner, K.K., 2006. An Observational Estimate of Volume and Freshwater Flux Leaving the Arctic Ocean through Nares Strait. *J. Phys. Oceanogr.* 36, 2025–2041. <https://doi.org/10.1175/JPO2962.1>
- Münchow, A., Padman, L., Fricker, H.A., 2014. Interannual changes of the floating ice shelf of Petermann Gletscher, North Greenland, from 2000 to 2012. *J. Glaciol.* 60, 489–499. <https://doi.org/10.3189/2014JoG13J135>
- Mundy, C.J., Barber, D.G., 2001. On the relationship between spatial patterns of sea-ice type and the mechanisms which create and maintain the North Water (NOW) polynya. *Atmosphere-Ocean* 39, 327–341. <https://doi.org/10.1080/07055900.2001.9649684>
- Murray, M.S., 1999. Local heroes. The long-term effects of short-term prosperity-an example from the Canadian Arctic. *World Archaeol.* 30, 466–483.
- Myers, P.G., 2005. Impact of freshwater from the Canadian Arctic Archipelago on Labrador Sea Water formation. *Geophys. Res. Lett.* 32. <https://doi.org/10.1029/2004GL022082>
- Nichols, R.L., 1969. Geomorphology of Inglefield Land, North Greenland, *Meddelelser om Grønland*. ed, 188. C.A. Reitzel, København.
- Nick, F.M., Luckman, A., Vieli, A., Van Der Veen, C.J., Van As, D., Van De Wal, R.S.W., Pattyn, F., Hubbard, A.L., Floricioiu, D., 2012. The response of Petermann Glacier, Greenland, to large calving events, and its future stability in the context of atmospheric and oceanic warming. *J. Glaciol.* 58, 229–239. <https://doi.org/10.3189/2012JoG11J242>
- Nürnberg, D., Wollenburg, I., Dethleff, D., Eicken, H., Kassens, H., Letzig, T., Reimnitz, E., Thiede, J., 1994. Sediments in Arctic sea ice: Implications for entrainment, transport and release. *Mar. Geol.* 119, 185–214.
- Nutt, D.C., 1966. The Drift of Ice Island WH-5. *Arctic* 19, 244–262. <https://doi.org/10.14430/arctic3432>
- Ó Cofaigh, C., Dowdeswell, J.A., 2001. Laminated sediments in glacial marine environments: diagnostic criteria for their interpretation. *Quat. Sci. Rev.* 20, 1411–1436.
- Oakey, G.N., Damaske, D., 2006. Continuity of basement structures and dyke swarms in the Kane Basin region of central Nares Strait constrained by aeromagnetic data. *Polarforschung* 74, 51–62.

- Oksanen, J., Blanchet, F.G., Friendly, M., Kindt, R., Legendre, P., McGlenn, D., Minchin, P.R., O'Hara, R.B., Simpson, G.L., Solymos, P., Stevens, M.H.H., Szoecs, E., Wagner, H., 2019. vegan: Community Ecology Package.
- Okulitch, A.V., Dawes, P.R., Higgins, A.K., Soper, N.J., Christie, R.L., 1990. Towards a Nares Strait solution: structural studies on southeastern Ellesmere Island and northwestern Greenland. *Mar. Geol.* 93, 369–384.
- Osterman, L.E., Nelson, A.R., 1989. Latest Quaternary and Holocene paleoceanography of the eastern Baffin Island continental shelf, Canada: benthic foraminiferal evidence. *Can. J. Earth Sci.* 26, 2236–2248.
- Outridge, P.M., Goodsite, M.E., Bennike, O., Rausch, N., Shotyk, W., 2016. Seabird Transfer of Nutrients and Trace Elements from the North Water Polynya to Land during the Mid-Holocene Warm Period, Carey Islands, Northwest Greenland. *Arctic* 69, 253. <https://doi.org/10.14430/arctic4577>
- Palfrey, K.M., Day, G.G., 1968. Oceanography of Baffin Bay and Nares Strait in the summer of 1966 and current measurements in Smith Sound, summer 1963. US Coast Guard Oceanographic Unit.
- Patterson, R.T., Guilbault, J.-P., Richardson, E.T., 2000. Oxygen Level Control on Foraminifera Distribution in Effingham Inlet, Vancouver Island, British Columbia, Canada. *J. Foraminifer. Res.* 30, 321–335. <https://doi.org/10.2113/0300321>
- Pegler, S.S., 2016. The dynamics of confined extensional flows. *J. Fluid Mech.* 804, 24–57.
- Perner, K., Moros, M., Jennings, A., Lloyd, J., Knudsen, K., 2013. Holocene palaeoceanographic evolution off West Greenland. *The Holocene* 23, 374–387. <https://doi.org/10.1177/0959683612460785>
- Pfirman, S., Wollenburg, I., Thiede, J., Lange, M.A., 1989. Lithogenic sediment on Arctic pack ice: Potential aeolian flux and contribution to deep sea sediments, in: *Paleoclimatology and Paleometeorology: Modern and Past Patterns of Global Atmospheric Transport*. Springer, pp. 463–493.
- Pieńkowski, A.J., England, J.H., Furze, M.F.A., MacLean, B., Blasco, S., 2014. The late Quaternary environmental evolution of marine Arctic Canada: Barrow Strait to Lancaster Sound. *Quat. Sci. Rev.* 91, 184–203. <https://doi.org/10.1016/j.quascirev.2013.09.025>
- Pieńkowski, A.J., England, J.H., Furze, M.F.A., Marret, F., Eynaud, F., Vilks, G., Maclean, B., Blasco, S., Scourse, J.D., 2012. The deglacial to postglacial marine environments of SE Barrow Strait, Canadian Arctic Archipelago: Deglacial to postglacial marine environments, Canadian Arctic Archipelago. *Boreas* 41, 141–179. <https://doi.org/10.1111/j.1502-3885.2011.00227.x>
- Polyak, L., Korsun, S., Febo, L.A., Stanovoy, V., Khusid, T., Hald, M., Paulsen, B.E., Lubinski, D.J., 2002. Benthic foraminiferal assemblages from the southern Kara Sea, a river-influenced Arctic marine environment. *J. Foraminifer. Res.* 32, 252–273. <https://doi.org/10.2113/32.3.252>
- Preußner, A., Heinemann, G., Willmes, S., Paul, S., 2015. Multi-Decadal Variability of Polynya Characteristics and Ice Production in the North Water Polynya by Means of Passive Microwave and Thermal Infrared Satellite Imagery. *Remote Sens.* 7, 15844–15867. <https://doi.org/10.3390/rs71215807>
- Rabe, B., Johnson, H.L., Münchow, A., Melling, H., 2012a. Geostrophic ocean currents and freshwater fluxes across the Canadian polar shelf via Nares Strait. *J. Mar. Res.* 70, 603–640. <https://doi.org/10.1357/002224012805262725>
- Rabe, B., Münchow, A., Johnson, H.L., Melling, H., 2010. Nares Strait hydrography and salinity field from a 3-year moored array. *J. Geophys. Res.* 115. <https://doi.org/10.1029/2009JC005966>
- Rainville, L., Lee, C., Woodgate, R., 2011. Impact of Wind-Driven Mixing in the Arctic Ocean. *Oceanography* 24, 136–145. <https://doi.org/10.5670/oceanog.2011.65>
- Rashid, H., Piper, D.J.W., Lazar, K.B., McDonald, K., Saint-Ange, F., 2017. The Holocene Labrador Current: Changing linkages to atmospheric and oceanographic forcing factors. *Paleoceanography* 32, 498–510. <https://doi.org/10.1002/2016PA003051>
- Rasmussen, T.A.S., Kliem, N., Kaas, E., 2011. The Effect of Climate Change on the Sea Ice and Hydrography in Nares Strait. *Atmosphere-Ocean* 49, 245–258. <https://doi.org/10.1080/07055900.2011.604404>
- Reilly, B.T., Stoner, J.S., Mix, A.C., Walczak, M.H., Jennings, A., Jakobsson, M., Dyke, L., Glueder, A., Nicholls, K., Hogan, K.A., Mayer, L.A., Hatfield, R.G., Albert, S., Marcott, S., Fallon, S., Cheseby, M., 2019. Holocene break-up and reestablishment of the Petermann Ice Tongue, Northwest Greenland. *Quat. Sci. Rev.* 218, 322–342. <https://doi.org/10.1016/j.quascirev.2019.06.023>

- Reimer, P.J., Bard, E., Bayliss, A., Beck, J.W., Blackwell, P.G., Ramsey, C.B., Buck, C.E., Cheng, H., Edwards, R.L., Friedrich, M., 2013. IntCal13 and Marine13 radiocarbon age calibration curves 0–50,000 years cal BP. *Radiocarbon* 55, 1869–1887.
- Retelle, M.J., 1986. Glacial geology and Quaternary marine stratigraphy of the Robeson Channel area, north-eastern Ellesmere Island, Northwest Territories. *Can. J. Earth Sci.* 23, 1001–1012. <https://doi.org/10.1139/e86-101>
- Reusche, M.M., Marcott, S.A., Ceperley, E.G., Barth, A.M., Brook, E.J., Mix, A.C., Caffee, M.W., 2018. Early to Late Holocene Surface Exposure Ages From Two Marine-Terminating Outlet Glaciers in Northwest Greenland. *Geophys. Res. Lett.* 45, 7028–7039. <https://doi.org/10.1029/2018GL078266>
- Ribeiro, S., Limoges, A., Massé, G., Colgan, W., Jackson, R., Mikkelsen, N., Johannsen, K.J., Georgiadis, E., Weckström, K., Kuijpers, A., Olsen, J., Olsen, S.M., Nissen, M., Strunk, A., Wetterich, S., Syväranta, J., Henderson, A.J., Mackay, H., Taipale, S., Jeppesen, E., Larsen, N.K., Crosta, X., Giraudeau, J., Holm, L., Nuttall, M., Grønnow, B., Mosbech, A., Davidson, T.A., submitted. Vulnerability of the North Water polynya ecosystem to climate change. *Nat. Clim. Change*.
- Rignot, E., Steffen, K., 2008. Channelized bottom melting and stability of floating ice shelves. *Geophys. Res. Lett.* 35. <https://doi.org/10.1029/2007GL031765>
- Rigor, I.G., Wallace, J.M., Colony, R.L., 2002. Response of Sea Ice to the Arctic Oscillation. *J. Clim.* 15, 2648–2663. [https://doi.org/10.1175/1520-0442\(2002\)015<2648:ROSITT>2.0.CO;2](https://doi.org/10.1175/1520-0442(2002)015<2648:ROSITT>2.0.CO;2)
- Rollinson, H.R., 1993. *Using Geochemical Data, Evolution, Presentation, Interpretation*, Longman Scientific & Technical. ed. Oxford/John Wiley, New York.
- Rontani, J.-F., Belt, S.T., Amiraux, R., 2018. Biotic and abiotic degradation of the sea ice diatom biomarker IP25 and selected algal sterols in near-surface Arctic sediments. *Org. Geochem.* 118, 73–88. <https://doi.org/10.1016/j.orggeochem.2018.01.003>
- Rose, G.A., 2005. Capelin (*Mallotus villosus*) distribution and climate: a sea “canary” for marine ecosystem change. *ICES J. Mar. Sci.* 62, 1524–1530.
- Ryan, P.A., Münchow, A., 2017. Sea ice draft observations in Nares Strait from 2003 to 2012: NARES STRAIT SEA ICE (2003-2012). *J. Geophys. Res. Oceans* 122, 3057–3080. <https://doi.org/10.1002/2016JC011966>
- Rykova, T., Straneo, F., Lilly, J.M., Yashayaev, I., 2009. Irminger Current anticyclones in the Labrador Sea observed in the hydrographic record, 1990–2004. *J. Mar. Res.* 67, 361–384.
- Rytter, F., Knudsen, K.L., Seidenkrantz, M.-S., Eiriksson, J., 2002. Modern distribution of benthic foraminifera on the north Icelandic Shelf and Slope. *J. Foraminifer. Res.* 32, 217–244. <https://doi.org/10.2113/32.3.217>
- Sadler, H.E., 1976. Water, Heat, and Salt Transports through Nares Strait, Ellesmere Island. *J. Fish. Res. Board Can.* 33, 2286–2295. <https://doi.org/10.1139/f76-275>
- Samelson, R.M., Agnew, T., Melling, H., Münchow, A., 2006. Evidence for atmospheric control of sea-ice motion through Nares Strait. *Geophys. Res. Lett.* 33. <https://doi.org/10.1029/2005GL025016>
- Samelson, R.M., Barbour, P.L., 2008. Low-Level Jets, Orographic Effects, and Extreme Events in Nares Strait: A Model-Based Mesoscale Climatology. *Mon. Weather Rev.* 136, 4746–4759. <https://doi.org/10.1175/2007MWR2326.1>
- Saunders, P.M., 1964. Sea smoke and steam fog. *Q. J. R. Meteorol. Soc.* 90, 156–165. <https://doi.org/10.1002/qj.49709038405>
- Schafer, C.T., Collins, E.S., Smith, J.N., 1991. Relationship of Foraminifera and thecamoebian distributions to sediments contaminated by pulp mill effluent: Saguenay Fiord, Quebec, Canada. *Mar. Micropaleontol.* 17, 255–283. [https://doi.org/10.1016/0377-8398\(91\)90016-Y](https://doi.org/10.1016/0377-8398(91)90016-Y)
- Schledermann, P., 1990. *Crossroads to Greenland: 3000 years of prehistory in the eastern High Arctic*. Arctic Institute of North America of the University of Calgary.
- Schledermann, P., 1980. Polynyas and Prehistoric Settlement Patterns. *ARCTIC* 33. <https://doi.org/10.14430/arctic2562>
- Schledermann, P., McCullough, K.M., 2003. Late Thule culture developments on the central east coast of Ellesmere Island. Sila-The Greenland Research Centre at the National Museum of Denmark.

- Schmitz, B., 1987. Barium, equatorial high productivity, and the northward wandering of the Indian continent. *Paleoceanography* 2, 63–77. <https://doi.org/10.1029/PA002i001p00063>
- Seidenkrantz, M.-S., 2013. Benthic foraminifera as palaeo sea-ice indicators in the subarctic realm – examples from the Labrador Sea–Baffin Bay region. *Quat. Sci. Rev.* 79, 135–144. <https://doi.org/10.1016/j.quascirev.2013.03.014>
- Serreze, M.C., Barrett, A.P., Slater, A.G., Woodgate, R.A., Aagaard, K., Lammers, R.B., Steele, M., Moritz, R., Meredith, M., Lee, C.M., 2006. The large-scale freshwater cycle of the Arctic. *J. Geophys. Res.* 111. <https://doi.org/10.1029/2005JC003424>
- Serreze, M.C., Stroeve, J., Barrett, A.P., Boisvert, L.N., 2016. Summer atmospheric circulation anomalies over the Arctic Ocean and their influences on September sea ice extent: A cautionary tale. *J. Geophys. Res. Atmospheres* 121, 11,463–11,485. <https://doi.org/10.1002/2016JD025161>
- Shadwick, E.H., Rintoul, S.R., Tilbrook, B., Williams, G.D., Young, N., Fraser, A.D., Marchant, H., Smith, J., Tamura, T., 2013. Glacier tongue calving reduced dense water formation and enhanced carbon uptake: Ocean changes following glacier calving. *Geophys. Res. Lett.* 40, 904–909. <https://doi.org/10.1002/grl.50178>
- Sharp, M., Burgess, D.O., Cawkwell, F., Copland, L., Davis, J.A., Dowdeswell, E.K., Dowdeswell, J.A., Gardner, A.S., Mair, D., Wang, L., Williamson, S.N., Wolken, G.J., Wyatt, F., 2014. Remote sensing of recent glacier changes in the Canadian Arctic, in: Kargel, J.S., Leonard, G.J., Bishop, M.P., Kääb, A., Raup, B.H. (Eds.), *Global Land Ice Measurements from Space*, Springer Praxis Books. Springer, Berlin, Heidelberg, pp. 205–228. https://doi.org/10.1007/978-3-540-79818-7_9
- Sheldon, C.M., Seidenkrantz, M.-S., Pearce, C., Kuijpers, A., Hansen, M.J., Christensen, E.Z., 2016. Holocene oceanographic changes in SW Labrador Sea, off Newfoundland. *The Holocene* 26, 274–289. <https://doi.org/10.1177/0959683615608690>
- Shroyer, E.L., Padman, L., Samelson, R.M., Münchow, A., Stearns, L.A., 2017. Seasonal control of Petermann Gletscher ice-shelf melt by the ocean's response to sea-ice cover in Nares Strait. *J. Glaciol.* 63, 324–330. <https://doi.org/10.1017/jog.2016.140>
- Shroyer, E.L., Samelson, R.M., Padman, L., Münchow, A., 2015. Modeled ocean circulation in Nares Strait and its dependence on landfast-ice cover. *J. Geophys. Res. Oceans* 120, 7934–7959. <https://doi.org/10.1002/2015JC011091>
- Smith, S.D., Muench, R.D., Pease, C.H., 1990. Polynyas and leads: An overview of physical processes and environment. *J. Geophys. Res. Oceans* 95, 9461–9479. <https://doi.org/10.1029/JC095iC06p09461>
- Snyder, S.W., 1990. Relationships between benthic foraminiferal assemblages and Neogene phosphatic sediments, North Carolina coastal plain and continental shelf, in: *Phosphate Deposits of the World. III: Neogene to Modern Phosphorites*. pp. 444–464.
- Solignac, S., de Vernal, A., Hillaire-Marcel, C., 2004. Holocene sea-surface conditions in the North Atlantic—contrasted trends and regimes in the western and eastern sectors (Labrador Sea vs. Iceland Basin). *Quat. Sci. Rev.* 23, 319–334. <https://doi.org/10.1016/j.quascirev.2003.06.003>
- Sperling, M., Weldeab, S., Schmiedl, G., 2002. Drying of samples may alter foraminiferal isotopic ratios and faunistic composition. *Micropaleontology* 48, 87–91. [https://doi.org/10.1661/0026-2803\(2002\)048\[0087:DOSMAF\]2.0.CO;2](https://doi.org/10.1661/0026-2803(2002)048[0087:DOSMAF]2.0.CO;2)
- Steele, M., Boyd, T., 1998. Retreat of the cold halocline layer in the Arctic Ocean. *J. Geophys. Res. Oceans* 103, 10419–10435. <https://doi.org/10.1029/98JC00580>
- Steele, M., Ermold, W., 2007. Steric sea level change in the Northern Seas. *J. Clim.* 20, 403–417.
- Steele, M., Morison, J., Ermold, W., Rigor, I., Ortmeyer, M., Shimada, K., 2004. Circulation of summer Pacific halocline water in the Arctic Ocean. *J. Geophys. Res. Oceans* 109. <https://doi.org/10.1029/2003JC002009>
- Steffen, K., Ohmura, A., 1985. Heat exchange and surface conditions in North Water, northern Baffin Bay. *Ann. Glaciol.* 6, 4.
- Steinsund, P.I., Hald, M., 1994. Recent calcium carbonate dissolution in the Barents Sea: Paleoceanographic applications. *Mar. Geol.* 117, 303–316. [https://doi.org/10.1016/0025-3227\(94\)90022-1](https://doi.org/10.1016/0025-3227(94)90022-1)

- Stirling, I., 1997. The importance of polynyas, ice edges, and leads to marine mammals and birds. *J. Mar. Syst.* 10, 9–21. [https://doi.org/10.1016/S0924-7963\(96\)00054-1](https://doi.org/10.1016/S0924-7963(96)00054-1)
- St-Onge, M.P., St-Onge, G., 2014. Environmental changes in Baffin Bay during the Holocene based on the physical and magnetic properties of sediment cores. *J. Quat. Sci.* 29, 41–56.
- Stroeve, J.C., Maslanik, J., Serreze, M.C., Rigor, I., Meier, W., Fowler, C., 2011. Sea ice response to an extreme negative phase of the Arctic Oscillation during winter 2009/2010. *Geophys. Res. Lett.* 38, n/a-n/a. <https://doi.org/10.1029/2010GL045662>
- Stuiver, M., Reimer, P.J., Reimer, R.W., 2020. CALIB 7.1 [WWW program].
- Svendsen, J.I., Mangerud, J., Elverhøi, A., Solheim, A., Schüttenhelm, R.T., 1992. The Late Weichselian glacial maximum on western Spitsbergen inferred from offshore sediment cores. *Mar. Geol.* 104, 1–17.
- Swift, J.H., Takahashi, T., Livingston, H.D., 1983. The contribution of the Greenland and Barents seas to the deep water of the Arctic Ocean. *J. Geophys. Res. Oceans* 88, 5981–5986. <https://doi.org/10.1029/JC088iC10p05981>
- Syvitski, J.P., 1991. Towards an understanding of sediment deposition on glaciated continental shelves. *Cont. Shelf Res.* 11, 897–937.
- Tang, C.C.L., Ross, C.K., Yao, T., Petrie, B., DeTracey, B.M., Dunlap, E., 2004. The circulation, water masses and sea-ice of Baffin Bay. *Prog. Oceanogr.* 63, 183–228. <https://doi.org/10.1016/j.pocean.2004.09.005>
- Taylor, W.E., 1968. The Amapik and Tyara sites: An archaeological study of Dorset culture origins. *Mem. Soc. Am. Archaeol.* iii–129.
- Teilmann, J., Born, E.W., Acquarone, M., 1999. Behaviour of ringed seals tagged with satellite transmitters in the North Water polynya during fast-ice formation 77, 13.
- Thomas, R., Frederick, E., Krabill, W., Manizade, S., Martin, C., 2009. Recent changes on Greenland outlet glaciers. *J. Glaciol.* 55, 147–162. <https://doi.org/10.3189/002214309788608958>
- Thornalley, D.J.R., Elderfield, H., McCave, I.N., 2009. Holocene oscillations in temperature and salinity of the surface subpolar North Atlantic. *Nature* 457, 711–714. <https://doi.org/10.1038/nature07717>
- Tjallingii, R., Röhl, U., Kölling, M., Bickert, T., 2007. Influence of the water content on X-ray fluorescence core-scanning measurements in soft marine sediments: XRF core scanning. *Geochem. Geophys. Geosystems* 8. <https://doi.org/10.1029/2006GC001393>
- Tremblay, J.-E., Gratton, Y., Fauchot, J., Price, N.M., 2002. Climatic and oceanic forcing of new, net, and diatom production in the North Water. *Deep Sea Res. Part II Top. Stud. Oceanogr.* 49, 4927–4946. [https://doi.org/10.1016/S0967-0645\(02\)00171-6](https://doi.org/10.1016/S0967-0645(02)00171-6)
- Tremblay, J.-É., Gratton, Yves, Carmack, Eddy C., Payne, Christopher D., Price, Neil M., 2002. Impact of the large-scale Arctic circulation and the North Water Polynya on nutrient inventories in Baffin Bay. *J. Geophys. Res.* 107. <https://doi.org/10.1029/2000JC000595>
- Tushingham, A.M., 1991. On the extent and thickness of the Innuitian Ice Sheet: a postglacial-adjustment approach. *Can. J. Earth Sci.* 28, 231–239.
- Van der Weijden, C.H., 2002. Pitfalls of normalization of marine geochemical data using a common divisor. *Mar. Geol.* 184, 167–187. [https://doi.org/10.1016/S0025-3227\(01\)00297-3](https://doi.org/10.1016/S0025-3227(01)00297-3)
- Van Wychen, W., Burgess, D.O., Gray, L., Copland, L., Sharp, M., Dowdeswell, J.A., Benham, T.J., 2014. Glacier velocities and dynamic ice discharge from the Queen Elizabeth Islands, Nunavut, Canada. *Geophys. Res. Lett.* 41, 484–490. <https://doi.org/10.1002/2013GL058558>
- Van Wychen, W., Davis, J., Burgess, D.O., Copland, L., Gray, L., Sharp, M., Mortimer, C., 2016. Characterizing interannual variability of glacier dynamics and dynamic discharge (1999-2015) for the ice masses of Ellesmere and Axel Heiberg Islands, Nunavut, Canada: GLACIER DYNAMICS OF THE CANADIAN ARCTIC. *J. Geophys. Res. Earth Surf.* 121, 39–63. <https://doi.org/10.1002/2015JF003708>
- Vare, L.L., Massé, G., Gregory, T.R., Smart, C.W., Belt, S.T., 2009. Sea ice variations in the central Canadian Arctic Archipelago during the Holocene. *Quat. Sci. Rev.* 28, 1354–1366. <https://doi.org/10.1016/j.quascirev.2009.01.013>
- Vellinga, M., Dickson, B., Curry, R., 2008. The changing view on how freshwater impacts the Atlantic meridional overturning circulation, in: *Arctic-Subarctic Ocean Fluxes*. Dordrecht, Netherlands, pp. 289–313.

- Vidussi, F., Roy, S., Lovejoy, C., Gammelgaard, M., Thomsen, H.A., Booth, B., Tremblay, J.-E., Mostajir, B., 2004. Spatial and temporal variability of the phytoplankton community structure in the North Water Polynya, investigated using pigment biomarkers. *Can. J. Fish. Aquat. Sci.* 61, 2038–2052. <https://doi.org/10.1139/f04-152>
- Vilks, G., 1969. Recent Foraminifera in the Canadian Arctic. *Micropaleontology* 15, 35–60. <https://doi.org/10.2307/1484859>
- Vincent, R.F., 2019. A Study of the North Water Polynya Ice Arch using Four Decades of Satellite Data. *Sci. Rep.* 9. <https://doi.org/10.1038/s41598-019-56780-6>
- Vincent, R.F., 2013. The 2009 North Water anomaly. *Remote Sens. Lett.* 4, 1057–1066. <https://doi.org/10.1080/2150704X.2013.837227>
- Vincent, R.F., Marsden, R.F., 2001. An analysis of the dissolution of ice in Nares Strait using AVHRR Imagery. *Atmosphere-Ocean* 39, 209–222. <https://doi.org/10.1080/07055900.2001.9649677>
- Vincent, W.F., Gibson, J.A.E., Jeffries, M.O., 2001. Ice-shelf collapse, climate change, and habitat loss in the Canadian high Arctic. *Polar Rec.* 37, 133–142. <https://doi.org/10.1017/S0032247400026954>
- Vinther, B.M., Clausen, H.B., Johnsen, S.J., Rasmussen, S.O., Andersen, K.K., Buchardt, S.L., Dahl-Jensen, D., Seierstad, I.K., Siggaard-Andersen, M.-L., Steffensen, J.P., 2006. A synchronized dating of three Greenland ice cores throughout the Holocene. *J. Geophys. Res. Atmospheres* 111.
- Wadley, M.R., Bigg, G.R., 2002. Impact of flow through the Canadian Archipelago and Bering Strait on the North Atlantic and Arctic circulation: An ocean modelling study. *Q. J. R. Meteorol. Soc.* 128, 2187–2203. <https://doi.org/10.1256/qj.00.35>
- Wang, J., Zhang, J., Watanabe, E., Ikeda, M., Mizobata, K., Walsh, J.E., Bai, X., Wu, B., 2009. Is the Dipole Anomaly a major driver to record lows in Arctic summer sea ice extent? *Geophys. Res. Lett.* 36. <https://doi.org/10.1029/2008GL036706>
- Weltje, G.J., Tjallingii, R., 2008. Calibration of XRF core scanners for quantitative geochemical logging of sediment cores: Theory and application. *Earth Planet. Sci. Lett.* 274, 423–438.
- White, A., Copland, L., 2019. Loss of floating glacier tongues from the Yelverton Bay region, Ellesmere Island, Canada. *J. Glaciol.* 65, 376–394. <https://doi.org/10.1017/jog.2019.15>
- Williams, K.M., 1990. Late Quaternary paleoceanography of the western Baffin Bay region: evidence from fossil diatoms. *Can. J. Earth Sci.* 27, 1487–1494. <https://doi.org/10.1139/e90-158>
- Wollenburg, J.E., Kuhnt, W., 2000. The response of benthic foraminifers to carbon flux and primary production in the Arctic Ocean. *Mar. Micropaleontol.* 40, 189–231. [https://doi.org/10.1016/S0377-8398\(00\)00039-6](https://doi.org/10.1016/S0377-8398(00)00039-6)
- Wollenburg, J.E., Mackensen, A., 1998. Living benthic foraminifers from the central Arctic Ocean: faunal composition, standing stock and diversity. *Mar. Micropaleontol.* 34, 153–185. [https://doi.org/10.1016/S0377-8398\(98\)00007-3](https://doi.org/10.1016/S0377-8398(98)00007-3)
- Wood, S., 2019. mgcv: Mixed GAM Computation Vehicle with Automatic Smoothness Estimation.
- Yao, T., Tang, C.L., 2003. The formation and maintenance of the North Water Polynya. *Atmosphere-Ocean* 41, 187–201. <https://doi.org/10.3137/ao.410301>
- Yashayaev, I., Loder, J.W., 2009. Enhanced production of Labrador Sea water in 2008. *Geophys. Res. Lett.* 36.
- Zaragosi, S., Bourillet, J.-F., Eynaud, F., Toucanne, S., Denhard, B., Toer, A.V., Lanfume, V., 2006. The impact of the last European deglaciation on the deep-sea turbidite systems of the Celtic-Armorian margin (Bay of Biscay). *Geo-Mar. Lett.* 26, 317–329. <https://doi.org/10.1007/s00367-006-0048-9>
- Zreda, M., England, J., Phillips, F., Elmore, D., Sharma, P., 1999. Unblocking of the Nares Strait by Greenland and Ellesmere ice-sheet retreat 10,000 years ago. *Nature* 398, 139–142. <https://doi.org/10.1038/18197>